

# **Intelligent Strategies for Mobile Robotics in Laboratory Automation**

**Habilitation Thesis**



**Submitted to**  
**the Faculty of Computer Sciences**  
**& Electrical Engineering,**  
**University of Rostock, Germany**

**by:**

**Dr. -Ing. Hui Liu, born on 7<sup>th</sup>, February 1983 in Xianyou, China**  
**Rostock, Germany, 2016**

Reviewers:

1. Reviewer:

Prof. Dr. -Ing. habil. Kerstin Thurow

Institute of Automation, University of Rostock, Germany

2. Reviewer:

Prof. Dr. -Ing. Norbert Stoll

Institute of Automation, University of Rostock, Germany

3. Reviewer:

Prof. Robin A. Felder, Ph.D.

Medical Automation Research Center, University of Virginia, USA

Data of Submission: 27<sup>th</sup>, May, 2016

Data of Defense: 24<sup>th</sup>, October, 2016

## Acknowledgement:

This habilitation thesis is impossible to be completed without the support, guidance and the help from the sponsored projects and the following important people.

First and foremost, I would like to express my highest gratitude to my supervisors *Prof. Kerstin Thurow* and *Prof. Norbert Stoll*, for their continuous and precious guidance. Their scientific and professional ideas leaded me during all my habilitation research activities. Having this precious chance to work with them is my great pleasure and it is also the base of my habilitation on mobile robotics.

Besides my supervisors, I would like to thank all my colleagues of the Institute of Automation and the Center for Life Science Automation (CELISCA) at University of Rostock, Germany. Especially I would like to thank *Prof. Dr. med. habil. Regina Stoll*, *apl. Prof. Dr.-Ing. habil. Mohit Kumar*, *Dr.-Ing. Steffen Junginger*, *Dr.-Ing. Thomas Roddelkopf*, *Dr.-Ing. Sebastian Neubert*, *PD Dr.-Ing. habil. Heidi Fleischer*, *Mr. Hans-Joachim Stiller*, *Mr. Lars Woinar*, *Mr. Ali Abdulla*, *Mr. Mazen Ghandour* and *Mr. Mohammed Myasar Ali*. They also provided me their incomparable suggestions to my habilitation work. I also would like to thank BMBF for the financial support to my group and me.

Last but not least, I would like to dedicate this thesis to my beloved family: *my wife Dr.-Ing. Yanfei Li*, *my son Mr. Xing Liu* and *daughter Ms. Shu Liu*, *my father Mr. Jinzheng Liu* and *my mother Mrs. Meiqiong Zheng*, for their great love, patience, unparalleled support and encouragement throughout my life!

# Contents

<b>Chapter 1</b>	<b>Introduction .....</b>	<b>1</b>
1.1	Development of Indoor Mobile Robotics.....	1
1.2	Related Works .....	3
1.2.1	Factory Transportation .....	3
1.2.2	Supermarket/Shopping Mall Transportation .....	4
1.2.3	Hospital Transportation.....	6
1.2.4	Laboratory Transportation/Delivery.....	8
1.2.5	Discussions.....	10
1.3	Architecture of this Habilitation.....	12
<b>Chapter 2</b>	<b>Intelligent Strategy .....</b>	<b>16</b>
2.1	Introduction.....	16
2.2	Framework of Intelligent Strategy .....	17
<b>Chapter 3</b>	<b>Multi-floor Indoor Navigation .....</b>	<b>24</b>
3.1	Introduction.....	24
3.2	StarGazer Sensor Based Robot Localization .....	28
3.3	Multi-floor Navigation Strategy.....	29
3.4	Robot-Door Integration in Multi-floors .....	32
3.5	Intelligent Robot Localization Signal Filter.....	35
3.5.1	Framework of the Proposed Intelligent Filter .....	35
3.5.2	Theories of the Modeling .....	37
3.5.2.1	Time Series Analysis Theory.....	37
3.5.2.2	Kalman Filter Theory .....	40
3.5.2.3	Modeling Steps of the Proposed Hybrid Method .....	42
3.5.3	Experiments and analysis.....	49
3.5.3.1	One-step Tracking/Forecasting Results .....	49
3.5.3.2	Two-step Forecasting Results .....	54
3.5.3.3	Real-time Performance of the Proposed ARIMA-KF .....	56
3.6	Execution of the Robot Navigation.....	56



<b>Chapter 4 Smart Collision Avoidance .....</b>	<b>58</b>
4.1 Introduction.....	58
4.2 Framework of the Proposed Smart Strategy .....	59
4.3 Face based Collision Avoidance.....	62
4.4 Gesture based Collision Avoidance.....	64
4.5 Modeling of the Embedded Algorithms .....	66
4.5.1 Modeling of LVQ Neural Network .....	66
4.5.2 Modeling of Support Vector Machine.....	68
4.6 Experiments and Analysis .....	70
4.6.1 Face based Strategy.....	70
4.6.2 Gesture based Strategy .....	73
4.7 Developed Controlling GUI.....	74
<b>Chapter 5 Intelligent Robot Power Forecasting.....</b>	<b>76</b>
5.1 Introduction .....	76
5.2 Power Measurement System .....	78
5.3 Robot Power Forecasting Method.....	79
5.3.1 Hybrid Forecasting Algorithm .....	79
5.3.2 Original Robot Power Sampling Data.....	80
5.3.3 Wavelet Decomposition of Mobile Robot Power Data .....	81
5.3.4 EMD Decomposition of Mobile Robot Power.....	83
5.3.5 ANFIS Forecasting Model .....	85
5.4 Experiments and Analysis .....	86
5.4.1 Results of the Hybrid WD-ANFIS Model.....	86
5.4.2 Results of the Hybrid EMD-ANFIS Model .....	88
5.4.3 Results of the MLP Model .....	89
5.4.4 Results of the ANFIS Model .....	91
5.4.5 Comparison of the Forecasting Results.....	92
5.4.6 Real-time Performance of the Proposed ARIMA-KF .....	93
<b>Chapter 6 Robot Arm Manipulator.....</b>	<b>94</b>
6.1 Introduction.....	94
6.2 Blind Arm Manipulator (BAM) .....	96
6.3 Vision based Arm Manipulator (VAM).....	98
6.4 MLP based Arm Joint Mapping .....	99

6.5	Arm Kinematics .....	101
6.6	Lab-ware Identification .....	103
6.7	Experiments and Analysis .....	104
6.7.1	BFGS based Mapping Results .....	105
6.7.2	GD-BP based Mapping Results.....	106
6.7.3	GDMA-BP based Mapping Results .....	108
6.7.4	CG-BP-FR based Mapping Results.....	110
6.7.5	Real-time Performance of the MLP .....	111
6.8	Developed Controlling GUI.....	112
<b>Chapter 7</b>	<b>Conclusions &amp; Outlook.....</b>	<b>114</b>
7.1	Conclusions .....	114
7.2	Outlook.....	118
<b>References</b>	.....	<b>120</b>
<b>Declaration</b>	.....	<b>145</b>
<b>Curriculum Vitae</b>	.....	<b>146</b>
<b>Theses</b>	.....	<b>157</b>
<b>Abstract</b>	.....	<b>161</b>
<b>Zusammenfassung</b>	.....	<b>164</b>

## List of Figures

Figure 1-1: Developing progress of the indoor mobile robotics	1
Figure 1-2: Car-wheel assembling and transporting robotic system	4
Figure 1-3: iCART II transportation system	4
Figure 1-4: Supermarket guiding robot	5
Figure 1-5: Supermarket guiding and carting robot	6
Figure 1-6: Robotic hospital transportation bed	7
Figure 1-7: Mobile robot Terapio for hospital healthcare purpose	7
Figure 1-8: MKR robots for hospital transportation tasks	7
Figure 1-9: Kinds of hospital transportation mobile robots proposed by companies	8
Figure 1-10: Caging transportation using swarm mobile robots	9
Figure 1-11: Local robot transportation	9
Figure 1-12: Framework of the proposed habilitation thesis	12
Figure 2-1: H20 mobile robots	16
Figure 2-2: System controlling Strategy	17
Figure 2-3: Process flows between the RRC and the HWMS	18
Figure 2-4: Process flows among the robotic hardware, the RBCs and the RRC	19
Figure 2-5: Process flows between the RBC, the MNC and the AM	21
Figure 2-6: Process flows between the RBC and the PFC	22
Figure 2-7: Process flows among the RBC, the GCAC and the FCAC	23
Figure 3-1: StarGazer based robot indoor navigation adopted at CELISC laboratory	29
Figure 3-2: Mobile robot multi-floor navigation mapping strategy	30
Figure 3-3: Mobile robot multi-floor path planning method	31

Figure 3-4: GUI of the multi-floor mobile robot transportation /movements	31
Figure 3-5: Laboratory door-opening/closing by the running mobile robots: (a) Automatic controlling for the laboratory doors; and (b) Automatic controlling for the elevator doors	32
Figure 3-6: The shortest path planning for the mobile robot transportation	33
Figure 3-7: Wireless communication channel for the robot-door controlling	34
Figure 3-8: A case of the status of the automated doors in a RBC center	34
Figure 3-9: A system log-file in the RBC monitoring the door opening/closing process	35
Figure 3-10: A system log-file in the RRC storing the door controlling error for the HWMS	35
Figure 3-11: Lighting interference conditions at CELISCA	36
Figure 3-12: The framework of the proposed robot positioning signal filtering method	37
Figure 3-13: Architecture of the original idea adopting in the KF	41
Figure 3-14: Computational framework of the KF	42
Figure 3-15: Robot transportation from the reformatting lab to the ICP lab at CELISCA	42
Figure 3-16: Robot indoor positioning coordinates by the StarGazer sensor: (a) the X coordinates; and (b) the Y coordinates	43
Figure 3-17: Autocorrelation parameters of the original robot X coordinates	43
Figure 3-18 Partial autocorrelation parameters of the original robot X coordinates	44
Figure 3-19 Autocorrelation parameters of the one-order difference processed robot X coordinates	45
Figure 3-20: Autocorrelation parameters of the one-order difference processed robot X coordinates	45
Figure 3-21: Partial autocorrelation parameters of the one-order difference processed robot X coordinates	46

Figure 3-22: Results at the 1st-600th sampling of the robot X positioning coordinates	50
Figure 3-23: Sub-zones for the results at the 1st-600th sampling of the robot X positioning coordinates	51
Figure 3-24: Results at the 1st-600th sampling of the robot Y positioning coordinates	51
Figure 3-25: Results at the 1st-600th sampling of the robot Y positioning coordinates	52
Figure 3-26: Two-step results at the 1st-600th sampling of the robot X positioning coordinates	55
Figure 3-27: Two-step results at the 1st-600th sampling of the robot X positioning coordinates	55
Figure 3-28: A case of the multi-floor mobile robot transportation at CELISCA laboratory	57
Figure 4-1: The framework of the proposed smart collision avoidance strategy	61
Figure 4-2: The definition of the smart collision avoidance	62
Figure 4-3: The framework of the proposed face moving recognition for the smart collision avoidance & HRI control	63
Figure 4-4: Five face orientation definition	63
Figure 4-5: Workflow of the proposed face orientation feature recognizing algorithm	64
Figure 4-6: Seven gesture definitions	65
Figure 4-7: Architecture of the LVQ neural network	66
Figure 4-6: Procedures of the human face orientation & moving recognition for the robots	61
Figure 4-7: Face moving recognition GUI	62
Figure 4-8: The built LVQ model	68
Figure 4-9: Architecture of the SVM model	69
Figure 4-10: Procedures of the human face orientation & moving recognition for the robots	71
Figure 4-11: Training performance of the proposed recognizing approach by different edge detection algorithms: (a) Sobel algorithm; (b) Prewitt algorithm; (c) Roberts algorithm; (d) Log algorithm; (e)	72

Zero-cross algorithm; and (f) Canny algorithm	
Figure 4-12: Face moving recognition GUI	75
Figure 4-13: Gesture controlling GUI	75
Figure 5-1: Robot power measurement GUIs	78
Figure 5-2: The proposed hybrid mobile robot power forecasting framework	79
Figure 5-3: Measured robot power voltage data from a H20 mobile robot	80
Figure 5-4: Four-layer based wavelet decomposing structure	82
Figure 5-5: Decomposed results of the measured robot power data by the WD algorithm	83
Figure 5-6: Decomposed results of the measured robot power data by the EMD algorithm	85
Figure 5-7: Scheme of the ANFIS network	85
Figure 5-8: Forecasting results for the originally measured robot power data by the proposed hybrid WD-ANFIS method	86
Figure 5-9: Forecasting results for the wavelet based decomposed data by the proposed hybrid WD-ANFIS method	88
Figure 5-10: Forecasting results for the originally measured robot power data by the proposed hybrid EMD-ANFIS method	89
Figure 5-11: Forecasting results for the originally measured robot power data by the proposed MLP neural network	90
Figure 5-12: Forecasting results for the originally measured robot power data by the proposed ANFIS neural network	91
Figure 6-1: Framework of the proposed BAM	97
Figure 6-2: The structure of the adopted three-layer MLP network	98
Figure 6-3: Framework of the proposed VAM	98
Figure 6-4: The computational schema of the MLP model	99
Figure 6-5: DOF configuration of the arms in H20 mobile robots	101
Figure 6-6: Results of the arm kinematic experiments: (a) FK model; and (b) IK model	102
Figure 6-7: Result of the arm workspace experiment	103

Figure 6-8: Result of the single lab-ware identification	103
Figure 6-9: Result of the multiple lab-ware identification	104
Figure 6-10: Result of the selected lab-ware identification	104
Figure 6-11: The schema of the experiment	104
Figure 6-12: The network training performance of the built MLP using the BFGS algorithm for the robot arm joint #8	105
Figure 6-13: The forecasting results by the built MLP with the BFGS algorithm for the robot arm joint #8	106
Figure 6-14: The network training performance of the built MLP using the GD-BP algorithm for the robot arm joint #8	107
Figure 6-15: The forecasting results by the built MLP with the GD-BP algorithm for the robot arm joint #8	107
Figure 6-16: The network training performance of the built MLP using the GDMA-BP algorithm for the robot arm joint #8	109
Figure 6-17: The forecasting results by the built MLP with the GDMA-BP algorithm for the robot arm joint #8	109
Figure 6-18: The network training performance of the built MLP using the CG-BP-FR algorithm for the robot arm joint #8	110
Figure 6-19: The forecasting results by the built MLP with the CG-BP-FR algorithm for the robot arm joint #8	111
Figure 6-20: Real cases of the proposed two arm manipulators: (a) BAM strategy; and (b) VAM strategy	112
Figure 6-21: Main GUI of the developed arm manipulator	113
Figure 6-22: Lab-ware identification GUI in the developed arm manipulator	113

## List of Tables

Table 3-1: The characteristics and accuracies of the available methods for the robot indoor navigation/localization	26
Table 3-2: The detailed results of the autocorrelation parameters given in Fig.3-17	44
Table 3-3: The detailed results of the partial autocorrelation parameters given in Fig.3-18	44
Table 3-4: The detailed results of the autocorrelation parameters given in Fig.3-20	46
Table 3-5: The detailed results of the partial autocorrelation parameters given in Fig.3-21	46
Table 3-6: The estimated errors of the robot one-step tracking /forecasting results by executing the proposed ARIMA-KF method	53
Table 3-7: The estimated errors of the robot one-step tracking /forecasting results by executing the mainstream ARIMA method	53
Table 3-8: The promoting percentages of the ARIMA method by the proposed ARIMA-KF method in the one-step results	54
Table 3-9: The estimated errors of the robot two-step forecasting results by executing the proposed ARIMA-KF method	55
Table 3-10: The estimated errors of the robot two-step forecasting results by executing the mainstream ARIMA method	56
Table 3-11: The time performance of the proposed ARIMA-KF model	56
Table 4-1: The defined controlling commands based on the dynamic gestures	65
Table 4-2: Successful rates of the proposed LVQ based recognizing approach by different edge detection algorithms	72
Table 4-3: Consumed times of the proposed LVQ based recognizing approach by different edge detection algorithms	73
Table 4-4: Experimental results of the built SVM to select the best ‘C’ parameter	73
Table 4-5: Experimental results of the built SVM for the gesture based collision avoidance	74
Table 5-1: The estimated errors of the robot power forecasting results by	87



executing the proposed hybrid WD-ANFIS method	
Table 5-2: The estimated errors of the robot power forecasting results by executing the proposed hybrid EMD-ANFIS method	89
Table 5-3: The estimated errors of the robot power forecasting results by executing the standard MLP neural network	90
Table 5-4: The estimated errors of the robot power forecasting results by executing the standard ANFIS neural network	91
Table 5-5: The results of the promoting error indexes among different models for the mobile robot power predictions	93
Table 5-6: The time performance of the involved different models in the robot power forecasting	93
Table 6-1: The D-H parameters of the H20 right arm	102
Table 6-1: The forecasted results of the robot arm joint #8 by the MLP neural network using the BFGS algorithm	106
Table 6-2: The forecasted results of the robot arm joint #8 by the MLP neural network using the GD-BP algorithm	108
Table 6-3: The forecasted results of the robot arm joint #8 by the MLP neural network using the GDMA-BP algorithm	109
Table 6-4: The forecasted results of the robot arm joint #8 by the MLP neural network using the CG-BP-FR algorithm	111
Table 6-5: The time performance of the involved different models in the robot arm controlling	112

## List of Abbreviations

- ✧ SMSF, *Single Mobile-robot Single Floor*;
- ✧ SMMF, *Single Mobile-robot Multi-floor*;
- ✧ MMSF, *Multiple Mobile-robot Single-floor*;
- ✧ MMMF, *Multiple Mobile-robot Multi-floor*;
- ✧ HRI, *Human Robot Interaction*;
- ✧ TSA, *Time Series Analysis*;
- ✧ KF, *Kalman Filter*;
- ✧ ARIMA, *Auto Regressive Integrated Moving Average*;
- ✧ KS, *Kinect Sensor (Microsoft)*;
- ✧ LVQ, *Learning Vector Quantization*;
- ✧ SVM, *Support Vector Machine*;
- ✧ ANFIS, *Adaptive Neuro Fuzzy Inference System*;
- ✧ WD, *Wavelet Decomposition*;
- ✧ EMD, *Empirical Mode Decomposition*;
- ✧ MLP, *Multi Layer Perceptron*;
- ✧ IMRTS, *Intelligent Mobile Robot Transportation System*;
- ✧ HWMS, *Hierarchical Workflow Management System*;
- ✧ RRC, *Robot Remote Center*;
- ✧ RBC, *Robot On-board Center*;
- ✧ AM, *Arm Manipulator*;
- ✧ MNC, *Multi-floor Navigation Component*;
- ✧ PFC, *Power Forecasting Component*;
- ✧ GCAC, *Gesture based Collision Avoidance Component*;
- ✧ AP, *Access Points*;
- ✧ PF, *Particle Filter*;
- ✧ CSS, *Camera Sensor Space*
- ✧ EKF, *Extended Kalman Filter*;

- ✧ KNN, *k-Nearest-Neighbor*;
- ✧ GPR, *Guassian Process Regression*;
- ✧ BF, *Bayes Filter*;
- ✧ FA-OSELM, *Feature Adaptive Online Sequential Extreme Learning Machine*;
- ✧ SLAM, *Simultaneous Localization and Mapping*;
- ✧ PLOT, *Polynomial Local Orientation Tensor*;
- ✧ RFID, *Radio Frequency Identification*;
- ✧ BAM, *Blind Arm Manipulator*;
- ✧ VAM, *Vision Arm Manipulator*;
- ✧ AK, *Arm Kinematics*;
- ✧ FK, *Forward Kinematics*;
- ✧ IK, *Inverse Kinematics*;
- ✧ ANN, *Artificial Neural Networks*
- ✧ MLP, *Multiple Layer Perceptron*;
- ✧ GD-BP, *Gradient Descent Back Propagation*;
- ✧ GDMA-BP, *Gradient Descent with Momentum and Adaptive Learning Rate Back Propagation*;
- ✧ CG-BP-FR, *Conjugate Gradient Back Propagation with Fletcher-Reeves Updates*;
- ✧ BFGS, *BFGS Quasi-Newton Back Propagation*;
- ✧ IR, *Infrared Radio*;
- ✧ DSP, *Digital Signal Processing*;
- ✧ AR, *Auto Regressive*;
- ✧ MA, *Moving Average*;
- ✧ ARMA, *Auto Regressive Moving Average*;
- ✧ AIC, *Akaike Information Criterion*;
- ✧ BIC, *Bayesian information criterion*;
- ✧ FPE, *Final Prediction Error*;
- ✧ YW, *Yule-Walker Estimation*;

- ✧ MLE, *Maximum Likelihood Estimation*;
- ✧ LSE, *Least Square Estimation*;
- ✧ PLL, *Pixel Level Likelihoods*;
- ✧ HMI, *Human-Machine Interface*;
- ✧ SEM, *Surface Electromyography Measurement*;
- ✧ HSM, *Human Skeleton Mapping*;
- ✧ MAE, *Mean Absolute Error*;
- ✧ MAPE, *Mean Absolute Percentage Error*;
- ✧ RMSE, *Root Mean Square Error*;
- ✧ PMAE, *Promotion of Mean Absolute Error*;
- ✧ PMAPE, *Promotion of Mean Absolute Percentage Error*;
- ✧ PRMSE, *Promotion of Root Mean Square Error*;

# Chapter 1 Introduction

## 1.1 Indoor Mobile Robotics

In recent years, the automation discipline has been developing considerably. It brings out important scientific and technical contributions in different fields, including the robotics integrated manufacturing [1]–[4], the traffic planning and controlling [5]–[8], the laboratory process controlling [9]–[12], etc. This habilitation thesis is based on the latest progress of the indoor mobile robotics.

The developing progress of the indoor mobile robotics is demonstrated in Fig. 1-1. From Fig. 1-1, it can be seen that there are four developing levels in indoor mobile robotics, which consists of the SMSF (*Single Mobile-robot Single Floor*), the SMMF (*Single Mobile-robot Multi-floor*), the MMSF (*Multiple Mobile-robot Single-floor*) and the MMMF (*Multiple Mobile-robot Multi-floor*).

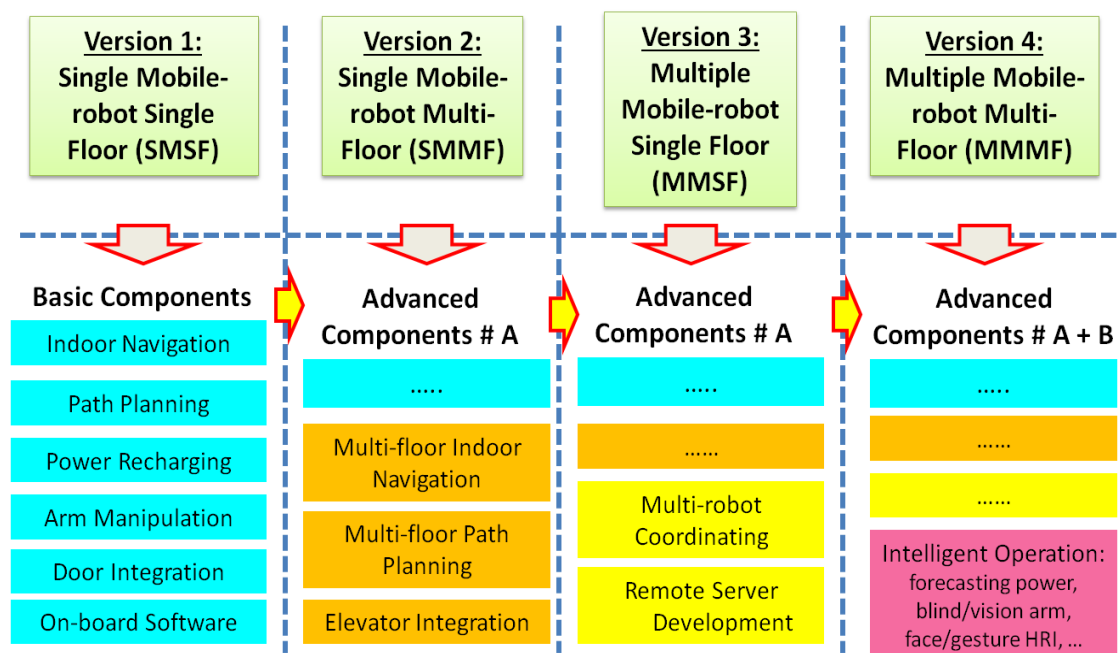


Figure 1.1: Developing progress of the indoor mobile robotics

The definitions of these mobile robotic systems can be given as follows:

**(a)** The SMSF level focuses on the development of the basic functions of the mobile robots. The involved technologies consist of the robot indoor navigation/localization, the robot path planning, the robot power recharging management, the arm manipulation, the robot-door integration and the development of robot on-board controlling software. Due to their features, the mobile robots in the SMSF level always run independently. Since they are not expected to be controlled remotely, they are not used to generate automatic indoor transportation processes.

**(b)** In the SMMF level, the mobile robots are controlled to run in the multi-floor indoor environments. Comparing to the mobile robots in the SMSF level, the mobile robots in the SMMF have some advanced robotic functions, such as, the multi-floor robot indoor navigation/localization, the multi-floor path planning and the elevator integration. Comparing to the single-floor navigation, the multi-floor navigation is more complicated. Besides the accuracy of the indoor navigation, the multi-floor one has to solve the flexible extension of the indoor navigation maps. Accordingly, the mobile robots need to solve the difficulty of the multi-floor path planning. In addition, the elevator handling is also critical for the mobile robots in the SMMF level.

**(c)** Different to the SMMF level, the mobile robots in the MMSF level do not need to cope with the multi-floor navigation and path planning but they have to face the issue of the multiple mobile-robot controlling. The MMSF systems will be applied for the single-floor situations and their developed software should schedule the multiple running mobile robots. The mobile robots in the MMSF level also have some advanced operating system components, which include the multi-robot coordinating & scheduling and the remote controlling software development. In the expected MMSF architecture, every mobile robot can be regarded as a special sensor and any new kinds of mobile robots can be integrated in the whole transportation system after convenient upgrading.

**(d)** The MMMF level is highest in the development of mobile robotics, which combines the SMMF and the MMSF. In the MMMF mobile robot systems, both of the multi-floor operation and the multiple mobile robot running are included. Additionally, in the latest versions of the MMMF systems, intelligent strategies are embedded to make the developed MMMF systems work smarter. Some advanced mobile robot functions are proposed in recent years, such as, the robot on-board power status is

forecasted to make the long-distance indoor transportation scientifically, the natural human features (*including face features and gesture features*) are proposed to realize the natural HRI (*Human-Robot Interaction*) based collision avoidance, etc. In the habilitation thesis, the intelligent strategies for the MMMF mobile robotic systems are focused.

## 1.2 Related Works

This section provides reviewing on some representative literatures on the mobile robot indoor transportation.

### 1.2.1 Factory Transportation

The mobile robots, which are applied in the latest factory transportation, are belonged to the definition of the MMSF mobile robotic systems [13]–[22]. In the factory transportation applications, the mobile robots usually run in the single floors.

*Lange et al.* presented a robot car-wheel assembling and transporting method based on standard industrial robots (*like KUKA*), as shown in Fig. 1-2 [23]. To compensate the temporal/spatial errors during the wheel assembling process, a sensor-driven controlling strategy was proposed. To decrease the delaying phenomenon of the installed three groups of sensors, a Kalman filter based processing model was built to realize the real-time forecasting computation.

*Horan et al.* put forward a large-loading transportation system based on OzTug robots for the manufacturing environments [24]. The OzTug mobile robots adopted in the paper could load up to 2,000 kg. To make the system simple and robust, the floor line-tracking mobile robot navigation method was utilized and a fuzzy based image processing controller was developed to track the transportation paths.

*Endo et al.* proposed a car transportation robotic system iCART using two mobile robots for narrow factory spaces [25]. In the iCART system, the leader-follower controlling strategy was presented to coordinate the adopted two mobile robots for the transportation target and at the same time the caster-like motion based adjusting method was utilized to solve the force-shifting problem during the transportation. The details of the coordinating control strategy can be found in [26]. To decrease the sizes of the carrying mobile robots, a upgraded version of the iCART (iCART II) was

developed as shown in Fig. 1-3 [27].

*Kang et al.* proposed an assistive mobile robot to help the disabled in factories [28]. To meet different factory requirements, different versions of the assistive mobile robot were designed as follows: the first version of the robot was equipped with a simple arm and forklift; the second one was supplemented an Omni-directional motion to let the robot move in small factory environments; and the third one was proposed to reduce the vibrating problem of the robot to focus on the comfort function.



Figure 1-2: Car-wheel assembling and transporting robotic system [23]

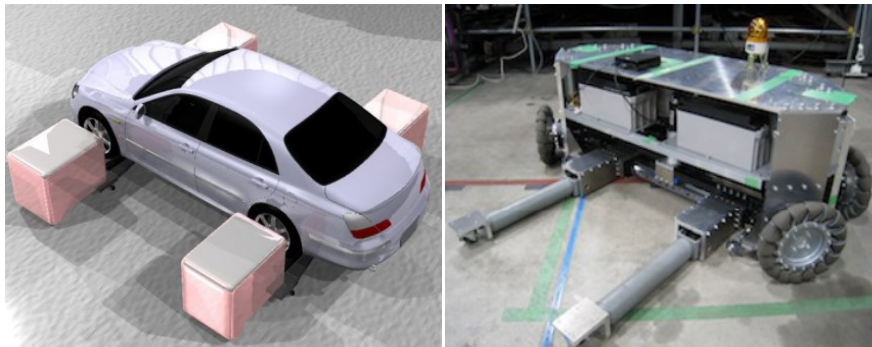


Figure 1-3: iCART II transportation system [27]

## 1.2.2 Supermarket/Shopping Mall Transportation

The mobile robots, which are adopted for the supermarket/mall shopping transportation, are belonged to the definition of the MMSF mobile robotic systems [29]–[37]. In this kind of indoor transportation, in most situations the mobile robots run independently and do not request the higher sever commands. The HRI functions



are emphasized in these mobile robots at supermarkets or shopping malls.

*Glas et al.* presented a shopping mobile robot for the big supermarket environments, as shown in Fig. 1-4 [38]. The mobile robot adopted the laser range finders to track people to assist people for the shopping guidance. The experiments provided in the paper showed that the developed mobile robot fits the indoor supermarkets well.

*Matshuira et al.* presented a shopping robotic system using various environmental cameras, as shown in Fig. 1-5 [39]. In this system, the customers only needed a membership card to drive any available guidance robot, and then the mobile robot lead the customers to different positions to do the heavy product transportation if necessary.

*Ng et al.* developed a carting car/robot for the supermarkets [40]. In their application the traditional floor line-tracking strategy was adopted for the carting robot. As mentioned in the paper, an Android platform based customer GUI is developed for the carting robot. The experimental results indicated that the line -tracking method was simple but effective for middle-size supermarket environments.

*Tomizawa et al.* developed a remote shopping robot system [41]. The customers can stay at home to remotely communicate with this system to buy fresh foods from supermarkets. The impressive innovation of the system was that the arm manipulator of the robot could grasp different types of fruits and vegetables using the camera based guidance.



Figure 1-4: Supermarket guiding robot [38]

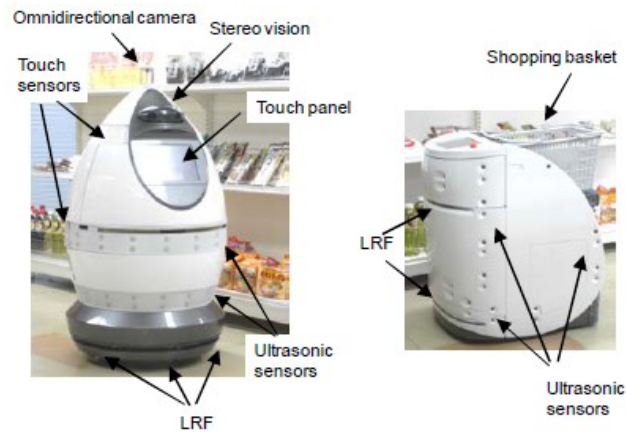


Figure 1-5: Supermarket guiding and carting robot [39]

### 1.2.3 Hospital Transportation

The mobile robots, which are used in the current hospital indoor transportation, are belonged to the boundaries between the SMMF mobile robotic systems and the MMSF ones [42]–[51]. Most of the developed mobile robots have the multi-pioneer communication functions and the higher controlling servers. Some of them are under development to have the multi-floor operating function.

*Wang et al.* proposed an intelligent robot bed for the hospital patient transportation, as shown in Fig.1-6 [52]. In the robotic transportation bed, the laser (Hokuyo URG-04LX) was adopted to detect the static and dynamic obstacles with a measuring range between  $4^{\circ}$  to  $240^{\circ}$ , the embedded board (Keil MCB2300 Micro-controller) was used to control all the bed hardware and the Labview programming platform was utilized for the control system development.

*Tasaki et al.* designed a new mobile robot *Terapio* for the healthcare purposes in patients' room at hospitals, as shown in Fig.1-7 [53]. The main functions of the robot were to do the transportation of various armamentarium supplies and the collection of the electronic health data. For these purposes, an Omni-directional motion module was included and an image processing based human tracking component was developed.

*Takahashi et al.* proposed a mobile robot MKR for the transport events in hospital areas, as given in Fig.1-8 [54]. In the published paper, the strategy for the MKR mobile robot to realize the high-quality indoor collision avoidance was proposed by using a new human-detecting algorithm. Their experimental results showed that the

presented MKR robot was suited for the hospital environments..

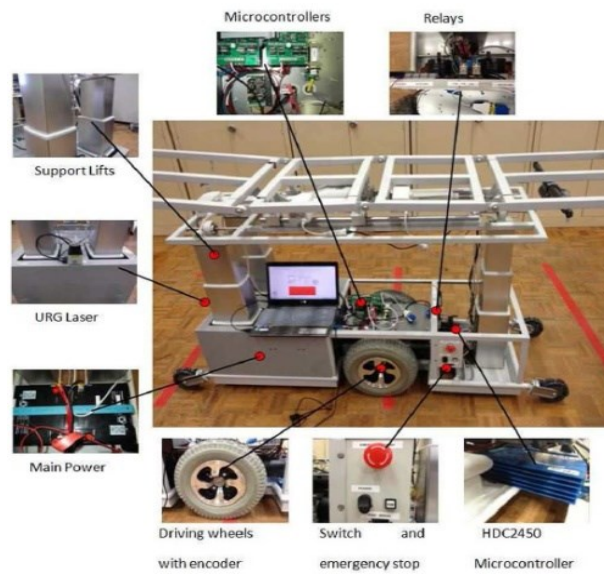


Figure 1-6: Robotic hospital transportation bed [52]

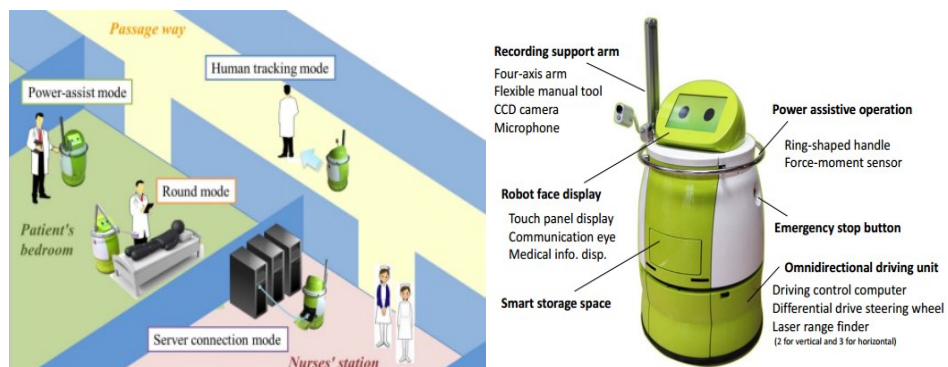


Figure 1-7: Mobile robot *Terapio* for hospital healthcare purpose [53]

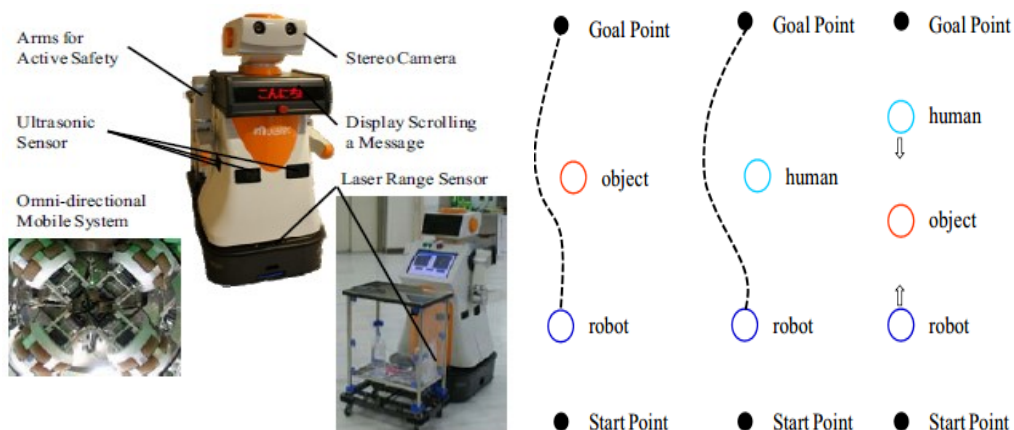


Figure 1-8: MKR robots for hospital transportation tasks [54]

Besides the upper important representative systems on the mobile robot transportation at hospitals, there is also some important work from industry, as shown in Fig. 1-9. For instance, *Aethon* Company released a TUG mobile robot for the hospitals. *Ortner* Company developed a series of transport mobile robots for the hospitals/laboratory clean rooms. *Swisslog* Company designed a group of mobile robot productions for the hospital transportation purposes.



Figure 1-9: Kinds of hospital transportation mobile robots proposed by companies: (a) left picture: <http://www.aethon.com/>; (b) middle picture: <http://www.rr-ortner.com/>; and (c) right picture: <http://www.swisslog.com/>

### 1.2.4 Laboratory Transportation/Delivery

The mobile robots, which are utilized in the current laboratory indoor transportation, fall into the definition of the MMSF mobile robot systems [55]–[62]. Similar to the mobile robots proposed for the indoor factories, the mobile robots here also have the higher controlling servers but there are still missing published applications on the multi-floor indoor laboratories. Since more and more modern indoor laboratories have multi-floor working environments, the multi-floor mobile robot operating function will become one of the most important robotic functions in near future.

*Dai et al.* studied the indoor transportation controlling strategy using swarm mobile robots (*ANTBOT robot*) in laboratory environments, as demonstrated in Fig.1-10 [63]. Three controlling strategies were put forward to cage a transporting target, which included the symmetric caging one, the heading consensus one and the transporting one. The A\* algorithm from the map theory was used to do the shortest path planning computation and the fuzzy-sliding controlling method was adopted to track the robots.

*Wojtczyk et al.* proposed a new mobile robot transporter in a small-size biotechnology laboratory, as given in Fig.1-11 [64]. The developed mobile robot consisted of several laser range finders, an arm manipulator with gripper tools, a force/torque sensor and a



camera. The laser range finders were utilized to do the local robot positioning, the manipulator was used to complete different types of experimental operations and the camera was for the face tracking of the laboratory personals.

*Najmabadi et al.* put forward a new scalable robotic-based system for the automation transportation and process-controlling in medium-sized biotechnology laboratories [65]. In the developed system, a new developing strategy named as the “*Tower-based configuration*” was proposed to provide the instrumentation processes consisting of shaking, incubation and vortexing. To verify the effectiveness of the proposed scalable robotic-based laboratory system, an experiment for the magnetic isolation of TAP tagged protein complexes protocol was presented. The result of the experiment indicated that the proposed system was effective.

*Gecks et al.* proposed an automated robot system (*QCX/Robolab*) based automated quality control and assurance application for the production laboratory [66]. In the application, a pneumatic tube transportation sub-system was adopted to realize the sample collection, transportation and distribution. The robot-controlled analysis functions included X-ray fluorescence/diffraction, particle size distribution and color detection. Based on the built network, all of the transportation and analysis operations were communicated and integrated.



Figure 1-10: Caging transportation using swarm mobile robots [63]

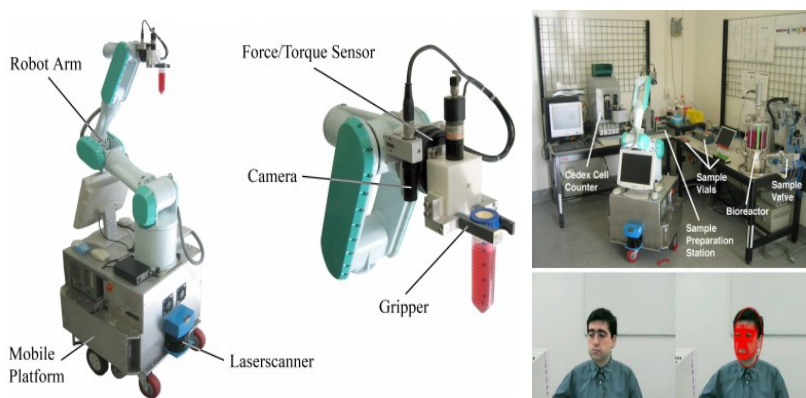


Figure 1-11: Local robot transportation [64]

### 1.2.5 Discussions

From the literatures reviewed in sections 1.2.1-1.2.4, it can be seen that:

**(a)** Mobile robots have been generally adopted for the indoor transportation activities in different fields. With more successful mobile robots coming into the market, the issue of the indoor mobile robot transportation will become more and more important. It is feasible to control various mobile robots for the transportation requirements.

**(b)** To have high-quality performance of the mobile robot transportation, a series of scientific and technical challenges has to be considered and solved, which always includes the robot indoor navigation/localization, the robot collision avoidance, the transportation path planning, the robot-robot/robot-human interface, the door controlling, etc. Especially when the processes of the mobile robot transportation are expected to be smart and flexible, additional efforts need to be spent on the intelligent controlling methods.

**(c)** The mobile robot transportation for different working environments have their own features. The supermarket/mall shopping transportation uses the camera-based image processing for the big indoors robot navigation and it focuses on the robot-customer interactions. Although there are often more than one mobile robots running in the supermarkets or shopping malls, they do not need any kinds of higher servers/controllers. So the mobile robot systems for the supermarket/shopping transportation are mostly developed using the SMSF working architecture. In this kind of mobile robot transportation, the high-quality robot-human performance is the most critical.

**(d)** The factory transportation generally adopts the simple floor line-tracking method for the robot navigation and it focuses on the physical strengths of the robots. Thus in most cases, the industrial robots but not the standard mobile robots are adopted in the factories. Even so, some mobile robots have been integrated in factory environments, they are not expected to run in multi-floors and they do not need to include the robot-human interacting operations. Additionally, by comparing to the mobile robots for supermarkets/shopping malls, the mobile robots in factories are always connected by the higher servers for the cooperating/parallel tasks. So they are mostly developed using the MMSF architecture.

(e) In the hospital indoor transportation, the mobile robots are adopted to transfer different kinds of targets (*e.g., medicines, medical waste, etc.*) among distribution indoor locations. Since the modern hospitals often have multi-floors, the mobile robots are expected to have the multi-floor transportation functions. So in most cases the mobile robots for the hospitals are designed using the SMMF architecture.

(f) This habilitation thesis focuses on the mobile robot transportation applications for life science laboratories. Comparing to the other types of mobile robot based indoor transportation, the transportation for the life science laboratories are more complicated and difficult. The reasons for this conclusion are explained as follows:

✧ Similar to the mobile robots in supermarkets, the mobile robots for the life science laboratories also need the high-quality HRI. However, the requested HRI level of the life science laboratories is higher than that of the supermarkets. For example, in the life science laboratories, the times of the HRI actions during the mobile robot transportation are strictly controlled by the life science experiments.

✧ Similar to the mobile robot transportation at hospitals, the mobile robots for the life science laboratories also have to face the multi-floor difficulty. There are lots of accurate life science experiments having strict parallel workflows, which require the mobile robot transportation in life sciences to be accurate and punctual. The challenge of the mobile robot transportation in life sciences is bigger than that at hospitals. Also by comparing to the mobile robot transportation in factories, the ones in life sciences are more accurate and more complicated. The expected mobile robots for life science laboratories should be developed using the MMMF controlling architecture.

✧ In life science laboratories, there are lots of different kinds of machines and devices. The expected mobile robot transportation are not allowed to affect the operating performance of the other laboratory devices and at the same time their own performance should also not be affected by the others. For instance, many mobile robots use the IR/laser/ultrasonic sensors for the indoor navigation, which can highly affect the other IR based experimental devices. To avoid any internal affecting issues, in chapter 3 a new robot indoor navigation method is proposed using the ceiling landmarks.

### 1.3 Architecture of this Habilitation

The research framework of the habilitation thesis is given in Fig. 1-12.

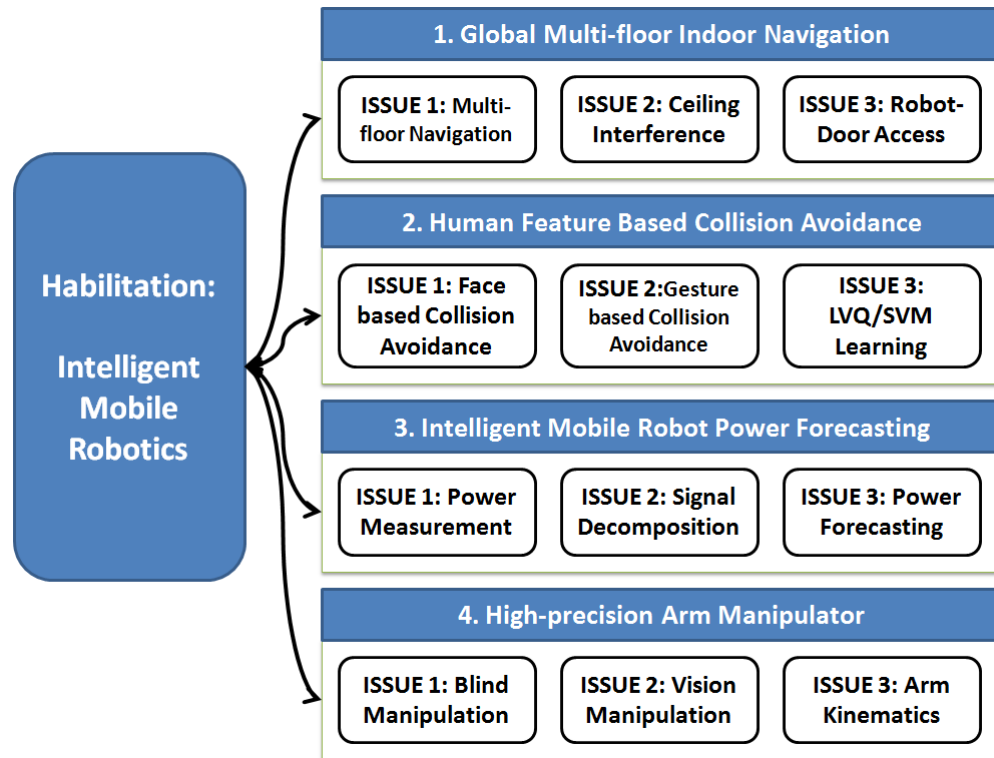


Figure 1-12: Framework of the proposed habilitation thesis

From Fig. 1-12, the following innovative contents can be explained in details as:

#### (a) Multi-floor Indoor Mobile Robot Navigation

Since modern laboratories are always established in buildings with multi-floors, global multi-floor indoor navigation is an initial question for any indoor mobile robot applications [67], [68]. Generally, at least the following challenges have to be solved in this topic, which include the multi-floor robot indoor localization, the multi-floor path planning and the robot-door access integration (including the room doors and the building elevator doors). There are already many published solutions for the mobile robot navigation in the single floors [69]–[74], but an approach for the multi-floor navigation method which meets all the upper mentioned aspects is still missing. Chapter 3 of the thesis will focus this issue.

In the chapter 3, a new global multi-floor indoor navigating method is proposed for the mobile robots at the indoor laboratories and a new intelligent signal filtering algorithm is presented to guarantee the robust performance of the



proposed global multi-floor navigation method combining the TSA (Time Series Analysis) theory and the KF (Kalman Filter). In the proposed navigation method, the adopted H20 mobile robots are equipped with a group of StarGazer sensors and a number of the corresponding landmarks are installed on the ceilings of the laboratories. To generate a continuous navigating map, the elevator access is considered. In the proposed robot positioning signal filtering strategy, the TSA is utilized to build the ARIMA (*Auto Regressive Integrated Moving Average*) model to recognize the robot nonlinear positioning relationships. Then the built ARIMA model is used to select the best initial parameters of the KF model for the robot indoor secure navigation under the ceiling interferences. Based on the proposed new method, the controlling GUI for the multi-robot multi-floor indoor navigation is provided.

#### **(b) Smart Collision Avoidance**

To have high-quality mobile robot applications inside the modern laboratory environments, the function of the robot collision avoidance is essential [75], [76]. The standard collision avoidance for the mobile robots is to detect the obstacles and find a new motion path to avoid the obstacles. One of the most successful algorithms to complete the standard collision avoidance is the artificial potential field [77]–[79], proposed by the robotic scientist Oussama Khatib, which has been generally adopted in the indoor mobile robots. Unfortunately, this kind of standard way cannot work effectively for the narrow indoor areas, which exist in modern laboratories commonly. Solving this problem is the focus of chapter 4.

In the chapter 4, a multi-layer smart collision avoidance method is presented for the mobile robot transportation. In the presented avoidance method, there are two different included strategies. The standard artificial potential field for the big areas, the human feature HRI based controlling method for the normally narrow areas and the especially narrow areas. For the human feature HRI based collision avoidance, a series of Microsoft KS (Kinect Sensors) are installed on all the H20 mobile robots. In this human feature HRI based smart collision avoidance, two intelligent methods are proposed by using the human faces and the human gestures, respectively. In the face based method, the dynamic human face orientations and their generating directions are used to control the coming mobile robots and the LVQ (Learning Vector Quantization) neural network is established

for the face orientation and moving recognition. In the gesture based method, the real-time human gestures are adopted for the robot controlling and the SVM (Support Vector Machine) is built to classify the different gesture commands.

### **(c) Intelligent Mobile Robot Power Forecasting**

Although there are many publications proposing technical solutions on the robot on-board power measurement and recharging [80]–[83], no publication is available on the indoor mobile robot power forecasting. Actually the robot power forecasting is really desired for the mobile robot transportation applications in big laboratory environments. In the multi-floor mobile robot transportation, the mobile robots cannot decide whether to execute the transportation commands only based on the current power values, otherwise they can be blocked during the transportation process due to the insufficient on-board power capacity. In these cases the on-board power forecasting becomes important and essential. Chapter 5 of the thesis solves the issue.

In the chapter 5, a new intelligent robot on-board power forecasting method is proposed by combining the single decomposing algorithms (*including the wavelet decomposition and the empirical mode decomposition*) and the ANFIS (*Adaptive Neuro Fuzzy Inference System*). The proposed power forecasting method can help the mobile robots making decisions cleverly for the transportation requests. In the proposed robot power forecasting method, the decomposing algorithms convert the originally measured robot on-board power into a series of sub-level signals and the ANFIS models are built to realize the real-time predicting computation. In the single decomposition, the WD (*Wavelet Decomposition*) and the EMD (*Empirical Mode Decomposition*) are both adopted and a comparison of their decomposing performance in the experiments is also provided. Additionally, the real-time performance of the proposed WD-ANFIS and EMD-ANFIS methods is investigated.

### **(d) Intelligent Arm Manipulation**

In the indoor laboratory applications, the expected arm manipulator of the mobile robots should balance the complexity and the accuracy [84]–[87]. Either from universities or from industries, all the developing effort everyone being spent is to promote the precision of the arm activities and decrease their costs. As we know,

in the robot arm manipulation the adoption of the image processing can increase the manipulating performance (*i.e., the accuracy and the flexibility*) [88]–[91]. The arm manipulation is the focus of the chapter 6.

In the chapter 6, a new intelligent arm manipulator is developed for the mobile robot transportation. In the developed intelligent arm manipulator, there are two kinds of methods included, the blind one and the vision one. In the proposed blind arm manipulator, the ultrasonic sensors existing on H20 mobile robot, originally for the collision avoidance, are used to find the expected arm manipulating workstations and an intelligent mapping method is presented to calculate the joint values of the robot arms using a MLP (*Multi Layer Perceptron*) neural network. In the proposed vision arm manipulator, the robot installed KS sensors are used to measure the manipulating targets and the arm kinematic models are built and embedded in the controller. Combining the two proposed two intelligent methods, the developed arm manipulator can realize the flexible grasping & placing with different expecting-error range [0.1cm, 1cm]. In addition, the multi-identification for the labwares located at different positions is also completed.

# Chapter 2 Intelligent Strategy

## 2.1 Introduction

As mentioned in chapter 1, the originality of the habilitation thesis is to develop a new Intelligent Mobile Robot Transportation System (*IMRTS*) for applications in life science automation. The expected IMRTS not only focuses on the standard functions of the mobile robots (*e.g., the robot indoor navigation, the collision avoidance, the robot recharging and the arm manipulation, etc.*) but also adopts the latest intelligent theories to improve the performance of these standard robotic functions as much as possible to let the IMRTS finally reach the “SMART” level. At the same time, the IMRTS also will meet some special requirements from the life sciences as: (a) convenient expandability; (b) fast integration; (c) robust performance; and (d) economic cost. So the research topic of the habilitation can be regarded as: “*mobile robotics*” + “*artificial intelligence*” + “*Laboratory automation*”.

One kind of mobile robots named as H20 from Canadian DrRobot Company has been adopted in this study at CELISCA laboratory, as shown in Fig. 2-1. The detailed parameters of the H20 mobile robots can be found in reference [92].



Figure 2-1: H20 mobile robots [92]

## 2.2 Framework of Intelligent Strategy

Based on the aims of the habilitation and the H20 robots' hardware configuration, the intelligent controlling framework of the proposed IMRTS is presented in Fig. 2-2.

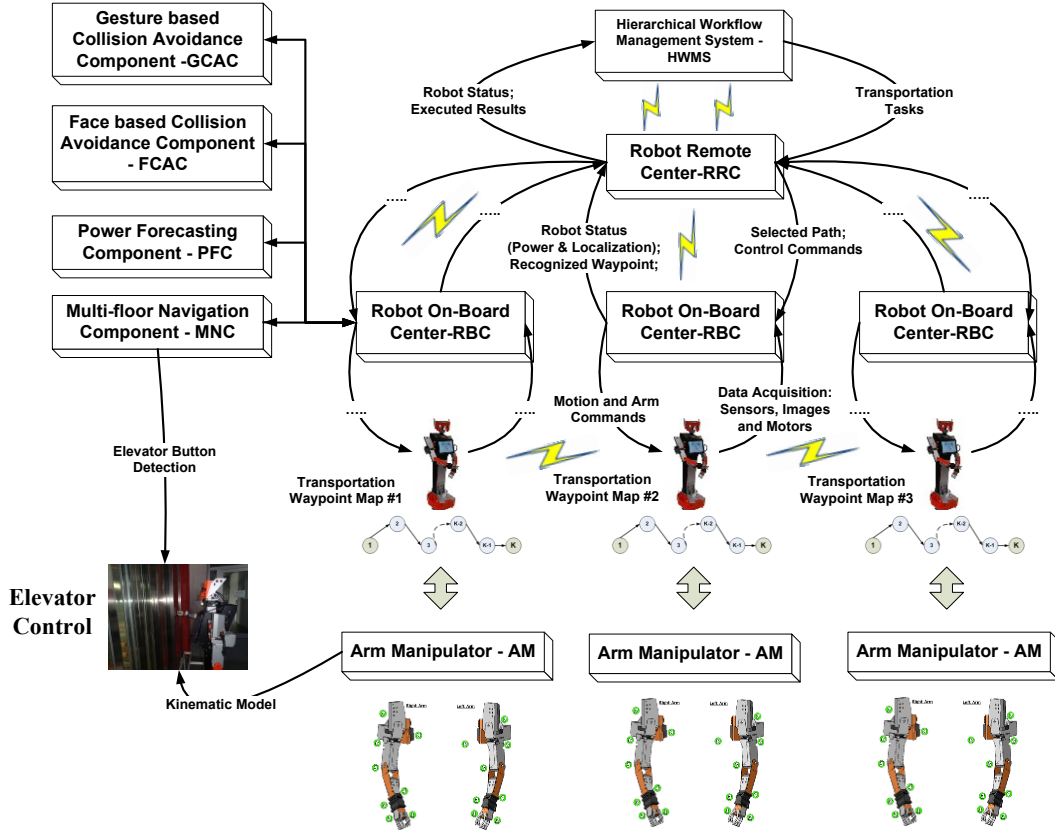


Figure 2-2: System controlling Strategy

As shown in Fig. 2-2, there are four controllers in the IMRTS system as: the Hierarchical Workflow Management System (HWMS), the Robot Remote Center (RRC), the Robot On-board Center (RBC) and the Arm Manipulator (AM). The RBC consists of four controlling components, including the Multi-floor Navigation Component (MNC), the Power Forecasting Component (PFC), the Gesture based Collision Avoidance Component (GCAC) and the Face based Collision Avoidance Component (FCAC). Their working relationships can be described as follows:

- (a) The HWMS is in the highest controlling level, which proposes different kinds of transportation tasks when they are desired in the automated laboratory workflows. The main functions of the HWMS are to manage, schedule and optimize the laboratory workflows. The HWMS adopts the standard wireless TCP/IP protocol to connect the RRC robot center. The processing relationships between the RRC and the HWMS are given in Fig. 2-3. The

details are explained as: **Firstly**, the HWMS sends a transportation command to the RRC like ‘*Move Object 1 from S-Lab, Device A, Position 1 to D-Lab, Device B, Position 2*’. **Secondly**, the RRC replies to the HWMS whether this transportation command can be executed by examining all the connected RBC centers/robots. If yes, the RRC will answer the HWMS the estimated time needed for the transportation, otherwise the RRC replies the HWMS that the transportation command cannot be executed. **Thirdly**, after finishing the transportation event, the RRC will report the results (*either be successful or be failure*) to the HWMS. If the robot has some problems (*like the front door cannot be opened rightly*) during the whole process, the RRC also will send the errors to the HWMS. **Fourthly**, both of the RRC and the HWMS have the error/emergency handling strategies.

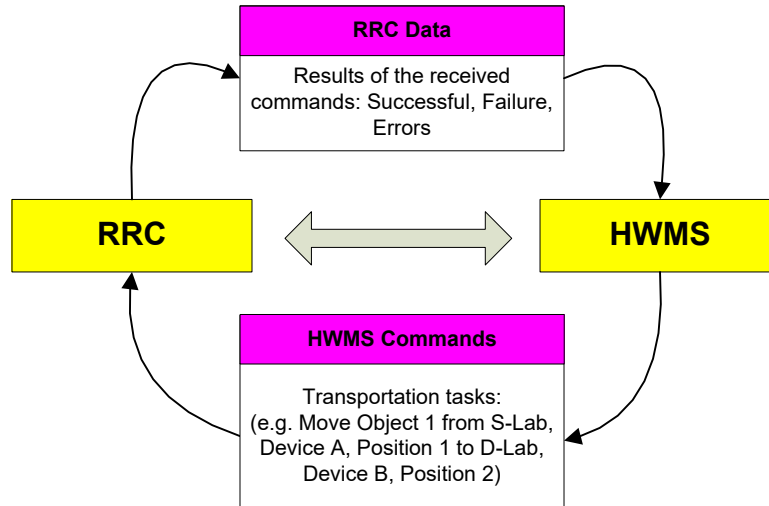


Figure 2-3: Process flows between the RRC and the HWMS

- (b) Both of the RRC and the RBCs are in the middle controlling level, which are developed to control the H20 robots to complete the transportation requests. The RRC is for receiving and understanding the HWMS commands while the RBCs are run in the on-board laptops of the H20 robots to control all the hardware modules and sensors inside the corresponding H20 mobile robots. Related to the HWMS, the RRC is a controlling client. But comparing to the RBCs, it is a server. The communication between the RRC and the RBCs is based on the wireless TCP/IP protocol. Their processing relationships are given in Fig. 2-4.

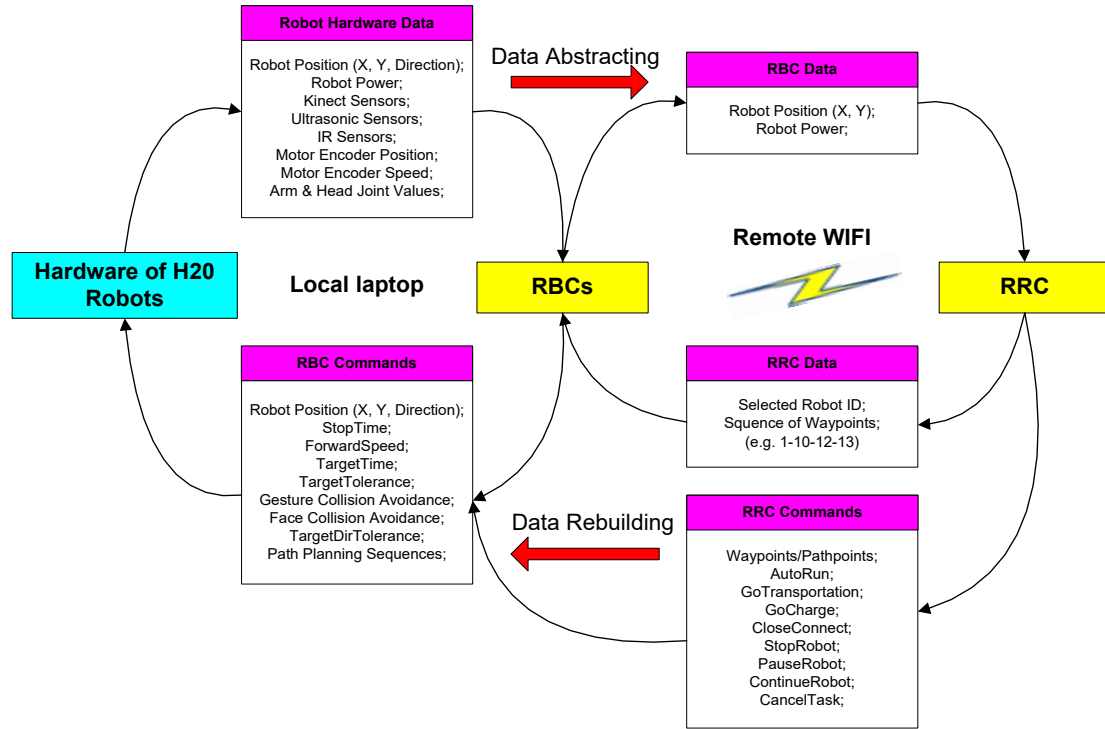


Figure 2-4: Process flows among the robotic hardware, the RBCs and the RRC

As illustrated in Fig. 2-4, the details of the processing flows are explained as: **Firstly**, no matter whether the RRC receives a new HWMS command, it always keeps wireless communication with all of the RBCs to receive the real-time status of the H20 mobile robots. To decrease the data volumes to avoid the communication-jamming phenomenon, only the essential robot data will be transferred from the RBCs to the RRC, including the robot positions and power values. **Secondly**, once the RRC receives a HWMS command, it will verify all the status of the connected H20 robots and select the best for the HWMS command. The selection is based on two methods, the first one is to choose the robot which is closest to the HWMS grasping position and the second one is to get the robot which power is highest at that moment. **Thirdly**, when a RBC is selected by the RRC for a HWMS transportation process, it will drive the robot equipping hardware (*including the motion and the arm manipulator*) to realize the transportation. The RRC does the path planning computation and the RRCs do the data rebuilding to generate the hardware controlling parameters based on the RRC path planned sequences. **Fourthly**, in case of any errors occurring during the processes, the RBC/RRC will handle the errors.

- (c) The MNC and the AM are both located in the specific executing level, which are presented to realize the global multi-floor robot motion and the robot arm manipulation, respectively. The MNC can be further explained as: to generate an automated continuous mobile robot transportation process for multi-floor environments, the elevator controlling is focused. At the same time, an intelligent strategy is proposed to forecast the multi-step robot indoor positions to solve the robot-losing problems under interferences based on the TSA method and the KF theory. The AM also can be further explained as: to realize the stratified arm manipulation of the mobile robots, the AM has two controlling strategies, the intelligent blind one and the sensing one. In the blind one, the MLP neural network model is established to build the dynamic mapping between the ultrasonic distances and the robot arm controlling joint values. In the sensing one, the Microsoft Kinect sensor based image processing method is applied in and the inverse/forward arm kinematic models are realized for the grasping/placing manipulations. The processing relationships among the RBC, the MNC and the Am are given in Fig. 2-5.

As given in Fig. 2-5, the processing relationships between the RBC and the MNC are given as: **Firstly**, the MNC measures the robot status data from the corresponding RBC, including the ceiling landmark IDs, the parameters of the motion encoders and the robot power status. **Secondly**, the MNC waits for the transportation request from the connected RBCs/RRC. Once a multi-floor transportation request is proposed, the MNC completes the robot multi-floor movements. When the MNC needs to control the elevators, it will apply for the RBCs to drive the AM to run in the same level/laptop to realize the mechanical pushing operation to the buttons of the elevators, or it will call the electronic controllers of the related elevators if the mechanical mode cannot push the buttons successfully.

Additionally, the processing relationships between the RBC and the AM are explained as: **firstly**, when the mobile robots arrive at the expected arm grasping/placing positions, the corresponding RBC will start the AM directly. **Secondly**, if the blind manipulating mode of the AM is enabled, the RBC will send the AM the measured ultrasonic distance and at the same time the embedded MLP neural network model in the RBC will generate the joint values for manipulations. If the sensing manipulating mode is enabled, it is



unnecessary for the RBC to send any ultrasonic data to the AM because the AM will complete the error compensation caused by the robot motion orientation through the arm side. In the sensing mode, the Kinect sensors are used to do the object recognition. *Thirdly*, if there are any errors occurring, the RBC and the AM will be noticed by each other.

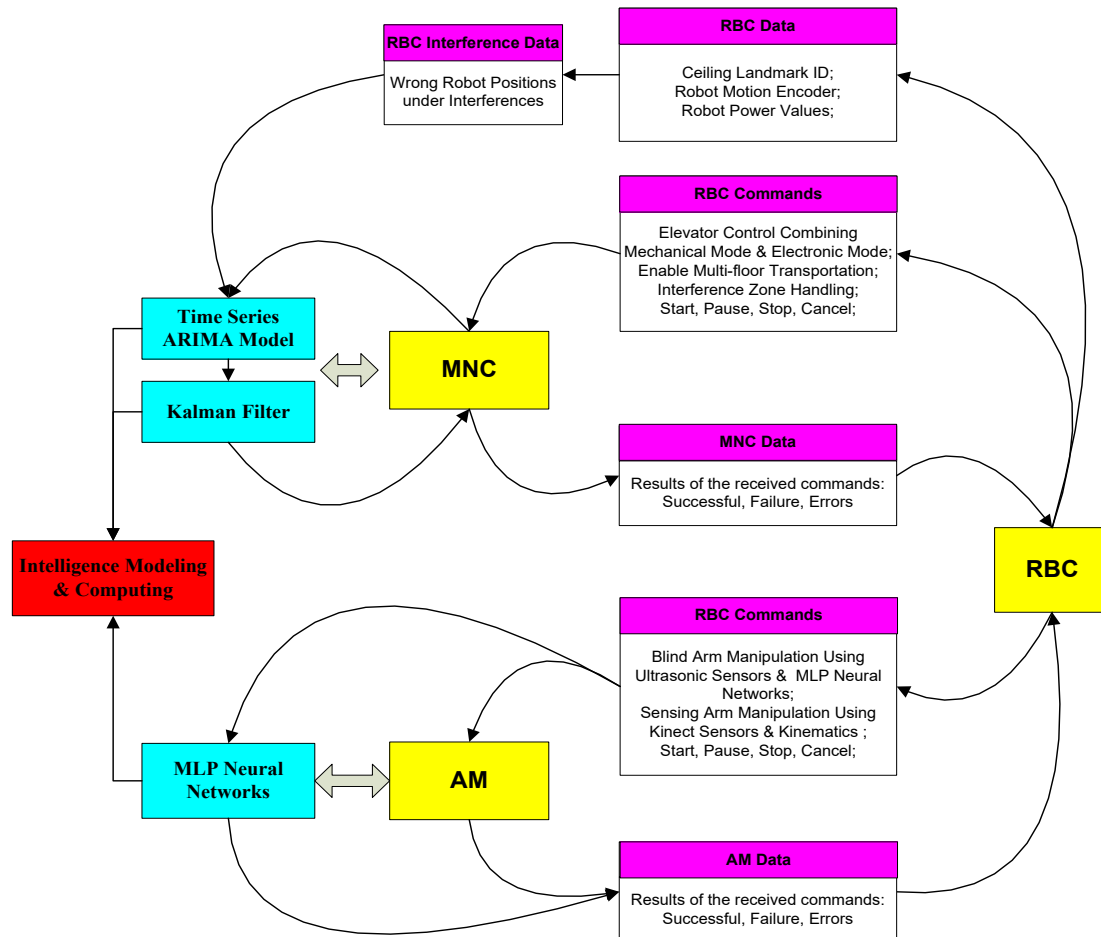


Figure 2-5: Process flows between the RBC, the MNC and the AM

- (d) The PFC is also one of the embedded software components running in the specific executing level. It realizes the robot on-board power tracking and forecasting to make smart decisions when the robots face situations whether they should start a long-distance multi-floor transportation process. The processing relationships between the PFC and the RBC are demonstrated in Fig. 2-6.

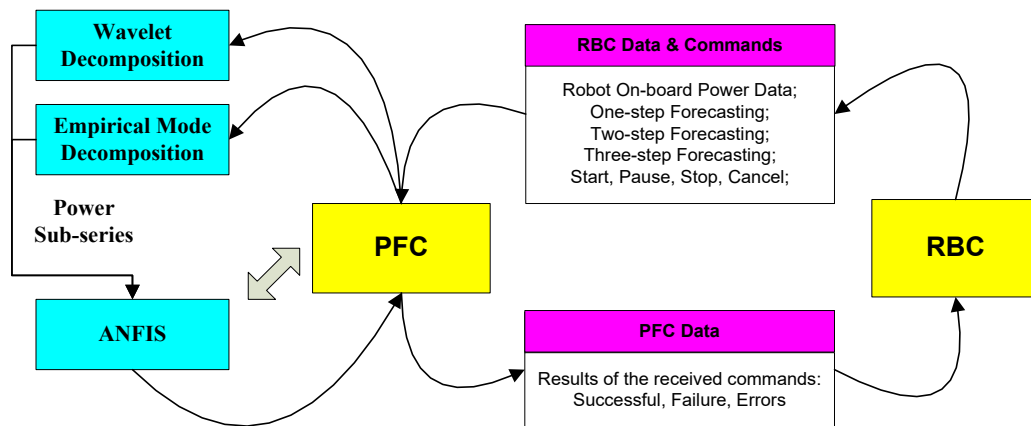


Figure 2-6: Process flows between the RBC and the PFC

From Fig. 2-6, the following explanations can be made as: **Firstly**, once a RBC starts to work, the related embedded PFC also will run at once. The PFC decomposes the raw robot on-board power data into a number of sub-series then builds the ANFIS model to complete the power predictions. **Secondly**, when there is transportation request proposed, the RBC will ask the PFC to generate the three-step ahead forecasting power then use the predicted power values to accept/reject the coming transportation requests. If the forecasting value is higher than the power threshold, the RBC will control the corresponding robot to start the motion otherwise this robot will be regarded as being unavailable for the transportation task. Based on this intelligent power forecasting strategy, the RBCs can select the best robot cleverly. **Thirdly**, another kind of popular signal decomposing algorithm (named as *Empirical Mode Decomposition - EMD*) is also included in the forecasting performance comparison.

- (e) Both of the GCAC and the FCAC are in the specific executing level. They are designed for the human gesture based robot collision avoidance and the face based robot collision avoidance, respectively. The GCAC adopts the Kinect sensors to understand the human commands by the moving positions of their gestures and the FCAC realizes the collision avoidance activities by using the human face orientations and motions. The former is proposed for these cases when the human arms are available and the latter is presented for the situations where it is impossible for the laboratory staff to use the arms to control the robots (*such as, inside the crowded elevators, the people are busy*

on some experiments, etc.). The processing relationships between the GCAC, the FCAC and the RBC are demonstrated in Fig. 2-7.

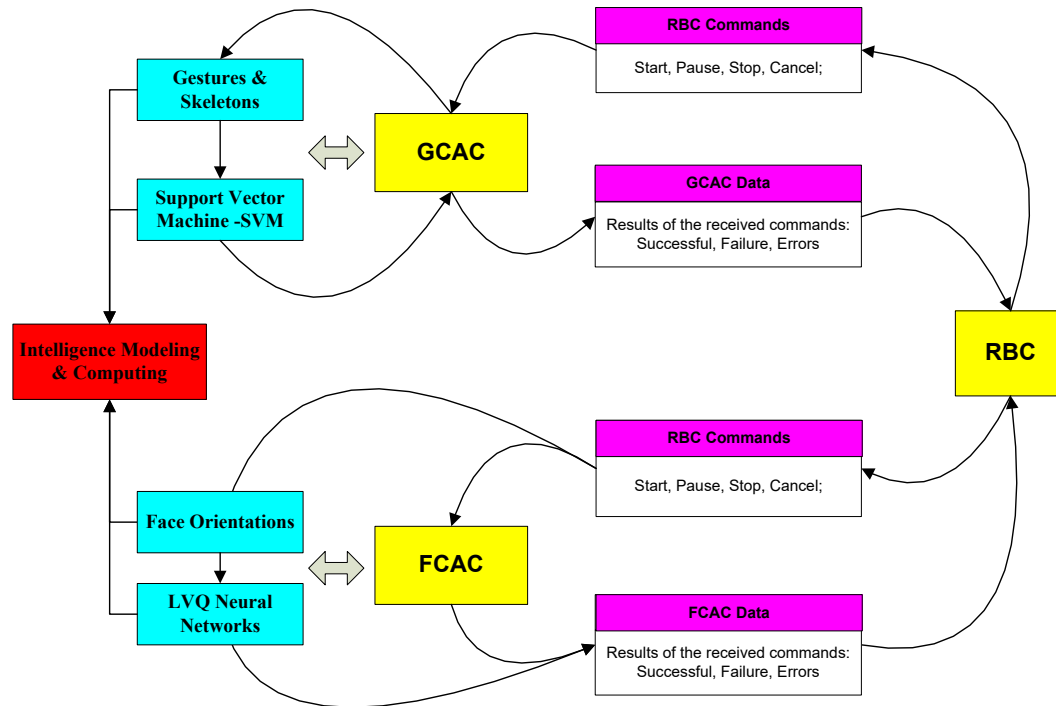


Figure 2-7: Process flows among the RBC, the GCAC and the FCAC

Also as shown in Fig. 2-7, the processing relationships between the RBC and the GCAC/FCAC are explained as follows: **Firstly**, during the mobile robot transportation process, when the robots meet any obstacles, they will stop, then measure the obstacles through their equipped Kinect sensors. If the obstacles are human, the robot on-board GCAC will wait for the human's gesture commands for the following avoidance. **Secondly**, when the GCAC detects the human gesture based avoiding commands, it will drive the embedded SVM model to classify the directions of the gesture moving, then finding a local path to avoid the human. **Thirdly**, during the avoiding process, the GCAC replaces the RBC to control the robot motion. When the avoidance is completed, the robot controlling rights will be returned to the corresponding RBC immediately. **Fourthly**, the processing relationships between the RBC and the FCAC are similar to the ones for the GCAC. The FCAC adopts the LVQ neural networks for the human face orientation recognition and at the same time the GCAC uses the SVM for the human gesture recognition.

# Chapter 3 Multi-floor Indoor Navigation

## 3.1 Introduction

High-quality indoor navigation is the first step to develop any kinds of indoor mobile robotic systems [93]–[98]. To meet the indoor navigation requirement for the mobile robots in life science laboratory building with multiple floors, two technical aspects should be solved as follows: **(a)** firstly, there should be a global navigating map which allows all the running mobile robots to find their relative indoors positions/coordinates for the motion controlling and the collision avoidance; and **(b)** secondly, the aim of this habilitation thesis is to develop an Intelligent Mobile Robot Transportation System (IMRTS) for application in life science automation. For this purpose, the expected indoor navigation method should be accurate, robust, low-cost and extendible.

This chapter focuses on presenting a global indoor navigation method for the multiple robots and the multiple laboratory floors. In recent years, some important robot indoor navigation approaches have been proposed. *Abadleh et al.* proposed a new indoor positioning/localization method named as CALL algorithm based on a floor plan, several wireless AP (*Access Points*) and smart-phones [99]. The experiments provided in their works indicated that the CALL algorithm was simple but had satisfactory accuracy. *Chavez-Romero et al.* presented a novel indoor localization approach for the robotic wheelchairs using the Particle Filter (PF) on Camera Sensor Space (CSS) [100]. To estimate the performance of the proposed strategy, a comparison of the proposed PF-CSS method and the Extended Kalman Filter (EKF) was provided and the results proved that the hybrid PF-CSS had better localization performance than the EKF. *Sun et al.* developed a Wi-Fi based mobile robot indoor localization system, which included two computational approaches, the KNN (*k-Nearest-Neighbor*) based fingerprint matching approach and the combining approach of the GPR (*Gaussian*

*Process Regression*) and the BF (*Bayes Filter*) [101]. The results provided in the paper indicated that the proposed system was suitable for the large indoor laboratory environments but only with low-accuracy request. **Jiang et al.** put forward a FA-OSELM (*Feature Adaptive Online Sequential Extreme Learning Machine*) algorithm to handle the dimension-changing problem of the WIFI based indoor localization [102]. With this new algorithm, the WIFI based indoor localization gets higher precision but need a small amount of access point data. The proposed method matched the lifelong indoor localization applications (*including the mobile robot cases*). **Lin et al.** presented a novel method for the robot SLAM (*Simultaneous Localization and Mapping*) using the stereo vision technology [103]. In the presented method, the distinctive invariant image features defined as PLOT (*Polynomial Local Orientation Tensor*) were extracted in real-time for the mobile robot indoor localization. The experimental results showed that the proposed method based on the PLOT feature information promoted the traditional SLAM algorithms considerably. **Olszewski et al.** designed an indoor localization system by the utilization of the RFID (*Radio Frequency Identification*) technique [104]. In the system, besides the RFID sensors for the localization, additional ultrasonic and IR sensors were equipped to detect the dynamic obstacles for the collision avoidance. **Abdelkrim et al.** proposed a new reactive robot navigation system in indoor environments using the Kinect sensors [105]. In the system, several Fuzzy logic controllers were developed for the real-time navigation computation. The proposed system was validated based on one kind of mobile robots named as Pioneer P3-AT. **Benavidez et al.** explained a framework for the navigation and target tracking of the mobile robots [106]. In the framework, the Microsoft Xbox Kinect sensor was adopted to measure the RGB images and the corresponding 3D depth data of the targets, the Fuzzy logic algorithm was used to do the real-time computation for the obstacle avoidance and the dynamic target tracking, and the neural networks based learning method was employed to recognize the pattern of the targets and to process the path planning tasks. **Wang et al.** proposed a new approach for the robot indoor localization only by using the existent room ceiling lights [107]. In the proposed approach, the image processing was adopted to recognize the ceiling light based landmarks and the Floyd algorithm was employed to calculate the shortest robot moving paths. Different to some other artificial landmarks [108]–[110], the ceiling light based landmarks do not need any installing work. **López et al.** integrated an indoor localization sensor manufactured by the Korea Hagisonic Company in their designed

robotic system [13]. The experiments indicated that the positioning performance of the StarGazer sensor was accurate. The same accuracy value was concluded by another performance experiment in reference [112]. *Kim et al.* proposed a new accurate dynamic localization system for the autonomous navigation of indoor mobile robots [113]. In the proposed system, a number of ultrasonic transmitters attached to the ceiling at known locations and at the same time the other ultrasonic receivers were installed on the top of the mobile robots. An EKF (Extended Kalman Filter) based controller with a state/observation vector was presented to estimate the mobile robots' positions based on the developed ultrasonic system. Based on the published literatures on the robot indoor navigation/localization, the characteristics and accuracies of different available methods are concluded in Table 3-1.

Table 3-1 The characteristics and accuracies of the available methods for the robot indoor navigation/localization

Method	Advantage	Disadvantage	Provided Accuracy
Ultrasonic Sensor/Laser based method [113-114]	<b>(a)</b> Convenient to be installed, extended and changed based on different situations; <b>(b)</b> Available for the multi-robot systems;	<b>(a)</b> Low-accuracy; <b>(b)</b> Easy to be affected by the environments; <b>(c)</b> High-cost; <b>(d)</b> Unavailable for the complex indoor environments;	Accuracy Error [5cm, 15cm];
WIFI/AP based method [99]	<b>(a)</b> Convenient to be installed, extended and changed based on different situations; <b>(b)</b> Available for the multi-robot systems; <b>(c)</b> Low-cost;	<b>(a)</b> Low-accuracy; <b>(b)</b> Easy to be affected by the environments;	Accuracy Error > 1 m;
Kinect Sensor CV based method [103]	<b>(a)</b> Low-cost; <b>(b)</b> Middle-accuracy;	<b>(a)</b> Difficult to be extended and changed based on different situations; <b>(b)</b> Easy to be affected by the around environments (such as the lighting);	Accuracy Error [5cm, 20cm];

RFID based method [104]	<b>(a)</b> Convenient to be installed, extended and changed based on different situations; <b>(b)</b> High-accuracy; <b>(c)</b> Low-cost;	<b>(a)</b> Unavailable for the multiple robots' collision avoidance; <b>(b)</b> Easy to be destroyed;	Accuracy Error [2cm, 30cm]
StarGazer based method [112]	<b>(a)</b> Convenient to be installed, extended and changed based on different situations; <b>(b)</b> Available for the multi-robot systems; <b>(c)</b> High-accuracy; <b>(d)</b> Low-cost;	Easy to be affected by the ceiling interferences;	Accuracy Error < 2 cm;

From Table 3-1, it can be seen that:

- (a)** Every proposed indoor navigation method has advantages and disadvantages.
- (b)** The ultrasonic sensor/laser based approaches can be installed for the big indoor environments but it does not fit the complex indoor environments due to the potential blocking/affecting problems of the ultrasonic signals [115]–[118]. So the ultrasonic sensor based methods are often combined with other methods (*such as the image process based strategies*) in the real applications [113], [114], [119], [120].
- (c)** The WIFI/AP or smart-phone based indoor wireless navigation methods are proposed in recent years, which have many advantages (*e.g., simplicity, low-cost, seamless, etc.*), but they are still under development to improve their current accuracies. The current accuracies are unsuitable for the real robotic applications [121]–[126].
- (d)** Although the Kinect sensor/CV based methods are convenient to be programmed and developed based on some current libraries (*e.g., Emgu CV, OpenCV, etc.*), their extension is unsatisfactory. When a Kinect sensor/CV based navigation system wants to be extended to different environments, more matching models need to be defined, which can cause considerable efforts [127]–[130]. Additionally, the Kinect sensor/CV based methods can be affected by the indoor environments easily [75], [131]–[133]. So they are suitable for the simple environments but not for the complex laboratory environments with multi-floors.

(e) The RFID based navigation methods have several advantages [134]–[138]. Such as, they are convenient to be installed, extended and changed for the different indoor environments, they have high-accuracy performance, etc. But they have a considerable disadvantage that they are unavailable for the multiple mobile robots' collision avoidance. Because one installed RFID tag can only be read by one robot at the same time. Also the RFID tags installed on the floors are easy to be destroyed [139], [140].

(f) By comparing the features of all the available indoor navigation methods, the StarGazer sensor based methods are finally adopted in the developed IMRTS system in the habilitation thesis. The advantages and disadvantages of the StarGazer sensors are given in details in Section 3.2.

### 3.2 StarGazer Sensor Based Robot Localization

As shown in Fig. 3-1, the StarGazer sensor (*Hagisonic Company, Korea*), which is adopted for the mobile robot indoor localization/navigation [141], consisting of an IR (*Infrared Radio*) camera, a DSP (*Digital Signal Processing*) processor and a number of ceiling landmarks. The working process of a StarGazer sensor is described as follows: (a) the IR projector inside the StarGazer sensor sends out the infrared rays to the installed ceiling landmarks; (b) the circle points of the landmarks reflect back the infrared rays so that the IR camera inside the StarGazer sensor can detect an image of the corresponding landmark; and (c) the DSP processor calculates the positions and angles by comparing the measured image sequences of the landmarks. The StarGazer sensors have been adopted for the indoor mobile robots in references [142]–[149].

The advantages of the StarGazer based indoor navigation can be summarized as: (a) the built navigating map is convenient to be extended to match any sizes of indoor laboratories by installing more landmarks; (b) compared to the ultrasonic ways, the ceiling landmarks do not cost any electrical power and do not affect the other indoor devices/sensors; (c) comparing to the image processing measures (*especially the popular SLAM algorithm*), the StarGazer has better real-time performance ( $<0.3s$ ); and (d) the StarGazer sensor achieves accurate positioning results ( $<2cm$ ) [141]. However, besides these advantages, due to its ceiling-reading mechanism, the sensor has an inevitable disadvantage that it can be affected by the ceiling interferences.



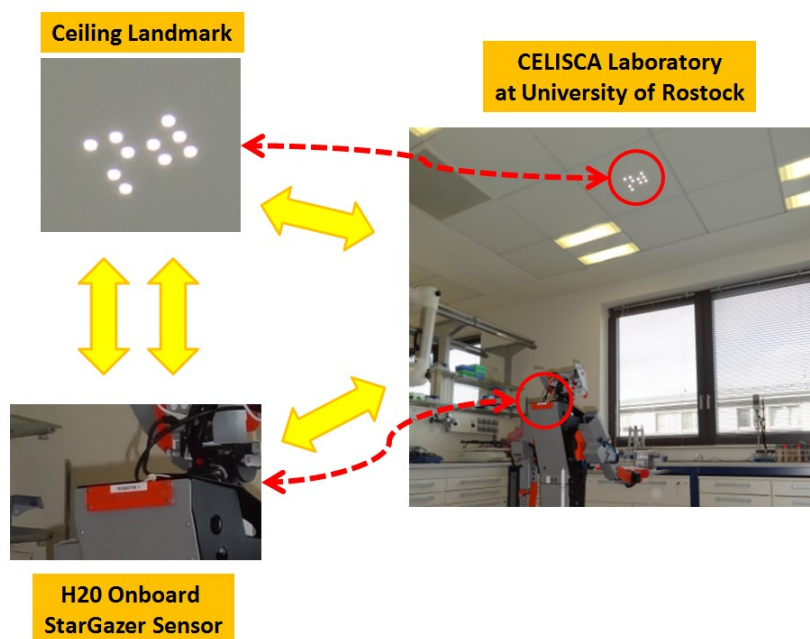


Figure 3-1: StarGazer based robot indoor navigation adopted at CELISCA laboratory

### 3.3 Multi-floor Navigation Strategy

In the hardware configuration of the StarGazer, there are two working modes, the mapping one and the alone one [141]. Based on the alone working mode of the StarGazer sensor, a new multi-floor indoor navigation method is proposed for the mobile robots in laboratory environments, as shown in Fig. 3-2.

As shown in Fig. 3-2, the proposed robot navigation method is described in details as follows: **(a)** the StarGazer sensor are equipped in the H20 robots and a series of landmarks are installed in the CELISCA laboratory ceilings; **(b)** all the ceiling landmarks are distributed an unique HEX ID and the StarGazer sensors server just as a HEX reader to measure the HEX IDs of the ceiling landmarks to calculate the indoor coordinates for the H20 robots; **(c)** since the elevators of the laboratories have to be included in the global multi-floor navigation map, there are also some landmarks being installed inside the elevators; and **(d)** to control the elevators for the mobile robot transportation, a hybrid elevator-controlling strategy is presented, including a mechanical robot arm-pushing method and an electronic wireless opening method. The detailed controlling approach of the doors of the rooms and elevators is provided in Section 3.4.



Figure 3-2: Mobile robot multi-floor navigation mapping strategy

To match the proposed multi-floor navigating map proposed in Fig. 3-2, a new hybrid robot path planning method is presented as given in Fig. 3-3. As given in Fig. 3-3, the proposed multi-floor robot path planning method is explained as follows: **(a)** the multi-floor laboratory is divided into a number of sub-zones. In the sub-zones, the transportation waypoints are defined to cover all the interesting robot-executing positions by using the robot RBC centers. It means the whole multi-floor navigating map is comprised of the defined sub-zones; **(b)** inside the sub-zones, all the shortest paths will be calculated for any pairs of way-points. Two new hybrid algorithms (*i.e.*, the *Floyd-Dijkstra algorithm* [150] and the *Floyd-GA algorithm* [151]) are presented to calculate the shortest robot navigation paths by our research group. In these two proposed path planning methods, the Floyd algorithm is adopted to calculate the shortest paths for any pairs of the starting positions and the ending positions, and the Dijkstra algorithm/genetic algorithm are used to find an alternative shortest path when the Floyd based calculated paths are unavailable due to the real-time changing of the robot transportation maps. The innovative combinations can guarantee the real-time performance of the robot path planning and at the same time decrease the computational burdens. The standard computational steps and features of the involved Floyd algorithm, Dijkstra algorithm and genetic algorithm can be seen in references [152]–[155], references [156]–[160], references [161]–[164], respectively; and **(c)** to connect the sub-zones and their shortest paths for the dynamic transportation

processes, there are a number of common way-points defined. These common waypoints can be redefined conveniently. Based on this proposed new robot path planning strategy, the controlling GUI for the multi-floor transportation is developed as shown in Fig.3-4.

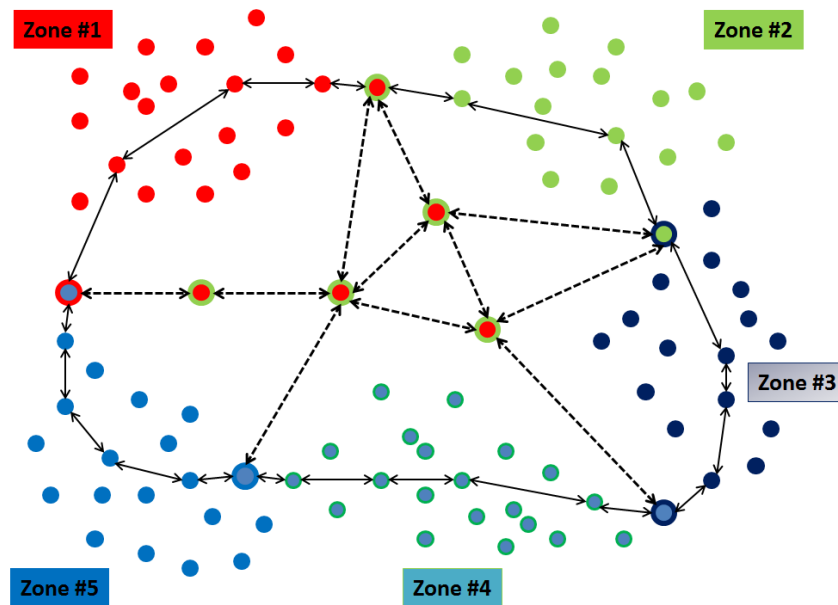


Figure 3-3: Mobile robot multi-floor path planning method

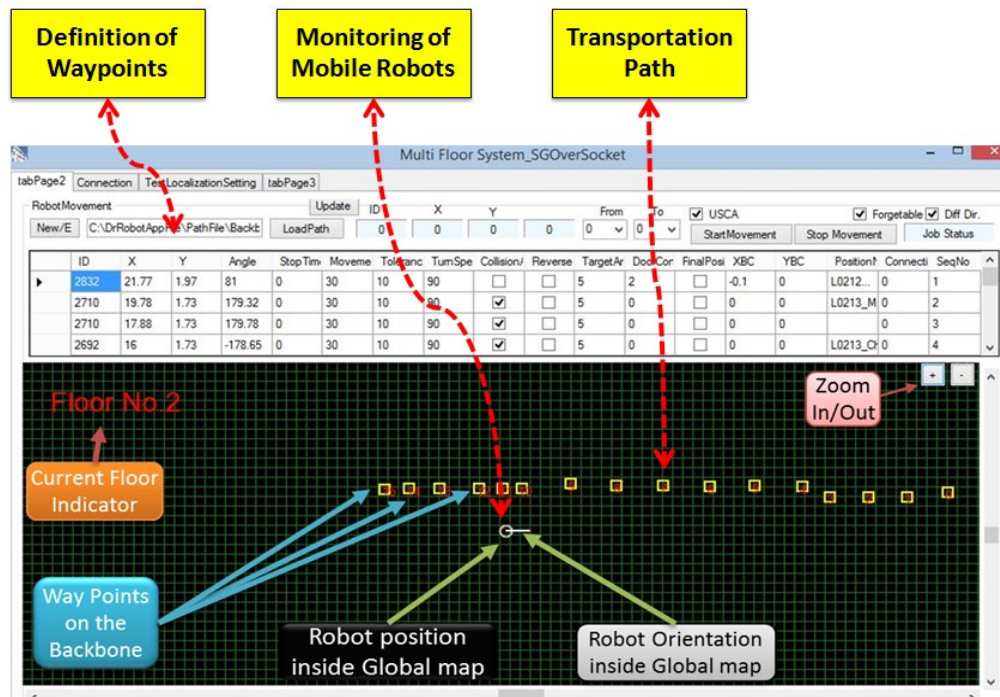


Figure 3-4: GUI of the multi-floor mobile robot transportation/movements

### 3.4 Robot-Door Integration in Multi-floors

Since the modern big laboratories have distributed rooms and elevators, the mobile robots have to open and close some doors automatically to form an automated process as demonstrated in Fig. 3-5. So the high quality robot-door integrating performance is desired in the mobile robot transportation.



Figure 3-5: Laboratory door-opening/closing by the running mobile robots: (a) Automatic controlling for the laboratory doors; and (b) Automatic controlling for the elevator doors

Several important technical issues have to be considered to develop an effective robot-door interface for the multi-floors, which include the monitoring of the door status, the robot-door collision avoidance, the door based global path planning, etc.

All of those upper mentioned technical challenges are considered in this section. Three solutions are presented for the robot-door integration as follows: **(a)** based on the adoption of the ceiling landmarks in the application, it has a chance to identify all the doors of the laboratories and the elevators with a unique HEX ID. The mobile robots can use these identified IDs to recognize the correct doors during the transportation process; **(b)** all of these doors are included inside the multi-floor path planning procedure so that the running mobile robots can control the corresponding doors correctly if necessary; **(c)** since the controlling features between the rooms and elevators are different, two controlling strategies are proposed. For the doors of the laboratory rooms, a wireless based controlling system is developed. For the doors of the elevators, a hybrid controlling method is designed; and **(d)** the secure protecting strategies are proposed for the failure door-opening/closing cases. When the mobile robots cannot read the real-time status of the front doors through the built wireless communication network, they will stop moving then start the error-handling process. At the same time, the robot on-board ultrasonic sensors are also adopted to detect the

mechanical status of the doors.

Based on the proposed multi-floor robot path planning method, as shown in Fig. 3-6, not only the arm manipulating and the robot motion controlling points are included, but also a number of assisting points including the door opening/closing points and the power recharging points are involved. All of the laboratory doors are marked with a unique transportation point number. When the robots reach those door points, their corresponding RBCs will send the remote commands to control the doors. At the same time, when any path planning initializes in the IMRTS system, those door points will be covered to decide the shortest transportation paths by considering their geometrical connecting conditions to the adjacent map points. All robots can open and close the doors of the laboratory rooms.

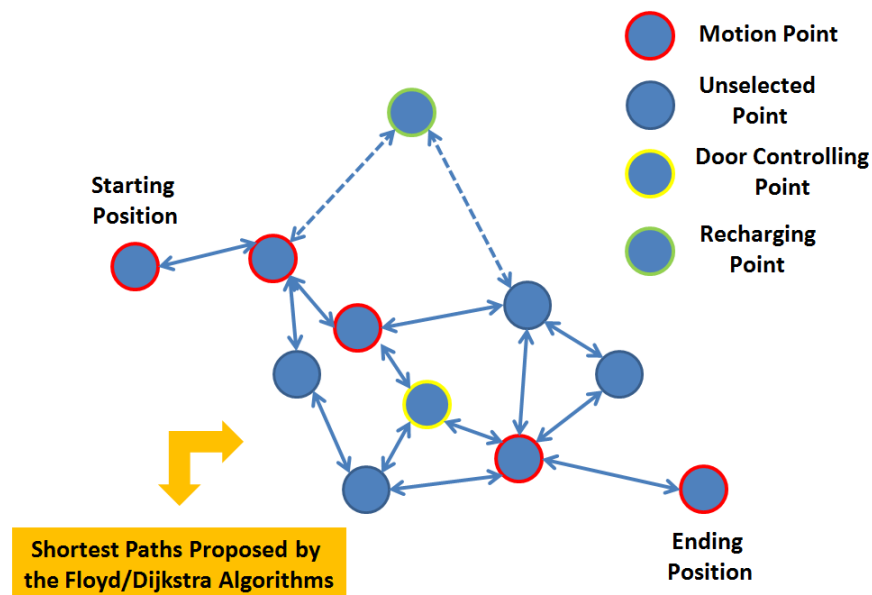


Figure 3-6: The shortest path planning for the mobile robot transportation

Additionally, as given in Fig.3-7, a wireless based controlling system named as ADAM controller is proposed to connect all laboratory doors and each ADAM controller is distributed a sole IP address [165]. On the other side, all of the robot on-board laptops (RBCs) are also given a unique IP address. Based on this wireless structure, The RBCs and the ADAM controllers can exactly recognize each other during the movements of the mobile robots. The developed door GUI of the RBC is demonstrated in Fig. 3-8. From Fig.3-8, it can be seen that all the doors are monitored by the corresponding RBC centers and any identified RBC can open/close those doors flexibly. When the mobile robots reach the defined door points, they only need to send out a door command to the



related I/O port of the ADAM controller.

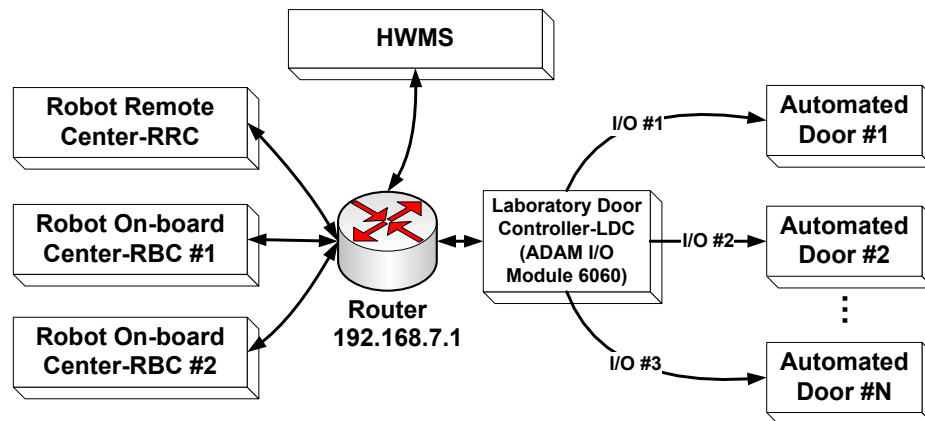


Figure 3-7: Wireless communication channel for the robot-door controlling [165]

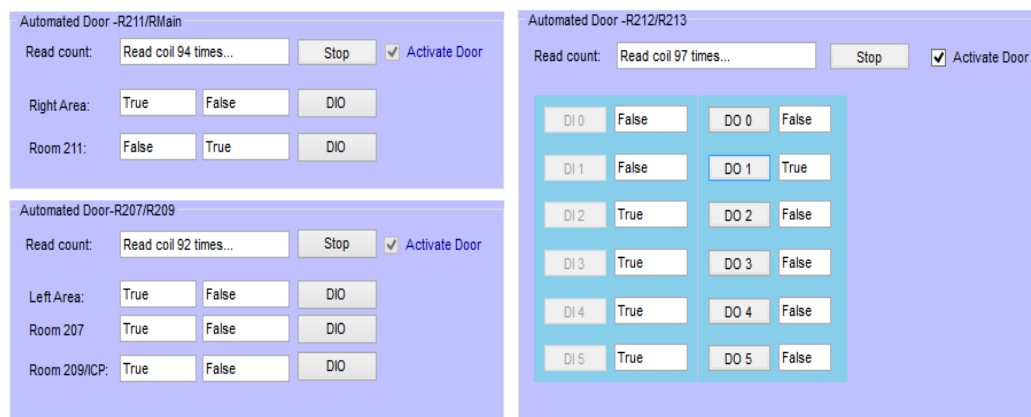


Figure 3-8: A case of the status of the automated doors in a RBC center [165]

For the possible failure situations of the mobile robot-door integration, there are two protecting levels used as follows: The first one is to protect the robots and the doors. A double-checking process is provided for those door points. If a mobile robot's on-board RBC cannot get the feedback messages from the corresponding door ADAM controller in any cases, the RBC will pause the robotic motion module until it gets the reply from the door controllers. The second one is for the whole transportation process. If a transportation task is blocked by a door-opening problem, the selected mobile robot is asked to report the door error message to the remote RRC center and the highest HWMS timely. It means if the robot's on-board RBC still cannot know the real-time status (*opened or closed*) of the front door after several reconnections, it will terminate the robot's motion process and switch to the error-sending process. Both of those two protecting levels have been embedded in the IMRTS system. Two real system log-files recorded by the RBCs is demonstrated in Fig.3-9 and Fig.3-10, respectively. From

Fig.3-9 and Fig.3-10, it can be seen that the mobile robot (*i.e.*, *Robot 4D*) executed the proposed two protecting levels rightly (*i.e.*, *to stop and send out an error message*).

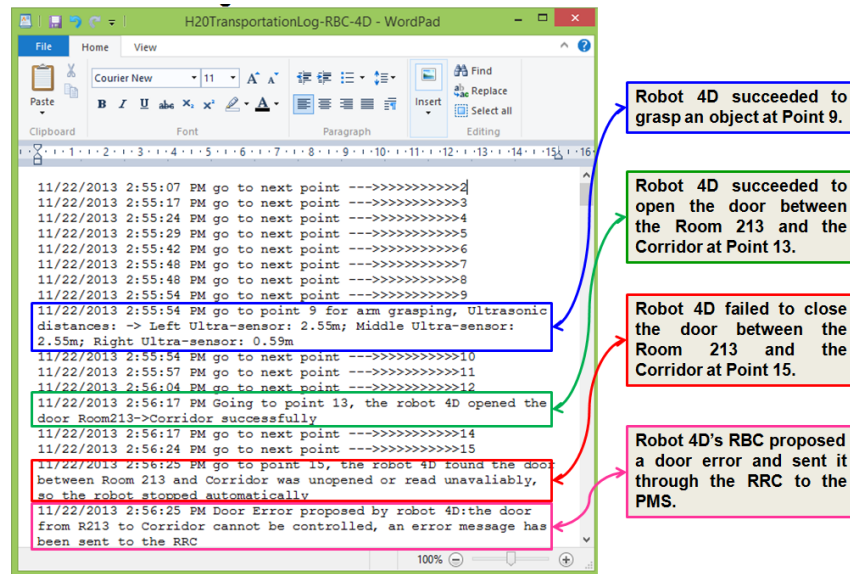


Figure 3-9: A system log-file in the RBC monitoring the door opening/closing process [165]

```
=====
22.11.2013 14:56:25 RRC:
<?xml version="1.0"?>
<H20M-Commands ID="6361" Type="Reply" Client="RRC">
  <Transport CommandName="Transport" Success="False" Possibility="False"
  ErrorText="Door Error proposed by robot 4D:the door between R213 to
  Corridor has an opening or reading error, the robot cannot pass through
  it" />
</H20M-Commands>
=====
```

Figure 3-10: A system log-file in the RRC storing the door controlling error for the HWMS [165]

## 3.5 Intelligent Robot Localization Signal Filter

### 3.5.1 Framework of the Proposed Intelligent Filter

As mentioned in Section 3.2, the StarGazer sensors are the base of the proposed multi-floor robot navigating strategy and the corresponding robot path planning method. Although the StarGazer sensors have lots of advantages in many aspects (*e.g.*, *extension, suitability, etc.*), based on the results of many experiments, we find that its robustness performance under interference conditions is unsatisfactory. As illustrated in Fig. 3-11, the ceiling lights above the elevators and the corridors, the security lights above the entrances and the strong-sunshine happening in the elevators all can cause the non-robustness of the navigation performance of the mobile robot on-board StarGazer sensors.

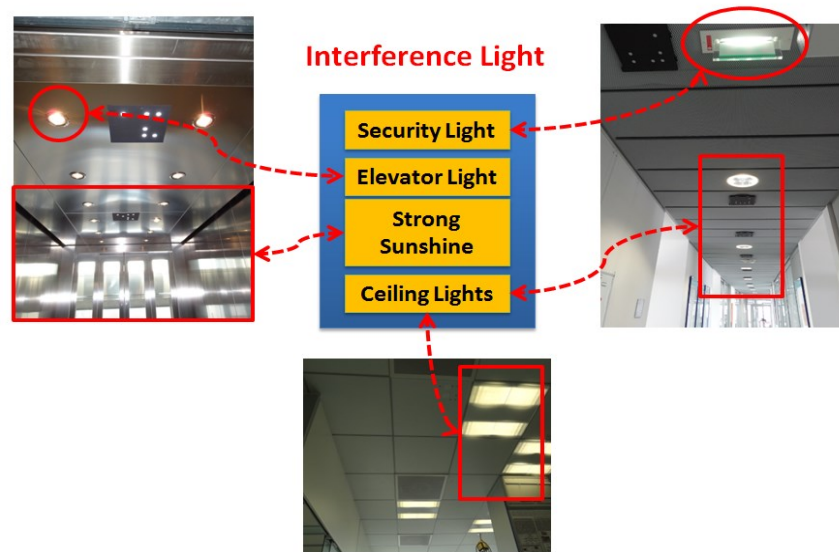


Figure 3-11: Lighting interference conditions at CELISCA

To solve the interference problem, an intelligent robot indoor positioning filter method is presented using the TSA (*Time Series Analysis*) theory and the KF (*Kalman Filter*), as given in Fig. 3-12. From Fig. 3-12, the contents of the proposed method are explained as follows:

- ✧ In the developed IMRTS system, once a mobile robot is started, the robot indoor coordinates will be measured automatically by the robot on-board RBC. So there is a good chance to forecast the coming coordinates of the mobile robots by using their corresponding historical coordinate data. Based on this new idea, the KF model is proposed to track and forecast the robot indoor localization coordinates. When the mobile robots are running under/near the interferences, once the measured coordinates from the StarGazer sensors are considerably different to the KF based forecasted coordinates, the RBC can control the corresponding H20 robot to leave/pass through the interference areas safely by using the forecasted robot coordinates.
- ✧ In the proposed robot positioning filter method, the following computational steps are included as: **(a)** firstly, to recognize the dynamic changing law of the robot indoor positioning, an ARIMA (*Auto Regressive Integrated Moving Average*) model from the TSA theory will be built based on the historical robot indoor coordinates. All of the historical data are stored inside a data class of the every RBC; and **(b)** secondly, the built ARIMA will be used to choose the initial parameters of the estimation equation and the measurement equations of the KF model. Once these initial parameters are selected, the iterative KF sequence



equations can be adopted to realize the tracking and forecasting computation.

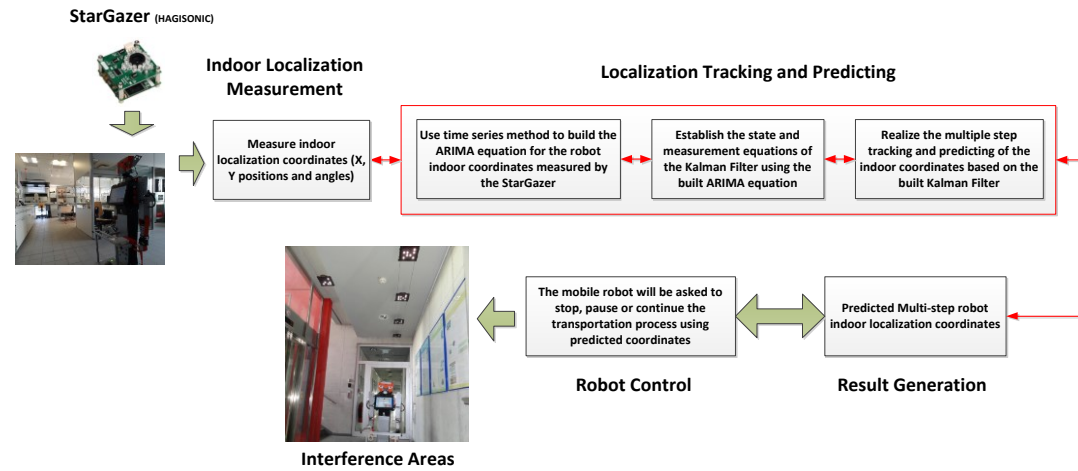


Figure 3-12: The framework of the proposed robot positioning signal-filtering method

The innovations of the proposed robot positioning filtering method are explained as follows: **(a)** for the engineering view, the proposed robot positioning filter method solves the ceiling interference problem of the adopted StarGazer sensors. Actually this kind of interference problems exists in the situations where the robots adopt the ceiling-reading strategy for the indoor navigation. This technical application can be extended to different kinds of mobile robots; and **(b)** for the scientific view, the proposed method presents a new idea how to establish an effective KF using the TSA models only based on the limited one-dimensional sampling data but ignoring the generating backgrounds of the signals.

### 3.5.2 Theories of the Modeling

#### 3.5.2.1 Time Series Analysis Theory

Time Series Analysis (TSA) is a mathematical method proposed to analyze the time series data/signals and establish the best TSA models to explore the changing laws of the measured time series [166]–[168]. Since the TSA has lots of computing advantages in some aspects (*e.g., the fast computation, the real-time modeling generation, the explicit equations, etc.*), it has been generally used in the non-stationary data/signal processing [169]–[175]. In the TSA theory, there are four standard types of models, including the AR (*Auto Regressive*) model, the MA (*Moving Average*) model, the

ARMA (*Auto Regressive Moving Average*) model and the ARIMA (*Auto Regressive Integrated Moving Average*) model.

- *Auto Regressive Model:*

$$X(t) = \varphi_1 X(t-1) + \varphi_2 X(t-2) + \dots + \varphi_m X(t-m) + a(t) \quad (Eq.3-1)$$

where  $\{X(t)\}$  is the originally measured time series,  $\{a(t)\}$  is the random error series meeting the signal distribution of a white noise with an equal variance,  $\{\varphi_m\}$  is the equation parameters of the AR models, and 'm' is the order of the AR models.

- *Moving Average Model:*

$$X(t) = a(t) - \theta_1 a(t-1) - \theta_2 a(t-2) - \dots - \theta_n a(t-n) \quad (Eq.3-2)$$

where  $\{X(t)\}$  is the originally measured time series,  $\{a(t)\}$  is the random error series,  $\{\theta_n\}$  is the equation parameters of the MA models, and 'n' is the order of the MA models.

- *Auto Regressive Moving Average Model:*

$$\begin{aligned} X(t) - \varphi_1 X(t-1) - \varphi_2 X(t-2) - \dots - \varphi_m X(t-m) \\ = a(t) - \theta_1 a(t-1) - \theta_2 a(t-2) - \dots - \theta_n a(t-n) \end{aligned} \quad (Eq.3-3)$$

where  $\{X(t)\}$  is the originally measured time series,  $\{a(t)\}$  is the random error series,  $\{\varphi_m\}$  is the equation parameters of the auto regressive components in the ARMA models,  $\{\theta_n\}$  is the equation parameters of the moving average components in the ARMA models, 'm' is the order of auto regressive components, and 'n' is the order of moving average components.

- *Auto Regressive Integrated Moving Average Model:*

$$\phi(B) \cdot K^d \cdot X(t) = \theta(B) \cdot a(t) \quad (Eq.3-4)$$

$$\begin{cases} B = X(t-1) / X(t) \\ K = 1 - B \\ \varphi(B) = 1 - \varphi_1 B - \varphi_2 B^2 - \varphi_3 B^3 - \dots - \varphi_m B^m \\ \theta(B) = 1 - \theta_1 B - \theta_2 B^2 - \theta_3 B^3 - \dots - \theta_n B^n \end{cases} \quad (Eq.3-5)$$

where  $\{X(t)\}$  is the originally measured time series,  $\{a(t)\}$  is the random error series, ' $B$ ' is the backward operating factor, ' $K$ ' is the difference computational factor, ' $m$ ' is the order of the auto regressive components in the ARIMA models, ' $d$ ' is the order of the difference computation, ' $n$ ' is the order of the moving average components in the ARIMA models,  $\{\varphi_m\}$  is the equation parameters of the auto regressive components and  $\{\theta_n\}$  is the equation parameters of the moving average components in the ARMA models.

In the TSA theory, a complete modeling process consists of three computational steps as follows: **(a)** the first one is to select the fitting model type for a group of time series data. The most popular way for the model selection is based on the auto correlation and the partial correlation from the original time series data; **(b)** the second step is to recognize the AR or MA components for the original time series and decide their best orders in their combinations. There are several algorithms available in this step, including the AIC (*Akaike Information Criterion*), the BIC (*Bayesian information criterion*) and the FPE (*Final Prediction Error*); and **(c)** the third step is to calculate the parameters of the finally recognized TSA models to get the specific equations. For the optimization of the model orders, several algorithms are proposed, such as the YW (*Yule-Walker Estimation*), the MLE (*Maximum Likelihood Estimation*) estimation, the LSE (*Least Square Estimation*), etc.

The FPE criterion is selected to decide the best order of the recognized TSA models. Here the standard AR model is taken as an example to describe the computational process of the FPE.

For any AR( $m$ ) model, the following equation should be met as:

$$\hat{\sigma}_a^2 = \hat{R}_0 - \sum_{j=1}^m \hat{\varphi}_j \hat{R}_j \quad (Eq.3-6)$$

where  $\{\hat{R}_j\}$  is the auto correlation series for the originally measured data and  $\{\varphi_m\}$  is the equation parameters of the AR( $m$ ) model.

The equation of the FPE( $n$ ) criterion is provided as:

$$FPE(n) = (1 + \frac{n}{N})(1 - \frac{n}{N})^{-1} (\hat{R}_0 - \sum_{j=1}^n \hat{\varphi}_j \hat{R}_j) \quad (Eq.3-7)$$

Then:

$$FPE(n) = \frac{(N+n)}{(N-n)} \sigma_a^2$$

$$\Rightarrow FPE(n_0) = \min_{0 \leq n \leq n_h} FPE(n) \quad (Eq.3-8)$$

where  $\sigma_a$  is the FPE error parameter and ‘ $N$ ’ is the total number of the originally measured time series.

Additionally, the following equation of the YW estimation is given as:

$$\begin{bmatrix} \varphi_{k1} \\ \varphi_{k2} \\ \dots \\ \varphi_{kk} \end{bmatrix} = \begin{bmatrix} \rho_0 & \rho_1 & \dots & \rho_{k-1} \\ \rho_1 & \rho_0 & \dots & \rho_{k-2} \\ \dots & \dots & \dots & \dots \\ \rho_{k-1} & \rho_{k-2} & \dots & \rho_0 \end{bmatrix}^{-1} \begin{bmatrix} \rho_1 \\ \rho_2 \\ \dots \\ \rho_k \end{bmatrix} \quad (Eq.3-9)$$

### 3.5.2.2 Kalman Filter Theory

Kalman Filter (KF) is an intelligent signal optimizing, tracking and predicting theory, which was proposed by famous scientist Kalman [83], [176]–[178]. Since it has strict mathematical derivation and has outstanding performance in the non-stationary and nonlinear signal processing, it has been applied in many scientific and engineering fields [68], [179]–[184]. In the KF theory, there are two equations built for the KF iterative close-looping computation, which are named as the state equation and the measurement equation.

- *KF State Equation:*

$$X(k+1) = \Phi(k+1, k)X(k) + \Gamma(k+1, k)w(k), \quad k = 0, 1, \dots \quad (Eq.3-10)$$

where  $\{X(k)\}$  is the real signal series, which are expected to be measured,  $\{w(k)\}$  is the existent random components of the real signals,  $\Phi(k+1, k)$  is the state-transferring matrix from the ‘ $k$ ’ step to the ‘ $k+1$ ’ step and  $\Gamma(k+1, k)$  is the incentive-transferring matrix from the ‘ $k$ ’ step to the ‘ $k+1$ ’ step.

- *KF Measurement Equation:*

$$Z(k+1) = H(k+1)X(k+1) + v(k+1), \quad k = 0, 1, \dots \quad (Eq.3-11)$$

where  $\{Z(k)\}$  is the signal measured series respecting to the real signal series  $\{X(k)\}$ ,  $\{v(k)\}$  is the corresponding signal measuring error series and  $H(k+1)$  is the signal measuring matrix in the ' $k+1$ ' step.

The relationship between the state equation and the measurement equation in the KF theory can be found as demonstrated in Fig.3-13.

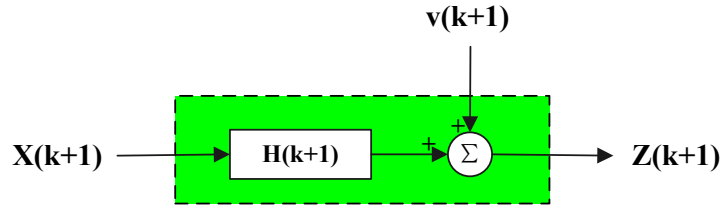


Figure 3-13: Architecture of the original idea adopting in the KF

● *Iterative Computation of KF Modeling:*

The reason why the KF can have outstanding capacity in the signal processing is that the KF has a power sequence of the iterative equations [185]. Based on these iterative equations, the KF is able to decrease the signal measuring errors and find the estimated results which are significantly close to the real signals [186], [187]. In fact, the KF can be adapted to three kinds of signal processing as: the filtering, the interpolation and the forecasting. The following iterative equations are adopted for the prediction of the mobile robot data in the chapter (see Fig. 3-14).

$$\begin{aligned} \hat{X}(k+1|k+1) &= \Phi(k+1|k)\hat{X}(k|k) + K(k+1)[Z(k+1) - H(k+1) \\ &\quad \times \Phi(k+1|k)\hat{X}(k|k)] \end{aligned} \quad (Eq.3-12)$$

$$\begin{aligned} K(k+1) &= P(k+1|k)H^T(k+1) \times [H(k+1)P(k+1|k) \\ &\quad \times H^T(k+1) + R(k+1)]^{-1} \quad (k = 0, 1, \dots) \end{aligned} \quad (Eq.3-13)$$

$$P(k+1|k) = \Phi(k+1, k)P(k|k)\Phi^T(k+1, k) + \Gamma(k+1, k)Q(k)\Gamma^T(k+1, k) \quad (Eq.3-14)$$

$$P(k+1|k+1) = [1 - K(k+1)H(k+1)]P(k+1|k) \quad k = 0, 1, \dots \quad (Eq.3-15)$$

$$\hat{X}(k+N|k) = \Phi(k+N, k) \hat{X}(k|k), k=0,1,\dots \quad (Eq.3-16)$$

$$\Phi(k+N, k) = \Phi(k+N, k+N-1)\Phi(k+N-1, k+N-2)\dots, k) \quad (Eq.3-17)$$

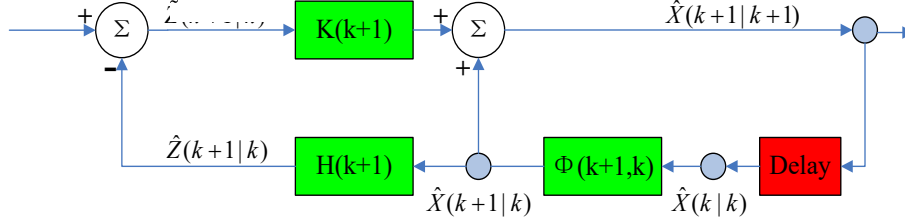


Figure 3-14: Computational framework of the KF

### 3.5.2.3 Modeling Steps of the Proposed Hybrid Method

To validate the performance of the proposed hybrid signal filtering method, a real mobile robot transportation experiment is provided, as shown in Fig. 3-15.

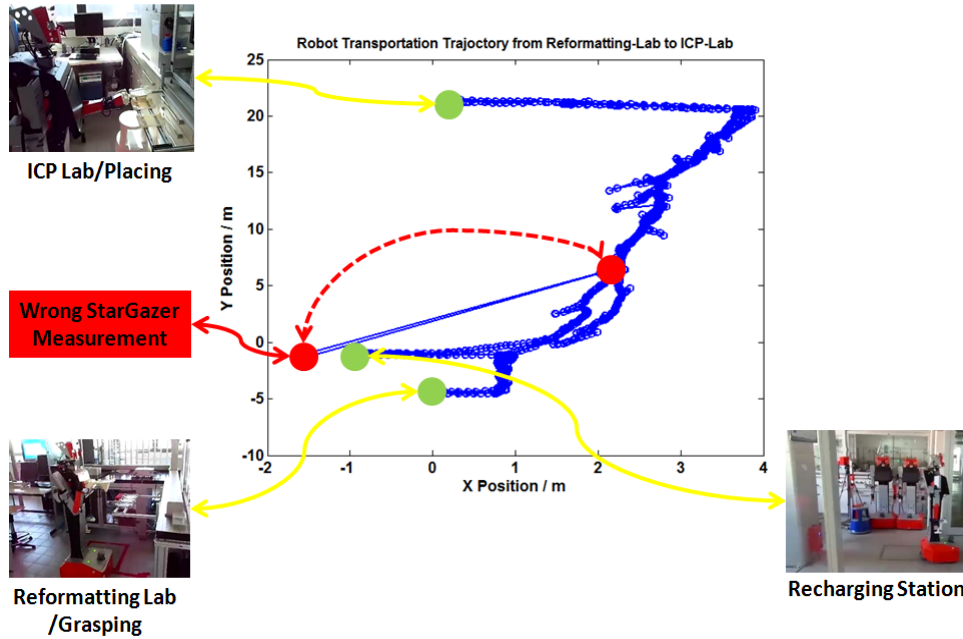


Figure 3-15: Robot transportation from the reformatting lab to the ICP lab at CELISCA

From Fig. 3-15, it can be seen that: the H20 robot completed a transportation event from the reformatting lab to the ICP lab in the CELISCA indoor environment (see the blue path trajectory). There was a wrong robot indoor point measured by the StarGazer sensor (see the red circle point). If the H20 adopted the wrong measure

point (including the X position and the Y position) for the indoor movement, this robot will be totally lost in motion and collide the building walls. The corresponding original robot indoor positions of the transportation experiments are given in Fig. 3-16. In this chapter, the proposed signal filtering method will be executed to find the mentioned wrong positioning point and forecast the right one.

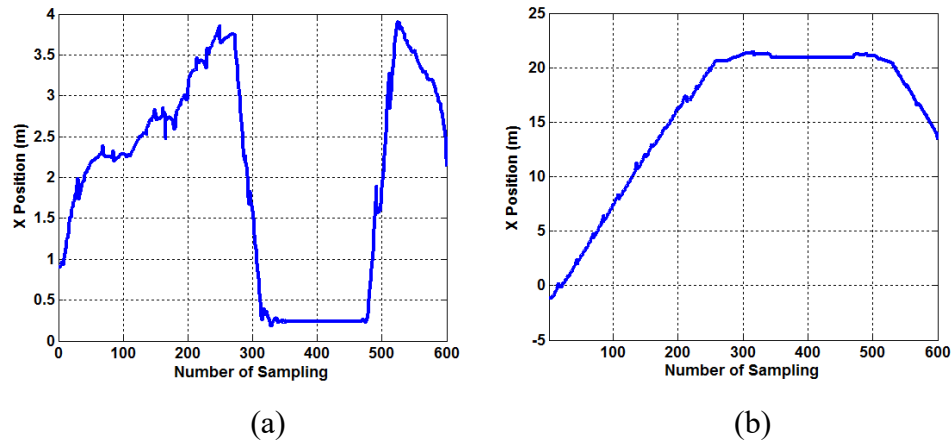


Figure 3-16: Robot indoors positioning coordinates by the StarGazer sensor: (a) the X coordinates; and (b) the Y coordinates

As explained in Section 3.5.2, in the TSA theory the methods of the autocorrelation and the partial autocorrelation are adopted to find the best model type and the corresponding model orders. In this chapter, they are also selected to find the most suitable time series model for the robot indoor positioning coordinates, which are demonstrated in Fig. 3-16. The related results for the robot X positioning coordinates are provided in Fig. 3-17, Fig. 3-18, Table 3-2 and Table 3-3.

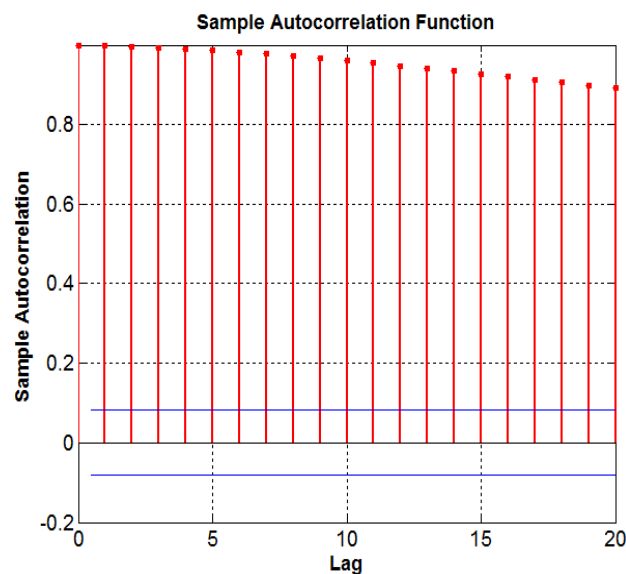


Figure 3-17: Autocorrelation parameters of the original robot X coordinates

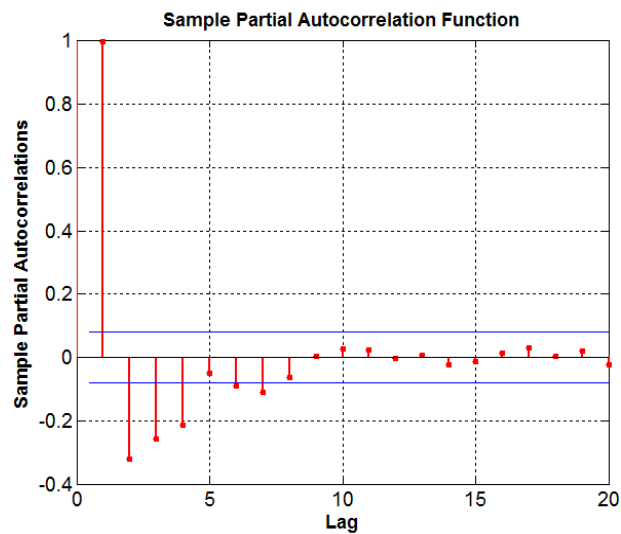


Figure 3-18 Partial autocorrelation parameters of the original robot X coordinates

Table 3-2 The detailed results of the autocorrelation parameters given in Fig.3-17

LAG 1	LAG 2	LAG 3	LAG 4
0.9982	0.9959	0.9932	0.9896
LAG 5	LAG 6	LAG 7	LAG 8
0.9859	0.9818	0.9771	0.9720
LAG 9	LAG 10	LAG 11	LAG 12
0.9665	0.9606	0.9544	0.9479
LAG 13	LAG 14	LAG 15	LAG 16
0.9412	0.9343	0.9273	0.9203
LAG 17	LAG 18	LAG 19	LAG 20
0.9133	0.9061	0.8989	0.8915

Table 3-3 The detailed results of the partial autocorrelation parameters given in Fig. 3-18

LAG 1	LAG 2	LAG 3	LAG 4
0.9982	0.3229	0.2579	0.2156
LAG 5	LAG 6	LAG 7	LAG 8
-0.0512	0.0901	0.1094	-0.0645
<b>LAG 9</b>	LAG 10	LAG 11	LAG 12
<b>0.0033</b>	0.0266	0.0239	-0.0016
LAG 13	LAG 14	LAG 15	LAG 16
0.0054	-0.0218	-0.0123	0.0133
LAG 17	LAG 18	LAG 19	LAG 20
0.0307	0.0039	0.0203	-0.0243



From Fig. 3-17, Fig. 3-18, Table 3-2 and Table 3-3, it can be seen that the results of the autocorrelation and partial correlation parameters for the mobile robot X coordinates show the strong-trailing and the oscillating character so that the signal difference processing should be executed to this group of original robot X coordinates. The one-order difference processing result and its corresponding auto-correlation and partial-correlation results are given in Figures 3-19~3-21 and Tables 3-4 and 3-5.

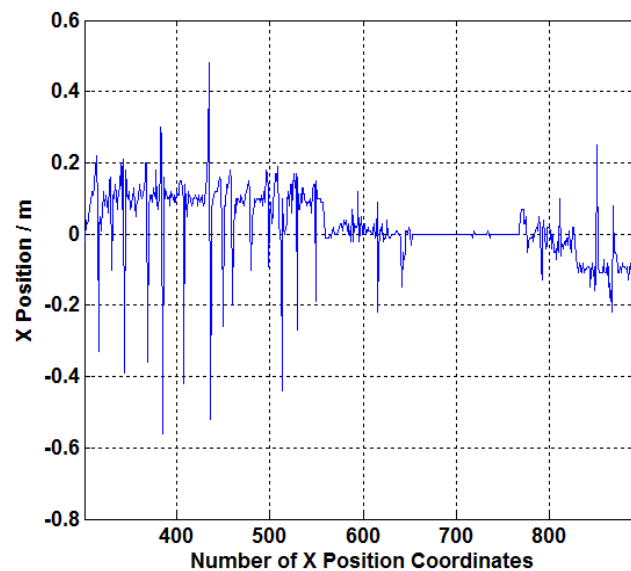


Figure 3-19 Autocorrelation parameters of the one-order difference processed robot X coordinates

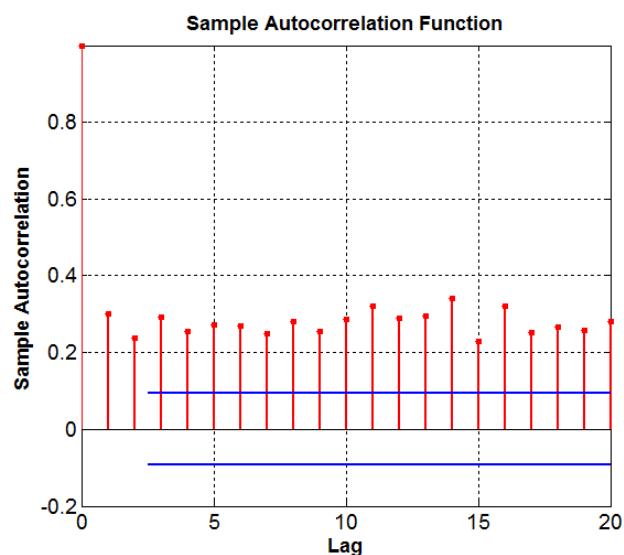


Figure 3-20: Autocorrelation parameters of the one-order difference processed robot X coordinates

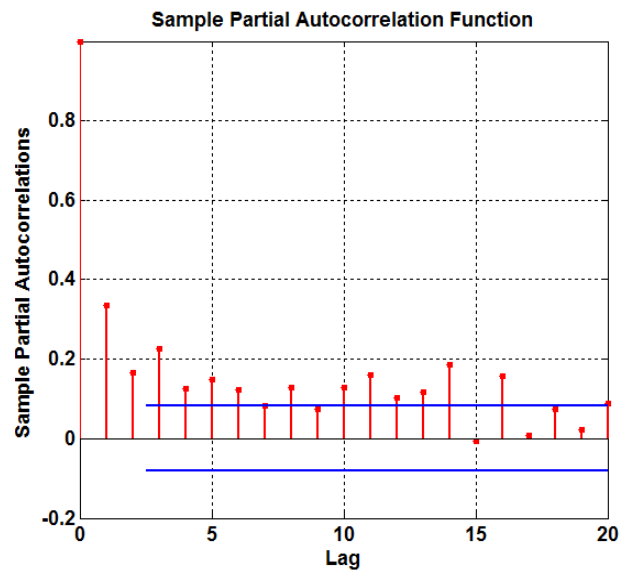


Figure 3-21: Partial autocorrelation parameters of the one-order difference processed robot X coordinates

Table 3-4 The detailed results of the autocorrelation parameters given in Fig. 3-20

LAG 1	LAG 2	LAG 3	LAG 4
0.3015	0.2386	0.2935	0.2542
LAG 5	LAG 6	LAG 7	LAG 8
0.2727	0.2707	0.2490	0.2807
LAG 9	LAG 10	LAG 11	LAG 12
0.2560	0.2871	0.3201	0.2888
LAG 13	LAG 14	LAG 15	LAG 16
0.2964	0.3423	0.2298	0.3198
LAG 17	LAG 18	LAG 19	LAG 20
0.2519	0.2661	0.2593	0.2795

Table 3-5 The detailed results of the partial autocorrelation parameters given in Fig. 3-21

LAG 1	LAG 2	LAG 3	LAG 4
0.3343	0.1655	0.2269	0.1263
LAG 5	LAG 6	<b>LAG 7</b>	LAG 8
0.1500	0.1227	<b>0.0832</b>	0.1292
LAG 9	LAG 10	LAG 11	LAG 12
0.0739	0.1293	0.1602	0.1041
LAG 13	LAG 14	LAG 15	LAG 16
0.1169	0.1869	-0.0068	0.1587
LAG 17	LAG 18	LAG 19	LAG 20
0.0092	0.0756	0.0235	0.0876

From Figures 3-19~3-21 and Tables 3-4 and 3-5, it can be found that: **(a)** since the results of the autocorrelation and partial correlation parameters for the mobile robot X coordinates show the trailing and oscillating character, the group of robot X position meets the AR model type; and **(b)** since the partial correlation of the robot X coordinates starts to fall into the thresholds when the lag is equal to seven (*the partial correlation value is equal to 0.0832*), the best order for the recognized AR model is chosen as seven. The YW matrix to realize the parameter estimation for the AR (7) is calculated as:

$$\begin{bmatrix} \varphi_1 \\ \varphi_2 \\ \dots \\ \varphi_7 \end{bmatrix} = \begin{bmatrix} 0.0104 & 0.0038 & 0.0035 & 0.0038 & 0.0034 & 0.0036 & 0.0036 \\ 0.0038 & 0.0104 & 0.0038 & 0.0035 & 0.0038 & 0.0034 & 0.0036 \\ 0.0035 & 0.0038 & 0.0104 & 0.0038 & 0.0035 & 0.0038 & 0.0034 \\ 0.0038 & 0.0035 & 0.0038 & 0.0104 & 0.0038 & 0.0035 & 0.0038 \\ 0.0034 & 0.0038 & 0.0035 & 0.0038 & 0.0104 & 0.0038 & 0.0035 \\ 0.0036 & 0.0034 & 0.0038 & 0.0035 & 0.0038 & 0.0104 & 0.0038 \\ 0.0036 & 0.0036 & 0.0034 & 0.0038 & 0.0035 & 0.0038 & 0.0104 \end{bmatrix}^{-1} \begin{bmatrix} 0.0038 \\ 0.0035 \\ 0.0038 \\ 0.0034 \\ 0.0036 \\ 0.0036 \\ 0.0034 \end{bmatrix}$$

(Eq.3-18)

Then the results are obtained as:

$$\{\varphi\} = \{0.1522, 0.0983, 0.1382, 0.0822, 0.1080, 0.1155, 0.0834\} \quad (\text{Eq.3-19})$$

The final equation of the AR(7) model built for the one-order difference processed robot X coordinate series can be gotten as:

$$(1 - 0.1522B - 0.0983B^2 - 0.1382B^3 - 0.0822B^4 - 0.1080B^5 - 0.1155B^6 - 0.0834B^7)X(t) = a(t) \quad (\text{Eq.3-20})$$

$$\begin{aligned} \Rightarrow X(t) = & 0.1522X(t-1) + 0.0983X(t-2) + 0.1382X(t-3) \\ & + 0.0822X(t-4) + 0.1080X(t-5) + 0.1155X(t-6) \\ & + 0.0834X(t-7) + a(t) \end{aligned} \quad (\text{Eq.3-21})$$

Based on Equations (3-4) and (3-5), the following final equation of the ATIMA(6,1,0) for the original robot X coordinates can be made as:

$$(1 - 0.1522B - 0.0983B^2 - 0.1382B^3 - 0.0822B^4 - 0.1080B^5 - 0.1155B^6 - 0.0834B^7)(1 - B)X(t) = a(t) \quad (\text{Eq.3-22})$$

$$\begin{aligned} \Rightarrow X(t) = & 1.1522 X(t-1) - 0.0539 X(t-2) + 0.0398 X(t-3) \\ & - 0.0559 X(t-4) + 0.0258 X(t-5) + 0.0075 X(t-6) \\ & - 0.0321 X(t-7) - 0.0834 X(t-8) + a(t) \end{aligned} \quad (Eq.3-23)$$

In the KF theory, there is an unsolved and fundamental problem, which is to apply the right KF model in engineering applications. *How to choose the right initial parameters of the KF model based on the measured time series signals?* For this issue, the traditional way is to select the KF initial parameters in random, then after running long-term/huge iteration training the built KF model using these random parameter possibly reaching a convergence state. Most published KF based applications [188]–[190] adopted this strategy. However, the solution is infeasible and non-effective. The time performance is focused in the mobile robot transportation. The mobile robots expect to find the interference areas as fast as possible. In the proposed ARIMA-KF based robot-positioning signal filtering framework, an original algorithm using the ARIMA model to optimize the initial parameters of the KF model is proposed.

In the TSA theory, the following equation can be set [191]:

$$X_i(t) = X[t - (i - 1)], (i = 1, 2, 3, \dots) \quad (Eq.3-24)$$

Based on Eq. (2-23), the upper Eq. (2-24) can be reformatted as:

$$\begin{aligned} \Rightarrow X_1(t+1) = & 1.1522 X_1(t) - 0.0539 X_2(t) + 0.0398 X_3(t) \\ & - 0.0559 X_4(t) + 0.0258 X_5(t) + 0.0075 X_6(t) \\ & - 0.0321 X_7(t) - 0.0834 X_8(t) + a(t+1) \end{aligned} \quad (Eq.3-25)$$

Then the following state equation of the KF model is calculated as:

$$\begin{bmatrix} X_1(t+1) \\ X_2(t+1) \\ X_3(t+1) \\ X_4(t+1) \\ X_5(t+1) \\ X_6(t+1) \\ X_7(t+1) \\ X_8(t+1) \end{bmatrix} = \begin{bmatrix} 1.1522 & -0.0539 & 0.0398 & -0.0559 & 0.0258 & 0.0075 & -0.0321 & -0.0834 \\ 1 & 0 & 0 & 0 & 0 & 0 & 0 & 0 \\ 0 & 1 & 0 & 0 & 0 & 0 & 0 & 0 \\ 0 & 0 & 1 & 0 & 0 & 0 & 0 & 0 \\ 0 & 0 & 0 & 1 & 0 & 0 & 0 & 0 \\ 0 & 0 & 0 & 0 & 1 & 0 & 0 & 0 \\ 0 & 0 & 0 & 0 & 0 & 1 & 0 & 0 \\ 0 & 0 & 0 & 0 & 0 & 0 & 1 & 0 \end{bmatrix} \times \begin{bmatrix} X_1(t) \\ X_2(t) \\ X_3(t) \\ X_4(t) \\ X_5(t) \\ X_6(t) \\ X_7(t) \\ X_8(t) \end{bmatrix} + a(t+1) \quad (Eq.3-26)$$

At the same time the measurement equation of the KF model is obtained as:

$$Z(t+1) = [1, 0, \dots, \hat{x}_1(t+1), X_2(t+1), X_3(t+1), X_4(t+1), X_5(t+1), X_6(t+1), X_7(t+1), X_8(t+1)] + v(t+1), (t = 0, 1, 2, \dots) \quad (Eq.3-27)$$

### 3.5.3 Experiments and analysis

In the experiment, the following considerations are included as: **(a)** not only the one-step forecasting performance is examined, but also the two-step forecasting results are checked. The one-step forecasting results are used to find the wrong reading robot positioning coordinates measured from the on-board StarGazer sensors, and the two-step forecasting results are provided to guide the missing mobile robots to pass through the interference areas safely; **(b)** the multi-step forecasting performance is desired to verify the robustness of the proposed hybrid method; and **(c)** to demonstrate the good algorithm performance of the proposed TSA-KF method, a comparison of the proposed ARIMA-KF method and the popular ARIMA model is also provided. In the chapter, three standard error estimating indexes are adopted in the experiment, including the MAE (*Mean Absolute Error*), the MAPE (*Mean Absolute Percentage Error*) and the RMSE (*Root Mean Square Error*).

(a) Mean Absolute Error (MAE):

$$\sigma = \frac{1}{n} \sum_{i=1}^M |X(i) - \hat{X}(i)| \quad (Eq.3-28)$$

(b) Mean Absolute Percentage Error (MAPE):

$$\tau = \frac{1}{n} \sum_{i=1}^M \left| \frac{X(i) - \hat{X}(i)}{\hat{X}(i)} \right| \quad (Eq.3-29)$$

(c) Root Mean Square Error (RMSE):

$$\delta = \sqrt{\frac{1}{n-1} \sum_{i=1}^M [X(i) - \hat{X}(i)]^2} \quad (Eq.3-30)$$

#### 3.5.3.1 One-step Tracking/Forecasting Results

The results of the experiment are shown in Figures 3-22, 3-23, 3-24 and 3-25. Based on

these experimental results, the corresponding estimating errors of the experimental results are given by Equations (3-28, 3-29 and 3-30) in Tables 3-6, 3-7 and 3-8.

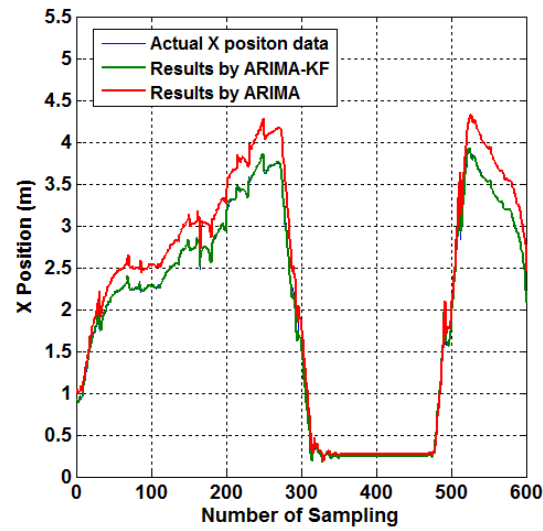
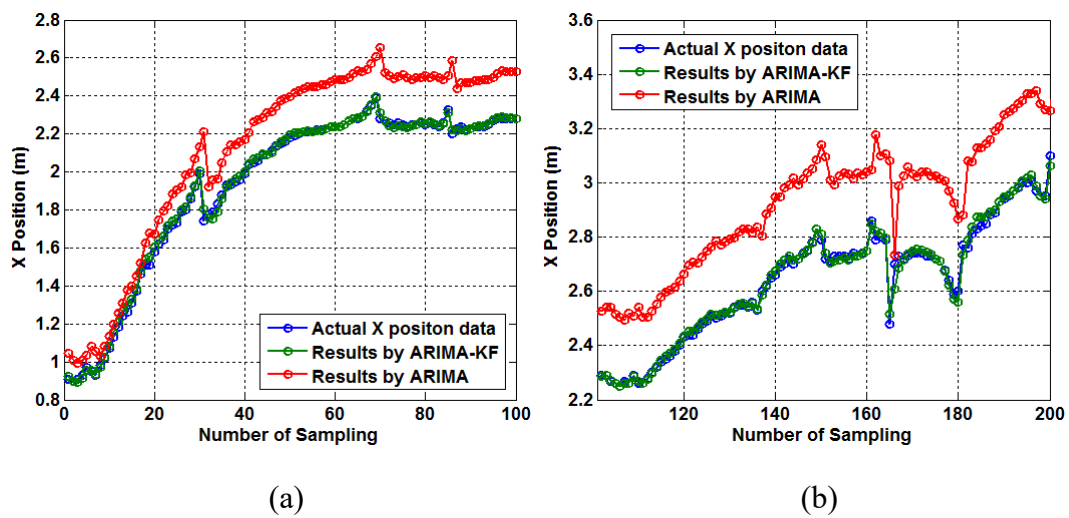


Figure 3-22: Results at the 1<sup>st</sup>-600<sup>th</sup> sampling of the robot X positioning coordinates



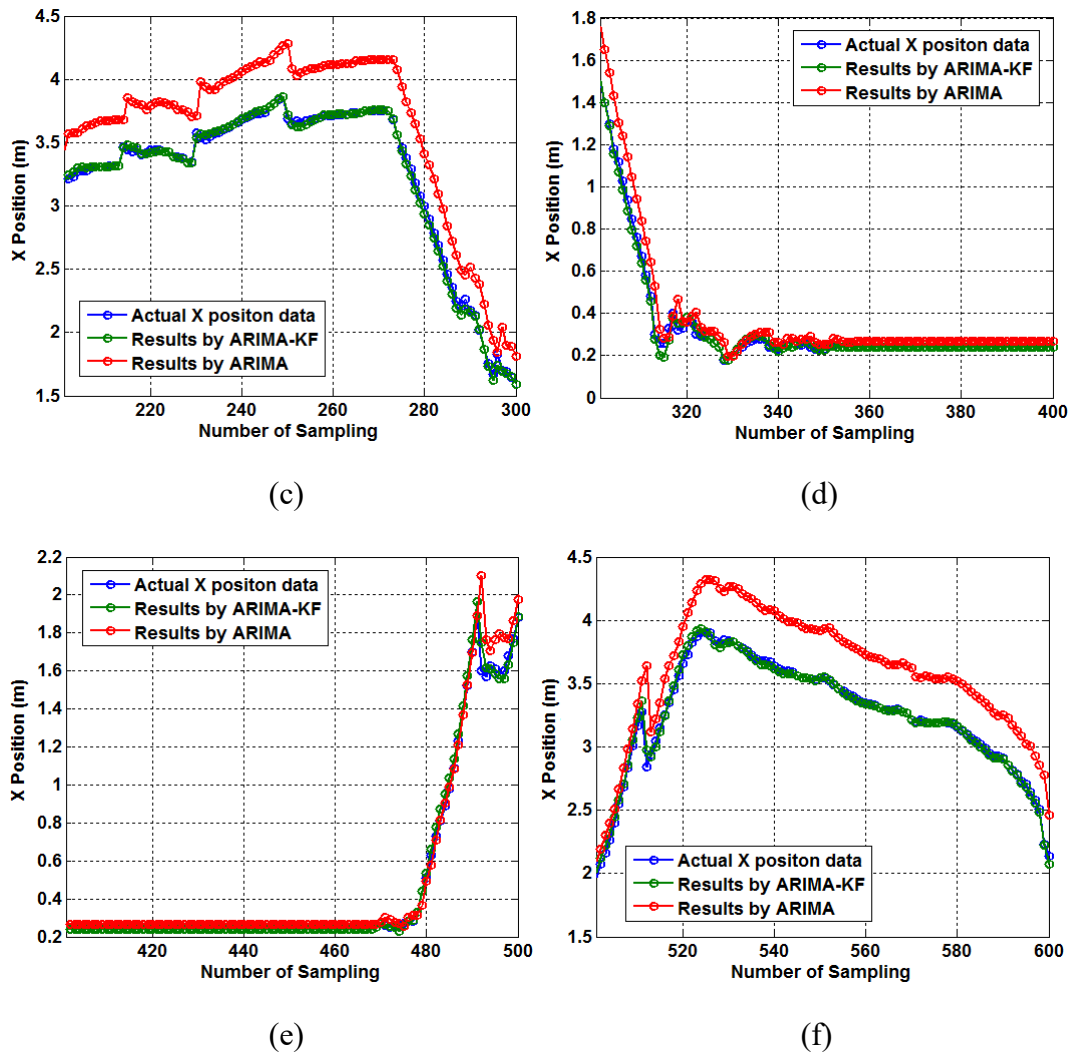


Figure 3-23: Sub-zones for the results at the 1<sup>st</sup>-600<sup>th</sup> sampling of the robot X positioning coordinates

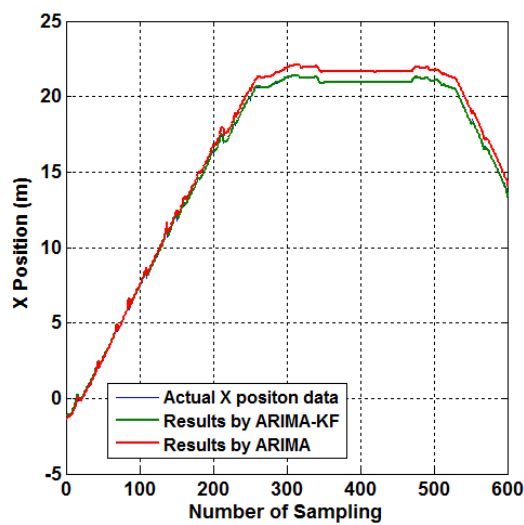


Figure 3-24: Results at the 1<sup>st</sup>-600<sup>th</sup> sampling of the robot Y positioning coordinates

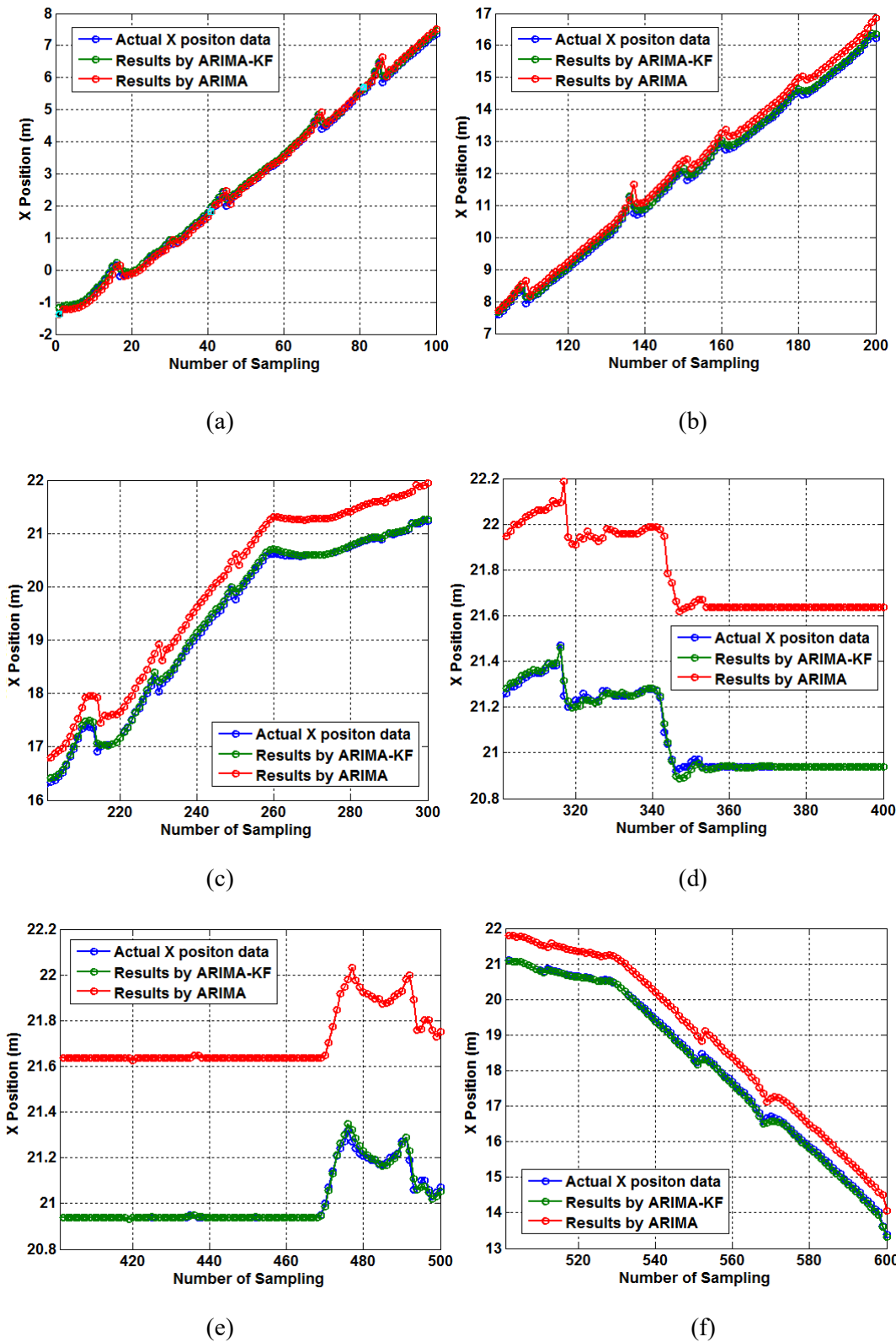


Figure 3-25: Results at the 1<sup>st</sup>-600<sup>th</sup> sampling of the robot Y positioning coordinates



Table 3-6 The estimated errors of the robot one-step tracking/forecasting results by executing the proposed ARIMA-KF method

Indexes	Hybrid TSA-KF Model		
	MAE (m)	MAPE (%)	RMSE (m)
Robot X Coordinate	0.0140	1.03	0.0232
Robot Y Coordinate	0.0395	1.49	0.0511

From Table 3-6, it can be seen that: **(a)** the proposed hybrid ARIMA-KF model forecasts the whole non-stationary robot positioning coordinates accurately; **(b)** for the robot X coordinate series, the MAE, MAPE and RMSE of the one-step results by the proposed ARIMA-KF model are only 0.014m, 1.03% and 0.0232m, respectively; and **(c)** for the robot Y coordinate series, the MAE, MAPE and RMSE of the one-step results by the proposed ARIMA-KF model are only 0.0395m, 1.49% and 0.0511m, respectively.

Table 3-7 The estimated errors of the robot one-step tracking/forecasting results by executing the mainstream ARIMA method

Indexes	ARIMA Model		
	MAE (m)	MAPE (%)	RMSE (m)
Robot X Coordinate	0.2014	10.44	0.1437
Robot Y Coordinate	1.8003	12.77	0.8334

From Table 3-7, it can be seen that: **(a)** the standard ARIMA model from the TSA theory forecasts the same group of non-stationary robot positioning coordinates with the lower accuracy; **(b)** for the robot X coordinate series, the MAE, MAPE and RMSE of the one-step results by the ARIMA model are 0.2014m, 10.44% and 0.1437m, respectively; and **(c)** for the robot Y coordinate series, the MAE, MAPE and RMSE of the one-step results by the ARIMA model are 1.8003m, 12.77% and 0.8334m, respectively.

Table 3-8 The promoting percentages of the ARIMA method by the proposed ARIMA-KF method in the one-step results

Indexes	ARIMA-KF vs. ARIMA		
	MAE	MAPE	RMSE
Robot X Coordinate	93.05 %	90.13 %	83.86 %
Robot Y Coordinate	97.81 %	88.33 %	93.87 %

From Table 3-8, it can be seen that:

(a) When comparing the proposed ARIMA-KF model with the standard ARIMA model, the former hybrid strategy has much better performance than the latter one. For the robot X coordinate series, the promoted percentages of the MAE, MAPE and RMSE to the ARIMA model by the proposed ARIMA-KF model in the one-step results are 99.03%, 90.13% and 83.86%, respectively. For the robot Y coordinate series, the promoted percentages of the MAE, MAPE and RMSE to the ARIMA model by the proposed ARIMA-KF model in the one-step results are 97.81%, 88.33% and 93.87%, respectively.

(b) The proposed hybrid ARIMA-KF method has high-level accuracy (*such as, the MAPE error of the one-step results is less than 5%*) to forecast the robot measured indoor coordinates for the robot safe transportation/motions under the ceiling interference situations. The standard ARIMA model, which is popular in the signal processing, has middle-level accuracy (*such as, the MAPE error of the one-step results is less than 10%*) in the experiment.

### 3.5.3.2 Two-step Forecasting Results

As discussed in Section 3.5.1, to guide the robot pass through the interferences and examine the performance of the proposed ARIMA-KF method, in the chapter the two-step forecasting experiments are also provided. The results of the two-step experiment are given in Fig. 3-26, Fig. 3-27 and Tables 3-9~3-10.

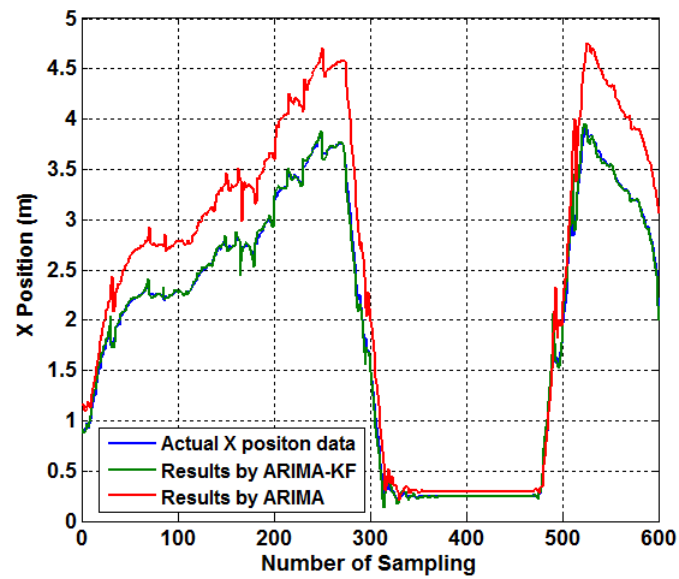


Figure 3-26: Two-step results at the 1<sup>st</sup>-600<sup>th</sup> sampling of the robot X positioning coordinates

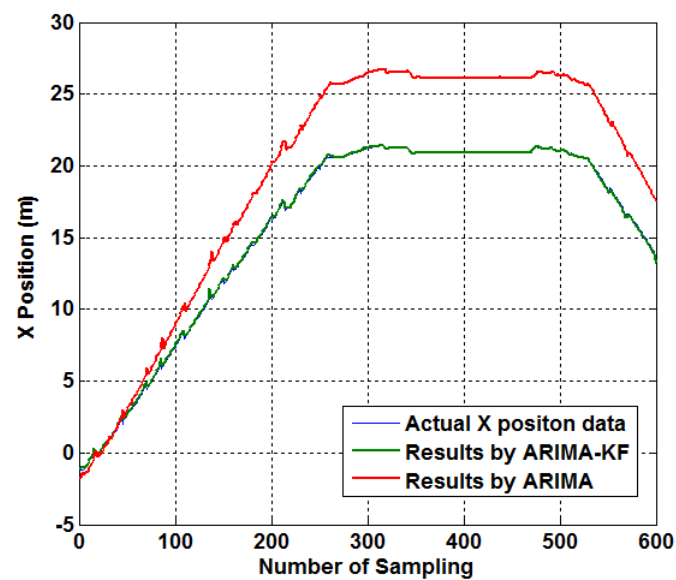


Figure 3-27: Two-step results at the 1<sup>st</sup>-600<sup>th</sup> sampling of the robot X positioning coordinates

Table 3-9 The estimated errors of the robot two-step forecasting results by executing the proposed ARIMA-KF method

Indexes	Hybrid TSA-KF Model		
	MAE (m)	MAPE (%)	RMSE (m)
Robot X Coordinate	0.0264	1.92	0.0432
Robot Y Coordinate	0.0811	2.82	0.0982

Table 3-10 The estimated errors of the robot two-step forecasting results by executing the mainstream ARIMA method

Indexes	ARIMA Model		
	MAE (m)	MAPE (%)	RMSE (m)
Robot X Coordinate	0.4334	22.48	0.3003
Robot Y Coordinate	3.8709	26.89	1.7940

From Fig. 3-26, Fig. 3-27 and Tables 3-9~3-10, it can be seen that: the proposed hybrid ARIMA-KF method still has high-level accuracy (*such as, the MAPE error of the two-step results is still less than 5%*). The standard ARIMA model starts to have unsatisfactory accuracy in the two-step results (*such as, the MAPE error of the two-step results is more than 20%*). It means the proposed ARIMA-KF method has good robustness, which is important in the mobile robot controlling. At the same time, the popular ARIMA model does not have good robustness which will block it been applied in the cases studied in the habilitation thesis.

### 3.5.3.3 Real-time Performance of the Proposed ARIMA-KF

Since the proposed ARIMA-KF method will be applied in the real mobile robot transportation system, the computational time of the proposed ARIMA-KF method is critical. To examine the time performance of the proposed ARIMA-KF method, an experiment is also made using a normal laptop (*CPU Intel i3-2350M 2.3GHz, RAM 6G*), with the results given in Table 3-11. From Table 3-11, the proposed method has satisfactory real-time performance.

Table 3-11 The time performance of the proposed ARIMA-KF model

Indexes	Consuming Time/s	
	One-step	Two-step
Robot X Coordinate	0.3561	0.3760
Robot Y Coordinate	0.3557	0.3716

## 3.6 Execution of the Robot Navigation

A case of the mobile robot transportation in the multi-floor environment at CELISCA laboratory is provided in Fig. 3-28. From Fig. 3-28, it can be see that the proposed

multi-floor indoor navigation method and the corresponding multi-floor path planning algorithm let the robots run correctly in the whole laboratory including the ceiling interference areas.



Figure 3-28: A case of the multi-floor mobile robot transportation at CELISCA laboratory

# Chapter 4 Smart Collision Avoidance

## 4.1 Introduction

Collision avoidance is one of the most impressive functions in the robotics [192]–[197]. Generally, the standard mobile robot collision avoidance is to measure the coming obstacles and find an alternative path to avoid any collision [198]–[204]. However, in some special cases this standard collision avoidance cannot be realized successfully in the life science environments [205]–[210]. There are many narrow zones (*e.g.*, *corridors*, *elevators*, *etc.*) which will cause the robots vibrate with the standard collision avoidance functions. In addition, a mobile robot cannot avoid a personal in the narrow corridors/elevator areas actively if it is carrying some targets on hands. The robot only can stop immediately when it finds any obstacles then waits for the personal's inputting commands. So a smart collision avoidance strategy is desired in the complex laboratory environments. This is the scope of this chapter.

In recent years, the smart robotic collision avoidance has taken lots of attention in the world. *Ratsamee et al.* [211] proposed a new social method allowing the indoor mobile robots to do various intelligent navigation in accordance to the human intentions for the intelligent collision avoidance. In their method, three different interacting behaviors were considered (*i.e.*, avoiding, un-avoiding and approaching). To let the mobile robots understand the human controlling behaviors, multiple RGB-D Kinect sensors were installed on the mobile robots to detect the face orientations of the cooperating human. Their experimental results provided in the paper showed that the proposed face orientation-detecting algorithm was effective for the mobile robot social navigation. *Machida et al.* [212] studied a human tracking system for mobile robots named as Pioneer 3-DX robots. In the system, a Microsoft Kinect sensor was mounted on a Pioneer 3-DX mobile robot to observe the relative positions between the front people

and the running mobile robot, a motor kinematic algorithm was established to control the dynamic motions of the mobile robot, and a Kalman Filter (KF) based estimator was built to predict the next positions of the tracked persons. The results from a real indoor experiment verified that the performance of the proposed HRI tracking system was quite satisfactory. *Beyl et al.* [213] presented a new approach which can accurately detect the human's movements. In the approach, multiple Microsoft Kinect sensors were installed at the corners of the operating environment and a new fusing algorithm was put forward to coordinate these sensors. The results validated that this multi-view recognizing strategy was robust to the environment interference and noise. *Lenz et al.* [214] proposed a new hardware-assisted multi-object tracking system for the HRI purpose based on the Particle Filter (PF) and the Pixel Level Likelihoods (PLL) method. The proposed model computed a full hypothesis map for each multi-target particle through the rendering engine of the graphical card. Their experiments showed that they tracked multi-objects very accurately. *Wang et al.* [215] developed a novel Human-Machine Interface (HMI) by combining the Surface Electromyography Measurement (SEM) to the human limbs and the Human Skeleton Mapping (HSM). Based on the developed HMI platform, a complete HMI experiment was investigated in the 3D space with complex hand speed profiles and some impressive results were gotten. *Awais et al.* [216] studied the performance of a robot collision avoidance experiment in a laboratory environment with unknown human intentions. In the experiment, both of the known and unknown aspects were considered: **(a)** in the known aspects, the robots selected the behaviors which had been executed and recorded before; and **(b)** in the unknown situations, the robots learned to guess the human intentions. The Reinforcement Learning (RL) algorithm was proposed to train the robots and the Particle Filter (PF) algorithm was adopted to calculate the probabilities for a new behavior. More technical strategies and applications in the human-robot interaction or smart collision avoidance can be found in references [217]–[222].

## 4.2 Framework of the Proposed Smart Strategy

The expected smart face HRI for the collision avoidance in the IMRTS system are illustrated in Fig. 4-1, with the explanations as follows:

**(a)** Suppose there are three floors in a life science laboratory building. In this building, it will take place four kinds of collision avoidance by the mobile robots. The most

normal one is the standard collision avoidance when the mobile robots have sufficient space at the corridors/rooms to generate an alternative path to avoid the obstacles actively (*see Case One in Fig. 4-1*). In this case, the standard artificial potential field method will be operated.

**(b)** The second one is the narrow collision avoidance when the mobile robots cannot have sufficient space at the corridors/rooms to find an avoiding path. In this case, the function of the artificial potential field method cannot be started otherwise the mobile robots will have the vibrating phenomenon. The mobile robots only can stop firstly then wait for the commands from the laboratory personals (*see Case Two in Fig. 4-1*). In this kind of robot collision avoidance, it is impossible for the robots to complete the collision avoidance by themselves. At those times, it is important that the people can avoid the robots initiatively or teach the robots where to go, such as the people use the hand gestures to control the robots equipping 3D cameras. Actually this type of collision avoidance is almost equal to a HRI event in robotics.

**(c)** The third one is the elevator based collision avoidance when the mobile robots take the elevators to go different building floors. In this case, the mobile robots will be together with people inside the elevators so that they will not do standard APF collision avoidance but need the inputting commands from people. This is also one kind of HRI events. Comparing to the upper second type, the third one requires higher intelligence. It is impossible to adopt the gesture based voidance controlling inside the elevators because the distances between the mobile robots and the around persons will be too short. To solve this problem, a face based HRI is executed in this third type of collision avoidance.

**(b)** The fourth one is the experimental cooperation based collision avoidance. When the mobile robots are reaching their expected grasping/placing positions and at the same time some people are doing the experiments there occupying the robots' positions, in that situation it is also impossible for the people to do the gesture based HRI so that the face based HRI is required.



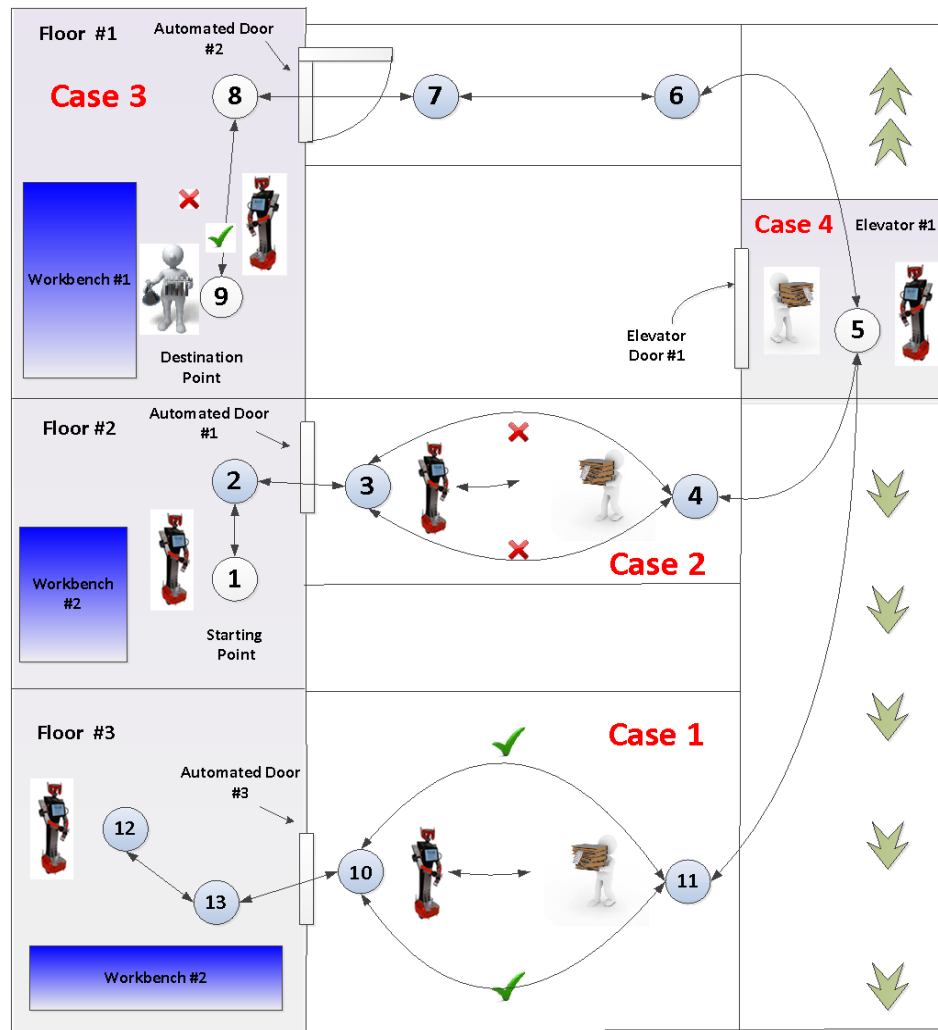


Figure 4-1: The application view of the proposed smart collision avoidance strategy

To meet all of the upper mentioned collision avoidance types, a smart mobile robot collision avoidance architecture is proposed as given in Fig.4-2. As shown in Fig.4-2, in the proposed strategy, there are three classifications of the collision avoidance are combined, which includes the static collision avoidance, the dynamic collision avoidance and the advanced human feature based collision avoidance. The proposed smart collision avoidance can be further explained as:

**(a)** the static collision avoidance is proposed for the mobile robots to measure the indoor laboratory environments to make sure that the mobile robots will not collide the static targets (*including standing people, static walls, standing robots, etc.*). In the static collision avoidance, the simple ‘measuring-stopping’ method is adopted. Once a running mobile robot detects the safe distance between the robot and the closest static obstacle is less than the defined safety distance, the corresponding mobile robot will stop running immediately and send out the error-handling messages to the higher

controlling servers. The dynamic collision avoidance is developed for the mobile robots to avoid the moving obstacles (*including moving laboratory personal, the other running mobile robots, etc.*). In the dynamic collision, the standard artificial potential filed method is embedded, which can be used in the standard-size laboratories.

**(b)** the advanced human face HRI based collision avoidance is presented for the mobile robots to follow the human feature real-time avoiding commands from the around personal to realize the human robot interactions. In the new HRI based collision avoidance, there are two different kinds, the human face based one and the human gesture based one. In the face based one, the mobile robot installed Kinect sensors will measure the real-time human face moving directions based on the face orientations so that the mobile robots can realize the secure collision avoidance. In the gesture based collision avoidance, the laboratory personal will use their hands/ gestures to control the mobile robots to complete the avoidance.

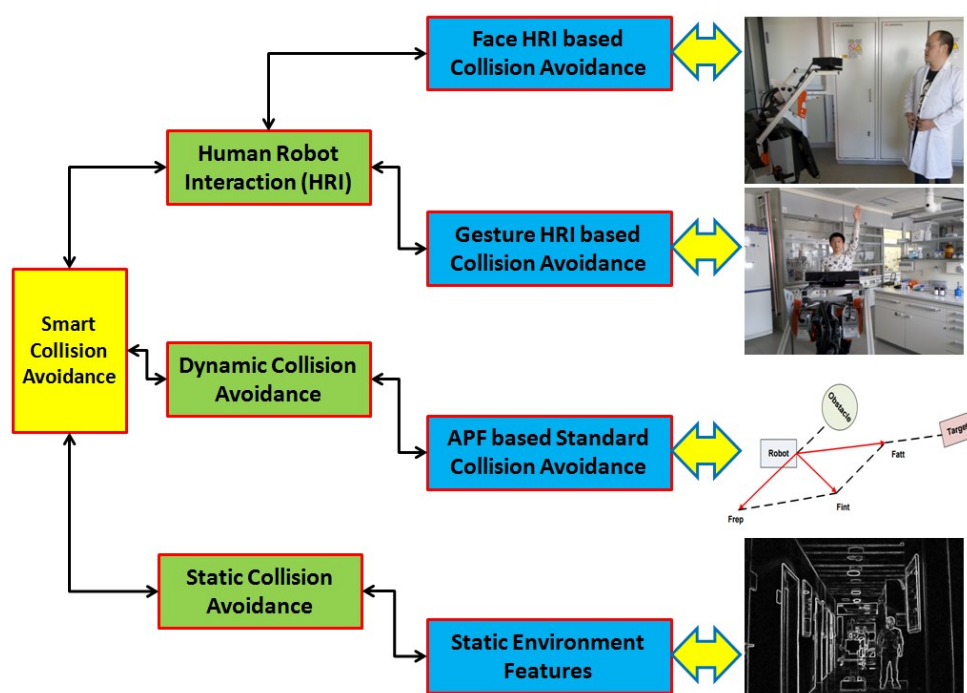


Figure 4-2: The definition of the smart collision avoidance

### 4.3 Face based Collision Avoidance

The proposed face HRI based collision avoidance method is illustrated in Fig. 4-3. From Fig. 4-3, the proposed method can be given as follows: **(a)** as presented in Section 4.2, the Microsoft Kinect sensors [223]–[227] are utilized to measure the face

movements of laboratory personnel. To have real-time performance of the face recognition, a new fast image processing strategy by using the edge detection and the image mesh is developed; **(b)** the Learning Vector Quantization (LVQ) Neural Network is established to recognize the face orientations and its corresponding movements; and **(c)** to have high-quality RHI controlling performance, all the parameters (*including the face enable conditions, the face moving degrees/angles and the selected master*) affecting the face recognition results are all considered. Five face orientations are defined for the face moving identification, including the left side, the forward side, the right side, the left-middle side and the right-middle side (*see Fig. 4-4*).

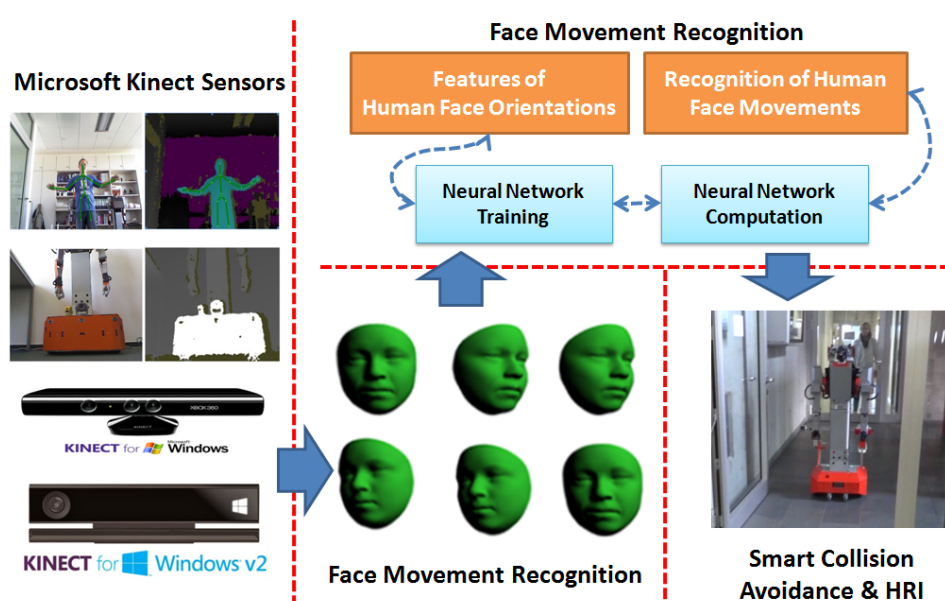


Figure 4-3: The framework of the proposed face moving recognition for the smart collision avoidance & HRI control [227]



Figure 4-4: Five face orientation definitions [227]

Since the extracted feature parameters will be input to the latter LVQ neural networks for the recognizing computation, those feature parameters should be extracted uniquely

and accurately. For this target, a new hybrid algorithm is presented by combining the image edge detection and the mesh generation.

The workflow of the proposed extracting algorithm is given in Fig. 4-5. Based on Fig. 4-5, the procedures of the face orientation feature recognizing algorithm can be explained as follows: **(a)** the pixels of the eye-eyebrow areas in the measured face images are selected to differentiate the orientations. All detected images will be divided into a number of rows and columns. The numbers of the rows and columns can be chosen up to the specific requirements. In the chapter, the numbers of the rows and the columns are equal to six and eight; and **(b)** the standard edge detection (*such as the Canny algorithm*) is executed for these images to find the eye-eyebrow features. The detailed procedures of the LVQ neural network for the face recognition can be found in Section 4.5.

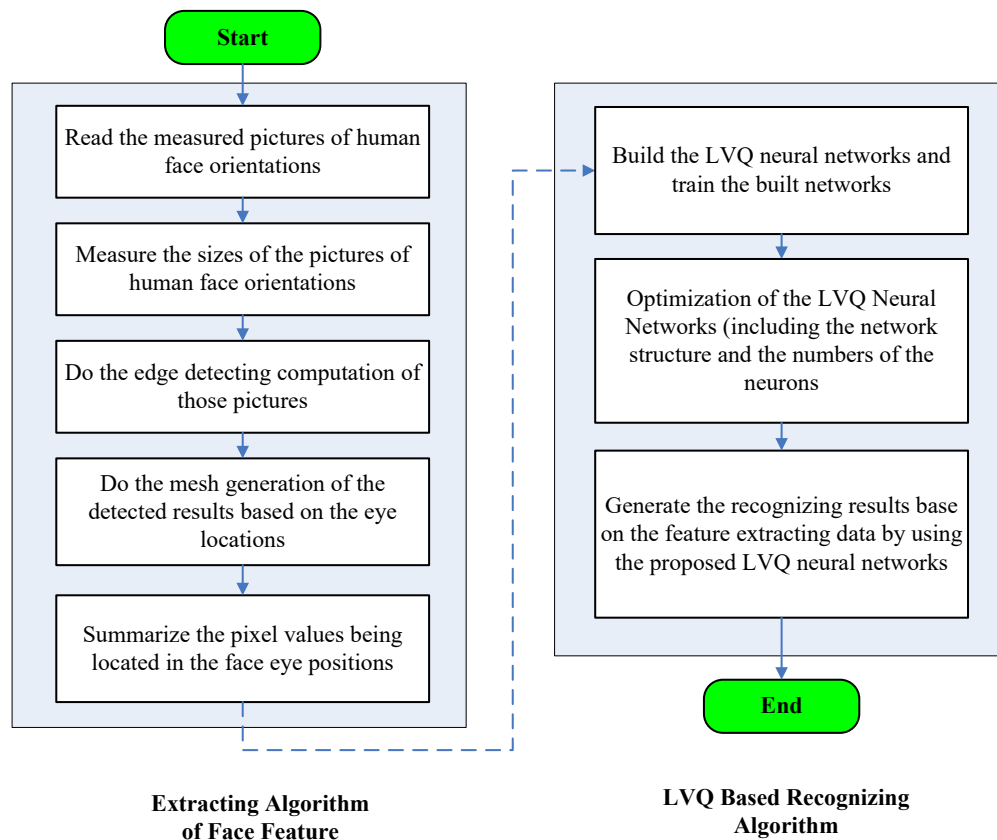


Figure 4-5: Workflow of the proposed face orientation feature-recognizing algorithm [227]

## 4.4 Gesture based Collision Avoidance

The proposed gesture HRI based collision avoidance method is illustrated in Fig. 4-6. From Fig. 4-6, the proposed method can be explained as follows: **(a)** as presented in

Section 4.2, the Microsoft Kinect sensors [223]–[227] are used to recognize the real-time gestures of laboratory personnel. Besides the dynamic gestures, the human skeletons are also measured. The Kinect sensors will firstly find the around people skeletons in the camera view then secondly capture the gestures' behaviors based on their hand skeletons; **(b)** the Support Vector Machine (SVM) is built to recognize the gesture orientations and its corresponding movements; and **(c)** to have high-quality RHI controlling performance, all the parameters (*including the gesture enable conditions, the gesture moving degrees/angles and the selected master*) affecting the face recognition results are all considered. By considering both of the simplicity and the explicitness of the gesture commands, in the proposed method seven gesture orientations are defined, which includes the dual-hand down, the dual-hand up, the left-hand open, the left-hand up, the right-hand open, the right-hand up and the dual-hand open. The corresponding robot controlling commands of these defined gesture behaviors are provided, which can be found in Table 4-1.

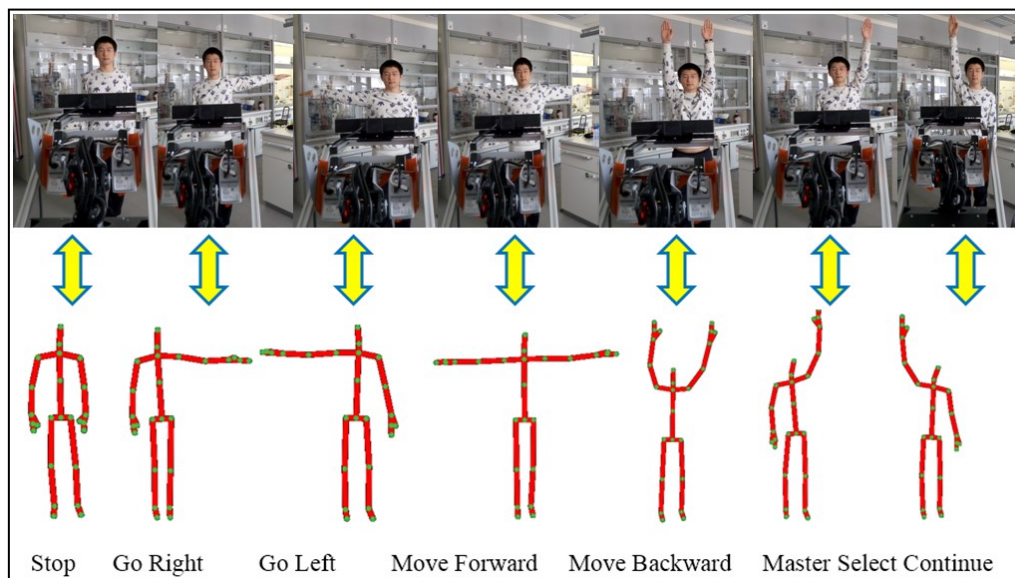


Figure 4-6: Seven gesture definitions

Table 4-1 The defined controlling commands based on the dynamic gestures

Behavior of Gesture	Robot Command Type	Model Type ID
Dual-hand Up	Move Backward	INT 1
Dual-hand Down	Stop Running	INT 2
Dual-hand Open	Move Forward	INT 3
Left-hand Up	Master Selection	INT 4

Left-hand Open	Go Left	INT 5
Right-hand Up	Continue/Keep Running	INT 6
Right-hand Open	Go Right	INT 7

## 4.5 Modeling of the Embedded Algorithms

### 4.5.1 Modeling of LVQ Neural Network

Learning Vector Quantization (LVQ) is a prototype-based supervised classification algorithm in control theory, which was invented by scientist *T. Kohonen* [228]–[233]. It is a supervised learning approach of vector quantization. The LVQ neural network is a standard input-forward neural network with the LVQ learning. The LVQ neural networks have unequalled performance in the classifications of nonlinear and random phenomenon [234]–[239]. A LVQ network has three layers as shown in Fig. 4-7, the inputting one, the competitive one and the outputting one. The competitive layer classifies the inputting vectors in a way which is the same as the competitive layers of clusters with SOM (*Self Organizing Map*) Neural Networks [240]–[244].

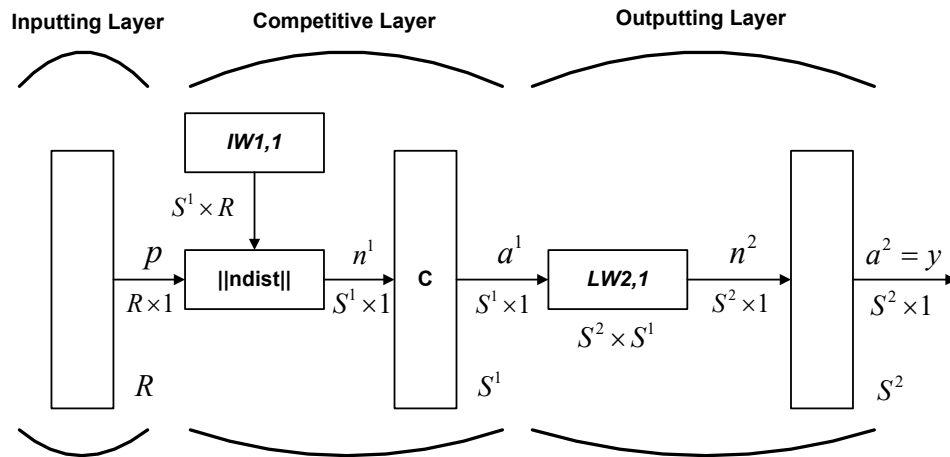


Figure 4-7: Architecture of the LVQ neural network [227]

In the LVQ neural networks, there are two computational procedures, the LVQ1 and the LVQ2. In this paper, to expedite the computational process to get satisfactory real-time performance for the running robotic systems, the LVQ1 is selected, with the following steps as [227][245]:

**Step (a):** Initialize the original network weights  $\omega_{ij}$  and the learning rate  $\eta$ ;

**Step (b):** Load the inputting vectors  $X$  to the network, and calculate the distances between the inputting vectors and the neurons of the competitive layer based on the following equation as:

$$d_i = \sqrt{\sum_{j=1}^R (x_j - \omega_{ij})^2}, i = 1, 2, \dots \quad (Eq. 4-1)$$

**Step (c):** Select the minim distance among the results attained in *Step (b)* and record the corresponding classification labels in the outputting layer as  $C_i$ .

**Step (d):** Compare the classification labels  $C_x$  from the inputting layer with the recorded labels in *Step (c)*. If they are equal, the following equation (4-2) will be used to adjust the network weights. Otherwise, the equation (3) will be chosen.

$$\omega_{ij-new} = \omega_{ij-old} + \eta(x - \omega_{ij-old}) \quad (Eq. 4-2)$$

$$\omega_{ij-new} = \omega_{ij-old} - \eta(x - \omega_{ij-old}) \quad (Eq. 4-3)$$

In the chapter, the LVQ is built as shown in Fig. 4-8. As given in Fig.4-8, the built LVQ neural network model includes three layers, the inputting layer, the hidden layer and the outputting layer. The inputting layer is proposed to load the selected human face features, the outputting layer is presented to generate the decided face orientations and the hidden layer is built to find the nonlinear relationships between the inputting neurons and the outputting neurons. The structure of the built LVQ model can given in details as follows: **(a)** the human face real-time images captured real-time face images captured by the Kinect sensors will be divided into six rows and eight columns. The numbers of the grid rows and columns can be changed based on the different interacting situations; **(b)** the locations of the selected face features (e.g., *the eyes, the eyebrow, the nose, etc*) are extracted. In summarized edge-processing pixels of these obvious face features' locations will be loaded into the inputting layer of the LVQ model. There are eight neurons in the inputting layer; and **(c)** there are one neuron in the outputting layer, which represents five different results of face orientations.

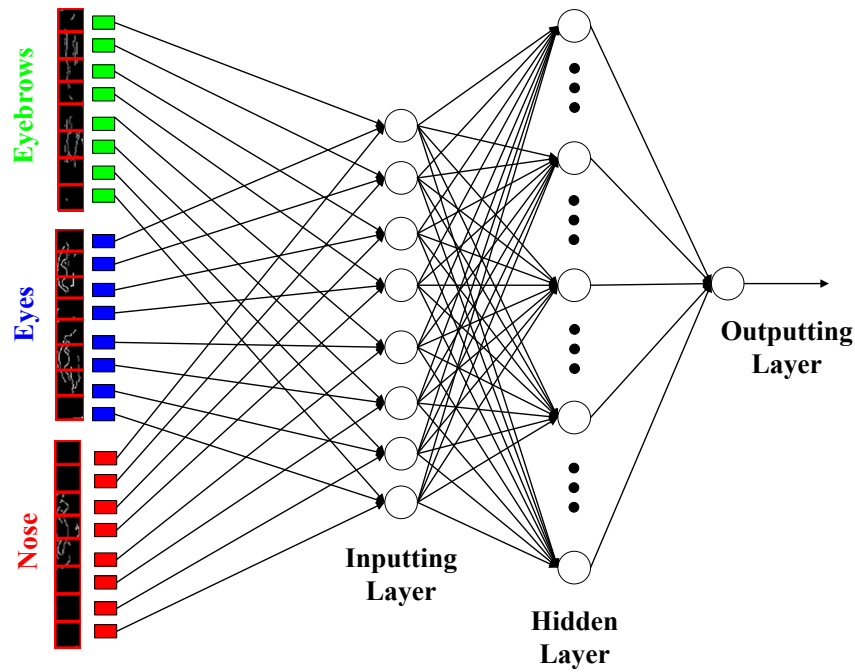


Figure 4-8: The built LVQ model

### 4.5.2 Modeling of Support Vector Machine

Support Vector Machine (SVM) is a supervised learning algorithm based on the notion of structural risk minimization strategy, firstly developed by scientist Vladimir N. Vapnik [5], which is proposed for the classification and regression of nonlinear data. By mapping the sampling space into a high dimensional space (*such as, the Hilbert space*), the SVM algorithm can convert a nonlinear separable problem in the sample space to a linear separable problem, which avoids the over-fitting phenomenon in the traditional machine learning algorithms [183][233]. The concept of the SVM classification is given in Fig. 4-9.



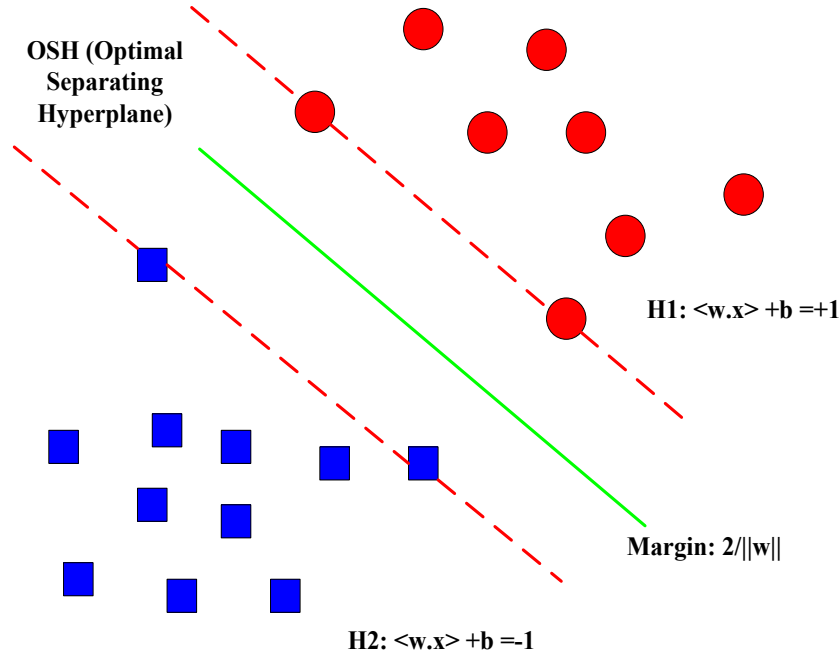


Figure 4-9: Architecture of the SVM algorithm

For an inputting data/images, the classification definition can be completed using the equation as follows [246]:

$$f(x) = \text{sign}(\langle \omega^* \cdot x \rangle + b^*) \quad (\text{Eq.4-4})$$

Given a dataset series  $\chi = \{(x_i, y_j)\}$ , if the OSH cannot be constructed in the inputting space, the improved nonlinear SVM will firstly maps the modeling data from the inputting space into the high dimensional feature space using the following mapping equation as:

To maximize the margin, the primal definitions are given as [246]:

$$\Phi: R^N \rightarrow R^M, M \gg N \quad (\text{Eq.4-5})$$

$$\text{Minimize} \quad \frac{1}{2} \|\omega\|^2 + C \sum_{i=1}^n \xi_i \quad (\text{Eq.4-6})$$

Where  $\xi_i$  is the error impacting for the mislabeled examples,  $C$  is the positive error weighting parameter which determines the trade-off between the maximal margin and the training error minimization.

$$\begin{aligned} \text{Subject to } & y_i(\langle \Phi(x_i), \omega \rangle + b) - 1 + \xi_i \geq 0, \\ & (\xi_i \geq 0, i = 1, 2, 3, \dots) \end{aligned} \quad (\text{Eq.4-7})$$

$$\text{Maximize } L_D(\alpha) = \sum_{i=1}^n \alpha_i - \frac{1}{2} \sum_{i,j=1}^n \alpha_i \alpha_j y_i y_j K(x_i, x_j) \quad (\text{Eq.4-8})$$

$$\begin{aligned} \text{Subject to } & 0 \leq \alpha_i \leq C \quad i = 1, 2, \dots \\ & \sum_{i=1}^n \alpha_i y_i = 0; \end{aligned} \quad (\text{Eq.4-9})$$

Additionally, the most common kernel functions needed in the SVM algorithm are also provided as follows [246]:

✧ *Polynomial based Classifier:*

$$K(x, x_i) = (x^T x_i + 1)^d \quad (\text{Eq.4-10})$$

✧ *Radial Basic Function based Classifier:*

$$K(x, x_i) = -\exp(\|x - x_i\|^2) / 2\sigma^2 \quad (\text{Eq.4-11})$$

✧ *Multi-Layer Perceptron based Classifier:*

$$K(x, x_i) = \tanh(x^T x_i - \Theta) \quad (\text{Eq.4-12})$$

## 4.6 Experiments and Analysis

### 4.6.1 Face based Strategy

An experiment is provided to validate the performance of the proposed face based strategy. The experiment executes the following contents: **(a)** select fifty random Kinect sensor based measured images to build the LVQ model; **(b)** use the following fifty images to verify the performance of the established LVQ model; **(c)** as mentioned in Section 4.3, the most popular edge detection algorithms in the image processing field are included in the recognizing comparison; and **(d)** since the proposed algorithm is expected to be applied in the running robotic systems, the model elapsing times of different models' computation are also investigated. As shown in Fig. 4-10, the

eye-eyebrow hybrid zones in the face image are abstracted as the recognizing features.

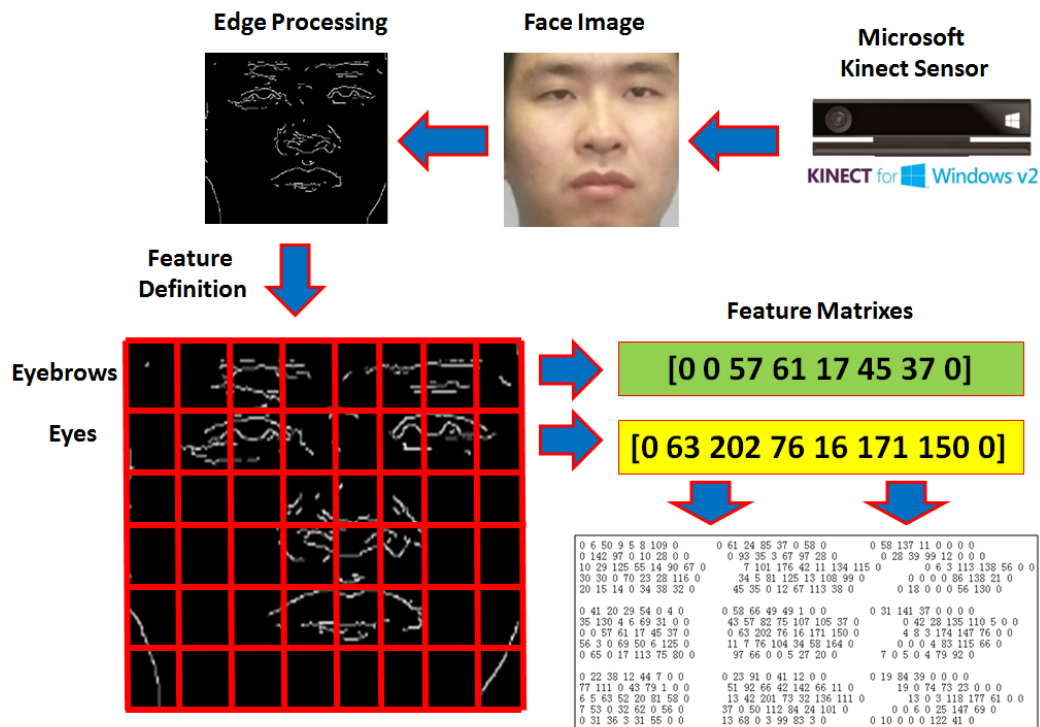


Figure 4-10: Procedures of the human face orientation & moving recognition for the robots

In this experiment, mostly all edge detecting algorithms are included to make a performance comparison in the LVQ model, including Sobel algorithm [247]–[250], Prewitt algorithm [251], [252], Roberts algorithm [253], [254], Log algorithm [255]–[257], Zero-cross algorithm [258]–[262] and Canny algorithm [263]–[266]. The calculated results with different edge detecting algorithms in the built MLP network are provided in Fig. 4-8. Based on the results displayed in Fig. 4-11, the final successful rates and model consuming times are concluded as given in Tables 4-2 and 4-3. From Tables 4-2 and 4-3, it can be seen that: **(a)** the proposed intelligent face orientation and moving recognition method using the eyebrow-eye features and the LVQ neural networks works very effectively; and **(b)** the Prewitt algorithm is the best in the edge detection calculation for the LVQ neural network based human face orientation recognition, by considering either the recognition accuracy 99 % or the real-time performance 3.17 s.

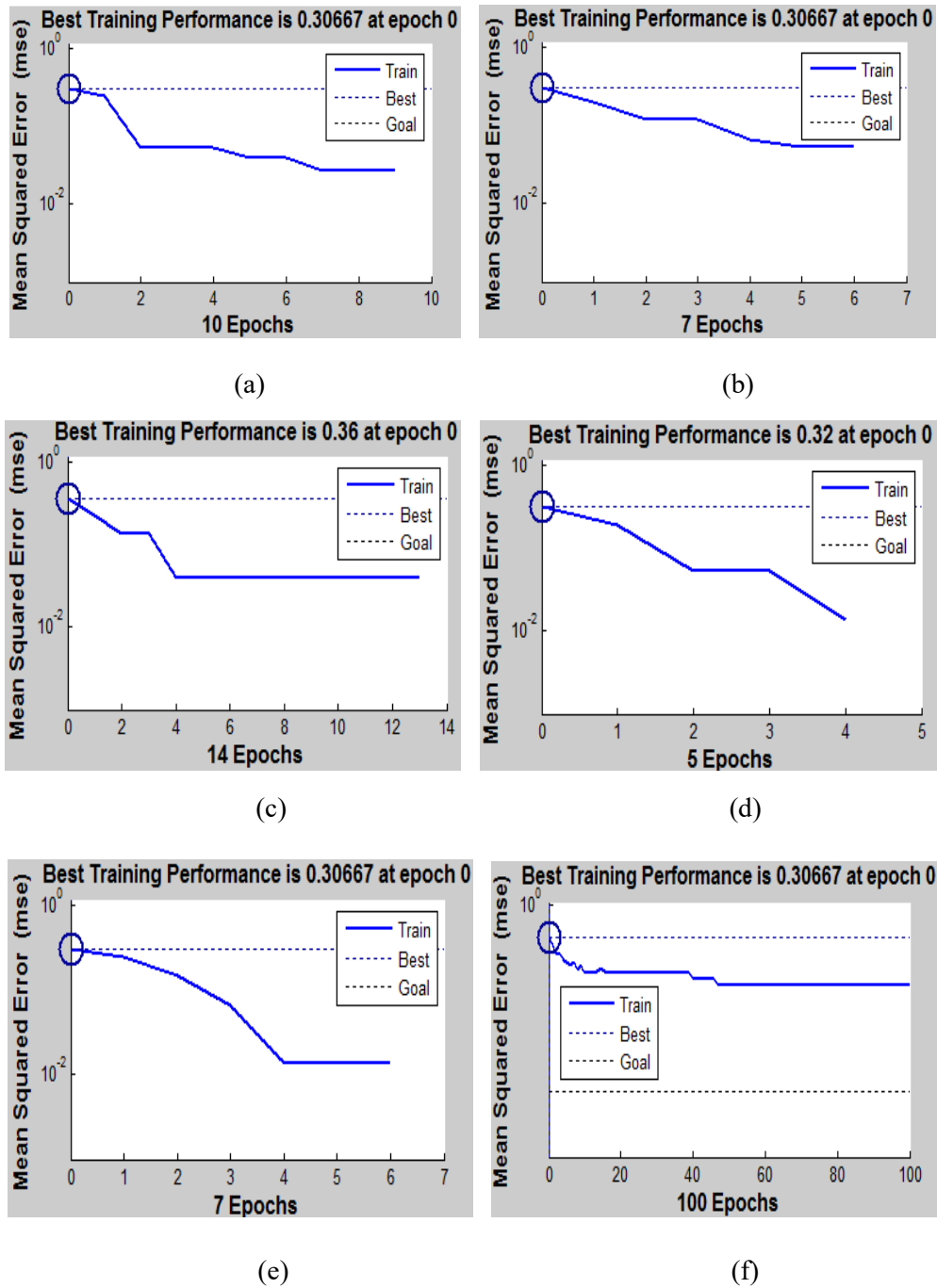


Figure 4-11: Training performance of the proposed recognizing approach by different edge detection algorithms: (a) Sobel algorithm; (b) Prewitt algorithm; (c) Roberts algorithm; (d) Log algorithm; (e) Zero-cross algorithm; and (f) Canny algorithm

Table 4-2 Successful rates of the proposed LVQ based recognizing approach by different edge detection algorithms

Sobel Algorithm	Prewitt Algorithm	Roberts Algorithm
94%	<b>99%</b>	98%
Log Algorithm	Zero-cross Algorithm	Canny Algorithm
97%	94%	79%

Table 4-3 Consumed times of the proposed LVQ based recognizing approach by different edge detection algorithms

Sobel Algorithm	Prewitt Algorithm	Roberts Algorithm
3.581520 s	<b>3.171716 s</b>	3.250973 s
Log Algorithm	Zero-cross Algorithm	Canny Algorithm
4.912319 s	4.863001 s	18.176525 s

#### 4.6.2 Gesture based Strategy

An experiment is also made to examine the performance of the proposed gesture based strategy. The experiment includes the following contents: **(a)** similar to the face based strategy, the built models need to complete the training procedures fast so that their real-time performance can be guaranteed. Once the models are trained/calibrated, they can cope with the real-time processing of the captured human feature images (*including the face images and the gesture images*); **(b)** the gesture samples from four people with different heights are included in distance [1,4] meters. Also for one gesture command, 16 samples are taken from every person so that there are  $7 \times 16 = 112$  samples for every person. Thus, the total training gesture data will reach 448 groups; and **(c)** in each gesture sample, four hand locations are involved, which includes the left wrist, the right wrist, the left elbow and the right elbow. Since it is possible the controlling personal will face the robots straightly, the training samples will have different angles range  $[-40^\circ, 40^\circ]$ .

In the SVM computation, the error weighting parameter ‘C’ is critical. To select the best parameter ‘C’, different selecting values are also compared in the experiment, with the results given in Table 4-4. As shown in Table 4-4, it can be seen that the values of  $C \geq 0.367$  have the minimum average errors and can reach the satisfactory classifying level of 99.78%.

Table 4-4 Experimental results of the built SVM to select the best ‘C’ parameter

Parameter ‘C’	Number of Errors	Average Error
$[2 \times 10^{-9}, 0.049]$	3	0.0067
0.135	2	0.0044
$> 0.367$	1	0.0022

Based on the decided SVM model, the successful rate performance of the developed gesture based strategy is obtained in Table 4-5. From Table 4-5, it can be found that the proposed new gesture based collision avoidance method is effective. Additionally, the real-time experiment of the proposed gesture based collision avoidance strategy using the SVM algorithm is also made and the experimental results show that all kinds of the gesture recognition can be completed in one second.

Table 4-5 Experimental results of the built SVM for the gesture based collision avoidance

ID	Distance between the closest person and the robot	Success Rate
1	2 m	96.8%
2	3 m	96.8%
3	4 m	96.8%

## 4.7 Developed Controlling GUI

In this chapter, the controlling GUIs for the face based collision avoidance and the gesture based one have been developed successfully as demonstrated in Fig. 4-12 and Fig. 4-13, respectively.

As shown in Fig. 4-12, the face GUI has the following functions as: **(a)** all of laboratory around the robots are detected and their face features are recognized. At the same time, the recognizing results of the face orientations and the moving directions are both provided in the GUI; and **(b)** to let the defined recognizing parameters can be adjusted conveniently by the users in different situations, the GUI provides the adjusting bars for different recognizing parameters, which include the face orientation angle parameter, the face moving velocity parameter, the robot safety distance parameter and the face sensitivity parameter. All of these embedded parameters are proposed to match different person's natural behaviors.

As shown in Fig. 4-13, the gesture GUI has the following functions as: **(a)** all of laboratory around the robots are detected and their body-skeletons are recognized. At the same time, the recognizing results of the gesture behaviors will be given in sound through the robot on-board laptops; and **(b)** to let the users monitor the recognizing results conveniently, the GUI also shows the detailed SVM matching values and the currently active gesture commands. In addition, the same to the face GUI, the gesture GUI also displays the communication socket status and the sending robot controlling

protocols to the remote controller (*i.e.*, the RBC).

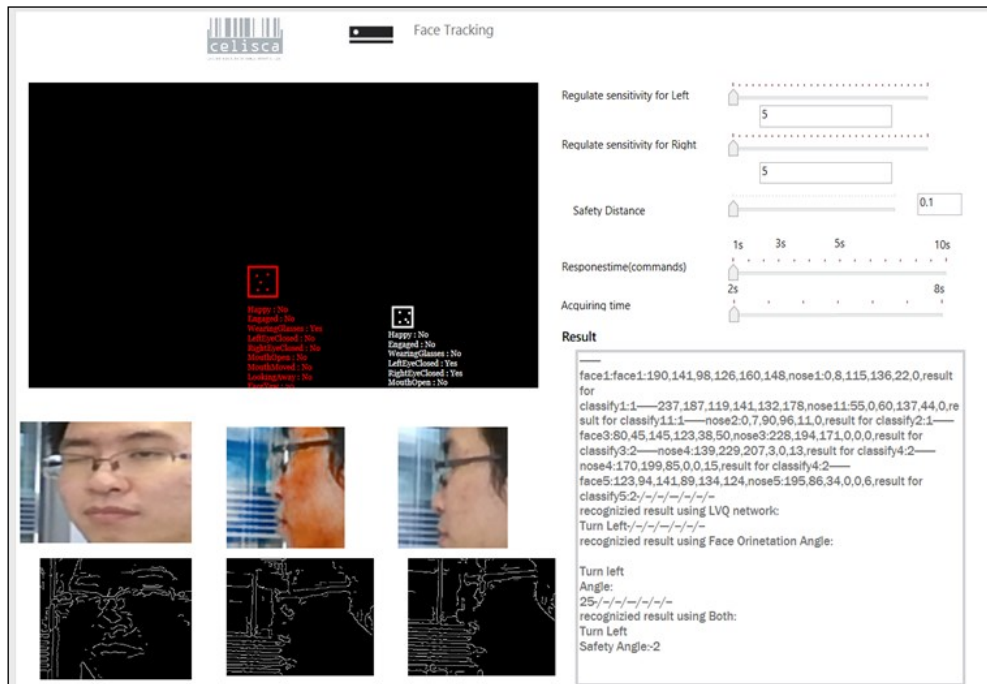


Figure 4-12: Face moving recognition GUI [267]

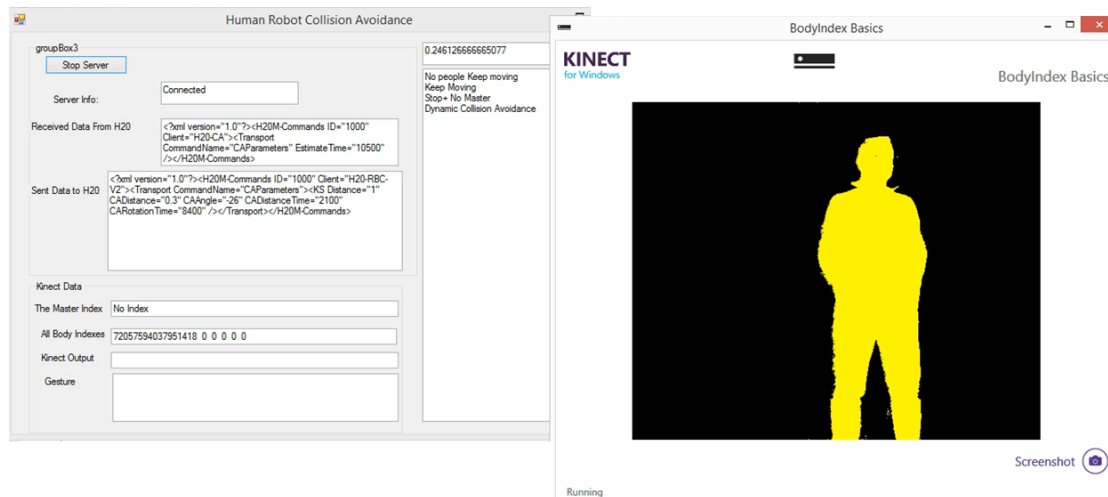


Figure 4-13: Gesture controlling recognition GUI

# Chapter 5 Intelligent Robot Power Forecasting

## 5.1 Introduction

Since the mobile robots need on-board batteries to go different areas for various tasks, the performance of the power recharging is one of the most important contents in the indoor mobile robotics [268]–[272].

This chapter focuses on the power management and optimization for the long-distance mobile robot transportation. In the issue, some important work has been published. *Mathew et al.* studied a multi-robot scheduling issue that the autonomous Unmanned Aerial Vehicles (UAVs) got effective recharging during the long run times [273]. The proposed method was to map the expected 3D UAV flight trajectories into a group of partial ground recharging zones, then the intelligent strategy was adopted to schedule and plan the real recharging paths with the minimum cost required. *Luo et al.* designed an innovative multiple sensor based fusing method to locate the poses of the mobile robots for the high-precision recharging [274]. *Vaughan et al.* proposed a new method using an autonomous robot as the automated dock to improve the successful rate of the recharging by the running mobile robots. The results given in their paper showed this special approach was very effective for the multiple mobile robots because it did not request many recharging positions [275]. *Su et al.* developed a safe self-diagnosis philosophy of the auto-recharging procedure for the mobile robotics. The contribution of their work was also to improve the docking accuracy and the recharging successful rate [276]. *Keshmiri et al.* presented an opportunistic control strategy to cope with the problem of the multiple robots and multiple recharging locations, which combined both of the centralized and the distributed methodologies [277]. *Mathew et al.* used the map theory to investigate the possibility and efficiency of the path planning computation for the robotic recharging. In the work, the authors considered the



recharging as a traveling salesman problem by searching for the shortest recharging path [278]. *Liu et al.* proposed a new application to select the best locations for the recharging stations in laboratory environments considering both of the transportation distances and the task intensities. An improved Artificial Immune Algorithm (AIA) had been presented to handle this application. The results in the paper demonstrated the best recharging positions can be optimized in a short time by adopting the proposed strategy [279]. From the upper literature reviewing, it indicates that there are already many attentions taken by the scientists in those topics (*including power measurement, recharging control, recharging station design & optimization, etc.*), but there is still no publication and realization on the tracking and predicting of the robots' real-time power for the mobile robot transportation. This issue is the focus of this paper.

In the power control for the indoor mobile robots, there are several important considerations as follows: **(a)** The effective recharging is important for any kinds of mobile robotic systems. This issue has been solved by our group in reference [279] and the details of the recharging procedures of the mobile robots are also provided in that paper; **(b)** The scientific distribution of the installed recharging stations is the second important consideration to develop an indoor mobile robot transportation system. One of the solutions is also proposed by our group by using the AIA in reference [279]. In our solution, both of the distances between the robots and the stations and the numbers of tasks are considered to select the best installing positions of the recharging stations; and **(c)** besides the upper two standard aspects of the robot power controlling, there is also a very essential and interesting scientific topic. That is how to utilize the corrected robot power data to improve the robot transportation performance, which content is the contribution of this chapter.

As explained in Chapter 2, in the IMRTS system the RRC will select the best mobile robot for a coming PMS transportation request based on either the distance standard or the power standard. In the power standard, the RRC will calculate all the connected mobile robots' current voltages and find the highest one for the transportation task. It means the robot having the highest accumulated power voltage will be selected. This simple strategy has been generally used in the mobile robotics. However, we find that this strategy has a big disadvantage. If the RRC only utilizes the current voltages, it does not know how long the selected voltage can last. Additionally, since the power parameter is one kind of non-stationary signals, it is so dynamic that it is impossible to use the linear methods to estimate the future power. Based on this consideration, the

mobile robot power forecasting is requested. If the robots can forecast their own on-board powers, they can decide whether to accept a coming task smartly.

## 5.2 Power Measurement System

The robot power measurement GUIs in the IMRTS system are given in Fig. 5-1.

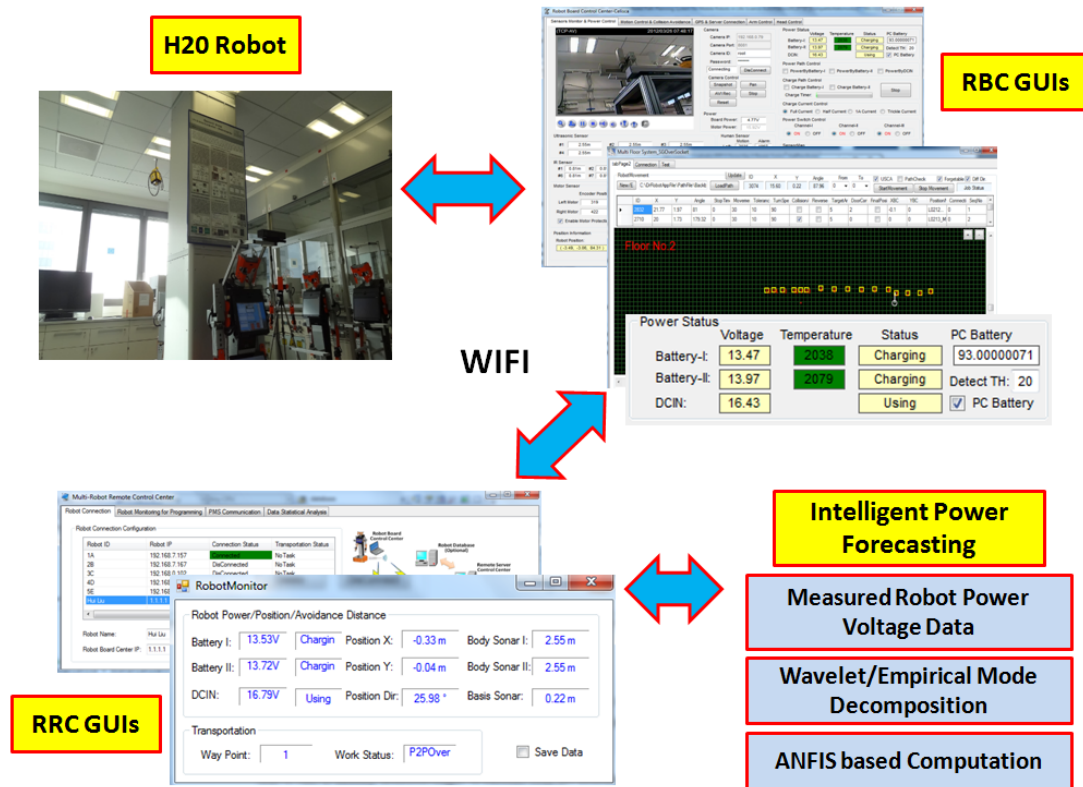


Figure 5-1: Robot power measurement GUIs

As shown in Fig. 5-1, the robot power measuring and forecasting processes can be explained as follows:

- The GUIs of the robot on-board controller (*i.e.*, the *RBC*) measure the two groups of robot inside batteries and send the measured raw data to the corresponding remote controller (*i.e.*, the *RRC*) through the WiFi communication.
- Once the *RRC* receives the robot power data from the connecting *RBCs*, it will start to decompose the raw robot power data and calculate their corresponding forecasting values.
- In the *RRC*, there is a robot power forecasting component embedded. The component adopts two signal processing algorithms (*i.e.*, the *wavelet decomposition*

and the empirical mode decomposition) to decompose the originally measured robot power data and use the built ANFIS model to complete the real-time forecasting computation.

### 5.3 Robot Power Forecasting Method

#### 5.3.1 Hybrid Forecasting Algorithm

A new hybrid forecasting method is proposed to predict the mobile robots' on-board power status by combining two popular signal processing theories (*i.e.*, the wavelet theory [280]–[285] and the empirical mode decomposition theory [286]–[291] ) and the ANFIS neural networks [292]–[297], as given in Fig. 5-2.

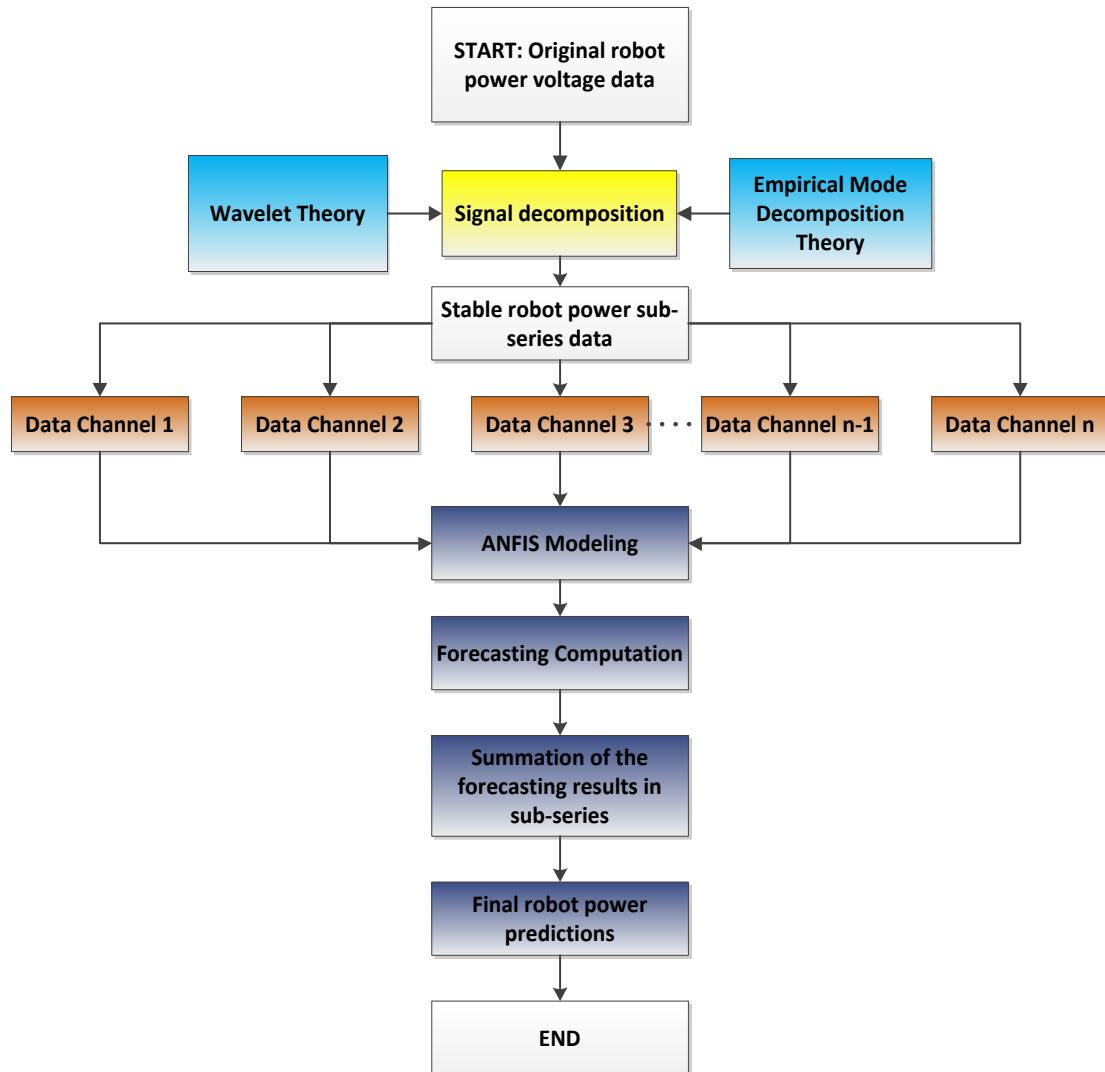


Figure 5-2: The proposed hybrid mobile robot power forecasting framework

As shown in Fig. 5-2, the proposed forecasting strategy is explained as follows: **(a)** since any power signal is non-stationary, two signal decomposing methods are adopted to decrease the instability of the raw mobile robot power voltage data. The purpose of the signal decomposition is to change the raw robot voltage data into a number of sub-channel data; **(b)** building the corresponding ANFIS based power forecasting models for all the sub-channel power data and completing the multi-step ahead predicting computation; and **(c)** summarizing the forecasting results in every sub-channel to obtain the final results to the original signal series. The forecasted results are adopted to select the best mobile robot and make the transportation decisions.

### 5.3.2 Original Robot Power Sampling Data

To validate the proposed robot power forecasting method, in this chapter a group of the really measured robot power voltages are used in the forecasting experiments, as given in Fig. 5-3. The former 1<sup>st</sup>-600<sup>th</sup> power voltage data will be given to establish the different kinds of models (*including the proposed EMD-ANFIS method, the proposed WD-ANFIS method, the standard MLP model and the standard ANFIS model*) and the latter 601<sup>st</sup>-800<sup>th</sup> data will be loaded into the built various models for checking the real performance.

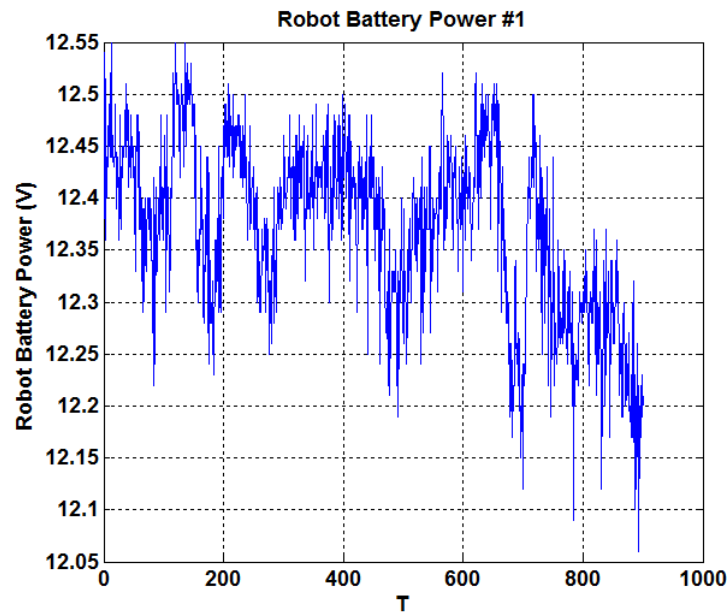


Figure 5-3: Measured robot power voltage data from a H20 mobile robot

### 5.3.3 Wavelet Decomposition of Mobile Robot Power Data

Wavelet method is one of the most effective signal decomposing algorithms [298]–[300]. Suppose  $X(t)$  is the original non-stationary signal, the wavelet decomposition of  $X(t)$  can be given as:

$$X_{\omega}(a, b) = \frac{1}{|a|} \int_{-\infty}^{+\infty} x(t) \bar{\psi}\left(\frac{t-b}{a}\right) dt \quad (Eq.5-1)$$

where the  $\psi(t)$  is mother wavelet, the ' $a$ ' is the scale controlling parameter and the ' $b$ ' is the position controlling parameter.

The rebuilding process of the  $X(t)$  after the decomposition can be illustrated as:

$$x(t) = C_{\psi}^{-1} \int_{-\infty}^{+\infty} \int_{-\infty}^{+\infty} \frac{1}{a^2} X_{\omega}(a, b) \psi\left(\frac{t-b}{a}\right) da db \quad (Eq.5-2)$$

where:

$$C_{\psi} = \int_{-\infty}^{+\infty} \frac{|\hat{\psi}(\omega)|^2}{|\omega|} d\omega \quad (Eq.5-3)$$

By considering the decomposed accuracy and the real-time generating performance, four-layer wavelet decomposition is selected, as demonstrated in Fig. 5-4. Based on this process, the original robot power voltages are decomposed as the results given in Fig. 5-5. As shown in Fig. 5-5, the decomposed sub-channel data are more stable than the original robot power series. In this chapter, the '*Daubechies*' wavelet [301]–[306] has been selected as the mother wavelet during the whole decomposition.

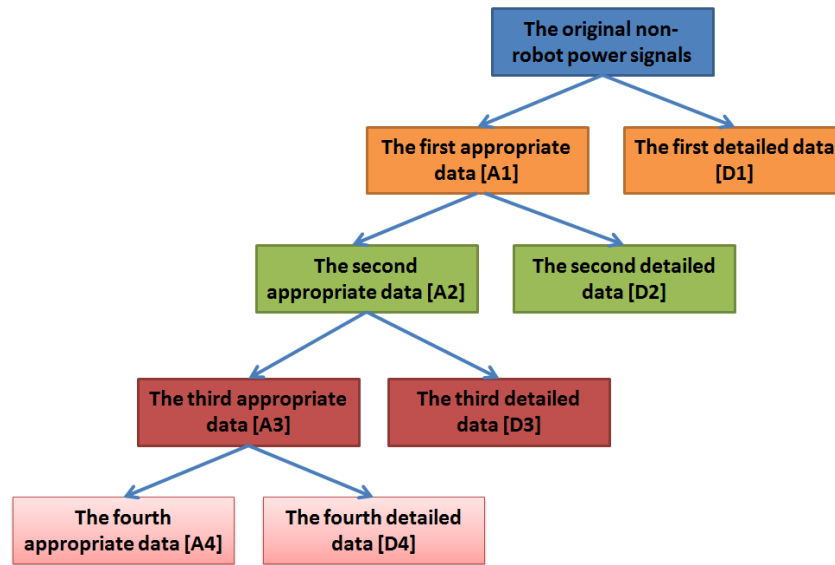
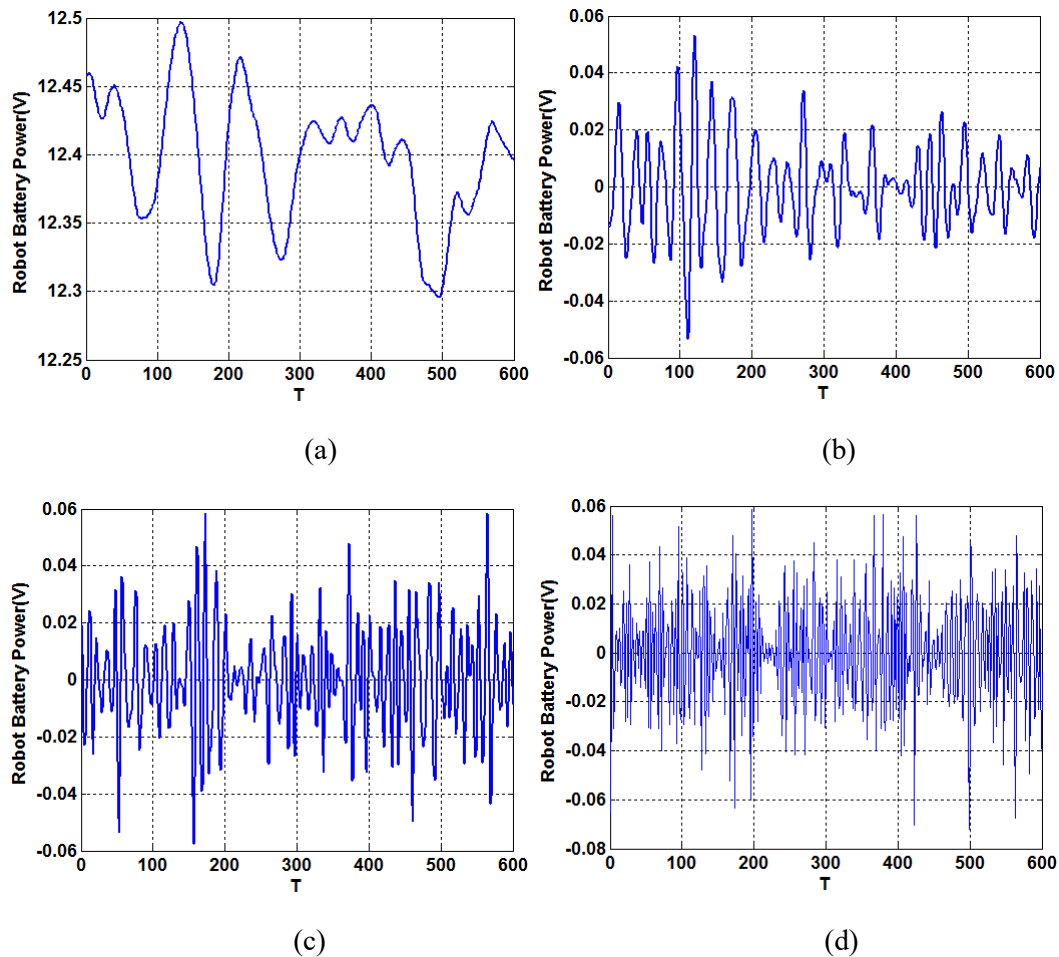
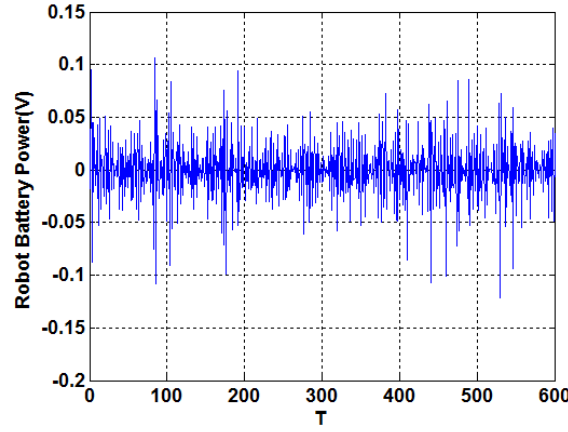


Figure 5-4: Four-layer based wavelet decomposing structure [300]





(e)

Figure 5-5: Decomposed results of the measured robot power data by the WD algorithm: (a) the fourth appropriate sub-layer; (b) the fourth detailed sub-layer; (c) the third detailed sub-layer; (d) the second detailed sub-layer; and (e) the first detailed sub-layer

### 5.3.4 EMD Decomposition of Mobile Robot Power

Empirical mode decomposition (EMD) is a time domain decomposing method, which converts a group of time series into multiple empirical modes, named as Intrinsic Mode Functions (IMF) [307]–[310]. Compared to the WD method, the EMD does not need to choose any parameters by manual in the whole computational process [309], [311]–[313].

The EMD considers any signal  $X(t)$  can be described using the equation as:

$$X(t) = \sum_{i=1}^n C_i(t) + R_n(t) \quad (Eq.5-4)$$

Where  $\{C_i(t)\}, (i=1,2,\dots)$  is the IMF in different decomposition and  $\{R_n(t)\}$  is the residue.

The computational steps of the standard EMD method are illustrated as follows [314]:

**Step1:** Identify all the local extrema of series  $\{X(t)\}$ , including local maxima and local minima.

**Step2:** Connect all the local maxima by a cubic spline line to generate its upper envelop  $\{X_{up}(t)\}$ . Similarly the lower envelop  $\{X_{low}(t)\}$  is made with all local minima.

**Step3:** Compute the mean envelop  $\{M(t)\}$  from the upper and lower envelops as follows:

$$M(t) = [X_{up}(t) + X_{low}(t)] / 2 \quad (Eq.5-5)$$

**Step4:** Extract the details as follows:

$$Z(t) = X(t) - M(t) \quad (Eq.5-6)$$

**Step5:** Check whether  $\{Z(t)\}$  is an IMF: (a) if  $\{Z(t)\}$  is an IMF then set  $C(t) = Z(t)$  and meantime replace  $\{X(t)\}$  with the residual  $R(t) = X(t) - C(t)$ ; (b) if  $\{Z(t)\}$  is not an IMF, replace  $\{X(t)\}$  with  $\{Z(t)\}$  then repeat *Step2-4* until the termination criterion is satisfied. The following equation can be regarded as the termination condition of this iterative calculation:

$$\sum_{t=1}^m \frac{[Z_{j-1}(t) - Z_j(t)]^2}{[Z_{j-1}(t)]^2} \leq \delta \quad (j=1,2,\dots \quad \dots \quad (Eq.5-7)$$

Where  $m$  is the length of signal,  $\delta$  is the terminated parameter, which is usually set as 0.2-0.3, and  $j$  denotes the times of iterative calculation. The  $\delta$  is usually determined by the requirements of application areas.

**Step6:** The procedure of *Step1-5* is repeated until all the IMFs are found.

The EMD decomposing results of the original robot measured power voltage data (see Fig. 5-1) is shown in Fig. 5-6.



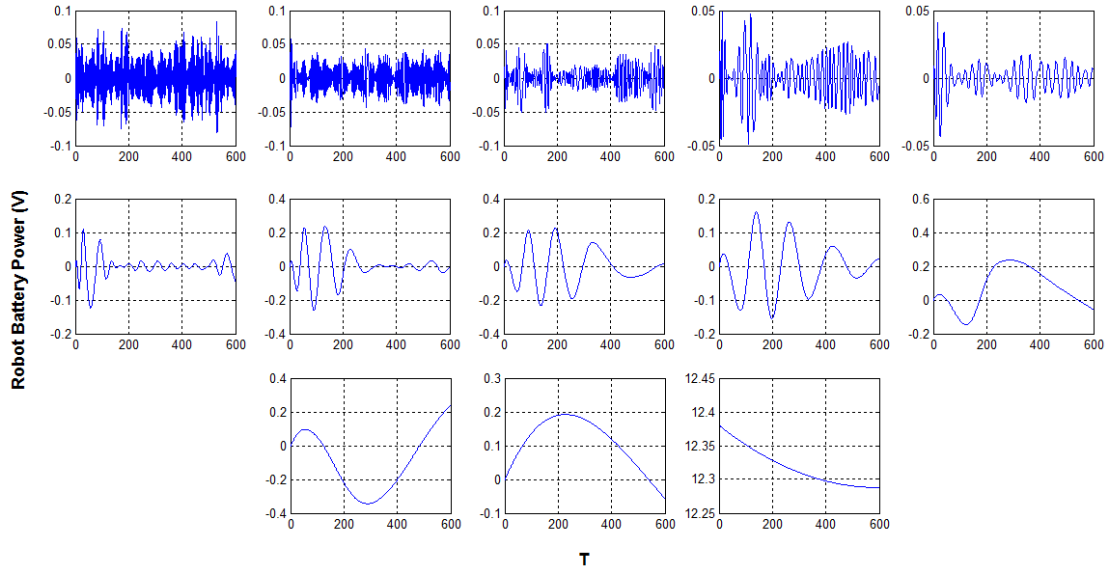


Figure 5-6: Decomposed results of the measured robot power data by the EMD algorithm

### 5.3.5 ANFIS Forecasting Model

Adaptive Neuro Fuzzy Inference System (ANFIS) is a popular signal mining approach in the field of artificial intelligence, combining the fuzzy inference system and the artificial neural networks [315]–[317]. In this chapter, the ANFIS network is adopted as the predictor to forecast the decomposed robot power data in the sub-channels. The frame of the ANFIS is given in Fig. 5-7.

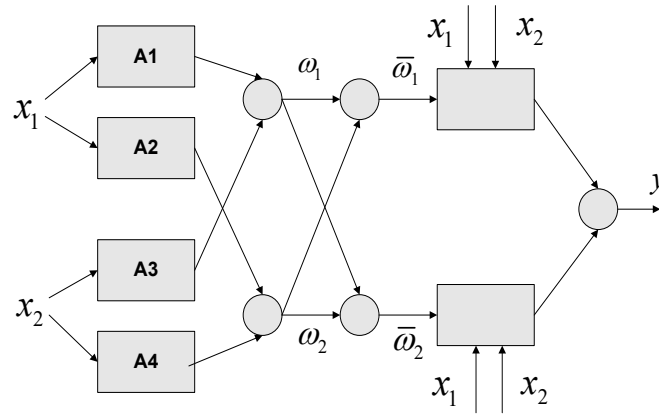


Figure 5-7: Scheme of the ANFIS network [300]

As shown in Fig. 5-7, a standard ANFIS network is comprised of an inputting layer, an outputting layer and several hidden layers. The  $x_1$  and  $x_2$  are the inputting power voltage parameters, the  $y$  is the outputting power voltage parameter, and the  $\omega_1$ ,  $\bar{\omega}_1$ ,  $\omega_2$  and  $\bar{\omega}_2$  are the network weighting parameters.

## 5.4 Experiments and Analysis

To validate the performance of the proposed strategy, a complete experiment for the originally measured robot raw voltage data is provided. The final forecasting results and their corresponding decomposed sub-layer data are illustrated in Figures 5-8~5-13. In addition, the error indexes for all the computational results using different models are also provided in Tables 5-1~5-4.

### 5.4.1 Results of the Hybrid WD-ANFIS Model

From Fig. 5-8 and Table 5-1, it can be analyzed that:

(a) the proposed intelligent WD-ANFIS method forecasts the robot power changing law accurately. The MAE, MAPE and RMSE error indexes of the proposed WD-ANFIS method are only 0.0272 V, 0.22 % and 0.0358 V, respectively. Even at the jumping sampled points, the proposed WD-ANFIS model has satisfactory performance.

(b) the reason for this kind of good performance is because the WD component inside the hybrid processing framework decomposes the originally non-stationary robot power data into the stable sub-layer data successfully so that the corresponding ANFIS component can forecast the decomposed signals precisely. The accuracies for different power zones calculated by the WD-ANFIS method are given in Table 5-2.

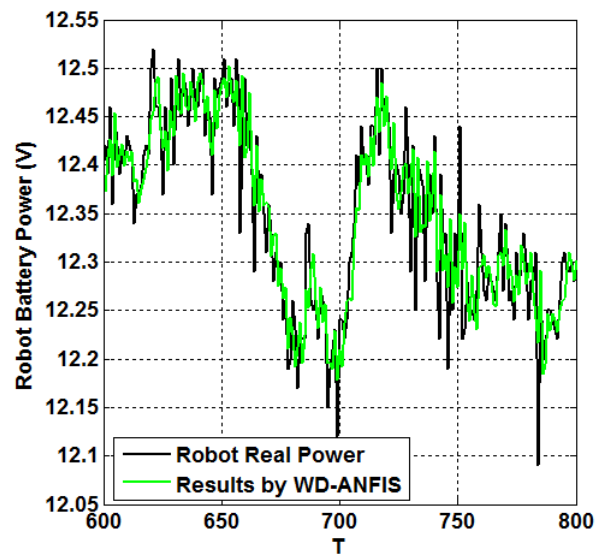
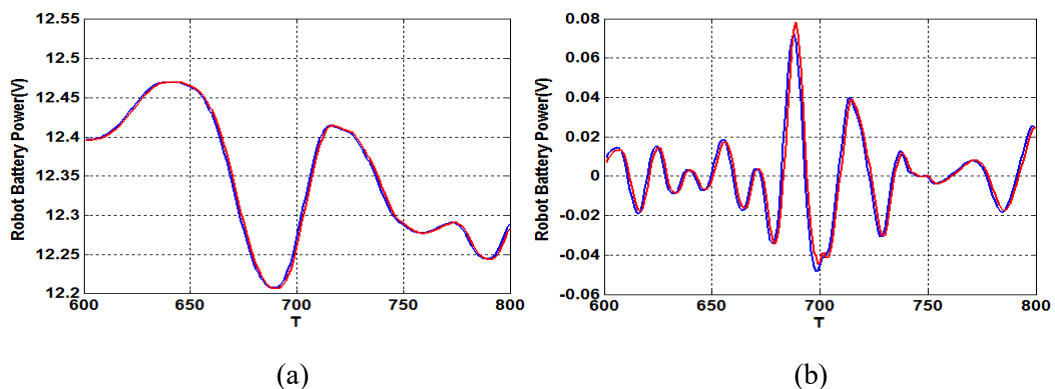


Figure 5-8: Forecasting results for the originally measured robot power data by the proposed hybrid WD-ANFIS method

Table 5-1 The estimated errors of the robot power forecasting results by executing the proposed hybrid WD-ANFIS method

Sampling	Hybrid WD-ANFIS Model		
	MAE (V)	MAPE (%)	RMSE (V)
<b>601<sup>st</sup>-800<sup>th</sup></b>	0.0272	0.22	0.0358
Sampling	Hybrid WD-ANFIS Model		
	MAE (V)	MAPE (%)	RMSE (V)
<b>601<sup>st</sup>-650<sup>th</sup></b>	0.0217	0.17	0.0265
Sampling	Hybrid WD-ANFIS Model		
	MAE (V)	MAPE (%)	RMSE (V)
<b>651<sup>st</sup>-700<sup>th</sup></b>	0.0284	0.23	0.0369
Sampling	Hybrid WD-ANFIS Model		
	MAE (V)	MAPE (%)	RMSE (V)
<b>701<sup>st</sup>-750<sup>th</sup></b>	0.0319	0.26	0.0400
Sampling	Hybrid WD-ANFIS Model		
	MAE (V)	MAPE (%)	RMSE (V)
<b>751<sup>st</sup>-800<sup>th</sup></b>	0.0268	0.22	0.0389

To verify the real performance of the hybrid WD-ANFIS method, the results of the ANFIS based prediction for every wavelet decomposed sub-layers are also illustrated in Fig. 5-9. As shown in Fig.5-9, the following interesting phenomenon can be found as: **(a)** compared to forecast the relatively stable signals, when the sub-signals are jumping or considerably non-stationary, it is more challenge for the ANFIS models to predict them accurately. This feature meets the objective fact; and **(b)** it is important for the ANFIS models to get the accurate forecasting results for the detailed wavelet based components to reach the satisfactory final results, because detailed WD based components have considerable amplitudes. The decomposed sub-layers with low amplitudes will not really affect the forecasting final results.



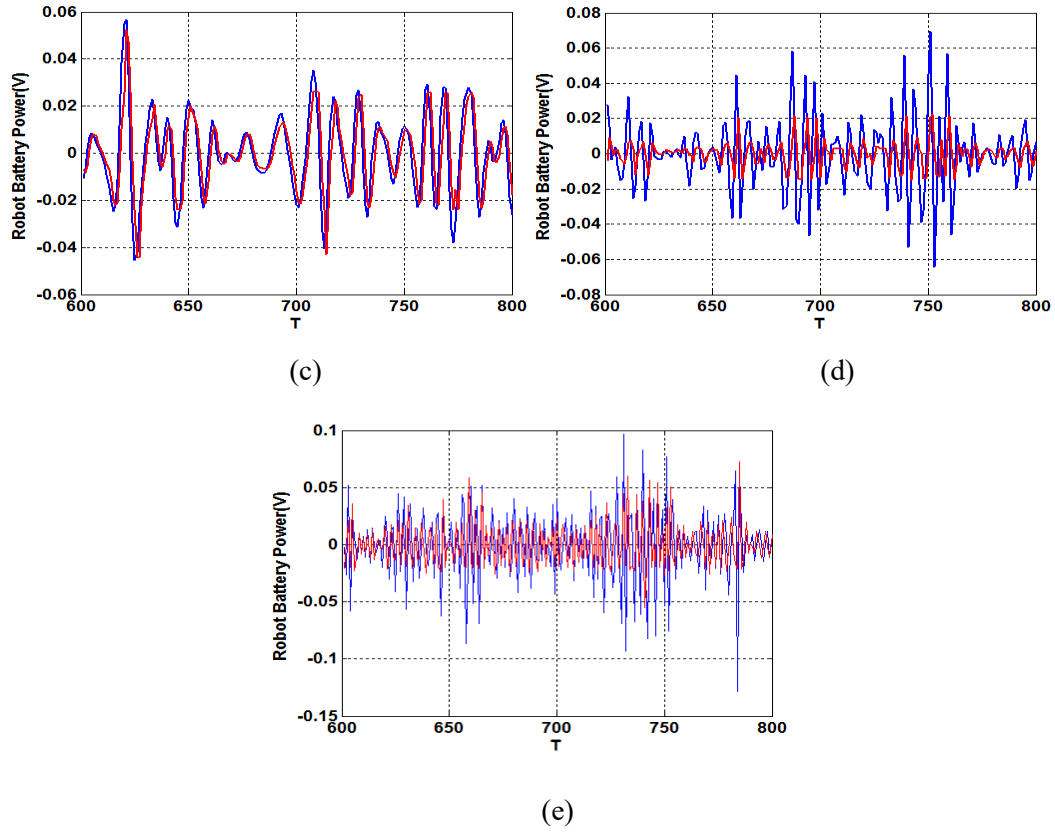


Figure 5-9: Forecasting results for the wavelet based decomposed data by the proposed hybrid WD-ANFIS method: (a) forecasting results of the fourth appropriate sub-layer; (b) forecasting results of the fourth detailed sub-layer; (c) forecasting results of the third detailed sub-layer; (d) forecasting results of the second detailed sub-layer; and (e) forecasting results of the first detailed sub-layer

### 5.4.2 Results of the Hybrid EMD-ANFIS Model

From Fig. 5-10 and Table 5-2, the similar analysis can be made to the ones proposed in Section 5.4.1 as follows: **(a)** the proposed EMD-ANFIS method has high-precision forecasting performance based on the successful combination of the EMD algorithm and the ANFIS model, which proves the signal decomposing algorithms (*including the wavelet decomposition and the empirical mode decomposition*) can improve the performance of the ANFIS neural network directly and considerably; and **(b)** The MAE, MAPE and RMSE error indexes of the proposed hybrid EMD-ANFIS method is only 0.0292 V, 0.24 % and 0.0386 V, respectively.

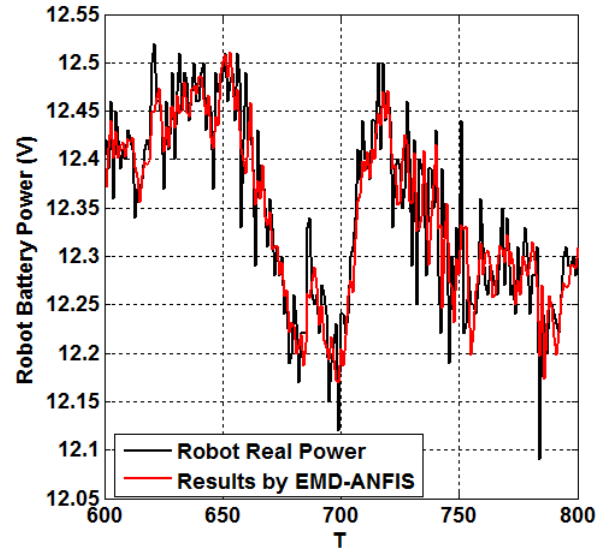


Figure 5-10: Forecasting results for the originally measured robot power data by the proposed hybrid EMD-ANFIS method

Table 5-2 The estimated errors of the robot power forecasting results by executing the proposed hybrid EMD-ANFIS method

Sampling	Hybrid EMD-ANFIS Model		
	MAE (V)	MAPE (%)	RMSE (V)
<b>601<sup>st</sup>-800<sup>th</sup></b>	0.0292	0.24	0.0386
Sampling	Hybrid EMD-ANFIS Model		
	MAE (V)	MAPE (%)	RMSE (V)
<b>601<sup>st</sup>-650<sup>th</sup></b>	0.0212	0.17	0.0272
Sampling	Hybrid EMD-ANFIS Model		
	MAE (V)	MAPE (%)	RMSE (V)
<b>651<sup>st</sup>-700<sup>th</sup></b>	0.0281	0.23	0.0368
Sampling	Hybrid EMD-ANFIS Model		
	MAE (V)	MAPE (%)	RMSE (V)
<b>701<sup>st</sup>-750<sup>th</sup></b>	0.0379	0.31	0.0480
Sampling	Hybrid EMD-ANFIS Model		
	MAE (V)	MAPE (%)	RMSE (V)
<b>751<sup>st</sup>-800<sup>th</sup></b>	0.0294	0.24	0.0404

### 5.4.3 Results of the MLP Model

As shown in Fig. 5-11 and Table 5-3, the standard MLP neural network could not track and forecast the robot power data accurately. Actually, the non-stationary and

nonlinear processing capacities of the MLP network have been proved before. So based on this phenomenon, it can be seen that it is difficult to realize the high-precision of the robot power data due to their jumping & non-stationary features.

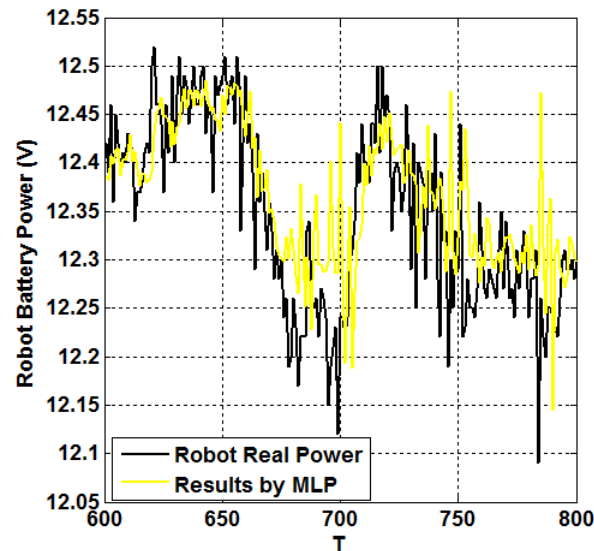


Figure 5-11: Forecasting results for the originally measured robot power data by the proposed MLP neural network

Table 5-3 The estimated errors of the robot power forecasting results by executing the standard MLP neural network

Sampling	MLP Neural Network		
	MAE (V)	MAPE (%)	RMSE (V)
<b>601<sup>st</sup>-800<sup>th</sup></b>	0.0517	0.42	0.0655
Sampling	MLP Neural Network		
	MAE (V)	MAPE (%)	RMSE (V)
<b>601<sup>st</sup>-650<sup>th</sup></b>	0.0298	0.24	0.0385
Sampling	MLP Neural Network		
	MAE (V)	MAPE (%)	RMSE (V)
<b>651<sup>st</sup>-700<sup>th</sup></b>	0.0645	0.53	0.0675
Sampling	MLP Neural Network		
	MAE (V)	MAPE (%)	RMSE (V)
<b>701<sup>st</sup>-750<sup>th</sup></b>	0.0555	0.45	0.0695
Sampling	MLP Neural Network		
	MAE (V)	MAPE (%)	RMSE (V)
<b>751<sup>st</sup>-800<sup>th</sup></b>	0.0570	0.47	0.0660

### 5.4.4 Results of the ANFIS Model

From Fig. 5-12 and Table 5-4, the similar analysis can be made to the ones discussed in Section 5.4.3.

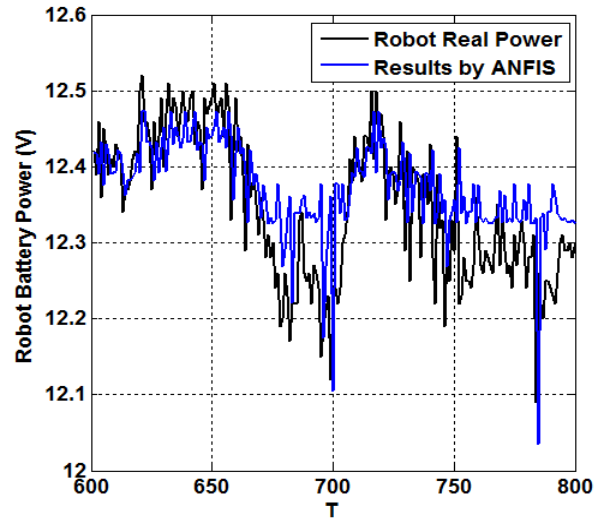


Figure 5-12: Forecasting results for the originally measured robot power data by the proposed ANFIS neural network

Table 5-4 The estimated errors of the robot power forecasting results by executing the standard ANFIS neural network

Sampling	ANFIS Neural Network		
	MAE (V)	MAPE (%)	RMSE (V)
<b>601<sup>st</sup>-800<sup>th</sup></b>	0.0605	0.49	0.0727
Sampling	ANFIS Neural Network		
	MAE (V)	MAPE (%)	RMSE (V)
<b>601<sup>st</sup>-650<sup>th</sup></b>	0.0380	0.31	0.0435
Sampling	ANFIS Neural Network		
	MAE (V)	MAPE (%)	RMSE (V)
<b>651<sup>st</sup>-700<sup>th</sup></b>	0.0722	0.59	0.0785
Sampling	ANFIS Neural Network		
	MAE (V)	MAPE (%)	RMSE (V)
<b>701<sup>st</sup>-750<sup>th</sup></b>	0.0561	0.46	0.0706
Sampling	ANFIS Neural Network		
	MAE (V)	MAPE (%)	RMSE (V)
<b>751<sup>st</sup>-800<sup>th</sup></b>	0.0757	0.62	0.0700

### 5.4.5 Comparison of the Forecasting Results

In the chapter, three error promoting indexes are adopted in the performance experiment, including the PMAE (*Promotion of Mean Absolute Error*), the PMAPE (*Promotion of Mean Absolute Percentage Error*) and the PRMSE (*Promotion of Root Mean Square Error*). The corresponding computational equations are given as below.

*Promotion of Mean Absolute Error (PMAE):*

$$PMAE = \frac{|MAE_1 - MAE_2|}{MAE_1} \times 100\% \quad (Eq.5-9)$$

*Promotion of Mean Absolute Percentage Error (PMAPE):*

$$PMAPE = \frac{|MAPE_1 - MAPE_2|}{MAPE_1} \times 100\% \quad (Eq.5-10)$$

*Promotion of Root Mean Square Error (PRMSE):*

$$PRMSE = \frac{|RMSE_1 - RMSE_2|}{RMSE_1} \times 100\% \quad (Eq.5-11)$$

Table 5-5 is provided to explore the promoting contributions of the adopted WD/EMD algorithms in the hybrid computational strategies. From Table 5-5, the following analysis can be made as:

**(a)** When comparing the proposed WD-ANFIS model with the standard ANFIS model, the PMAE, the PMAPE and the PRMSE in the experiment are 55.04%, 55.10% and 50.76%, respectively. The feature proves that the adoption of the wavelet decomposition inside the robot power control is correct.

**(b)** When comparing the proposed EMD-ANFIS model with the standard ANFIS model, the promoting percentages of the MAE, the MAPE and the RMSE are 51.74%, 51.02% and 46.91%, respectively. The character also indicates that it is feasible to use the empirical mode decomposition in the robot power prediction. The promoting percentages of the empirical mode decomposition to the ANFIS are considerable but not as much as the ones generated by the wavelet decomposition.



(c) When analyzing the performance of the standard ANFIS and the standard MLP in the robot power forecasting experiment, both of them have middle-level accuracies and the MLP model defeated the ANFIS model slightly. The PMAE, the PMAPE and the PRMSE of the MLP model to the ANFIS model are 14.55%, 14.29% and 9.90%, respectively.

Table 5-5 The results of the promoting error indexes among different models for the mobile robot power predictions

WD-ANFIS Model vs. ANFIS Model		
PMAE (%)	PMAPE (%)	PRMSE (%)
55.04	55.10	50.76
EMD-ANFIS Model vs. ANFIS Model		
PMAE (%)	PMAPE (%)	PRMSE (%)
51.74	51.02	46.91
ANFIS Model vs. MLP Model		
PMAE (%)	PMAPE (%)	PRMSE (%)
14.55	14.29	9.90

#### 5.4.6 Real-time Performance of the Proposed ARIMA-KF

To examine the time performance of the involved models applying in the robot power control, an experiment is also provided based on a normal laptop (*CPU Intel i3-2350M 2.3GHz, RAM 6G*), with the results given in Table 5-6. From Table 5-6, it can be seen that both of the proposed WD-ANFIS method and EMD-ANFIS method have satisfactory real-time performance.

Table 5-6 The time performance of the involved different models in the robot power forecasting

Methods	Consuming Time/s
Hybrid WD-ANFIS	3.581885
Hybrid EMD-ANFIS	4.298262
Standard ANFIS	0.716377
Standard MLP	2.120446

# Chapter 6 Robot Arm Manipulator

## 6.1 Introduction

In the robotics, the high-precision arm manipulator is desired [318]–[323]. During the mobile robot transportation, the robots are controlled to distribute zones/rooms to complete different kinds of arm manipulation (*including grasping and placing*).

In the issue of the indoor mobile robot arm manipulation, some important work has been published. *Aoyagi et al.* proposed a precise parameter-calibration method in a kinematic model for a robot arm [257]. A laser tracking system was employed for the calibration process to minimize the manipulating errors, a neural network was built to further decrease the errors and a genetic algorithm based model was put forward to optimize the measuring positions. The results provided proved that the proposed intelligent framework obtained good performance. *Guo et al.* presented a six-joint robotic arm based on PLC controlling component [324]. The proposed robot arm consisted of five servo motors and one pneumatics gripper. The corresponding PLC component was comprised of a controller module, a touch panel, two positioning modules, an inputting/outputting module and five servo amplifiers. The experiments provided in the paper showed that the PLC based programming measure was suitable for designed a robot arm. *Reinbacher et al.* studied the possibility to adopt a Kinect depth camera as the standard robot arm mounted measurement unit. For that purpose, they solved a series of technical problems, including reducing the sensor working distance to a few centimeters, replacing the Laser projector unit by a focusable projector, etc. Their results showed that the Kinect camera was an ideal sensor for the robotic arm recognition and controlling [325]. *Yoo et al.* developed a weight subtask controlling strategy for a redundant robot arm based on the fuzzy theory [326]. In the work, the innovation was to use the fuzzy rules to get the weights of the elements in

the pseudo-inverse then designed a task-space controller to track the desired space trajectory and subtask inputs. The results of an experiment with a seven-degree arm manipulator robot showed the effectiveness of the proposed approach. *Chen et al.* presented a camera version based method for a humanoid robot arm. In the method, besides the normal camera measurement, an extended Kalman filter was developed to adjust the calibration parameters of the cameras dynamically. That proposed method had been applied in the motion controlling of a real robotic arm, and the results showed that the vision controller worked satisfactorily [327]. *Esfandiar et al.* aimed at proposing an optimal ‘position to position’ path planning method for a flexible arm manipulator [328]. For the target, the Harmony Search (HS) based optimizing algorithm was adopted, and the maximum load and minimum transferring time of the manipulator were selected as the target functions during the HS searching process. The findings in the paper indicated that the proposed method was powerful to cope with the nonlinear dynamic features of the manipulator. *Huang et al.* proposed a 3D position controller for a robot arm. In the controller, two CCD cameras were adopted to recognize the shapes of the objects and an inverse kinematics model was utilized to manipulate the robot arm. At the same time, to improve the recognizing accuracy of the CCD framework, a fuzzy based position error compensator was provided [329]. Besides those arm controlling applications, there are also some simulating progresses presented by scientists. *Manigpan et al.* studied a simulation of a 6 DOF articulated robot arm using BP neural network to solve the problem regarding inverse kinematic computation. Their results showed that by adopting the BP mapping the robot arm could move to the target positions very accurately and the average error was only around four degrees [330]. *Lakshmi et al.* proposed an Adaptive Neuron-Fuzzy (ANFIS) approach to plan the joint variables of a 4 DOF selective compliant assembly robot arm. Their works displayed that the ANFIS model improved the accuracy of the kinematic mathematic models considerably [331]. From those upper literatures, it can be concluded that: **(a)** in the arm manipulation, different types of sensors (*e.g., cameras, Kinect sensors, ultrasonic sensors, etc.*) are equipped in the robot arms to measure the environments and the targets; and **(b)** to attain high-precision results, an intelligent computation is always preferred. For example, to adopt the fuzzy algorithm to process the arm trajectory planning computation [293].

In the chapter, there are some special requirements to the arm manipulators of the mobile robots in life sciences, including: **(a)** the arm grasping/placing function meets

various accuracies. In the chapter, two levels of manipulating accuracies are defined, the 2 cm one and the 0.5 cm one. Certainly, the levels of the various accuracies can be extended conveniently; **(b)** the proposed manipulating methods meet the real-time performance request for the robot transportation system; and **(c)** the proposed arm manipulator is economic but robust. For these expectations, two strategies are proposed in this chapter, the blind one and the visual one. In the proposed Blind Arm Manipulator (BAM), a group of ultrasonic sensors are adapted to measure the distances between the arm grasping/placing workstations and the positions of the robots, and an artificial neural network based controller is presented to establish the relationships between the measured distances and the controlling values of the joints of the robot arms. The BAM strategy has many advantages such as the simplicity, the real-time performance and the middle-level accuracy ( $< 2\text{cm}$ ). In the Visual Arm Manipulator (VAM), an Microsoft Kinect Sensor (KS) is equipped with every mobile robot to realize the target recognition and a series of Kinematic Models (KM) is established to calculate the arm trajectory controlling process to complete the arm grasping/placing.

The innovation of the BAM strategy are given as: the BAM presents a new intelligent framework allowing the arm manipulation reach a satisfactory operating level but does not adopt external sensors to increase the development complexity. The innovation of the VAM strategy can also be explained as: compared to the BAM, due to the utilization of the KS, the VAM can reach higher accuracy ( $< 0.5\text{ cm}$ ).

## 6.2 Blind Arm Manipulator (BAM)

Fig. 6-1 demonstrates the framework of the proposed BAM, which contents are given as follows:

- Two robot existent on-board ultrasonic sensors, originally proposed for the function of collision avoidance, are utilized for the blind arms. During the mobile robot transportation process, when a H20 robot arrives at the predefined grasping position, those two ultrasonic sensors will measure two channels of distances between the robot bases and the front automated tables/workbenches.
- To establish the relationship between the ultrasonic distances and the robot arm joint controlling values, an artificial neural network based forecasting strategy is presented. Both of the accuracy and the time performance for the artificial neural network in the robot arm joint mapping and controlling are focused.

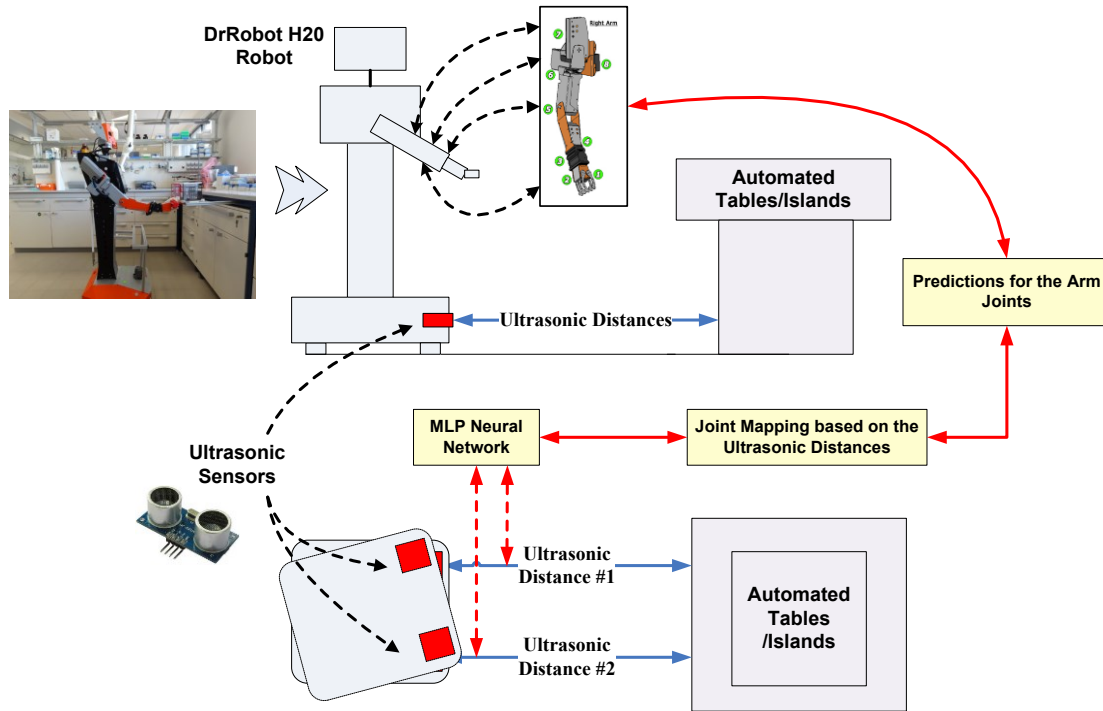


Figure 6-1: Framework of the proposed BAM [332]

In the artificial neural network (ANN) theory, the MLP (*Multiple Layer Perceptron*) neural network is popular due to its excellent nonlinear processing capacity [333]–[338]. By considering the real-time performance required in the robot arm control, a three-layer MLP network is established as illustrated in Fig. 6-2.

As shown in Fig. 6-2, three system levels are included in the proposed BAM arm controller, the measuring level, the computing level and the controlling level. In the measuring level, two H20 robot on-board ultrasonic sensors, which are originally installed for the robotic collision avoidance, are adopted to measure the distances between the robot positions and the front work stations. These measured ultrasonic distances will be sent to the MLP network as the inputting neurons. In the computing level, the MLP neural network is built to compute the robot arm joint controlling values. In the controlling level, the developed robot arm manipulator will adopt the calculated results from the MLP network to control the arm movements. The expected robot arm joint controlling parameter is selected as the MLP outputting neurons.

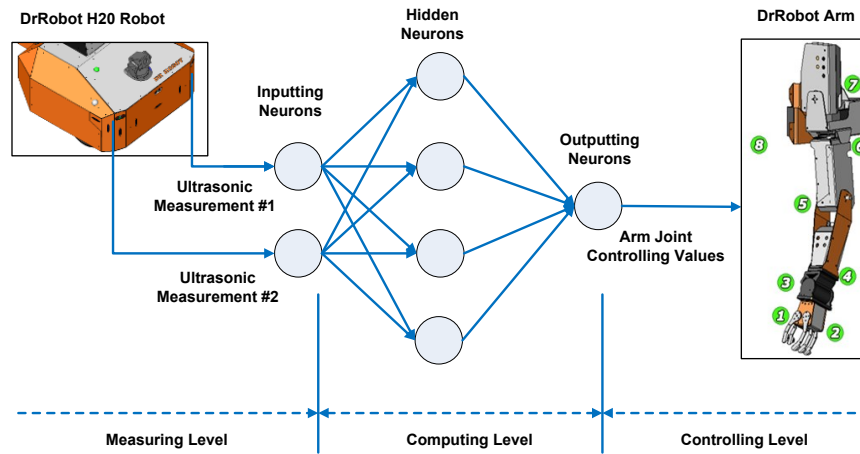


Figure 6-2: The structure of the adopted three-layer MLP network [332]

### 6.3 Vision based Arm Manipulator (VAM)

Fig. 6-3 illustrates the architecture of the proposed VAM, which contents are explained as follows:

- Different to the proposed BAM strategy adopting the ultrasonic sensors, in the VAM strategy a Microsoft Kinect sensor is installed in the H20 robots to find and measure the lab-ware targets. The standard SURF (*Speeded Up Robust Features*) image processing algorithm is used.
- Different to the BAM strategy based on the artificial neural network, in the VAM strategy the arm kinematic models are built to control the arms.

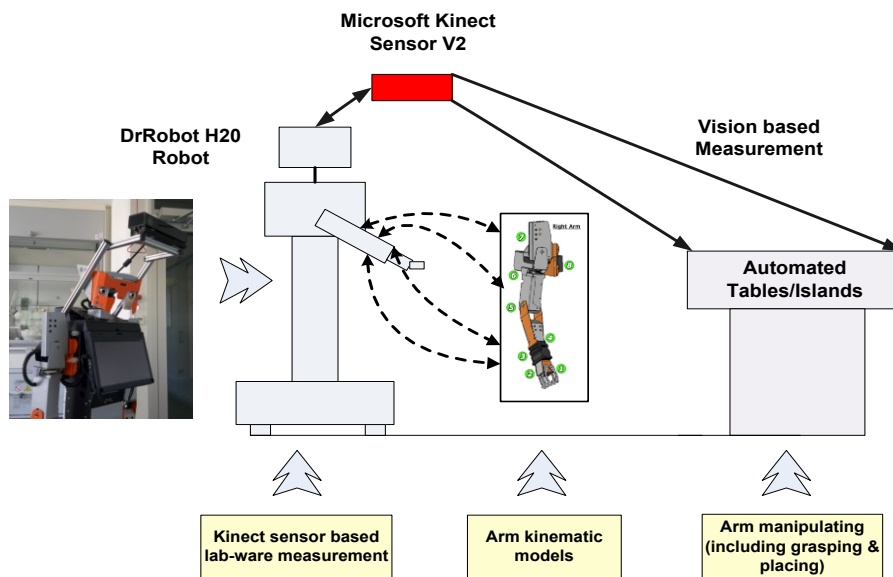


Figure 6-3: Framework of the proposed VAM

## 6.4 MLP based Arm Joint Mapping

The computational schema of the MLP neural network adopted, as shown in Fig. 6-4. The MLP modeling procedure consists of two steps: the training step and the forecasting step. In the network training step, the historical ultrasonic distances and arm joint data are used. In the network forecasting/mapping step, the trained MLP will generate the joint controlling values by inputting the new ultrasonic distance data.

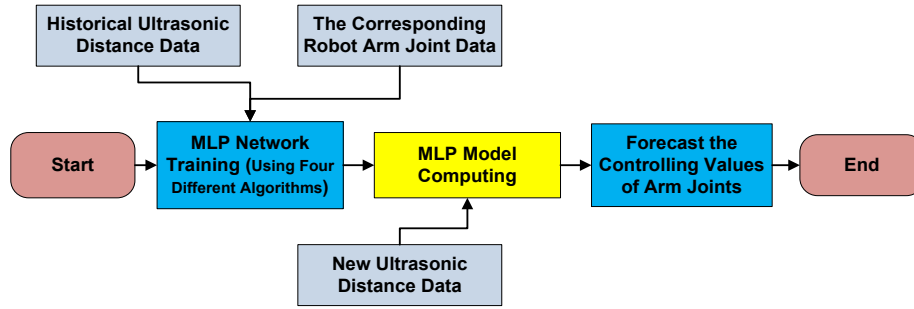


Figure 6-4: The computational schema of the MLP model [332]

**Suppose:** the number of the inputting neurons is equal to  $M$ , the number of the hidden neurons is equal to  $Q$ , the number of the outputting neurons is equal to  $L$ ,  $W_{ij}$  is the connecting weight for the ‘ $j$ ’ neuron in the hidden layer respecting to the ‘ $i$ ’ neuron in the inputting layer,  $W_{jk}$  is the connecting weight for the ‘ $k$ ’ neuron in the outputting layer respecting to the ‘ $j$ ’ neuron in the hidden layer.

The computational equation of the ‘ $j$ ’ neuron in the hidden layer is given as:

$$o_{pj} = f(net_{pj}) = f\left(\sum_{i=1}^Q W_{ij} o_{pi} - \theta_j\right) \quad (Eq.6-1)$$

The computational equation of the ‘ $k$ ’ neuron in the outputting layer is given as:

$$o_{pk} = f(net_{pk}) = f\left(\sum_{j=1}^Q W_{jk} o_{pj} - \theta_k\right) \quad (Eq.6-2)$$

Respecting to the  $S$  function there is an equation as:

$$f'(net) = f(net)[1 - f(net)] \quad (Eq.6-3)$$

The error network function under the ‘ $p$ ’ mode can be given as:

$$E_p = \frac{1}{2} \sum_{k=1}^L (d_{pk} - o_{pk})^2 \quad (Eq. 6-4)$$

For the all training data (*P series*), the overall network error can be provided as:

$$E = \sum_{p=1}^P E_p = \frac{1}{2} \sum_{p=1}^P \sum_{k=1}^L (d_{pk} - o_{pk}) \quad (Eq. 6-5)$$

The weights between the hidden layer and the outputting layer can be adjusted as:

$$\begin{cases} \Delta W_{jk} = -\eta \frac{\partial E_p}{\partial W_{jk}} \\ \frac{\partial E_p}{\partial W_{jk}} = \frac{\partial E_p}{\partial net_{jk}} \frac{\partial net_{jk}}{\partial W_{jk}} \end{cases} \quad (Eq. 6-6)$$

The corresponding back propagation error can be given as:

$$\begin{aligned} \delta_{pk} &= -\frac{\partial E_p}{\partial net_{pk}} = -\frac{\partial E_p}{\partial o_{pk}} \frac{\partial o_{pk}}{\partial net_{pk}} \\ &= (d_{pk} - o_{pk}) f'(net_{pk}) \\ &= o_{pk} (1 - o_{pk}) (d_{pk} - o_{pk}) \end{aligned} \quad (Eq. 6-7)$$

Because:

$$\begin{aligned} \frac{\partial net_{pk}}{\partial W_{jk}} &= \frac{\partial}{\partial W_{jk}} \left( \sum_{j=1}^Q W_{jk} o_{pj} - \theta_k \right) = o_{pj} \\ &= o_{pk} (1 - o_{pk}) (d_{pk} - o_{pk}) \end{aligned} \quad (Eq. 6-8)$$

Then, the final adjusting equation can be obtained as:

$$\begin{cases} \Delta W_{jk} = \eta o_{pk} (1 - o_{pk}) (d_{pk} - o_{pk}) o_{pj} = \eta \delta_{pk} o_{pj} \\ \Delta \theta_k = \eta o_{pk} (1 - o_{pk}) (d_{pk} - o_{pk}) = \eta \delta_{pk} \end{cases} \quad (Eq. 6-9)$$

Based on the upper computational mechanism, the network error-adjusting equations can be described as:

$$\begin{cases} W_{jk}(n+1) = W_{jk}(n) + \eta \delta_{pk}(n) o_{pj}(n) \\ W_{ij}(n+1) = W_{ij}(n) + \eta \delta_{pj}(n) o_{pi}(n) \\ \theta_k(n+1) = \theta_k(n) + \eta \delta_{pk}(n) \\ \theta_j(n+1) = \theta_j(n) + \eta \delta_{pj}(n) \end{cases} \quad (Eq. 6-10)$$



## 6.5 Arm Kinematics

The H20 mobile robot has dual arms with 6 revolute joints, which can reach 60 cm and lift weight of 800g. The arm has 6 DOFs (*Degree of Freedom*). Two of the 6 DOFs are located in the shoulder, two in the elbow and the last two are assigned on the wrist. The DOF configuration of the H20 robots' arms is shown in Fig. 6-5.

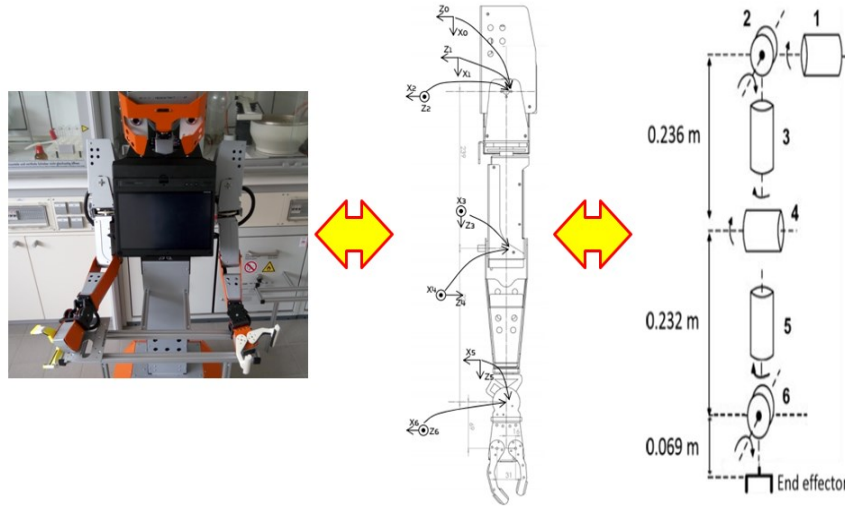


Figure 6-5: DOF configuration of the arms in H20 mobile robots

In the solving of the arm kinematics in the H20 robots, the D-H (*Denavit-Hartenberg*) rules are adopted to describe the locations of all arm joints and at the same time the forward & inverse arm kinematics are considered [339]–[342]. The D-H parameters of the H20 right arm are given in Table 6-1. Based on the obtained D-H parameters, the HT (*Homogeneous Transformation*) matrix of the H20 arms can be made as [343]:

$${}^{i-1}_iT = \begin{bmatrix} \cos\theta_i & -\sin\theta_i & 0 & a_{(i-1)} \\ \sin\theta_i \cos\alpha_{(i-1)} & \cos\theta_i \cos\alpha_{(i-1)} & -\sin\alpha_{(i-1)} & -\sin\alpha_{(i-1)}d_i \\ \sin\theta_i \sin\alpha_{(i-1)} & \cos\theta_i \sin\alpha_{(i-1)} & \cos\alpha_{(i-1)} & \cos\alpha_{(i-1)}d_i \\ 0 & 0 & 0 & 1 \end{bmatrix} \quad (Eq.6-11)$$

where ‘ $a$ ’ is the link length, ‘ $\alpha$ ’ is the link twist, ‘ $\theta$ ’ is the joint angle, ‘ $d$ ’ is the link offset and ‘ $i$ ’ is the link number in the kinematic chain.

Table 6-1 The D-H parameters of the H20 right arm

ID	Link Length	Link Twist	Link Offset	Joint Angle	Joint Limits	
1	0°	0	0	$\theta_1$	-20°	192°
2	-90°	0	0	$\theta_2$	-200°	-85°
3	-90°	0	0.236	$\theta_3$	-195°	15°
4	90°	0	0	$\theta_4$	-129°	-90°
5	-90°	0	0.232	$\theta_5$	0°	180°
6	90°	0	0	$\theta_6$	-60°	85°

To validate the efficiency of the solved forward & inverse models for the latter arm manipulations, three types of experiments are provided based on the Robotics Toolbox of Matlab platform. The experimental results of the FK (Forward Kinematics) and the IK (Inverse Kinematics) are given in Fig. 6-6. The experimental result of the three-dimensional arm workspace is shown in Fig. 6-7. From Figures 6-6 and 6-7, it can be seen that the proposed arm kinematic models for H20 mobile robots are correct, which can be applied in the real arm manipulators. [More details can be found at: *Ali, M. M.; Liu, H.; Stoll, N.; Thurow, K.: Kinematic Analysis of 6-DOF Arms for H20 Mobile Robots and Labware Manipulation for Transportation in Life Science Labs. Journal of Automation, Mobile Robotics & Intelligent Systems, 2016*]

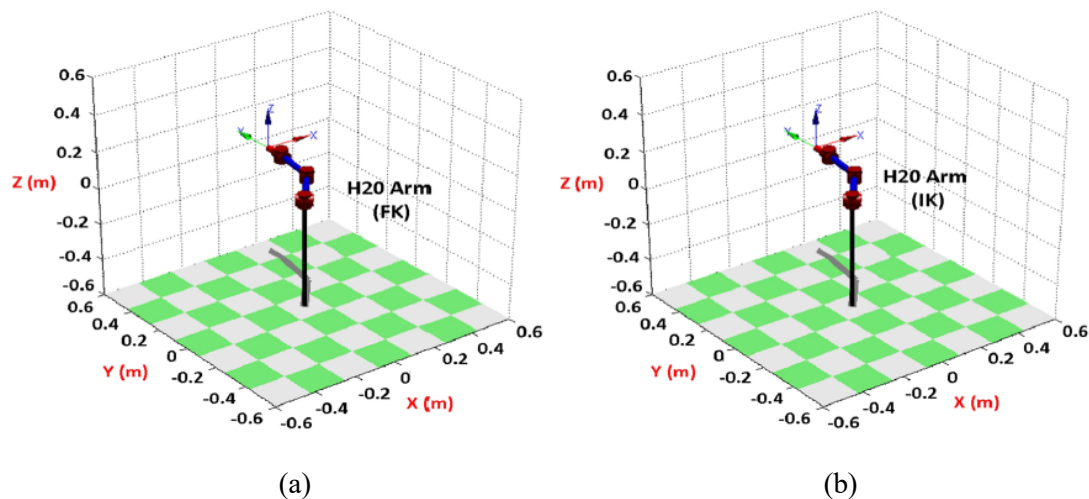


Figure 6-6: Results of the arm kinematic experiments: (a) FK model; and (b) IK model

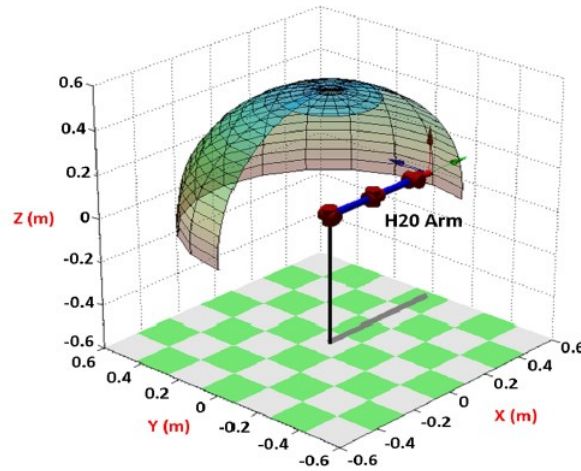


Figure 6-7: Result of the arm workspace experiment

## 6.6 Lab-ware Identification

In an effective arm manipulator, the function of lab-ware identification is desired. When the mobile robots arrive at the expected arm manipulating positions, they need the lab-ware identification function to insure that the correct lab-ware target will be grasped or placed. In the developed IMRTS system, three types of smart lab-ware identification functions are defined, which consists of the SLI (*Single Lab-ware Identification*), the MLI (*Multiple Lab-ware Identification*) and the SLI (*Selected Lab-ware Identification*) [344]. The type of the lab-ware identification will be decided by the camera views of the mobile robots, which can be switched automatically.

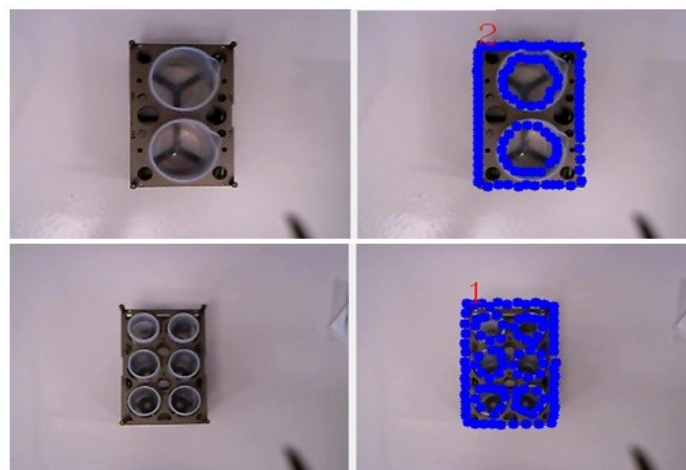


Figure 6-8: Results of the single lab-ware identification [344]

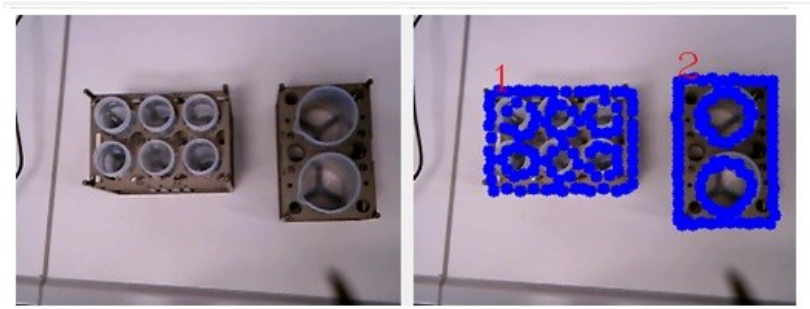


Figure 6-9: Results of the multiple lab-ware identification [344]

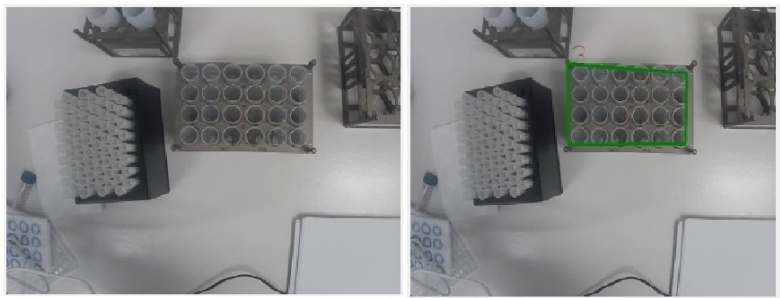


Figure 6-10: Results of the selected lab-ware identification [344]

6.7 Experiments and Analysis

An experiment is provided in this chapter to validity the effectiveness of the adoption of the MLP neural networks in the robot arm manipulation. As demonstrated in Fig. 6-11, a H20 mobile robot from *DrRobot Canada* [92] is expected to grasp an object at a position in front of an automated workstation. For this experiment, 11 groups of the ultrasonic distances between the robot positions and the workstations and their corresponding arm controlling joint data are prepared.

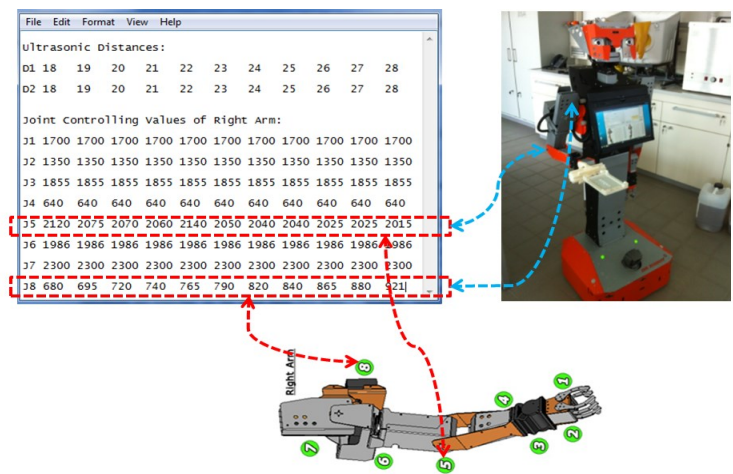


Figure 6-11: The schema of the experiment [332]

From the data shown in Fig. 6-11, it can be seen that only two joint values are changed with the different robot orientations. It means the MLP model only needs to forecast the results for these two joints. Different to the kinematic model based method, the proposed MLP based method does not need to calculate all of the joints for the robot arms, which can have the real-time performance and the simplicity of the arm designs. This feature is also an advantage of the intelligent arm controlling strategies like the MLP neural network adopted in this chapter. In the MLP theory, there are many network training algorithms. In this chapter, four of them, which are most popular, are included in the experiment to compare the different performance, including GD-BP algorithm (*Gradient Descent Back Propagation*), GDMA-BP algorithm (*Gradient Descent with Momentum and Adaptive Learning Rate Back Propagation*), CG-BP-FR algorithm (*Conjugate Gradient Back Propagation with Fletcher-Reeves Updates*) and BFGS algorithm (*BFGS Quasi-Newton Back Propagation*) [332].

### 6.7.1 BFGS based Mapping Results

The results of the BFGS based computation are given in Fig. 6-12 and Fig. 6-13. The corresponding actual and forecasting values are provided in Table 6-2. From Fig. 6-12, it can be seen that the MLP network adopted the BFGS training algorithm to spend 22 iterative steps to reach the accuracy threshold ( $MSE\ 0.0019565$ ). From Fig. 6-13 and Table 6-2, it can be seen that: **(a)** the built MLP network with the BFGS algorithm has satisfactory arm joint forecasting results; and **(b)** the average accuracy of the arm joint #8 respecting to all of the ultrasonic distances is 99.6245 %.

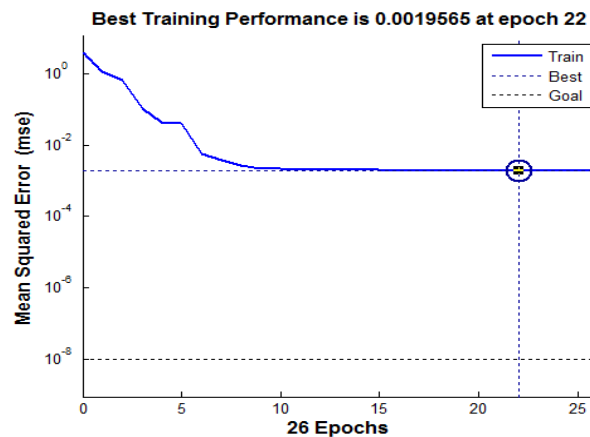


Figure 6-12: The network training performance of the built MLP using the BFGS algorithm for the robot arm joint #8

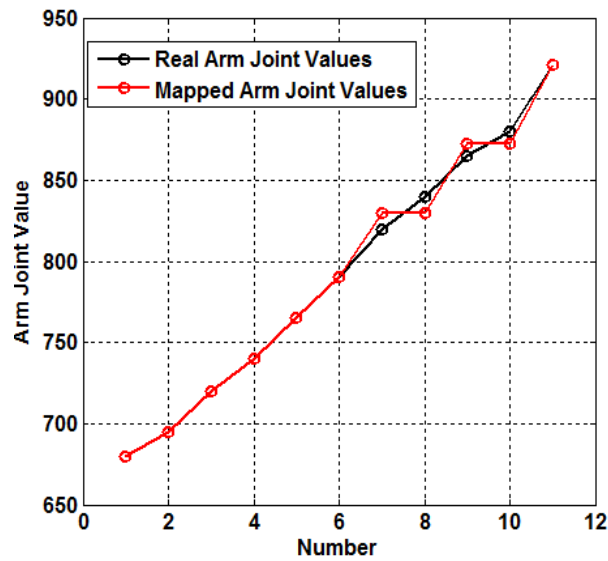


Figure 6-13: The forecasting results by the built MLP with the BFGS algorithm for the robot arm joint #8

Table 6-2 The forecasted results of the robot arm joint #8 by the MLP neural network using the BFGS algorithm

ID	Actual Value	Mapped Value	MAPE/%
1	680	680	100%
2	695	695	100%
3	720	720	100%
4	740	740	100%
5	765	765	100%
6	790	790	100%
7	820	830	98.78%
8	840	830	98.81%
9	865	872	99.13%
10	880	872	99.15%
11	921	921	100%

### 6.7.2 GD-BP based Mapping Results

The results of the GD-BP based computation are given in Fig. 6-14 and Fig. 6-15. The corresponding actual and forecasting values are provided in Table 6-3. From Fig. 6-14, it can be seen that the MLP network utilized the GD-BP training algorithm to spend

194 iterative steps to reach the accuracy threshold ( $MSE\ 0.0023558$ ). From Fig. 6-15 and Table 6-3, it can be seen that: **(a)** the built MLP network with the BFGS algorithm has good arm joint forecasting results; and **(b)** the average accuracy of the arm joint #8 respecting to all of the ultrasonic distances is 97.9691 %.

When comparing the performance of the GD-BP algorithm with that of the BFGS algorithm (*see Section 6.4.1*), the BFGS has better performance than the GD-BP, either in the required iterative steps or in the arrived network accuracy.

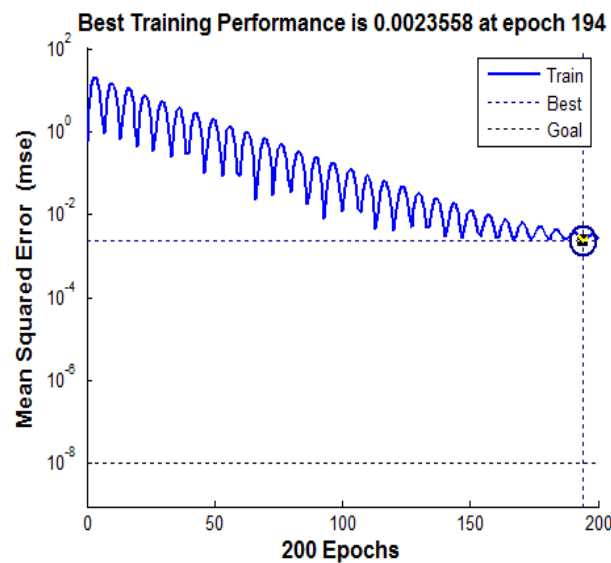


Figure 6-14: The network training performance of the built MLP using the GD-BP algorithm for the robot arm joint #8

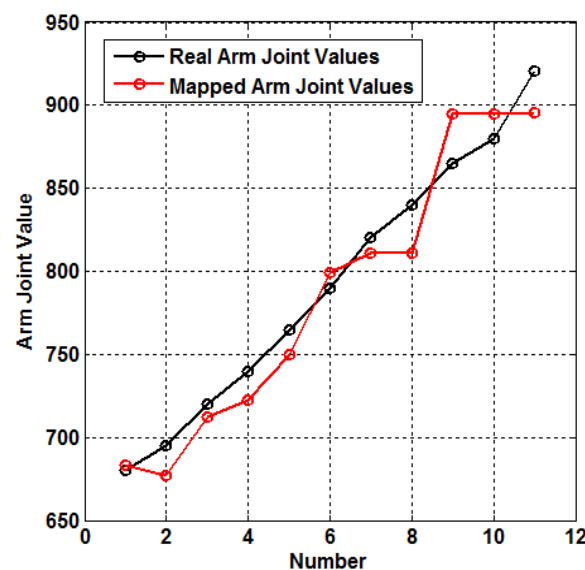


Figure 6-15: The forecasting results by the built MLP with the GD-BP algorithm for the robot arm joint #8



Table 6-3 The forecasted results of the robot arm joint #8 by the MLP neural network using the GD-BP algorithm

ID	Actual Value	Mapped Value	MAPE/%
1	680	683.6115	99.47%
2	695	676.8262	97.39%
3	720	712.0110	98.89%
4	740	722.1275	97.58%
5	765	749.9785	98.04%
6	790	799.4684	98.80%
7	820	810.8332	98.88%
8	840	810.8332	96.53%
9	865	895.0803	96.52%
10	880	895.0803	98.29%
11	921	895.8606	97.27%

### 6.7.3 GDMA-BP based Mapping Results

The results of the GDMA-BP based computation are given in Fig. 6-16 and Fig. 6-17. The corresponding actual and forecasting values are provided in Table 6-4. From Fig. 6-16, it can be seen that the MLP network utilized the GDMA -BP training algorithm to spend 156 iterative steps to reach the accuracy threshold ( $MSE\ 0.0019743$ ). From Fig. 6-17 and Table 6-4, it can be seen that: **(a)** the built MLP network with the GDMA-BP algorithm has good arm joint forecasting results; and **(b)** the average accuracy of the arm joint #8 respecting to all of the ultrasonic distances is 99.1473 %.

When comparing the performance of the GDMA-BP algorithm with those of the BFGS algorithm (*see Section 6.4.1*) and the GD-BP algorithm (*see Section 6.4.2*), it can be concluded that the BFGS has better performance than both of the GD-BP and the GDMA-BP while the GDMA-BP has better performance than the GD-BP, either in the required iterative steps or in the arrived network accuracy.



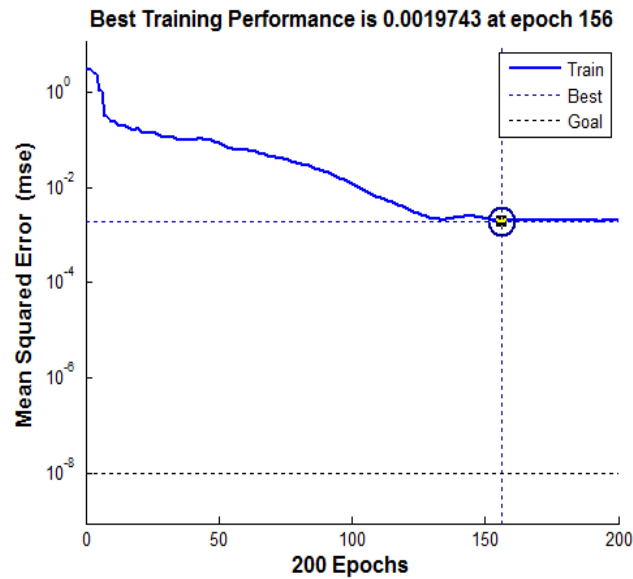


Figure 6-16: The network training performance of the built MLP using the GDMA-BP algorithm for the robot arm joint #8

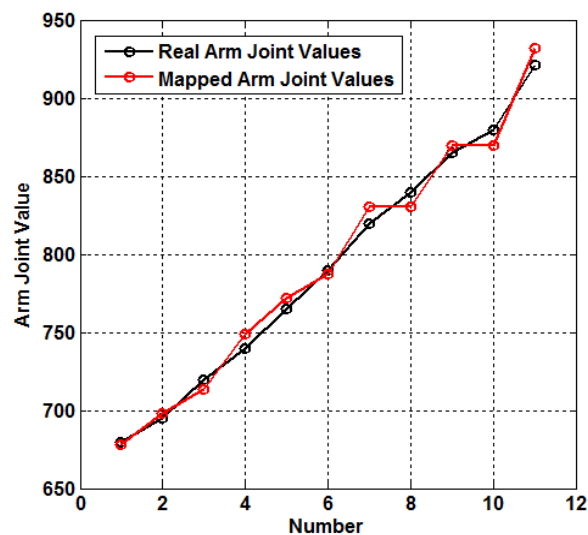


Figure 6-17: The forecasting results by the built MLP with the GDMA-BP algorithm for the robot arm joint #8

Table 6-4 The forecasted results of the robot arm joint #8 by the MLP neural network using the GDMA-BP algorithm

ID	Actual Value	Mapped Value	MAPE/%
1	680	677.7844	99.67%
2	695	697.8151	99.59%
3	720	713.1176	99.04%
4	740	748.6452	98.83%
5	765	772.0108	99.08%
6	790	787.5600	99.69%

7	820	830.0444	98.78%
8	840	830.0444	98.81%
9	865	869.3862	99.49%
10	880	869.3862	98.79%
11	921	931.6291	98.85%

#### 6.7.4 CG-BP-FR based Mapping Results

The results of the CG-BP-FR based computation are given in Fig. 6-18 and Fig. 6-19. The corresponding actual and forecasting values are provided in Table 6-5. From Fig. 6-18, it can be seen that the MLP network utilized the CG-BP-FR training algorithm to spend 53 iterative steps to reach the accuracy threshold ( $MSE\ 0.0019565$ ). From Fig. 6-19 and Table 6-5, it can be seen that: **(a)** the built MLP network with the CG-BP-FR algorithm has good arm joint forecasting results; and **(b)** the average accuracy of the arm joint #8 respecting to all of the ultrasonic distances is 99.4618 %.

When comparing the performance of the CG-BP-FR algorithm with those of the other adopted network training algorithms, it can be concluded that: the BFGS has the best performance among all of the algorithms; The CG-BP-FR ranks the second best one; The GDMA-BP is the third one; and the GD-BP is the fourth one.

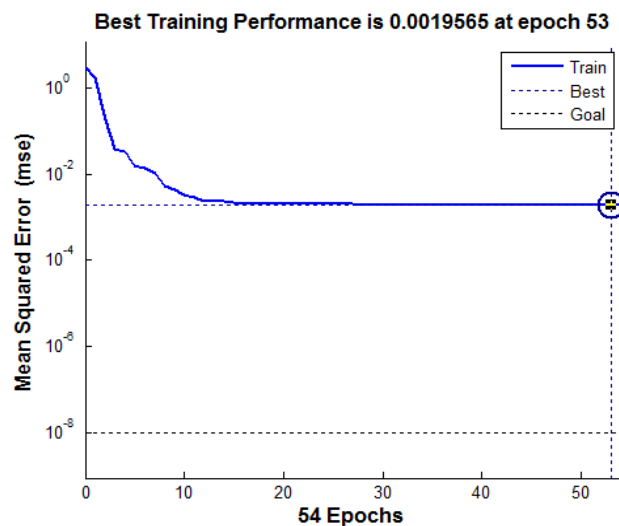


Figure 6-18: The network training performance of the built MLP using the CG-BP-FR algorithm for the robot arm joint #8

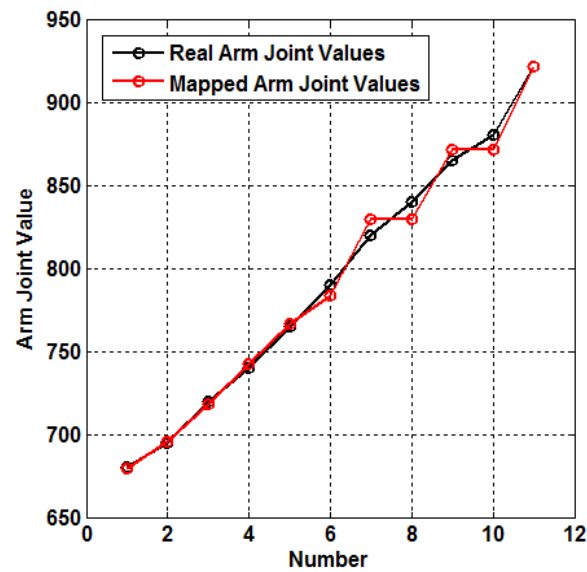


Figure 6-19: The forecasting results by the built MLP with the CG-BP-FR algorithm for the robot arm joint #8

Table 6-5 The forecasted results of the robot arm joint #8 by the MLP neural network using the CG-BP-FR algorithm

ID	Actual Value	Mapped Value	MAPE/%
1	680	679.2023	99.88%
2	695	695.3248	99.95%
3	720	717.9752	99.72%
4	740	742.5933	99.65%
5	765	766.3401	99.82%
6	790	783.8690	99.22%
7	820	829.5576	98.83%
8	840	829.5576	98.76%
9	865	871.2151	99.28%
10	880	871.2151	99.00%
11	921	921.2827	99.97%

### 6.7.5 Real-time Performance of the MLP

To examine the time performance of the involved models, an experiment is provided based on a normal laptop (*CPU Intel i3-2350M 2.3GHz, RAM 6G*), with the results given in Table 6-6. From Table 6-6, it can be seen that: **(a)** both of the adopting training algorithms with the built MLP model have satisfactory time performance; and **(b)** the BFGS still ranks the best position in the computational time performance,

besides the iterative step and accuracy discussed before.

Table 6-6 The time performance of the involved different models in the robot arm controlling

Methods	Consuming Time/s
GD-BP Algorithm	0.717838
GDMA-BP Algorithm	0.739387
CG-BP-FR Algorithm	0.985031
BFGS Algorithm	0.724849

## 6.8 Developed Controlling GUI

Based on the proposed two new arm manipulating strategies, two different robot arm manipulators are developed for the intelligent mobile robot transportation, as given in Fig. 6-20. As shown in Fig.6-20, the BAM method uses the ultrasonic sensors in the robot bases to measure the robot orientations' distances then calculate the arm joint controlling values using the built MLP models and the VAM method adopts the installed Kinect sensors to detect the lab-wares directly using the built SURF vision models for the manipulating-error compensation.

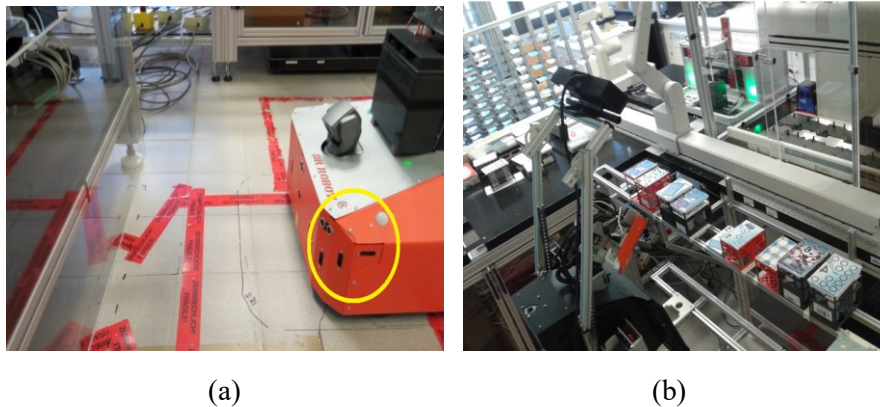


Figure 6-20: Real cases of the proposed two arm manipulators: (a) BAM strategy; and (b) VAM strategy

In the developed arm manipulators, the software GUIs are given in Figures 6-21 and 6-22. As shown in Fig. 6-21, the main GUI of the developed arm manipulator can realize the following functions as: **(a)** once the main GUI starts, it will connect to all of the arm motor modules and the corresponding RBC controller; **(b)** after the successful connections to the hardware and the server software, the main GUI will complete the whole kinematic computation; **(c)** the coordinates of the installed Kinect sensors will be mapped and transferred to the coordinates of the robot arms so that the

arms can realize the expected operations; and **(d)** the type of the manipulators (*i.e.*, the *BAM* and the *VAM*) will be selected by the corresponding RBC controller. When the RBC controls the VAM to do the vision based grasping & placing actions, the VAM will start the lab-ware identification GUI, as shown in Fig. 6-22.

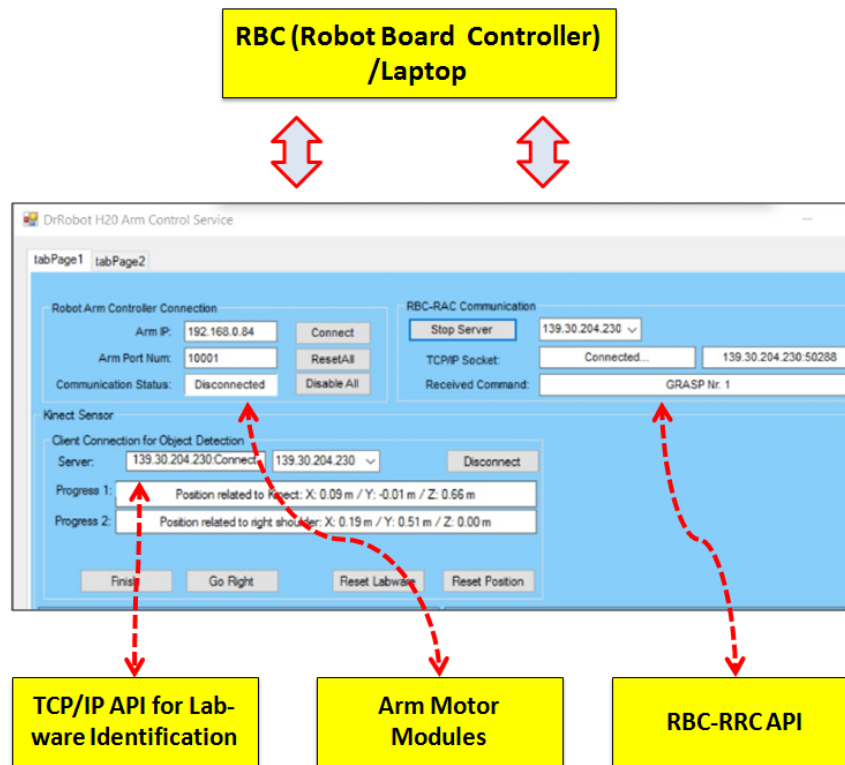


Figure 6-21: Main GUI of the developed arm manipulator

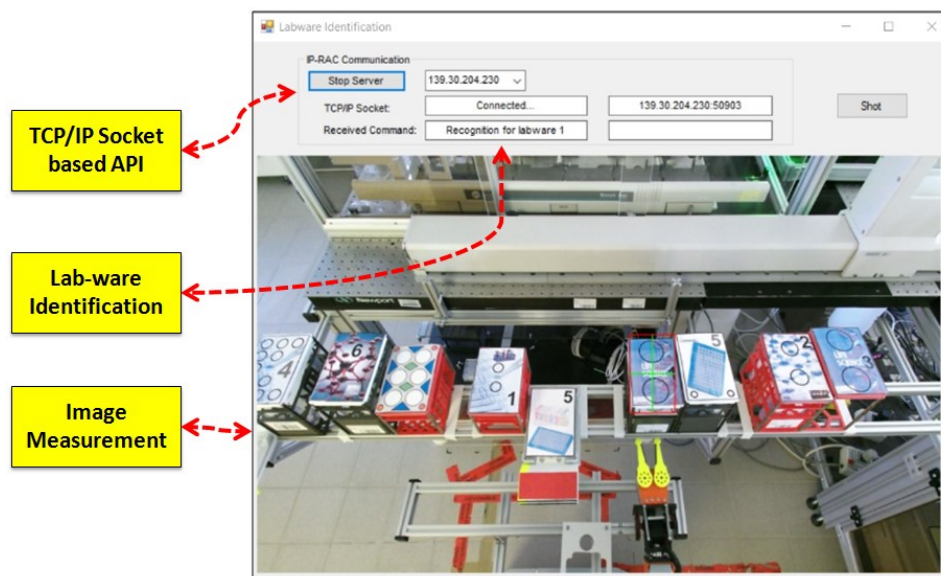


Figure 6-22: Lab-ware Identification GUI in the developed arm manipulator

# Chapter 7 Conclusions & Outlook

## 7.1 Conclusions

In this habilitation thesis, a series of intelligent strategies are proposed for the mobile robotics in laboratory automation. In the habilitation thesis, the main innovations are concluded as below:

- ***Issue of the Multi-floor Robot Indoor Navigation:***

In this issue, a new StarGazer based multi-floor navigation mapping method is proposed and a corresponding multi-segment shortest mobile robot path planning approach is presented. Based on these proposed new strategies, any sizes and types of the modern laboratories can be equipped with a universal mobile robot navigating map. The built multi-floor navigation map can be extended conveniently and identifies all of the areas of the laboratories with a unique ID. The mobile robots can recognize the big laboratory environments freely.

To correct the wrong measured indoor coordinates of the StarGazer sensors under the ceiling interferences, a new robot indoor positioning forecasting method is presented by adopting the Time Series Analysis (TSA) theory and the Kalman Filter (KF) theory. With this proposed positioning forecasting method, the mobile robots can run safely even under the strong ceiling interferences. In the proposed forecasting method, the ARIMA model from the TSA theory is adopted to build the models to recognize the changing laws of the mobile robot indoor coordinates and the KF model is used to do the one-step tracking and the two-step forecasting computation for the mobile robots.

The proposed robot indoor positioning predicting strategy consists of two new ideas. Firstly, this is the first time to propose the hybrid ARIMA-KF method to realize the robot indoor positioning prediction for the complex laboratories' ceiling interferences. Secondly, the proposed ARIMA-KF structure provides a smart idea to use the ARIMA

model to select the best initial parameters of the KF models in front of the original signals. The results of the experiments provided in the chapter indicate that the proposed TSA-KF method is effective in the mobile robot indoor coordinate signal forecasting and has better tracking and forecasting accuracy than the standard ARIMA models. For example, in the experiment the MAE, MAPE and RMSE of the one-step results by the proposed ARIMA-KF model are 0.014m, 1.03% and 0.0232m, respectively. With the same group of robot indoor coordinates, the MAE, MAPE and RMSE of the one-step results by the ARIMA model are 0.2014m, 10.44% and 0.1437m, respectively.

● ***Issue of the Human Feature based Collision Avoidance:***

In the issue, a multi-layer intelligent framework is presented for the mobile robot collision avoidance in laboratories, which consists of the standard collision avoidance in the normal zones, the human feature guiding HRI collision avoidance in the narrow and special zones. The proposed human feature HRI based collision avoidance is consisted of two different working modes, the face feature based one and the gesture feature based one.

The innovative results of the proposed face feature based strategy are concluded as follows:

(a) The hybrid eye-eyebrow zones are selected to recognize the human face orientations and identify the face moving directions. To control the mobile robot smoothly, five face orientation parameters are defined, including the left side, the middle-left side, the forward side, the middle-right side and the right side.

(b) The parameters of the eyes and the eyebrows are abstracted using the image edge detection. To compare the performance of the different edge detecting algorithms, an experiment is executed. The involved edge detecting algorithms include *the Sobel algorithm, the Prewitt algorithm, the Roberts algorithm, the Log algorithm, the Zero-cross algorithm and the Canny algorithm*.

(c) To measure the real-time images of the human faces, the Microsoft Kinect sensors are equipped with all the mobile robots. In the Kinect sensor based measurement, the eyebrow-eye matrixes of the human faces, the blinking status of the human eyes and the distances between the sensors and the avoiding people are all included. Among the measured parameters, the blinking status of the eyes are used to start the face

controlling procedures, the eyebrow-eye edge detecting matrixes are adopted to identify the moving directions of the faces, and the distances between the robots and the front persons are utilized to find the closest person.

(d) The LVQ neural network is established to classify the relationships between the measured eyebrow-eye matrixes and the human face controlling. Since the proposed method is expected to be applied in the running systems, both of the recognizing accuracy and the model-consuming time are considered. The built MLP model trained by the Prewitt Algorithm only needs 3.17s to realize the 99% successful rate of the human face classification.

The innovative results of the proposed gesture feature based strategy are given as follows:

(a) The human body skeletons and gestures are selected to recognize the human gesture based controlling commands. To control the mobile robot smoothly, seven different gesture controlling parameters are defined.

(b) The SVM model is built to classify the dynamic measured human gesture behaviors and identify the real-time gesture controlling commands. The same to the upper proposed face based strategy, since the proposed gesture method will also be used in the running systems, both of the recognizing accuracy and the model-consuming time are focused. The built SVM model only needs less than one second to realize the 99.78% successful rate in the gesture classification and recognition.

#### ● ***Issue of the Robot Power Forecasting based Control:***

In the issue, the following important work is concluded as follows:

(a) A multi-channel robot power measuring system is developed. Based on the developed robot power measurement system, all the real-time power status of the connecting mobile robots can be sampled the higher system components.

(b) A new intelligent forecasting method is proposed to predict the future power status of the running mobile robots. The forecasted results can let the mobile robots decide whether to accept a coming transportation request clearer. In the proposed intelligent strategy, two mainstream non-stationary signal decomposing algorithms (*i.e., the wavelet decomposition and the empirical mode decomposition*) are included to



decompose the measured robot power data into a number of stable robot power sub-series, and at the same time the ANFIS neural networks are built for the decomposed robot power sub-series.

(c) To indicate the performance of the proposed hybrid WD-ANFIS and EMD-ANFIS methods, a series of comparison is provided. The involved comparing methods beside the proposed ones include the standard ANFIS neural network and the standard MLP neural network. The results of the experiments show that: both of the proposed WD-ANFIS and EMD-ANFIS methods forecast the robot power accurately; the wavelet and EMD decomposition promote the capacity of the standard ANFIS model considerably. The PMAE, the PMAPE and the PRMSE of the ANFIS by the WD algorithm are 55.04%, 55.10% and 50.76%, respectively. The PMAE, the PMAPE and the PRMSE of the ANFIS by the EMD algorithm are 51.74%, 51.02% and 46.91%, respectively.

(d) The real-time performances of the proposed hybrid intelligent methods are also investigated. The results indicate that the WD-ANFIS model and the EMD-ANFIS model need 3.58s and 4.30s to reach the satisfactory results, respectively. It proves that the proposed intelligent methods have good time -consuming performance.

#### ● *Issue of the Robot Arm Manipulation:*

In the issue, a hybrid robot arm manipulator is proposed, which includes two arm controlling methods, the BAM one and the VAM one.

In the presented two arm manipulating methods, the following innovative works are executed as:

(a) A new intelligent blind strategy named BAM is proposed to use the real-time measuring distances between the running robots and the expected workstations to calculate the controlling values of the corresponding robot arms for grasping and placing manipulations. The proposed strategy does not request additional cameras and the solving of the arm kinematic models but just utilizes the existent ultrasonic sensors in the robots. So it has the simplicity and low-cost features.

(b) To calculate the arm joint controlling values effectively, the intelligent MLP neural network is established. To build the best MLP neural network, four mainstream network training algorithms are compared, including the BFGS algorithm, the GD-BP algorithm, the CGMA-BP algorithm and the CG-BP-FR algorithm. The comparing

results show that the BFGS algorithm is most suitable for the MLP neural network in the robot arm manipulations (*the successful Rate 99.62%*).

(c) As discussed in chapter 6, the proposed blind arm manipulating strategy goes for the simplicity. To increase the accuracy definition of the blind method ( $< 2\text{cm}$ ) to reach a higher level ( $< 0.5\text{ cm}$ ), a new intelligent vision strategy named VAM is proposed. The VAM method adopts the robot installed Microsoft Kinect sensors to recognize the targeted lab-wares and compensate the errors caused by the robots' orientations to realize the accurate arm manipulations. For the flexible arm manipulating activities, the arm forward and inverse kinematic models are solved and embedded in the developed arm manipulator. At the same time, the multiple lab-ware identification function is also designed in the arm manipulator. By using the proposed VAM strategy, the robot arms can reach high-accuracy ( $< 0.5\text{ cm}$ ) with 100% successful rate.

(d) In the BAM, the real-time performance of the MLP neural network using different network training algorithms is also investigated. The results indicate that the MLP neural network using all included algorithms have good real-time performance (*the consuming time less than 1s*). The BFGS algorithm is the fastest one among all of the involved algorithms (*the consuming time 0.72s*).

## 7.2 Outlook

The future works of the habilitation thesis are given as follows:

(a) The first focus is how to extend the multi-floor navigation map to the multi-building map. More and more modern laboratories have multi-buildings with multi-floors; the combination of the indoor and outdoor mobile robot transportation will be highly expected in future. For this purpose, it can be foreseen that one of the most important work will lay on building an effective data/controlling API between the indoor ceiling landmark based robot navigation strategy and the outdoor GPS based robot navigation method.

(b) The second focus is to investigate the developed systems and controllers as much as possible. It is well-known that there are always some gaps between the target based technical solutions and the all-weather system operating. The new innovations only can come if the sufficient investigation is executed to the current systems.

(c) The third focus is to increase the impacting of the human inside the mobile robot

transportation activities. In this thesis the human face based robot collision avoidance controller has been presented and some of face features (*i.e., the blinking eyes, the rotating heads and the moving hands/gestures*) are selected to interact with the running mobile robots. In the next version, more kinds of human features (*i.e., the human sound, the fingers, etc.*) will be defined and included in the robot-human interfaces for the various purposes.

**(d)** The last focus is to increase the integrating percentages between the mobile robot controlling systems and the higher HWMS/PMS systems.

## References

- [1] M. R. Pedersen, L. Nalpantidis, R. S. Andersen, C. Schou, S. Bøgh, V. Krüger, and O. Madsen, “Robot skills for manufacturing: From concept to industrial deployment,” *Robotics and Computer-Integrated Manufacturing*, vol. 37, pp. 282–291, 2016.
- [2] O. Stocklosa, T. Borangiu, S. Raileanu, O. Morariu, and C. Morariu, “Visual guidance of robots integrated in intelligent manufacturing,” *UPB Scientific Bulletin, Series C: Electrical Engineering*, vol. 77, no. 2, pp. 65–80, 2015.
- [3] M. H. Korayem, A. Tajik, H. Tourajizadeh, M. Taherifar, A. Imanian, and S. Khayatzadeh, “Design and manufacturing a torque measurement mechanism for the motors of ICaSbot robot and developing its applications,” *International Journal of Advanced Manufacturing Technology*, vol. 71, no. 1–4, pp. 439–458, 2014.
- [4] A. Cherubini, R. Passama, A. Crosnier, A. Lasnier, and P. Fraisse, “Collaborative manufacturing with physical human-robot interaction,” *Robotics and Computer-Integrated Manufacturing*, vol. 40, pp. 1–13, 2016.
- [5] S. B. Wali, M. A. Hannan, A. Hussain, and S. A. Samad, “An Automatic Traffic Sign Detection and Recognition System Based on Colour Segmentation, Shape Matching, and SVM,” *Mathematical Problems in Engineering*, vol. 2015, pp. 1–12, 2015.
- [6] M. A. Hannan, C. T. Gee, and M. S. Javadi, “Automatic vehicle classification using fast neural network and classical neural network for traffic monitoring,” *Turkish Journal of Electrical Engineering and Computer Sciences*, vol. 23, pp. 2031–2042, 2015.
- [7] Y. Feng, J. Sun, and P. Chen, “Vehicle trajectory reconstruction using automatic vehicle identification and traffic count data,” *Journal of Advanced Transportation*, vol. 49, no. 2, pp. 174–194, 2015.
- [8] M. Dubská, A. Herout, R. Juránek, and J. Sochor, “Fully automatic roadside camera calibration for traffic surveillance,” *IEEE Transactions on Intelligent Transportation Systems*, vol. 16, no. 3, pp. 1162–1171, 2015.
- [9] W. Chao and A. Kolski-Andreaco, “August 2014: This month in JoVe - Chemical sensing robots, tracking blood cell development, rodents on the treadmill, and simulating urban runoff,” *Journal of Visualized Experiments*, no. 90, pp. 1–2, 2014.
- [10] M. Turduev, G. Cabrita, M. Kirtay, V. Gazi, and L. Marques, “Experimental studies on chemical concentration map building by a multi-robot system using bio-inspired algorithms,” *Autonomous Agents and Multi-Agent Systems*, vol. 28, no. 1, pp. 72–100, 2014.
- [11] L. O. De, O. Castillo, A. Meléndez, P. Melin, L. Astudillo, and C. Sánchez, “Optimization of reactive fuzzy controllers for mobile robots based on the chemical reactions algorithm,” *Studies in Computational Intelligence*, vol. 601, pp. 253–266, 2015.
- [12] T. Van, Y. Wang, H. Ao, and T. Khac, “Sliding Mode Control Based on Chemical Reaction Optimization and Radial Basis Functional Link Net for De-Icing Robot Manipulator,” *Journal of Dynamic Systems, Measurement and Control, Transactions of the ASME*, vol. 137, no. 5, 2015.
- [13] P. Waurzyniak, “Fast, lightweight robots help factories go faster,” *Manufacturing Engineering*, vol. 154, no. 3, pp. 55–65, 2015.

- [14] E. Erdem, V. Patoglu, and Z. G. Saribatur, "Integrating hybrid diagnostic reasoning in plan execution monitoring for cognitive factories with multiple robots," *Proceedings IEEE International Conference on Robotics and Automation*, pp. 2007–2013, 2015.
- [15] D. Claes and K. Tuyls, "Human robot-team interaction: Towards the factory of the future," *Communications in Computer and Information Science*, vol. 519, pp. 61–72, 2015.
- [16] M. Shipulski, "Robots and factories are no longer differentiators: Real competitive advantage lies outside of the process of making things," *Assembly*, vol. 57, no. 8, 2014.
- [17] Z. G. Saribatur, E. Erdem, and V. Patoglu, "Cognitive factories with multiple teams of heterogeneous robots: Hybrid reasoning for optimal feasible global plans," *Proceedings IEEE International Conference on Intelligent Robots and Systems*, pp. 2923–2930, 2014.
- [18] W. Knight, "Introducing the friendlier, more agile factory robot," *Technology Review*, vol. 116, no. 6, pp. 26–27, 2013.
- [19] R. Brooks, "Robots at work: Toward a smarter factory," *Futurist*, vol. 47, no. 3, pp. 24–27, 2013.
- [20] J. Gonçalves, J. Lima, P. J. Costa, and A. P. Moreira, "Modeling and simulation of the EMG30 geared motor with encoder resorting to simtwo: The official robot@factory simulator," *Lecture Notes in Mechanical Engineering*, vol. 7, pp. 307–314, 2013.
- [21] A. Valera, J. Gomez-Moreno, A. Sánchez, C. Ricolfe-Viala, R. Zotovic, and M. Valés, "Industrial robot programming and upnp services orchestration for the automation of factories," *International Journal of Advanced Robotic Systems*, vol. 9, pp. 1–11, 2012.
- [22] S. Harris, "Humanoid robot could help out in understaffed factories," *Engineer*, vol. 13-DECEMBER, pp. 1–2, 2010.
- [23] F. Lange, J. Werner, J. Scharrer, and G. Hirzinger, "Assembling wheels to continuously conveyed car bodies using a standard industrial robot," *Proceedings 2010 IEEE International Conference on Robotics and Automation (ICRA)*, pp. 3863–3869, 2010.
- [24] B. Horan, Z. Najdovski, T. Black, S. Nahavandi, and P. Crothers, "OzTug mobile robot for manufacturing transportation," *Proceedings 2011 IEEE International Conference on Systems, Man, and Cybernetics (SMC)*, pp. 3554–3560, 2011.
- [25] M. Endo, K. Hirose, Y. Hirata, K. Kosuge, T. Kanbayashi, M. Oomoto, K. Akune, H. Arai, H. Shinoduka, and K. Suzuki, "A car transportation system by multiple mobile robots - iCART -," *Proceedings IEEE/RSJ International Conference on Intelligent Robots and Systems (IROS 2008)*, pp. 2795–2801, 2008.
- [26] M. Endo, K. Hirose, Y. Hirata, K. Kosuge, Y. Sugahara, K. Suzuki, K. Murakami, K. Nakamura, M. Nakanishi, and T. Kanbayashi, "A coordinated control algorithm based on the caster-like motion for a car transportation system -iCART-," *Proceedings IEEE International Conference on Robotics and Automation (ICRA2009)*, pp. 2350–2355, 2009.
- [27] K. Kashiwazaki, N. Yonezawa, M. Endo, K. Kosuge, Y. Sugahara, Y. Hirata, T. Kanbayashi, K. Suzuki, K. Murakami, and K. Nakamura, "A car transportation system using multiple mobile robots: iCART II," *Proceedings 2011 IEEE/RSJ International Conference on Intelligent Robots and Systems (IROS)*, pp. 4593–4600, 2011.
- [28] J. W. Kang, B. S. Kim, and M. J. Chung, "Development of Assistive Mobile Robots Helping

the Disabled Work in a Factory Environment,” Proceedings *IEEE/ASME International Conference on Mechatronic and Embedded Systems and Applications (MESA2008)*, pp. 426–431, 2008.

[29] C. Datta, A. Kapuria, and R. Vijay, “A pilot study to understand requirements of a shopping mall robot,” presented at the HRI 2011 - Proceedings 6th ACM/IEEE International Conference on Human-Robot Interaction, pp. 127–128, 2011.

[30] M. Prischepa and V. Budkov, “Hierarchical dialogue system for guide robot in shopping mall environments,” *Lecture Notes in Computer Science (including subseries Lecture Notes in Artificial Intelligence and Lecture Notes in Bioinformatics)*, vol. 6836 LNAI, pp. 163–170, 2011.

[31] T. Kanda, M. Shiomi, Z. Miyashita, H. Ishiguro, and N. Hagita, “A communication robot in a shopping mall,” *IEEE Transactions on Robotics*, vol. 26, no. 5, pp. 897–913, 2010.

[32] Y. Wu, “Intelligent robot operating in major shopping malls in the application of cost control,” *Advances in Intelligent and Soft Computing*, vol. 119, pp. 683–687, 2011.

[33] H. Kaindl, B. Putz, D. Ertl, H. Hüttenrauch, and C. Bogdan, “A walking aid integrated in a semi-autonomous robot shopping cart,” Proceedings 4th International Conference on Advances in Computer-Human Interactions, pp. 218–221, 2011.

[34] M. Garcia-Arroyo, L. F. Marin-Urias, A. Marin-Hernandez, and G. D. J. Hoyos-Rivera, “Design, integration, and test of a shopping assistance robot system,” Proceedings 7th Annual ACM/IEEE International Conference on Human-Robot Interaction, pp. 135–136, 2012.

[35] M. Shiomi, K. Shinozawa, Y. Nakagawa, T. Miyashita, T. Sakamoto, T. Terakubo, H. Ishiguro, and N. Hagita, “Recommendation Effects of a Social Robot for Advertisement-Use Context in a Shopping Mall,” *International Journal of Social Robotics*, vol. 5, no. 2, pp. 251–262, 2013.

[36] N. Doering, S. Poeschl, H.-M. Gross, A. Bley, C. Martin, and H.-J. Boehme, “User-Centered Design and Evaluation of a Mobile Shopping Robot,” *International Journal of Social Robotics*, vol. 7, no. 2, pp. 203–225, 2015.

[37] T. Zhao and Y. Wang, “Market based multi-robot coordination for a cooperative collecting and transportation problem,” Proceedings *IEEE SOUTHEASTCON Conference*, pp. 1–6, 2013.

[38] D. F. Glas, Y. Morales, T. Kanda, H. Ishiguro, and N. Hagita, “Simultaneous people tracking and robot localization in dynamic social spaces,” *Auton Robot*, vol. 39, no. 1, pp. 43–63, 2015.

[39] N. Matsuhira, F. Ozaki, S. Tokura, T. Sonoura, T. Tasaki, H. Ogawa, M. Sano, A. Numata, N. Hashimoto, and K. Komoriya, “Development of robotic transportation system - Shopping support system collaborating with environmental cameras and mobile robots -,” Proceedings *2010 41st International Symposium on and 2010 6th German Conference on Robotics (ROBOTIK)*, pp. 1–6, 2010.

[40] Y. L. Ng, C. S. Lim, K. A. Danapalasingam, M. L. P. Tan, and C. W. Tan, “Automatic human guided shopping trolley with smart shopping system,” *Jurnal Teknologi*, vol. 73, no. 3, pp. 49–56, 2015.

[41] T. Tomizawa, A. Ohya, and S. Yuta, “Remote Shopping Robot System, -Development of a hand mechanism for grasping fresh foods in a supermarket,” Proceedings *2006 IEEE/RSJ International Conference on Intelligent Robots and Systems*, pp. 4953–4958, 2006.

[42] S. Ljungblad, J. Kotrbova, M. Jacobsson, H. Cramer, and K. Niechwiadowicz, “Hospital

- robot at work: Something alien or an intelligent colleague?," *Proceedings ACM Conference on Computer Supported Cooperative Work*, pp. 177–186, 2012.
- [43] H. Li, M. H. Gail, B. Scott, H. T. Gold, D. Walter, M. Liu, C. P. Gross, and D. V. Makarov, "Are hospitals 'keeping up with the Joneses'? : Assessing the spatial and temporal diffusion of the surgical robot," *Healthcare*, vol. 2, no. 2, pp. 152–157, 2014.
- [44] C. Murray, E. Ortiz, and C. Kubin, "Application of a robot for critical care rounding in small rural hospitals," *Critical Care Nursing Clinics of North America*, vol. 26, no. 4, pp. 477–485, 2014.
- [45] J. Lee, "Surgical-robot costs put small hospitals in a bind.," *Modern healthcare*, vol. 44, no. 16, pp. 12–14, 2014.
- [46] B. Ilias, R. Nagarajan, M. Murugappan, K. Helmy, O. Awang, and R. Abdul, "Hospital nurse following robot: Hardware development and sensor integration," *International Journal of Medical Engineering and Informatics*, vol. 6, no. 1, pp. 1–13, 2014.
- [47] J. H. Pyun, H. K. Kim, J. Y. Kim, S. B. Kim, S. Cho, S. G. Kang, Y. H. Ko, J. Cheon, J. G. Lee, J. J. Kim, and S. H. Kang, "Standardized analysis of complications after robot-assisted radical cystectomy: Korea university hospital experience," *Korean Journal of Urology*, vol. 56, no. 1, pp. 48–55, 2015.
- [48] F. Zhou, M. Zhou, X. Yuan, and H. Zhang, "Design, implementation and application of real-time obstacle avoidance method for hospital wards inspection robot," *ICIC Express Letters, Part B: Applications*, vol. 6, no. 7, pp. 1865–1871, 2015.
- [49] G. Sivarajan, G. B. Taksler, D. Walter, C. P. Gross, R. E. Sosa, and D. V. Makarov, "The Effect of the diffusion of the surgical robot on the hospital-level utilization of partial Nephrectomy," *Medical Care*, vol. 53, no. 1, pp. 71–78, 2015.
- [50] H. S. Ahn, M. H. Lee, and B. A. Macdonald, "Healthcare robot systems for a hospital environment: CareBot and ReceptionBot," *Proceedings IEEE International Workshop on Robot and Human Interactive Communication*, pp. 571–576, 2015.
- [51] K. Wittig, N. Ruel, J. Barlog, L. Crocitto, K. Chan, C. Lau, T. Wilson, and B. Yuh, "Critical Analysis of Hospital Readmission and Cost Burden after Robot-Assisted Radical Cystectomy," *Journal of Endourology*, vol. 30, no. 1, pp. 83–91, 2016.
- [52] C. Wang, A. V. Savkin, R. Clout, and H. T. Nguyen, "An Intelligent Robotic Hospital Bed for Safe Transportation of Critical Neurosurgery Patients Along Crowded Hospital Corridors," *IEEE Transactions on Neural Systems and Rehabilitation Engineering*, vol. 23, no. 5, pp. 744–754, 2015.
- [53] R. Tasaki, M. Kitazaki, J. Miura, and K. Terashima, "Prototype design of medical round supporting robot 'Terapio';," *Proceedings 2015 IEEE International Conference on Robotics and Automation (ICRA)*, pp. 829–834, 2015.
- [54] M. Takahashi, T. Suzuki, F. Cinquegrani, R. Sorbello, and E. Pagello, "A mobile robot for transport applications in hospital domain with safe human detection algorithm," *Proceedings 2009 IEEE International Conference on Robotics and Biomimetics (ROBIO)*, pp. 1543–1548, 2009.
- [55] H. D. Nayar, "Field applications for advanced robotics," *Proceedings Annual Offshore Technology Conference*, pp. 1109–1120, 2015.

- [56] J. Ma, H. Kharboutly, A. Benali, F. B. Amar, and M. Bouzit, "Design of omnidirectional mobile platform for balance analysis," *IEEE/ASME Transactions on Mechatronics*, vol. 19, no. 6, pp. 1872–1881, 2014.
- [57] A. Liekna and J. Grundspenkis, "Towards practical application of swarm robotics: Overview of swarm tasks," *Engineering for Rural Development*, 2014, vol. 13, pp. 271–277.
- [58] L. Ribas-Xirgo, A. Miro-Vicente, I. F. Chaile, and A. J. Velasco-Gonzalez, "Multi-agent model of a sample transport system for modular in-vitro diagnostics laboratories," *Proceedings IEEE International Conference on Emerging Technologies and Factory Automation*, pp. 1–8, 2012.
- [59] V. Sunspiral, D. W. Wheeler, D. Chavez-Clemente, and D. Mittman, "Development and field testing of the FootFall planning system for the ATHLETE robots," *Journal of Field Robotics*, vol. 29, no. 3, pp. 483–505, 2012.
- [60] Y. Wang, P. G. D. Siriwardana, and S. De, "Multi-robot cooperative transportation of objects using machine learning," *International Journal of Robotics and Automation*, vol. 26, no. 4, pp. 369–375, 2011.
- [61] S. Hu and D. Sun, "Automated transportation of single cells using robot-tweezer manipulation system," *Journal of Laboratory Automation*, vol. 16, no. 4, pp. 263–270, 2011.
- [62] D. Kaliukhovich, V. Golovko, and A. Paczynski, "Control algorithms for the mobile robot 'MAX' on a task of line following provided by intelligent image processing," *Solid State Phenomena*, vol. 147–149, pp. 35–42, 2009.
- [63] Y. Dai, Y. Kim, S. Wee, D. Lee, and S. Lee, "Symmetric caging formation for convex polygonal object transportation by multiple mobile robots based on fuzzy sliding mode control," *ISA Transactions*, vol. 60, pp. 321–332, 2016.
- [64] M. Wojtczyk, G. Panin, C. Lenz, T. Roder, S. Nair, E. Roth, A. Knoll, R. Heidemann, K. Joeris, C. Zhang, M. Burnett, and T. Monica, "A vision based human robot interface for robotic walkthroughs in a biotech laboratory," *Proceedings 4th ACM/IEEE International Conference on Human-Robot Interaction (HRI)*, pp. 309–310, 2009.
- [65] P. Najmabadi, A. A. Goldenberg, and A. Emili, "A scalable robotic-based laboratory automation system for medium-sized biotechnology laboratories," *Proceedings IEEE International Conference on Automation Science and Engineering*, pp. 166 – 171, 2005.
- [66] W. Gecks and S. T. Pedersen, "Robotics-an efficient tool for laboratory automation," *IEEE Transactions on Industry Applications*, vol. 28, no. 4, pp. 938–944, 1992.
- [67] J. Martínez-Gómez, I. García-Varea, M. Cazorla, and V. Morell, "ViDRILo: The visual and depth robot indoor localization with objects information dataset," *International Journal of Robotics Research*, vol. 34, no. 14, pp. 1681–1687, 2015.
- [68] H.-Y. Chung, C.-C. Hou, and Y.-S. Chen, "Indoor Intelligent Mobile Robot Localization Using Fuzzy Compensation and Kalman Filter to Fuse the Data of Gyroscope and Magnetometer," *IEEE Transactions on Industrial Electronics*, vol. 62, no. 10, pp. 6436–6447, 2015.
- [69] S.-Y. An, L.-K. Lee, and S.-Y. Oh, "Ceiling vision-based active SLAM framework for dynamic and wide-open environments," *Autonomous Robots*, vol. 40, no. 2, pp. 291–324, 2016.
- [70] J. Martínez-Carranza, R. Bostock, S. Willcox, I. Cowling, and W. Mayol-Cuevas, "Indoor



- MAV auto-retrieval using fast 6D relocalisation,” *Advanced Robotics*, vol. 30, no. 2, pp. 119–130, 2016.
- [71] C. Fernández-Caramés, F. J. Serrano, V. Moreno, B. Curto, J. F. Rodríguez-Aragón, and R. Alves, “A real-time indoor localization approach integrated with a Geographic Information System (GIS),” *Robotics and Autonomous Systems*, vol. 75, pp. 475–489, 2016.
- [72] Z. Huang, J. Zhu, L. Yang, B. Xue, J. Wu, and Z. Zhao, “Accurate 3-D Position and Orientation Method for Indoor Mobile Robot Navigation Based on Photoelectric Scanning,” *IEEE Transactions on Instrumentation and Measurement*, vol. 64, no. 9, pp. 2518–2529, 2015.
- [73] S. Gai, S.-M. Oh, and B.-J. Yi, “ASC localization in noisy environment based on wireless sensor network,” *Intelligent Service Robotics*, vol. 8, no. 4, pp. 201–213, 2015.
- [74] H. Cheng, H. Chen, and Y. Liu, “Topological Indoor Localization and Navigation for Autonomous Mobile Robot,” *IEEE Transactions on Automation Science and Engineering*, vol. 12, no. 2, pp. 729–738, 2015.
- [75] S. Wen, X. Chen, C. Ma, H. K. Lam, and S. Hua, “The Q-learning obstacle avoidance algorithm based on EKF-SLAM for NAO autonomous walking under unknown environments,” *Robotics and Autonomous Systems*, vol. 72, pp. 29–36, 2015.
- [76] C.-H. Lin and K.-T. Song, “Robust ground plane region detection using multiple visual cues for obstacle avoidance of a mobile robot,” *Robotica*, vol. 33, no. 2, pp. 436–450, 2015.
- [77] O. Montiel, R. Sepúlveda, and U. Orozco-Rosas, “Optimal Path Planning Generation for Mobile Robots using Parallel Evolutionary Artificial Potential Field,” *Journal of Intelligent and Robotic Systems: Theory and Applications*, vol. 79, no. 2, pp. 237–257, 2015.
- [78] R. R. Nair, L. Behera, V. Kumar, and M. Jamshidi, “Multisatellite formation control for remote sensing applications using artificial potential field and adaptive fuzzy sliding mode control,” *IEEE Systems Journal*, vol. 9, no. 2, pp. 508–518, 2015.
- [79] J.-H. Park and U.-Y. Huh, “Local path planning for mobile robot using artificial neural network - Potential field algorithm,” *Transactions of the Korean Institute of Electrical Engineers*, vol. 64, no. 10, pp. 1479–1485, 2015.
- [80] G. Wang, Z. Dai, Y. Guan, P. Dong, and L. Wu, “Power management of hybrid power systems with Li-Fe batteries and supercapacitors for mobile robots,” *Advances in Mechanical Engineering*, pp. 1–11, 2014.
- [81] J. Gao, G. Yan, Z. Wang, P. Jiang, and D. Liu, “A capsule robot powered by wireless power transmission: Design of its receiving coil,” *Sensors and Actuators, A: Physical*, vol. 234, pp. 133–142, 2015.
- [82] A. S. Potts and C. Da, “Optimal power loss motion planning in legged robots,” *Robotica*, vol. 34, no. 2, pp. 423–448, 2016.
- [83] M. Partovibakhsh and G. Liu, “An adaptive unscented kalman filtering approach for online estimation of model parameters and state-of-charge of lithium-ion batteries for autonomous mobile robots,” *IEEE Transactions on Control Systems Technology*, vol. 23, no. 1, pp. 357–363, 2014.
- [84] B. R. Jouybari, K. G. Osgouie, and A. Meghdari, “Optimization of kinematic redundancy and workspace analysis of a dual-arm cam-lock robot,” *Robotica*, vol. 34, no. 1, pp. 23–42, 2016.

- [85] A. D'Ausilio, L. Badino, P. Cipresso, A. Chirico, E. Ferrari, G. Riva, and A. Gaggioli, "Automatic imitation of the arm kinematic profile in interacting partners," *Cognitive Processing*, vol. 16, pp. 197–201, 2015.
- [86] P. Long, W. Khalil, and S. Caro, "Kinematic and dynamic analysis of lower-mobility cooperative arms," *Robotica*, vol. 33, no. 9, pp. 1813–1834, 2015.
- [87] M. R. C. Qazani, S. Pedrammehr, A. Rahmani, B. Danaei, M. M. Ettetfagh, A. K. S. Rajab, and H. Abdi, "Kinematic analysis and workspace determination of hexarot-a novel 6-DOF parallel manipulator with a rotation-symmetric arm system," *Robotica*, vol. 33, no. 8, pp. 1686–1703, 2015.
- [88] P. Gil, C. Mateo, and F. Torres, "3D visual sensing of the human hand for the remote operation of a robotic hand," *International Journal of Advanced Robotic Systems*, vol. 11, no. 1, pp. 1–13, 2014.
- [89] Z. Tomori, P. Vanko, and B. Vaitovic, "Using of low-cost 3D cameras to control interactive exhibits in science centre," *Advances in Intelligent Systems and Computing*, vol. 316, pp. 273–281, 2015.
- [90] D. Kruse, J. T. Wen, and R. J. Radke, "A sensor-based dual-arm tele-robotic system," *IEEE Transactions on Automation Science and Engineering*, vol. 12, no. 1, pp. 4–18, 2015.
- [91] S. Buitrago, O. L. Ramos, and D. Amaya, "Control algorithm for an industrial robotic arm using computer vision," *International Review of Mechanical Engineering*, vol. 9, no. 2, pp. 182–190, 2015.
- [92] "Dr Robot Inc. [Online]. Available: <http://www.drrobot.com/>. [Accessed: 17-January-2016]."
- [93] A. Sheinker, B. Ginzburg, N. Salomonski, L. Frumkis, B.-Z. Kaplan, and M. B. Moldwin, "A method for indoor navigation based on magnetic beacons using smartphones and tablets," *Measurement: Journal of the International Measurement Confederation*, vol. 81, pp. 197–209, 2016.
- [94] L. Huang, D. He, Z. Zhang, and P. Zhang, "Path Navigation For Indoor Robot With Q-Learning," *Intelligent Automation and Soft Computing*, vol. 1, pp. 1–7, 2016.
- [95] C. Sprunk, J. Röwekämper, G. Parent, L. Spinello, G. D. Tipaldi, W. Burgard, and M. Jalobeanu, "An experimental protocol for benchmarking robotic indoor navigation," *Springer Tracts in Advanced Robotics*, vol. 109, pp. 487–504, 2016.
- [96] S. Taneja, B. Akinci, J. H. Garrett Jr., and L. Soibelman, "Algorithms for automated generation of navigation models from building information models to support indoor map-matching," *Automation in Construction*, vol. 61, pp. 24–41, 2016.
- [97] G. Gerstweiler, E. Vonach, and H. Kaufmann, "HyMoTrack: A mobile AR navigation system for complex indoor environments," *Sensors (Switzerland)*, vol. 16, no. 1, pp. 1–19, 2015.
- [98] M. M. Atia, S. Liu, H. Nematallah, T. B. Karamat, and A. Noureldin, "Integrated indoor navigation system for ground vehicles with automatic 3-D alignment and position initialization," *IEEE Transactions on Vehicular Technology*, vol. 64, no. 4, pp. 1279–1292, 2015.
- [99] A. Abadleh, S. Han, S. J. Hyun, B. Lee, and M. Kim, "Construction of indoor floor plan and localization," *Wireless Netw*, vol. 22, no. 1, pp. 175–191, May 2015.

- [100] R. Chavez-Romero, A. Cardenas, M. Maya, A. Sanchez, D. Piovesan, R. Chavez-Romero, A. Cardenas, M. Maya, A. Sanchez, and D. Piovesan, "Camera Space Particle Filter for the Robust and Precise Indoor Localization of a Wheelchair," *Journal of Sensors*, vol. 1, pp. 1–12, 2015.
- [101] Y. Sun, M. Liu, and M. Q.-H. Meng, "WiFi signal strength-based robot indoor localization," *Proceedings 2014 IEEE International Conference on Information and Automation (ICIA)*, pp. 250–256, 2014.
- [102] X. Jiang, J. Liu, Y. Chen, D. Liu, Y. Gu, and Z. Chen, "Feature Adaptive Online Sequential Extreme Learning Machine for lifelong indoor localization," *Neural Comput & Applic*, vol. 27, no. 1, pp. 215–225, 2014.
- [103] R. Lin, M. Li, and L. Sun, "Image features-based mobile robot visual SLAM," *Proceedings 2013 IEEE International Conference on Robotics and Biomimetics (ROBIO)*, pp. 2499–2504, 2013.
- [104] B. Olszewski, S. Fenton, B. Tworek, J. Liang, and K. Yelamarthi, "RFID positioning robot: An indoor navigation system," *Proceedings 2013 IEEE International Conference on Electro/Information Technology (EIT)*, pp. 1–6, 2013.
- [105] N. Abdelkrim, K. Issam, K. Lyes, and C. Khaoula, "Fuzzy logic controllers for Mobile robot navigation in unknown environment using Kinect sensor," *Proceedings 2014 International Conference on Systems, Signals and Image Processing (IWSSIP)*, pp. 75–78, 2014.
- [106] P. Benavidez and M. Jamshidi, "Mobile robot navigation and target tracking system," *Proceedings 6th International Conference on System of Systems Engineering (SoSE)*, pp. 299–304, 2011.
- [107] H. Wang, H. Yu, and L. Kong, "Ceiling Light Landmarks Based Localization and Motion Control for a Mobile Robot," *Proceedings IEEE International Conference on Networking, Sensing and Control*, pp. 285–290, 2007.
- [108] X. Chen, R. Li, X. Wang, Y. Tian, and Q. Huang, "A novel artificial landmark for monocular global visual localization of indoor robots," *Proceedings International Conference on Mechatronics and Automation (ICMA)*, pp. 1314–1319, 2010.
- [109] Y.-C. Lee, Christiand, H. Chae, and W. Yu, "Artificial landmark map building method based on grid SLAM in large scale indoor environment," *Proceedings IEEE International Conference on Systems Man and Cybernetics (SMC)*, pp. 4251–4256, 2010.
- [110] X. He, Z. Cai, D. Huang, and Y. Wang, "Integrated indoor navigation system for aerial vehicle using visual odometry and artificial landmark matching," *Proceedings IEEE Chinese Conference on Guidance, Navigation and Control Conference (CGNCC)*, pp. 2059–2064, 2014.
- [111] J. López, C. Watkins, D. Pérez, and M. Díaz-Cacho, "Evaluating different landmark positioning systems within the RIDE architecture," *Journal of Physical Agents*, vol. 7, no. 1, pp. 3–11, 2013.
- [112] I. Ul-Haque and E. Prassler, "Experimental Evaluation of a Low-cost Mobile Robot Localization Technique for Large Indoor Public Environments," *Proceedings 41st International Symposium on and 2010 6th German Conference on Robotics (ROBOTIK)*, pp. 1–7, 2010.
- [113] S. J. Kim and B. K. Kim, "Dynamic ultrasonic hybrid localization system for indoor

- mobile robots,” *IEEE Transactions on Industrial Electronics*, vol. 60, no. 10, pp. 4562–4573, 2013.
- [114] N. Y. Ko and T.-Y. Kuc, “Fusing range measurements from ultrasonic beacons and a laser range finder for localization of a mobile robot,” *Sensors (Switzerland)*, vol. 15, no. 5, pp. 11050–11075, 2015.
- [115] Z. Li and Z. Huang, “Design of a type of cleaning robot with ultrasonic,” *Journal of Theoretical and Applied Information Technology*, vol. 47, no. 3, pp. 1218–1222, 2013.
- [116] W.-S. Moon, B.-S. Cho, and K. R. Baek, “Optimization of code combination in multi-code ultrasonic sensors for multi-robot systems,” *Journal of Institute of Control, Robotics and Systems*, vol. 19, no. 7, pp. 614–619, 2013.
- [117] U. Yayan, H. Yucel, and A. Yazıcı, “A Low Cost Ultrasonic Based Positioning System for the Indoor Navigation of Mobile Robots,” *Journal of Intelligent and Robotic Systems: Theory and Applications*, vol. 78, no. 3–4, pp. 541–552, 2015.
- [118] L. Chassagne, O. Bruneau, A. Bialek, C. Falguière, E. Broussard, and O. Barrois, “Ultrasonic Sensor Triangulation for Accurate 3D Relative Positioning of Humanoid Robot Feet,” *IEEE Sensors Journal*, vol. 15, no. 5, pp. 2856–2865, 2015.
- [119] A. Medina-Santiago, J. L. Camas-Anzueto, J. A. Vazquez-Feijoo, L. Hernández-De, and R. Mota-Grajales, “Neural control system in obstacle avoidance in mobile robots using ultrasonic sensors,” *Journal of Applied Research and Technology*, vol. 12, no. 1, pp. 104–110, 2014.
- [120] H. C. Yun and T. H. Park, “Auto-parking controller of omnidirectional mobile robot using image localization sensor and ultrasonic sensors,” *Journal of Institute of Control, Robotics and Systems*, vol. 21, no. 6, pp. 571–576, 2015.
- [121] Y. Zhuang, H. Lan, Y. Li, and N. El-Sheimy, “PDR/INS/WiFi integration based on handheld devices for indoor pedestrian navigation,” *Micromachines*, vol. 6, no. 6, pp. 793–812, 2015.
- [122] J. Cheng, L. Yang, Y. Li, and W. Zhang, “Seamless outdoor/indoor navigation with WIFI/GPS aided low cost Inertial Navigation System,” *Physical Communication*, vol. 13, no. PA, pp. 31–43, 2014.
- [123] M. M. Atia, M. J. Korenberg, and A. Noureldin, “Particle-filter-based WiFi-aided reduced inertial sensors navigation system for indoor and GPS-denied environments,” *International Journal of Navigation and Observation*, vol. 1, pp. 1–13, 2012.
- [124] F. Evennou and F. Marx, “Advanced integration of WiFi and inertial navigation systems for indoor mobile positioning,” *Eurasip Journal on Applied Signal Processing*, vol. 1, pp. 1–11, 2006.
- [125] Y. Li, Y. Zhuang, H. Lan, P. Zhang, X. Niu, and N. El-Sheimy, “WiFi-aided magnetic matching for indoor navigation with consumer portable devices,” *Micromachines*, vol. 6, no. 6, pp. 747–764, 2015.
- [126] H.-H. Liu, W.-H. Lo, C.-C. Tseng, and H.-Y. Shin, “A WiFi-Based Weighted Screening Method for Indoor Positioning Systems,” *Wireless Personal Communications*, vol. 79, no. 1, pp. 611–627, 2014.
- [127] K. Choi, J. Park, Y.-H. Kim, and H.-K. Lee, “Monocular SLAM with undelayed

- initialization for an indoor robot,” *Robotics and Autonomous Systems*, vol. 60, no. 6, pp. 841–851, 2012.
- [128] R. Lin, Y. Wang, and S. Yang, “RGBD SLAM for indoor environment,” *Advances in Intelligent Systems and Computing*, vol. 215, pp. 161–175, 2014.
- [129] J. Jung, T. Oh, and H. Myung, “Magnetic field constraints and sequence-based matching for indoor pose graph SLAM,” *Robotics and Autonomous Systems*, vol. 70, pp. 92–105, 2015.
- [130] J. Jung, S. Yoon, S. Ju, and J. Heo, “Development of kinematic 3D laser scanning system for indoor mapping and as-built BIM using constrained SLAM,” *Sensors (Switzerland)*, vol. 15, no. 10, pp. 26430–26456, 2015.
- [131] J. Lv, Y. Kobayashi, T. Emaru, and A. A. Ravankar, “Indoor slope and edge detection by using two-dimensional EKF-SLAM with orthogonal assumption,” *International Journal of Advanced Robotic Systems*, vol. 12, pp. 1–16, 2015.
- [132] Y.-S. Jeon, J. Choi, and J. O. Lee, “Development of a SLAM System for Small UAVs in Indoor Environments using Gaussian Processes,” *Journal of Institute of Control, Robotics and Systems*, vol. 20, no. 11, pp. 1098–1102, 2014.
- [133] S.-Y. Hwang and J.-B. Song, “Monocular vision-based SLAM in indoor environment using corner, lamp, and door features from upward-looking camera,” *IEEE Transactions on Industrial Electronics*, vol. 58, no. 10, pp. 4804–4812, 2011.
- [134] M. Cremer, U. Dettmar, C. Hudusch, R. Kronberger, R. Lerche, and A. Pervez, “Localization of Passive UHF RFID Tags Using the AoA Transmitter Beamforming Technique,” *IEEE Sensors Journal*, vol. 16, no. 6, pp. 1762–1771, 2016.
- [135] N. Decarli, F. Guidi, and D. Dardari, “Passive UWB RFID for Tag Localization: Architectures and Design,” *IEEE Sensors Journal*, vol. 16, no. 5, pp. 1385–1397, 2016.
- [136] A. Aguilar-Garcia, S. Fortes, E. Colin, and R. Barco, “Enhancing RFID indoor localization with cellular technologies,” *Eurasip Journal on Wireless Communications and Networking*, vol. 2015, no. 1, pp. 1–22, 2015.
- [137] F. Martinelli, “A Robot Localization System Combining RSSI and Phase Shift in UHF-RFID Signals,” *IEEE Transactions on Control Systems Technology*, vol. 23, no. 5, pp. 1782–1796, 2015.
- [138] M. Scherhäufl, M. Pichler, and A. Stelzer, “UHF RFID Localization Based on Evaluation of Backscattered Tag Signals,” *IEEE Transactions on Instrumentation and Measurement*, vol. 64, no. 11, pp. 2889–2899, 2015.
- [139] S. Dhananjeyan, S. Mohana, A. Kalaiyarasi, and P. G. Kuppusamy, “Design and development of blind navigation system using GSM and RFID technology,” *Indian Journal of Science and Technology*, vol. 9, no. 2, pp. 1–5, 2016.
- [140] C. Tsirmpas, A. Rompas, O. Fokou, and D. Koutsouris, “An indoor navigation system for visually impaired and elderly people based on Radio Frequency Identification (RFID),” *Information Sciences*, vol. 320, pp. 288–305, 2015.
- [141] “HAGISONIC Inc. [Online]. Available: <http://eng.hagisonic.kr/main.html>. [Accessed: 17-January-2016].” .
- [142] K. Thurow and H. Liu, “Mobile robotics for life science laboratories,” Book Chapter:

*Mobile Robotics: Principles, Techniques and Applications*, Nova Science Publishers (USA), pp. 1–23, 2015.

[143] A. A. Abdulla, H. Liu, N. Stoll, and K. Thurow, “Multi-floor navigation method for mobile robot transportation based on StarGazer sensors in life science automation,” *Proceedings IEEE Instrumentation and Measurement Technology Conference*, pp. 428–433, 2015.

[144] M. Ghandour, H. Liu, N. Stoll, and K. Thurow, “Improving the navigation of indoor mobile robots using Kalman filter,” *Proceedings IEEE Instrumentation and Measurement Technology Conference*, pp. 1434–1439, 2015.

[145] S. W. Yoon, S.-B. Park, and J. S. Kim, “Kalman filter sensor fusion for Mecanum wheeled automated guided vehicle localization,” *Journal of Sensors*, pp. 1–7, 2015.

[146] H. Liu, N. Stoll, S. Junginger, and K. Thurow, “A fast approach to arm blind grasping and placing for mobile robot transportation in laboratories,” *International Journal of Advanced Robotic Systems*, vol. 11, no. 1, pp. 1–12, 2014.

[147] L.-K. Chen and M.-Y. Hsiao, “Control of service robot by integration of multiple intermittent sensors,” *Advanced Materials Research*, vol. 939, pp. 609–614, 2014.

[148] H. Liu, N. Stoll, S. Junginger, and K. Thurow, “Mobile robot for life science automation,” *International Journal of Advanced Robotic Systems*, vol. 10, pp. 1–14, 2013.

[149] I. S. Kim, W. K. Hyun, J. J. Yu, and S. S. Park, “An effective localization and navigation method based on sensor fusion for mobile robot moving in unknown indoor environment,” *Proceedings 14th International Symposium on Artificial Life and Robotics*, pp. 557–560, 2009.

[150] H. Liu, N. Stoll, S. Junginger, and K. Thurow, “A Floyd-Dijkstra hybrid application for mobile robot path planning in life science automation,” *Proceedings IEEE International Conference on Automation Science and Engineering*, pp. 279–284, 2012.

[151] H. Liu, N. Stoll, S. Junginger, and K. Thurow, “A floyd-genetic algorithm based path planning system for mobile robots in laboratory automation,” *Proceedings IEEE International Conference on Robotics and Biomimetics(ROBIO)*, pp. 1550–1555, 2012.

[152] A. V. Gerbessiotis and C. J. Siniolakis, “A probabilistic analysis of the Floyd-Rivest expected time selection algorithm,” *International Journal of Computer Mathematics*, vol. 82, no. 5, pp. 509–519, 2005.

[153] K. C. Kiwiel, “On Floyd and Rivest’s SELECT algorithm,” *Theoretical Computer Science*, vol. 347, no. 1–2, pp. 214–238, 2005.

[154] S. Hougardy, “The Floyd-Warshall algorithm on graphs with negative cycles,” *Information Processing Letters*, vol. 110, no. 8–9, pp. 279–281, 2010.

[155] Y. Zhang, J. Tang, S. Lv, and X. Luo, “Floyd-A\* algorithm solving the least-time itinerary planning problem in urban scheduled public transport network,” *Mathematical Problems in Engineering*, pp. 1–16, 2014.

[156] G.-Z. Tan, H. He, and A. Sloman, “Global optimal path planning for mobile robot based on improved Dijkstra algorithm and ant system algorithm,” *Journal of Central South University of Technology (English Edition)*, vol. 13, no. 1, pp. 80–86, 2006.

[157] Z. Zhang and Z. Zhao, “A multiple mobile robots path planning algorithm based on

- a-star and dijkstra algorithm,” *International Journal of Smart Home*, vol. 8, no. 3, pp. 75–86, 2014.
- [158] J. Guo, Y. Gao, and G. Cui, “The navigation of mobile robot based on hybrid Dijkstra algorithm,” *Journal of Computational Information Systems*, vol. 10, no. 9, pp. 3879–3886, 2014.
- [159] K. Uchida, “Discrete ray tracing based on Dijkstra Algorithm for diffraction and reflection,” *International Journal of Microwave and Optical Technology*, vol. 10, no. 6, pp. 377–384, 2015.
- [160] D. Ghosh, S. Kumar, and P. Bhulania, “A novel solution of dijkstra’s algorithm for shortest path routing with polygonal obstacles in wireless networks using fuzzy mathematics,” *Advances in Intelligent Systems and Computing*, vol. 380, pp. 489–497, 2016.
- [161] M. Gemeinder and M. Gerke, “GA-based path planning for mobile robot systems employing an active search algorithm,” *Applied Soft Computing Journal*, vol. 3, no. 2, pp. 149–158, 2003.
- [162] J. C. Mohanta, D. R. Parhi, and S. K. Patel, “Path planning strategy for autonomous mobile robot navigation using Petri-GA optimisation,” *Computers and Electrical Engineering*, vol. 37, no. 6, pp. 1058–1070, 2011.
- [163] I. Châari, A. Koubâa, S. Trigui, H. Bennaceur, A. Ammar, and K. Al-Shalfan, “SmartPATH: An efficient hybrid ACO-GA algorithm for solving the global path planning problem of mobile robots,” *International Journal of Advanced Robotic Systems*, vol. 11, no. 1, pp. 1–15, 2014.
- [164] A. Watkins, “GA-based path planning for mobile robots: An empirical evaluation of seven techniques,” *Journal of Computers (Finland)*, vol. 8, no. 8, pp. 1912–1922, 2013.
- [165] H. Liu, N. Stoll, S. Junginger, and K. Thürow, “Mobile robotic transportation in laboratory automation: Multi-robot control, robot-door integration and robot-human interaction,” *Proceedings IEEE International Conference on Robotics and Biomimetics*, pp. 1033–1038, 2014.
- [166] R. N. Calheiros, E. Masoumi, R. Ranjan, and R. Buyya, “Workload prediction using ARIMA model and its impact on cloud applications’ QoS,” *IEEE Transactions on Cloud Computing*, vol. 3, no. 4, pp. 449–458, 2015.
- [167] M.-D. Ma and J.-Y. Li, “Improved variable EWMA controller for general ARIMA processes,” *IEEE Transactions on Semiconductor Manufacturing*, vol. 28, no. 2, pp. 129–136, 2015.
- [168] M. Ndong, D. Kâ, A. Diop, and S. Dossou-Gbété, “Estimation for seasonal fractional ARIMA with stable innovations via the empirical characteristic function method,” *Statistics*, vol. 50, no. 2, pp. 298–311, 2016.
- [169] Z. Rzepecka, J. Z. Kalita, K. Stępiak, and P. Wielgosz, “Time series analysis of radio signals wet tropospheric delays for short-term forecast,” *Acta Geodynamica et Geomaterialia*, vol. 12, no. 4, pp. 345–354, 2015.
- [170] M. Majidpour, C. Qiu, P. Chu, R. Gadh, and H. R. Pota, “Fast prediction for sparse time series: Demand forecast of EV charging stations for cell phone applications,” *IEEE Transactions on Industrial Informatics*, vol. 11, no. 1, pp. 242–250, 2015.
- [171] D. S. P. Salazar, P. J. L. Adeodato, and A. L. Arnaud, “Continuous dynamical

combination of short and long-term forecasts for nonstationary time series,” *IEEE Transactions on Neural Networks and Learning Systems*, vol. 25, no. 1, pp. 241–246, 2014.

[172] H. Ghosh, Prajneshu, and S. Samanta, “Fitting of self-exciting threshold autoregressive moving average nonlinear time-series model through genetic algorithm and development of out-of-sample forecasts,” *Statistics*, vol. 48, no. 5, pp. 1166–1184, 2014.

[173] C. Antoniou, E. Papadimitriou, and G. Yannis, “Road Safety Forecasts in Five European Countries Using Structural Time Series Models,” *Traffic Injury Prevention*, vol. 15, no. 6, pp. 598–605, 2014.

[174] S. Abdolahi, S. Hadinia, and K. Babaei, “The study of usefulness of different earnings forecast models (usefulness of different earnings forecast models by management compared to earnings forecast through time series models),” *Life Science Journal*, vol. 10, pp. 225–232, 2013.

[175] M. Huang and Y. Tian, “A novel visual modeling system for time series forecast: Application to the domain of hydrology,” *Journal of Hydroinformatics*, vol. 15, no. 1, pp. 21–37, 2013.

[176] Q. Xiao, H. Fu, Z. Wang, Y. Zhang, and Y. Wu, “The stability analysis of the adaptive three-stage Kalman filter,” *Signal Processing*, vol. 118, pp. 1–24, 2016.

[177] P. A. C. Lopes, J. A. B. Gerald, and M. S. Piedade, “The Random Walk Model Kalman Filter in Multichannel Active Noise Control,” *IEEE Signal Processing Letters*, vol. 22, no. 12, pp. 2244–2248, 2015.

[178] G. Du and P. Zhang, “A novel human-manipulators interface using hybrid sensors with Kalman filter and particle filter,” *Robotics and Computer-Integrated Manufacturing*, vol. 38, pp. 93–101, 2016.

[179] W. Li, Y. Jia, and J. Du, “Event-triggered Kalman consensus filter over sensor networks,” *IET Control Theory and Applications*, vol. 10, no. 1, pp. 103–110, 2016.

[180] J. Pan, X. Yang, H. Cai, and B. Mu, “Image noise smoothing using a modified Kalman filter,” *Neurocomputing*, vol. 173, pp. 1625–1629, 2016.

[181] B. Fridholm, T. Wik, and M. Nilsson, “Kalman filter for adaptive learning of look-up tables with application to automotive battery resistance estimation,” *Control Engineering Practice*, vol. 48, pp. 78–86, 2016.

[182] D. Viegas, P. Batista, P. Oliveira, and C. Silvestre, “On the stability of the continuous-time Kalman filter subject to exponentially decaying perturbations,” *Systems and Control Letters*, vol. 89, pp. 41–46, 2016.

[183] J. Meng, G. Luo, and F. Gao, “Lithium polymer battery state-of-charge estimation based on adaptive unscented kalman filter and support vector machine,” *IEEE Transactions on Power Electronics*, vol. 31, no. 3, pp. 2226–2238, 2016.

[184] B. L. Boada, M. J. L. Boada, and V. Diaz, “Vehicle sideslip angle measurement based on sensor data fusion using an integrated ANFIS and an Unscented Kalman Filter algorithm,” *Mechanical Systems and Signal Processing*, vol. 72–73, pp. 832–845, 2016.

[185] C. K. Chui, and G. R. Chen, *Kalman Filtering with Real-Time Applications*. Springer Science & Business Media, ISBN: 978-3-540-87848-3, Germany, 2009.

[186] S. S. Haykin, S. S. Haykin, and S. S. Haykin, *Kalman filtering and neural networks*.



Wiley Online Library, ISBN: 978-0-471-36998-1, USA, 2001.

- [187] G. Evensen, *Data assimilation: the ensemble Kalman filter*. Springer Science & Business Media, ISBN: 978-3-642-03711-5, Germany, 2009.
- [188] D. Li, J. Ouyang, H. Li, and J. Wan, "State of charge estimation for LiMn<sub>2</sub>O<sub>4</sub> power battery based on strong tracking sigma point Kalman filter," *Journal of Power Sources*, vol. 279, pp. 439–449, 2015.
- [189] W. Bukhari and S.-M. Hong, "Real-time prediction and gating of respiratory motion using an extended Kalman filter and Gaussian process regression," *Physics in Medicine and Biology*, vol. 60, no. 1, pp. 233–252, 2015.
- [190] G. Giorgi, "An event-based kalman filter for clock synchronization," *IEEE Transactions on Instrumentation and Measurement*, vol. 64, no. 2, pp. 449–457, 2015.
- [191] H. Liu, H.-Q. Tian, and Y.-F. Li, "Comparison of two new ARIMA-ANN and ARIMA-Kalman hybrid methods for wind speed prediction," *Applied Energy*, vol. 98, pp. 415–424, 2012.
- [192] M. Shiomi, F. Zanlungo, K. Hayashi, and T. Kanda, "Towards a Socially Acceptable Collision Avoidance for a Mobile Robot Navigating Among Pedestrians Using a Pedestrian Model," *International Journal of Social Robotics*, vol. 6, no. 3, pp. 443–455, 2014.
- [193] P. Ratsamee, Y. Mae, K. Ohara, T. Takubo, and T. Arai, "Human-robot collision avoidance using a modified social force model with body pose and face orientation," *International Journal of Humanoid Robotics*, vol. 10, no. 1, 2013.
- [194] A. Cherubini and F. Chaumette, "Visual navigation of a mobile robot with laser-based collision avoidance," *International Journal of Robotics Research*, vol. 32, no. 2, pp. 189–205, 2013.
- [195] A. Soriano, E. J. Bernabeu, A. Valera, and M. Vallés, "Collision avoidance of mobile robots using multi-agent systems," *Advances in Intelligent Systems and Computing*, vol. 217, pp. 429–437, 2013.
- [196] A. Yang, W. Naeem, M. Fei, L. Liu, and X. Tu, "Synthesis of multi-robot formation manoeuvre and collision avoidance," *Communications in Computer and Information Science*, vol. 462, pp. 533–542, 2014.
- [197] Y. Chen and Q. Chen, "Real-time self-collision avoidance for humanoid robot based on dynamic task-prior system," *International Journal of Robotics and Automation*, vol. 29, no. 3, pp. 234–244, 2014.
- [198] N. Asakawa and Y. Kanjo, "Collision avoidance of a welding robot for a large structure (application of potential field)," *International Journal of Automation Technology*, vol. 7, no. 2, pp. 190–195, 2013.
- [199] J. Ruchti, R. Senkbeil, J. Carroll, J. Dickinson, J. Holt, and S. Biaz, "Unmanned aerial system collision avoidance using artificial potential fields," *Journal of Aerospace Information Systems*, vol. 11, no. 3, pp. 140–144, 2014.
- [200] H.-T. Chiang, N. Malone, K. Lesser, M. Oishi, and L. Tapia, "Aggressive moving obstacle avoidance using a stochastic reachable set based potential field," *Springer Tracts in Advanced Robotics*, vol. 107, pp. 73–89, 2015.

- [201] L. A. García-Delgado, J. R. Noriega, D. Berman-Mendoza, A. L. Leal-Cruz, A. Vera-Marquina, R. Gómez-Fuentes, A. García-Juárez, A. G. Rojas-Hernández, and I. E. Zaldívar-Huerta, “Repulsive Function in Potential Field Based Control with Algorithm for Safer Avoidance,” *Journal of Intelligent and Robotic Systems: Theory and Applications*, vol. 80, no. 1, pp. 59–70, 2015.
- [202] M. Defoort, A. Doniec, and N. Bouraqadi, “Decentralized robust collision avoidance based on receding horizon planning and potential field for multi-robots systems,” *Lecture Notes in Electrical Engineering*, vol. 85, pp. 201–215, 2011.
- [203] E. Oland and R. Kristiansen, “Collision and terrain avoidance for UAVs using the potential field method,” *Proceedings IEEE Aerospace Conference*, pp. 201–215, 2013.
- [204] N. Noto, H. Okuda, Y. Tazaki, and T. Suzuki, “Steering assisting system for obstacle avoidance based on personalized potential field,” *Proceedings IEEE Conference on Intelligent Transportation Systems*, pp. 1702–1707, 2012.
- [205] Y. Girdhar and G. Dudek, “Modeling curiosity in a mobile robot for long-term autonomous exploration and monitoring,” *Autonomous Robots*, pp. 1–12, 2015.
- [206] A. Schierl, A. Angerer, A. Hoffmann, M. Vistein, and W. Reif, “A taxonomy of distribution for cooperative mobile manipulators,” *Proceedings 12th International Conference on Informatics in Control, Automation and Robotics*, pp. 74–83, 2015.
- [207] A. M. Pinto, A. P. Moreira, M. V. Correia, and P. G. Costa, “A flow-based motion perception technique for an autonomous robot system,” *Journal of Intelligent and Robotic Systems: Theory and Applications*, vol. 75, no. 3–4, pp. 475–492, 2014.
- [208] G. Prencipe, “Autonomous mobile robots: A distributed computing perspective,” *Lecture Notes in Computer Science (including subseries Lecture Notes in Artificial Intelligence and Lecture Notes in Bioinformatics)*, vol. 8243, pp. 6–21, 2013.
- [209] N. A. Sabto and M. Al, “Mobile robot localization based on RSSI measurements using an RFID sensor,” *Proceedings IADIS International Conference Intelligent Systems and Agents*, pp. 59–66, 2011.
- [210] N. Elkmann, E. Schulenburg, and M. Fritzsche, “Mobile robot system ‘LISA’ for safe human-robot interaction,” *Proceedings IASTED International Conference on Robotics*, pp. 47–54, 2010.
- [211] P. Ratsamee, Y. Mae, K. Ohara, M. Kojima, and T. Arai, “Social navigation model based on human intention analysis using face orientation,” *Proceedings IEEE/RSJ International Conference on Intelligent Robots and Systems (IROS)*, pp. 1682–1687, 2013.
- [212] E. Machida, M. Cao, T. Murao, and H. Hashimoto, “Human motion tracking of mobile robot with Kinect 3D sensor,” *Proceedings SICE Annual Conference (SICE)*, pp. 2207–2211, 2012.
- [213] T. Beyl, P. Nicolai, J. Raczowsky, H. Worn, M. D. Comparetti, and E. De Momi, “Multi kinect people detection for intuitive and safe human robot cooperation in the operating room,” *Proceedings 16th International Conference on Advanced Robotics (ICAR)*, pp. 1–6, 2013.
- [214] C. Lenz, G. Panin, T. Roder, M. Wojtczyk, and A. Knoll, “Hardware-assisted multiple object tracking for human-robot-interaction,” *Proceedings ACM/IEEE International Conference*

on *Human-Robot Interaction (HRI)*, pp. 283–284, 2009.

[215] B. Wang, C. Yang, and Q. Xie, “Human-machine interfaces based on EMG and Kinect applied to teleoperation of a mobile humanoid robot,” *Proceedings 10th World Congress on Intelligent Control and Automation (WCICA)*, pp. 3903–3908, 2012.

[216] M. Awais and D. Henrich, “Human-Robot Interaction in an Unknown Human Intention Scenario,” *Proceedings 11th International Conference on Frontiers of Information Technology (FIT)*, pp. 89–94, 2013.

[217] Y. Zheng, “Near infrared face recognition using orientation-based face patterns,” *Proceedings International Conference on Biometrics Special Interest Group (BIOSIG)*, pp. 1–4, 2012.

[218] C.-C. Chang and H. Aghajan, “Linear Dynamic Data Fusion Techniques for Face Orientation Estimation in Smart Camera Networks,” *Proceedings First ACM/IEEE International Conference on Distributed Smart Cameras*, pp. 44–51, 2007.

[219] K. Nakamura and H. Takano, “Unregistered Face Discrimination by the Face Orientation and Size Recognition,” *Proceedings International Joint Conference on Neural Networks*, pp. 1924–1928, 2007.

[220] K. C. Yow and R. Cipolla, “Detection of human faces under scale, orientation and viewpoint variations,” *Proceedings International Conference on Automatic Face and Gesture Recognition*, pp. 295–300, 1996.

[221] R. C. Luo, C. T. Liao, and Y. J. Chen, “Robot - human face tracking and recognition using relative affine structure,” *Proceedings IEEE Workshop on Advanced robotics and Its Social Impacts*, pp. 1–6, 2008.

[222] C.-S. Fahn and C.-S. Lo, “A high-definition human face tracking system using the fusion of omni-directional and PTZ cameras mounted on a mobile robot,” *Proceedings 5th IEEE Conference on Industrial Electronics and Applications (ICIEA)*, pp. 6–11, 2010.

[223] M.-C. Hu, C.-W. Chen, W.-H. Cheng, C.-H. Chang, J.-H. Lai, and J.-L. Wu, “Real-Time Human Movement Retrieval and Assessment With Kinect Sensor,” *IEEE Transactions on Cybernetics*, vol. 45, no. 4, pp. 742–753, 2015.

[224] M. T. Nouei, A. V. Kamyad, A. R. Soroush, and S. Ghazalbash, “A comprehensive operating room information system using the Kinect sensors and RFID,” *Journal of Clinical Monitoring and Computing*, vol. 29, no. 2, pp. 251–261, 2015.

[225] N. M. DiFilippo and M. K. Jouaneh, “Characterization of Different Microsoft Kinect Sensor Models,” *IEEE Sensors Journal*, vol. 15, no. 8, pp. 4554–4564, 2015.

[226] A. Procházka, O. Vyšata, M. Vališ, O. Ťupa, M. Schätz, and V. Mařík, “Use of the image and depth sensors of the Microsoft Kinect for the detection of gait disorders,” *Neural Computing and Applications*, vol. 26, no. 7, pp. 1621–1629, 2015.

[227] H. Liu, N. Stoll, S. Junginger, and K. Thurow, “Human face orientation recognition for intelligent mobile robot collision avoidance in laboratory environments using feature detection and LVQ neural networks,” *Proceedings IEEE International Conference on Robotics and Biomimetics (ROBIO)*, pp. 2003–2007, 2015.

[228] X. Liu, H. Du, G. Wang, S. Zhou, and H. Zhang, “Automatic diagnosis of premature

- ventricular contraction based on Lyapunov exponents and LVQ neural network,” *Computer Methods and Programs in Biomedicine*, vol. 122, no. 1, pp. 47–55, 2015.
- [229] J. Amezcua, P. Melin, and O. Castillo, “Design of an optimal modular LVQ network for classification of arrhythmias based on a variable training-test datasets strategy,” *Advances in Intelligent Systems and Computing*, vol. 323, pp. 369–375, 2015.
- [230] J. Amezcua and P. Melin, “Optimization of the LVQ network architecture with a modular approach for arrhythmia classification using PSO,” *Studies in Computational Intelligence*, vol. 601, pp. 119–126, 2015.
- [231] B. Mokbel, B. Paassen, F.-M. Schleif, and B. Hammer, “Metric learning for sequences in relational LVQ,” *Neurocomputing*, vol. 169, pp. 306–322, 2015.
- [232] B. Fan, N. Hu, and Z. Cheng, “Fault degradation state recognition for planetary gear set based on LVQ neural network,” *Lecture Notes in Mechanical Engineering*, vol. 19, pp. 9–18, 2015.
- [233] A. Bekaddour, A. Bessaid, and F. T. Bendimerad, “Multi Spectral Satellite Image Ensembles Classification Combining k-means, LVQ and SVM Classification Techniques,” *Journal of the Indian Society of Remote Sensing*, vol. 43, no. 4, pp. 671–686, 2015.
- [234] T. Villmann, S. Haase, and M. Kaden, “Kernelized vector quantization in gradient-descent learning,” *Neurocomputing*, vol. 147, no. 1, pp. 83–95, 2015.
- [235] V. de, S. C. Pauws, and M. Biehl, “Insightful stress detection from physiology modalities using Learning Vector Quantization,” *Neurocomputing*, vol. 151, no. P2, pp. 873–882, 2015.
- [236] P. Li, S. Zhang, H. Feng, and Y. Li, “Speaker identification using spectrogram and learning vector quantization,” *Journal of Computational Information Systems*, vol. 11, no. 9, pp. 3087–3095, 2015.
- [237] R. Liu, B. Li, L. Zhang, and L. Jiao, “A new two-step learning vector quantization algorithm for image compression,” *Transactions of the Institute of Measurement and Control*, vol. 37, no. 1, pp. 3–14, 2015.
- [238] D. Nebel, B. Hammer, K. Froberg, and T. Villmann, “Median variants of learning vector quantization for learning of dissimilarity data,” *Neurocomputing*, vol. 169, pp. 295–305, 2015.
- [239] L. H. A. Wahab, A. Susanto, S. Insap, and M. Tjokronegoro, “Computational cost of learning vector quantization algorithm for malaria parasite classification in realtime test,” *International Journal of Imaging and Robotics*, vol. 16, no. 1, pp. 101–107, 2016.
- [240] T. Oliva, M. Fernandes, J. Amorim, and V. Vasconcelos, “Video-tracking of zebrafish (*Danio rerio*) as a biological early warning system using two distinct artificial neural networks: Probabilistic neural network (PNN) and self-organizing map (SOM),” *Aquatic Toxicology*, vol. 165, pp. 241–248, 2015.
- [241] A. A. Konaté, H. Pan, S. Fang, S. Asim, Y. Y. Ziggah, C. Deng, and N. Khan, “Capability of self-organizing map neural network in geophysical log data classification: Case study from the CCSD-MH,” *Journal of Applied Geophysics*, vol. 118, pp. 37–46, 2015.
- [242] M. Pandey, A. K. Pandey, A. Mishra, and B. D. Tripathi, “Application of chemometric

analysis and self Organizing Map-Artificial Neural Network as source receptor modeling for metal speciation in river sediment,” *Environmental Pollution*, vol. 204, pp. 64–73, 2015.

[243] A. Yasuda, Y. Onuki, Y. Obata, and K. Takayama, “Latent structure modeling underlying theophylline tablet formulations using a Bayesian network based on a self-organizing map clustering,” *Drug Development and Industrial Pharmacy*, vol. 41, no. 7, pp. 1148–1155, 2015.

[244] Y. Wang, L. Wang, D. Li, X. Cheng, and Y. Xiao, “Self-Organizing Map Neural Network-Based Depth-of-Interaction Determination for Continuous Crystal PET Detectors,” *IEEE Transactions on Nuclear Science*, vol. 62, no. 3, pp. 766–772, 2015.

[245] X. Ma, W. Liu, Y. Li, and R. Song, “LVQ neural network based target differentiation method for mobile robot,” *Proceedings 12th International Conference on Advanced Robotics*, pp. 680–685, 2005.

[246] Y. Chen, K. Tseng, “Multiple-angle Hand Gesture Recognition by Fusing SVM Classifiers,” *Proceedings 3rd International Conference on Automation Science and Engineering*, pp. 527–530, 2007.

[247] A. Romero-Manchado and J. I. Rojas-Sola, “Application of gradient-based edge detectors to determine vanishing points in monoscopic images: Comparative study,” *Image and Vision Computing*, vol. 43, pp. 1–15, 2015.

[248] A. Asjad and D. Mohamed, “A new approach for salt dome detection using a 3D multidirectional edge detector,” *Applied Geophysics*, vol. 12, no. 3, pp. 334–342, 2015.

[249] Y. Xu, Y. Sun, and Z. Wang, “Human segmentation for video sequences in natural environments,” *Journal of Computational Information Systems*, vol. 11, no. 9, pp. 3131–3138, 2015.

[250] A. Sengur, Y. Guo, M. Ustundag, and Ö. F. Alcin, “A Novel Edge Detection Algorithm Based on Texture Feature Coding,” *Journal of Intelligent Systems*, vol. 24, no. 2, pp. 235–248, 2015.

[251] X. Tian, “A novel image edge detection algorithm based on prewitt operator and wavelet transform,” *International Journal of Advancements in Computing Technology*, vol. 4, no. 19, pp. 73–82, 2012.

[252] F. G. Ergin, B. B. Watz, K. Erglis, and A. Cēbers, “Time-resolved velocity measurements in a magnetic micromixer,” *Experimental Thermal and Fluid Science*, vol. 67, pp. 6–13, 2015.

[253] H. X. Gong and L. Hao, “Roberts edge detection algorithm based on GPU,” *Journal of Chemical and Pharmaceutical Research*, vol. 6, no. 7, pp. 1308–1314, 2014.

[254] W. Xiulei, C. Ming, W. Xianglin, and Z. Guomin, “Defending DDoS attacks in software defined networking based on improved Shiryayev-Roberts detection algorithm,” *Journal of High Speed Networks*, vol. 21, no. 4, pp. 295–298, 2015.

[255] A. Afshari, S. R. Shadizadeh, and M. A. Riahi, “The use of artificial neural networks in reservoir permeability estimation from well logs: Focus on different network training algorithms,” *Energy Sources, Part A: Recovery, Utilization and Environmental Effects*, vol. 36, no. 11, pp. 1195–1202, 2014.

- [256] M. Aleardi, "Seismic velocity estimation from well log data with genetic algorithms in comparison to neural networks and multilinear approaches," *Journal of Applied Geophysics*, vol. 117, pp. 13–22, 2015.
- [257] S. Aoyagi, M. Suzuki, T. Takahashi, J. Fujioka, and Y. Kamiya, "Calibration of kinematic parameters of robot arm using laser tracking system: Compensation for non-geometric errors by neural networks and selection of optimal measuring points by genetic algorithm," *International Journal of Automation Technology*, vol. 6, no. 1, pp. 29–37, 2012.
- [258] S. Hu, Z. Liu, Y. L. Guan, W. Xiong, G. Bi, and S. Li, "Sequence design for cognitive CDMA communications under arbitrary spectrum hole constraint," *IEEE Journal on Selected Areas in Communications*, vol. 32, no. 11, pp. 1974–1986, 2014.
- [259] Q. Hao, J. Cao, Y. Hu, Y. Yang, K. Li, and T. Li, "Differential optical-path approach to improve signal-to-noise ratio of pulsed-laser range finding," *Optics Express*, vol. 22, no. 1, pp. 563–575, 2014.
- [260] H. Monga and R. S. Kaler, "Analytical Design, Simulation & Evaluation of Proposed OCDMA with Message Priority Fast Routing Codes," *National Academy Science Letters*, vol. 37, no. 6, pp. 509–512, 2014.
- [261] M. D. Toy, "A supercell storm simulation using a nonhydrostatic cloud-resolving model based on a hybrid isentropic-sigma vertical coordinate," *Monthly Weather Review*, vol. 141, no. 4, pp. 1204–1215, 2013.
- [262] Y. Pei, "Inhomogeneity of weak edge image level set segmentation algorithm," *International Review on Computers and Software*, vol. 7, no. 7, pp. 3698–3703, 2012.
- [263] Z. Hou, "Dual threshold and edge image optimization of canny algorithm in the road extraction from remote sensing image," *International Journal of Earth Sciences and Engineering*, vol. 8, no. 1, pp. 188–194, 2015.
- [264] Q. Xu, S. Varadarajan, C. Chakrabarti, and L. J. Karam, "A distributed canny edge detector: Algorithm and FPGA implementation," *IEEE Transactions on Image Processing*, vol. 23, no. 7, pp. 2944–2960, 2014.
- [265] T. Xiao, W. Yin-He, and W. Qin-Ruo, "A face recognition method based on complex network, canny algorithm and image contours," *International Review on Computers and Software*, vol. 8, no. 1, pp. 204–210, 2013.
- [266] M. J. Ebrahim and H. Pourghassem, "A novel automatic synthetic segmentation algorithm based on mean shift clustering and canny edge detector for aerial and satellite images," *International Review on Computers and Software*, vol. 7, no. 3, pp. 1122–1129, 2012.
- [267] J. Zhang, "Human-Mobile Robot Interaction and Controlling Software Development Using Novel Face Orientation Recognition Strategy," *Master Thesis, University of Rostock, Germany*, 2016.
- [268] Y. Saito, K. Asai, Y. Choi, T. Iyota, K. Watanabe, and Y. Kubota, "Development of a battery support system for the prolonged activity of mobile robots," *Electronics and Communications in Japan*, vol. 94, no. 3, pp. 60–71, 2011.
- [269] F. Zhang, G. Liu, L. Fang, and H. Wang, "Estimation of battery state of charge with H $\infty$  observer: Applied to a robot for inspecting power transmission lines," *IEEE Transactions on*

*Industrial Electronics*, vol. 59, no. 2, pp. 1086–1095, 2012.

[270] V. Berenz, F. Tanaka, and K. Suzuki, “Autonomous battery management for mobile robots based on risk and gain assessment,” *Artificial Intelligence Review*, vol. 37, no. 3, pp. 217–237, 2012.

[271] J. Zhang, G. Song, Y. Li, G. Qiao, and Z. Li, “Battery swapping and wireless charging for a home robot system with remote human assistance,” *IEEE Transactions on Consumer Electronics*, vol. 59, no. 4, pp. 747–755, 2013.

[272] I. Shnaps and E. Rimon, “On-line coverage of planar environments by a battery powered autonomous mobile robot,” *Springer Tracts in Advanced Robotics*, vol. 107, pp. 571–589, 2015.

[273] N. Mathew, S. L. Smith, and S. L. Waslander, “Multirobot Rendezvous Planning for Recharging in Persistent Tasks,” *IEEE Transactions on Robotics*, vol. 31, no. 1, pp. 128–142, 2015.

[274] R. C. Luo, C. T. Liao, and S. C. Lin, “Multi-sensor fusion for reduced uncertainty in autonomous mobile robot docking and recharging,” *Proceedings IEEE/RSJ International Conference on Intelligent Robots and Systems*, pp. 2203–2208, 2009.

[275] A. Couture-Beil and R. T. Vaughan, “Adaptive mobile charging stations for multi-robot systems,” *Proceedings IEEE/RSJ International Conference on Intelligent Robots and Systems*, pp. 1363–1368, 2009.

[276] K. L. Su, T. L. Chien, and C. Y. Liang, “Develop a self-diagnosis function auto-recharging device for mobile robot,” *Proceedings IEEE International Workshop on Safety, Security and Rescue Robotics*, Proceedings, pp. 1–6, 2005.

[277] S. Keshmiri, “Multi-robot, multi-rendezvous recharging paradigm: An opportunistic control strategy,” *Proceedings IEEE International Symposium on Robotic and Sensors Environments (ROSE)*, pp. 31–36, 2011.

[278] N. Mathew, S. L. Smith, and S. L. Waslander, “A graph-based approach to multi-robot rendezvous for recharging in persistent tasks,” *Proceedings 2013 IEEE International Conference on Robotics and Automation (ICRA)*, pp. 3497–3502, 2013.

[279] H. Liu, N. Stoll, S. Junginger, and K. Thürow, “An application of charging management for mobile robot transportation in laboratory environments,” *Proceedings IEEE Instrumentation and Measurement Technology Conference*, pp. 435–439, 2013.

[280] L. Zhao and Y. Jia, “Transcale control for a class of discrete stochastic systems based on wavelet packet decomposition,” *Information Sciences*, vol. 296, no. 1, pp. 25–41, 2015.

[281] G. De, A. Ficarella, and A. Lay-Ekuakille, “Monitoring Cavitation Regime from Pressure and Optical Sensors: Comparing Methods Using Wavelet Decomposition for Signal Processing,” *IEEE Sensors Journal*, vol. 15, no. 8, pp. 4684–4691, 2015.

[282] C. Sours, H. Chen, S. Roys, J. Zhuo, A. Varshney, and R. P. Gullapalli, “Investigation of multiple frequency ranges using discrete wavelet decomposition of resting-state functional connectivity in mild traumatic brain injury patients,” *Brain Connectivity*, vol. 5, no. 7, pp. 442–450, 2015.

[283] G. De, A. Ficarella, and A. Lay-Ekuakille, “Cavitation Regime Detection by LS-SVM and ANN with Wavelet Decomposition Based on Pressure Sensor Signals,” *IEEE Sensors Journal*,

vol. 15, no. 10, pp. 5701–5708, 2015.

[284] N. M. Makbol, B. E. Khoo, and T. H. Rassem, “Block-based discrete wavelet transform-singular value decomposition image watermarking scheme using human visual system characteristics,” *IET Image Processing*, vol. 10, no. 1, pp. 34–52, 2016.

[285] Y. Qin, B. Tang, and Y. Mao, “Adaptive signal decomposition based on wavelet ridge and its application,” *Signal Processing*, vol. 120, pp. 480–494, 2016.

[286] K. S. Wu, W. D. Liao, C.-N. Lin, and T.-S. Chen, “A high payload hybrid data hiding scheme with LSB, EMD and MPE,” *Imaging Science Journal*, vol. 63, no. 3, pp. 174–181, 2015.

[287] M. Mohebbi, “A novel application of higher order statistics of R-R interval signal in EMD domain for predicting termination of atrial fibrillation,” *Journal of Biological Systems*, vol. 23, no. 1, pp. 115–130, 2015.

[288] S. Ramezania and O. Bahar, “EMD-based output-only identification of mode shapes of linear structures,” *Smart Structures and Systems*, vol. 16, no. 5, pp. 919–935, 2015.

[289] Y. V. Vizilter and S. V. Sidiyakin, “Comparison of shapes of two-dimensional figures with the use of morphological spectra and EMD metrics,” *Pattern Recognition and Image Analysis*, vol. 25, no. 3, pp. 365–372, 2015.

[290] M. Xu, P. Shang, and A. Lin, “Cross-correlation analysis of stock markets using EMD and EEMD,” *Physica A: Statistical Mechanics and its Applications*, vol. 442, pp. 82–90, 2016.

[291] M. K. I. Molla, K. Hirose, and M. K. Hasan, “Voiced/non-voiced speech classification using adaptive thresholding with bivariate EMD,” *Pattern Analysis and Applications*, vol. 19, no. 1, pp. 139–144, 2016.

[292] A. Karami and M. Guerrero-Zapata, “An ANFIS-based cache replacement method for mitigating cache pollution attacks in Named Data Networking,” *Computer Networks*, vol. 80, pp. 51–65, 2015.

[293] Y. Liu and Y. Zhang, “Iterative local ANFIS-based human welder intelligence modeling and control in pipe GTAW process: A data-driven approach,” *IEEE/ASME Transactions on Mechatronics*, vol. 20, no. 3, pp. 1079–1088, 2015.

[294] S. H. Jung and S.-U. Choi, “Prediction of composite suitability index for physical habitat simulations using the ANFIS method,” *Applied Soft Computing Journal*, vol. 34, pp. 502–512, 2015.

[295] I. G. Sardou and M. T. Ameli, “ANFIS-based non-dominated sorting genetic algorithm II for scenario-based joint energy and reserves market clearing considering TCSC device,” *International Transactions on Electrical Energy Systems*, vol. 25, no. 12, pp. 3349–3373, 2015.

[296] P. Shen, “ANFIS control double-inverted pendulum,” *Chemical Engineering Transactions*, vol. 46, pp. 895–900, 2015.

[297] D. P. Rini, S. M. Shamsuddin, and S. S. Yuhaniz, “Particle swarm optimization for ANFIS interpretability and accuracy,” *Soft Computing*, vol. 20, no. 1, pp. 251–262, 2016.

[298] A. M. S. U. Doulah, S. . Fattah, W.-P. Zhu, and M. O. Ahmad, “Wavelet Domain Feature Extraction Scheme Based on Dominant Motor Unit Action Potential of EMG Signal for Neuromuscular Disease Classification,” *IEEE Transactions on Biomedical Circuits and Systems*, vol. 8, no. 2, pp. 155–164, Apr. 2014.



- [299] S. Banerjee and M. Mitra, "Application of Cross Wavelet Transform for ECG Pattern Analysis and Classification," *IEEE Transactions on Instrumentation and Measurement*, vol. 63, no. 2, pp. 326–333, Feb. 2014.
- [300] H. Liu, N. Stoll, S. Junginger, and K. Thurow, "A new approach to battery power tracking and predicting for mobile robot transportation using wavelet decomposition and ANFIS networks," *Proceedings 2014 IEEE International Conference on Robotics and Biomimetics*, pp. 253–258, 2014.
- [301] S. K. Madishetty, A. Madanayake, R. J. Cintra, V. S. Dimitrov, and D. H. Mugler, "VLSI architectures for the 4-tap and 6-tap 2-D Daubechies wavelet filters using algebraic integers," *IEEE Transactions on Circuits and Systems I: Regular Papers*, vol. 60, no. 6, pp. 1455–1468, 2013.
- [302] K. L. V. Iyer, X. Lu, Y. Usama, V. Ramakrishnan, and N. C. Kar, "A twofold Daubechies-wavelet-based module for fault detection and voltage regulation in SEIGs for distributed wind power generation," *IEEE Transactions on Industrial Electronics*, vol. 60, no. 4, pp. 1638–1651, 2013.
- [303] R. Singh and A. Khare, "Fusion of multimodal medical images using Daubechies complex wavelet transform - A multiresolution approach," *Information Fusion*, vol. 19, no. 1, pp. 49–60, 2014.
- [304] P. Balakrishnan, M. M. Hasan, and K. A. Wahid, "An efficient algorithm for daubechies lifting wavelets using algebraic integers," *Canadian Journal of Electrical and Computer Engineering*, vol. 37, no. 3, pp. 127–134, 2014.
- [305] M. R. E. Dishabi and M. A. Azgomi, "Differential privacy preserving clustering using Daubechies-2 wavelet transform," *International Journal of Wavelets, Multiresolution and Information Processing*, vol. 13, no. 4, 2015.
- [306] J. Chen, W. Tang, and M. Xu, "A mesh-free analysis of the ship structures based on daubechies wavelet basis theory," *Journal of Information and Computational Science*, vol. 12, no. 5, pp. 1675–1684, 2015.
- [307] B. I. Kbaier, P. Lazure, and I. Puillat, "Advanced Spectral Analysis and Cross Correlation Based on the Empirical Mode Decomposition: Application to the Environmental Time Series," *IEEE Geoscience and Remote Sensing Letters*, vol. 12, no. 9, pp. 1968–1972, 2015.
- [308] Y. Yang, J. Deng, and D. Kang, "An improved empirical mode decomposition by using dyadic masking signals," *Signal, Image and Video Processing*, vol. 9, no. 6, pp. 1259–1263, 2015.
- [309] Z. Liu, T. Chai, W. Yu, and J. Tang, "Multi-frequency signal modeling using empirical mode decomposition and PCA with application to mill load estimation," *Neurocomputing*, vol. 169, pp. 392–402, 2015.
- [310] X. Yin, B. Xu, C. Jiang, Y. Fu, Z. Wang, H. Li, and G. Shi, "NIRS-based classification of clench force and speed motor imagery with the use of empirical mode decomposition for BCI," *Medical Engineering and Physics*, vol. 37, no. 3, pp. 280–286, 2015.
- [311] A. R. Hassan and M. I. H. Bhuiyan, "Computer-aided sleep staging using Complete Ensemble Empirical Mode Decomposition with Adaptive Noise and bootstrap aggregating," *Biomedical Signal Processing and Control*, vol. 24, pp. 1–10, 2016.

- [312] L. Yang, F. Zhou, L. Yang, and H. Zhou, "Optimal averages for nonlinear signal decompositions - Another alternative for empirical mode decomposition," *Signal Processing*, vol. 121, pp. 17–29, 2016.
- [313] R. A. Rios and M. De, "Applying Empirical Mode Decomposition and mutual information to separate stochastic and deterministic influences embedded in signals," *Signal Processing*, vol. 118, pp. 159–176, 2015.
- [314] H. Liu, C. Chen, H. Tian, and Y. Li, "A hybrid model for wind speed prediction using empirical mode decomposition and artificial neural networks," *Renewable Energy*, vol. 48, pp. 545–556, 2012.
- [315] M. Liu, M. Dong, and C. Wu, "A New ANFIS for Parameter Prediction With Numeric and Categorical Inputs," *IEEE Transactions on Automation Science and Engineering*, vol. 7, no. 3, pp. 645–653, 2010.
- [316] P. Garcia, C. . Garcia, L. M. Fernandez, F. Llorens, and F. Jurado, "ANFIS-Based Control of a Grid-Connected Hybrid System Integrating Renewable Energies, Hydrogen and Batteries," *IEEE Transactions on Industrial Informatics*, vol. 10, no. 2, pp. 1107–1117, 2014.
- [317] A. Al-Hmouz, J. Shen, R. Al-Hmouz, and J. Yan, "Modeling and Simulation of an Adaptive Neuro-Fuzzy Inference System (ANFIS) for Mobile Learning," *IEEE Transactions on Learning Technologies*, vol. 5, no. 3, pp. 226–237, 2012.
- [318] G. Ma, Z. Jiang, H. Li, J. Gao, Z. Yu, X. Chen, Y.-H. Liu, and Q. Huang, "Hand-eye servo and impedance control for manipulator arm to capture target satellite safely," *Robotica*, vol. 33, no. 4, pp. 848–864, 2015.
- [319] J.-W. Lu, X.-M. Sun, A. F. Vakakis, and L. A. Bergman, "Influence of backlash in gear reducer on dynamic of single-link manipulator arm," *Robotica*, vol. 33, no. 8, pp. 1671–1685, 2015.
- [320] H. Ananthanarayanan and R. Ordóñez, "Real-time Inverse Kinematics of  $(2n + 1)$  DOF hyper-redundant manipulator arm via a combined numerical and analytical approach," *Mechanism and Machine Theory*, vol. 91, pp. 209–226, 2015.
- [321] F. da, O. Saotome, M. N. Pontuschka, G. L. B. Lima, F. de, and N. Seito, "Interaction between motions of robotic manipulator arms and the non-fixed base in on-orbit operations," *Journal of Aerospace Technology and Management*, vol. 7, no. 4, pp. 443–453, 2015.
- [322] Y. Ren, Y. Liu, M. Jin, and H. Liu, "Biomimetic object impedance control for dual-arm cooperative 7-DOF manipulators," *Robotics and Autonomous Systems*, vol. 75, pp. 273–287, 2016.
- [323] X. Liu, P. Zhang, and G. Du, "Hybrid adaptive impedance-leader-follower control for multi-arm coordination manipulators," *Industrial Robot*, vol. 43, no. 1, pp. 112–120, 2016.
- [324] J.-H. Guo, K.-L. Su, and B.-Y. Li, "Development of a PLC based robot arm," *ICIC Express Letters, Part B: Applications*, vol. 6, no. 3, pp. 637–642, 2015.
- [325] C. Reinbacher, M. Ruther, and H. Bischof, "RopNect: Hand mounted depth sensing using a commodity gaming sensor," *Proceedings 21st International Conference on Pattern Recognition (ICPR)*, pp. 461–464, 2012.
- [326] Y. J. Yoo, D. S. Jung, Y. J. Jang, and S. C. Won, "Fuzzy weighted subtask controller for

- redundant manipulator,” *Robotica*, vol. 33, no. 2, pp. 295–313, 2015.
- [327] G. Chen, Z. Xia, X. Ming, S. Lining, J. Ji, and Z. Du, “Camera calibration based on Extended Kalman Filter using robot’s arm motion,” *Proceedings IEEE/ASME International Conference on Advanced Intelligent Mechatronics*, pp. 1839–1844, 2009.
- [328] H. Esfandiari and M. H. Korayem, “Optimal point to point path planning of flexible manipulator under large deformation by using harmony search method,” *Journal of Theoretical and Applied Mechanics*, vol. 54, no. 1, pp. 179–183, 2016.
- [329] C.-H. Huang, C.-S. Hsu, P.-C. Tsai, R.-J. Wang, and W.-J. Wang, “Vision based 3-D position control for a robot arm,” *Proceedings IEEE International Conference on Systems, Man, and Cybernetics (SMC)*, pp. 1699–1703, 2011.
- [330] S. Manigpan, S. Kiattisin, and A. Leelasantitham, “A simulation of 6R industrial articulated robot arm using backpropagation neural network,” *Proceedings 2010 International Conference on Control Automation and Systems (ICCAS)*, pp. 823–826, 2010.
- [331] K. V. Lakshmi and Mashuq-un-Nabi, “An adaptive Neuro-Fuzzy control approach for motion control of a robot arm,” *Proceedings 2012 International Conference on Informatics, Electronics Vision (ICIEV)*, pp. 832–836, 2012.
- [332] H. Liu, N. Stoll, S. Junginger, and K. Thürow, “A new method for mobile robot arm blind grasping using ultrasonic sensors and Artificial Neural Networks,” *Proceedings 2013 IEEE International Conference on Robotics and Biomimetics*, pp. 1360–1364, 2013.
- [333] J. I. Peláez, J. M. Doña, J. F. Fornari, and G. Serra, “Ischemia classification via ECG using MLP neural networks,” *International Journal of Computational Intelligence Systems*, vol. 7, no. 2, pp. 344–352, 2014.
- [334] B. Sokouti, S. Haghipour, and A. D. Tabrizi, “A framework for diagnosing cervical cancer disease based on feedforward MLP neural network and ThinPrep histopathological cell image features,” *Neural Computing and Applications*, vol. 24, no. 1, pp. 221–232, 2014.
- [335] G. Badalians, H. Masihi, M. Azimipour, A. Abrishami, and M. Mirabi, “Optimizing stabilization of waste-activated sludge using Fered-Fenton process and artificial neural network modeling (KSOFM, MLP),” *Environmental Science and Pollution Research*, vol. 21, no. 11, pp. 7177–7186, 2014.
- [336] M. Rafei, S. E. Sorkhabi, and M. R. Mosavi, “Multi-objective optimization by means of multi-dimensional mlp neural networks,” *Neural Network World*, vol. 24, no. 1, pp. 31–56, 2014.
- [337] E. Asnaashari, M. Asnaashari, A. Ehtiati, and R. Farahmandfar, “Comparison of adaptive neuro-fuzzy inference system and artificial neural networks (MLP and RBF) for estimation of oxidation parameters of soybean oil added with curcumin,” *Journal of Food Measurement and Characterization*, vol. 9, no. 2, pp. 215–224, 2015.
- [338] M. Taki, Y. Ajabshirchi, S. F. Ranjbar, A. Rohani, and M. Matloobi, “Heat transfer and MLP neural network models to predict inside environment variables and energy lost in a semi-solar greenhouse,” *Energy and Buildings*, vol. 110, pp. 314–329, 2016.
- [339] J.-T. Zou and K.-L. Su, “Design and implementation of a robot arm for humanoid robot,” *ICIC Express Letters*, vol. 7, no. 5, pp. 1597–1604, 2013.
- [340] L. J. Everett and J. Lei, “Improved manipulator performance through local D-H

- calibration,” *Journal of Robotic Systems*, vol. 12, no. 7, pp. 505–514, 1995.
- [341] Y. Chen and Y. Wei, “Simulation of a robot machining system based on heterogeneous-resolution representation,” *Computer-Aided Design and Applications*, vol. 13, no. 1, pp. 77–85, 2016.
- [342] M.-H. Chiang and H.-T. Lin, “Development of a 3D parallel mechanism robot arm with three vertical-axial pneumatic actuators combined with a stereo vision system,” *Sensors*, vol. 11, no. 12, pp. 11476–11494, 2011.
- [343] M. M. Ali, H. Liu, R. Stoll, and K. Thurow, “Arm grasping for mobile robot transportation using Kinect sensor and kinematic analysis,” *Proceedings IEEE International Instrumentation and Measurement Technology Conference (I2MTC)*, pp. 516–521, 2015.
- [344] M. Sabhadiya, “Calibration and Optimization of Arm Grasping & Placing for Mobile Robot Transportation,” *Master Thesis, University of Rostock, Germany*, 2016.

## Declaration

This habilitation thesis ‘*Intelligent Strategies for Mobile Robotics in Laboratory Automation*’ is a presentation of my original habilitation research. Wherever contributions of others are involved, every effort is made to indicate this clearly, with due reference to the literature, and acknowledgement of collaborative research and discussions.

Myself have done the work of this habilitation thesis at the University of Rostock, Germany. The habilitation thesis has not been accepted for any degree and is not concurrently submitted in candidature of any other degree.

Rostock, 29 February, 2016

Hui Liu

## Curriculum Vitae

**Dr. -Ing. Hui Liu**



### 1. Personal Information

- ✧ **Name:** Hui Liu
- ✧ **Nationality:** Chinese
- ✧ **Birthday:** 07-02-1983
- ✧ **Family status:** married, 2 children

### 2. Education Qualifications

- ✧ **Dr. -Ing.**, Automation Engineering, University of Rostock, Faculty of Computer Science and Electrical Engineering, Germany, 2013.  
Dissertation Title: Mobile Robot Transportation in Laboratory Automation
- ✧ **Master Degree Honors I**, Mechanical and Control Engineering, Central South University, Faculty of Traffic and Transportation Engineering, China, 2008.
- ✧ **Bachelor Degree Honors I**, Mechanical and Control Engineering, Central South University, Faculty of Traffic and Transportation Engineering, China, 2004.

### 3. Work Experiences

- ✧ **2015-2016:**  
Leader of BMBF Junior Research Group (*Equivalent to Assistant Professor in US System/Lecturer in UK System*) of 'Life Science Automation - Systems & Process Technologies', Leader of Research Group 'Mobile Robotics', Senior Scientist at the Center for Life Science Automation (CELISCA) & Institute of Automation, University of Rostock, Germany; (*working on habilitation degree for the professorship*)
- ✧ **2014-2015:**  
Associate Leader of BMBF Junior Research Group of 'Life Science Automation - Systems & Process Technologies', Group Leader of Research Group 'Mobile Robotics', Postdoctoral Scientist at the Center for Life Science Automation (CELISCA) & Institute of Automation, University of Rostock, Germany.

✧ **2011-2013:**

Doctoral Scientist (*Supervisors: Prof. Kerstin Thurow, Prof. Norbert Stoll*) at Center for Life Science Automation (CELISCA) & Institute of Automation, University of Rostock, Germany.

✧ **2009-2010:**

Scientific Visitor at the Laboratory for Motion Generation and Analysis, Department of Mechanical and Aerospace Engineering, Faculty of Engineering, Monash University, Australia.

✧ **2008-2011:**

Lecturer (*Institute Director: Prof. Hongqi Tian*) at the key laboratory of traffic safety on track of Ministry of Education of China, Central South University, China.

✧ **2005-2008:**

Master of Engineering in Mechanical and Control Engineering (Honors I, State Medal, the top one student in all faculty master students), Central South University, China.

✧ **2004-2005:**

Engineer in Bureau of Railway of Shanghai City, China.

✧ **2000-2004:**

Bachelor of Engineering in Mechanical and Control Engineering (Honors I, University Medal, the top 5% student in all faculty undergraduate students), Central South University, China

## 4. Research Interests:

- ✧ Mobile Robotics
- ✧ Laboratory Automation
- ✧ Wind Engineering & Wind Energy System
- ✧ Hybrid Artificial Intelligence

## 5. Experiences as Reviewer

✧ **Reviewers of Journals:**

- IEEE Transactions on Neural Networks and Learning Systems (IF: 4.37)

- IEEE Transactions on Power System (IF: 3.530)
- IET Renewable Power Generation (IF: 2.280)
- IET Generation, Transmission & Distribution (IF: 1.866)
- Renewable & Sustainable Energy Reviews (IF: 5.901)
- International Journal of Electrical Power & Energy Systems (IF: 3.432)
- Information Sciences (IF: 4.038)
- Robotics and Autonomous Systems (IF: 1.256)
- Applied Energy (IF: 5.261)
- Neurocomputing (IF: 2.005)
- Energy Conversion and Management (IF: 3.590)
- Applied Soft Computing (IF: 2.810)
- Chaos, Solitons & Fractals (IF: 1.503)
- Advances in Mechanical Engineering (IF: 0.5)
- KSCE Journal of Civil Engineering (IF: 0.511)
- Progress in Computational Fluid Dynamics (IF: 0.6)

✧ **Members of Technical Program Committees of International Conferences:**

- IEEE Power and Energy Conference 2012 (IEEE PECON 2012);
- IEEE International Conference on Clear Energy & Technologies 2013 (IEEE CEAT 2013)
- IEEE International Conference on Image Information Processing 2013 (IEEE ICIIP 2013)
- IEEE International Conference on Image Information Processing 2015 (IEEE ICIIP 2015)
- International work-conference on Time Series 2014 (ITISE 2014);
- International work-conference on Time Series 2015 (ITISE 2015);
- IEEE Second International Symposium on Computer Vision and the Internet (IEEE VersionNet 2015)
- IEEE Game Physics and Mechanics International Conference 2015 (GAMEPEC 2015)

✧ **Reviewers of International Conferences:**

- IEEE I2MTC 2013, IEEE CASE 2012-2015, IEEE ROBIO 2012, IEEE ICOEIS 2012, IEEE PECON 2012-2014, IEEE CEAT 2013, IEEE ICIIP 2013, IEEE InCIEC 2013, IEEE ISBEIA 2012-2013, IEEE ICACCI-2014, etc.



## 6. Theses/Dissertations as Supervisors

### ✧ Master Theses:

- 1) Thesis Topic: Remote Controlling Software Development for Mobile Robot Transportation, Student Name: Mr. Ali Ghar, Discipline: Communication Engineering, in process, *Co-supervision with Prof. Kerstin Thurow.*
- 2) Thesis Topic: Human-Mobile Robot Interaction and Controlling Software Development Using Novel Pace Orientation Recognition Strategy, Student Name: Mr. Jian Zhang, Discipline: Communication Engineering, completed on 16.03.2016, *Co-supervision with Prof. Kerstin Thurow.*
- 3) Thesis Topic: Calibration and Optimization of Arm Grasping & Placing for Mobile Robot Transportation, Student Name: Mr. Maheshkumar Sabhadiya, Discipline: Computational Engineering, completed on 30.03.2016, *Co-supervision with Prof. Kerstin Thurow.*
- 4) Thesis Topic: Graphical Display Components for Robot indoor localization, Student Name: Mr. Yaman Neameh, Discipline: Computational Engineering, completed on 24.09.2012, *Co-supervision with Prof. Kerstin Thurow and Dr. Steffen Junginger.*
- 5) Thesis Topic: Database Programming for Mobile Robot, Student Name: Mr. B. Chaitanya Krishna Reddy, Discipline: Computational Engineering, completed on 08.10.2012, *Co-supervision with Prof. Norbert Stoll and Dr. Steffen Junginger.*
- 6) Thesis Topic: Mobile Robot Localization Using Microsoft Kinect Sensor, Student Name: Mr. Mohammed Myasar Ali, Discipline: Computational Engineering, completed on 26.03.2013, *Co-supervision with Prof. Norbert Stoll and Dr. Steffen Junginger.*
- 7) Thesis Topic: Accuracy Measurement of StarGazer Based Indoor Localization for Mobile Robots in Laboratories, Student Name: Mr. Xiaozhou Li, Discipline: Electronic Engineering, completed on 20.09.2013, *Co-supervision with Prof. Norbert Stoll and Dr. Steffen Junginger.*
- 8) Thesis Topic: System Integration for Mobile Robots in Bio-labs, Student Name: Mr. Sohail Mughal, Discipline: Computational Engineering, completed on 19.05.2014, *Co-supervision with Prof. Norbert Stoll and Dr. Steffen Junginger.*
- 9) Thesis Topic: Indoor Navigation with the Dr. Robot Jaguar, Student Name: Mr. Ankit R. Ramani, Discipline: Computational Engineering, completed on 25.06.2014, *Co-supervision with Prof. Norbert Stoll and Dr. Steffen Junginger.*

### ✧ PhD Dissertations in Progress:

- 1) Thesis Topic: Mobile Robot High-precision Arm Manipulation, Candidate: M.Sc. Mohammed Myasar Ali, Discipline: Automation Engineering/Mobile Robotics, *Co-supervision with Prof. Kerstin Thurow and Prof. Norbert Stoll.*
- 2) Thesis Topic: Mobile Robot Indoor Multi-floor Transportation, Candidate: M. Sc. Ali Abdulla, Discipline: Automation Engineering/Mobile Robotics, *Co-supervision with Prof. Kerstin Thurow and Prof. Norbert Stoll.*
- 3) Thesis Topic: Mobile Robot Secure Indoor Navigation and Collision Avoidance, Candidate: M.Sc. Mazen Ghandour, Discipline: Automation Engineering/Mobile Robotics, *Co-supervision with Prof. Kerstin Thurow and Prof. Norbert Stoll.*

## 7. Awards:

- 1) 2015 Highly Cited Research Paper. Awarded by Applied Energy, Elsevier, 2016
- 2) International Eni Award 2013 Nomination (*The most famous award in Energy and Environment*). Nominated by Eni Award Scientific Secretariat, 2012.
- 3) Excellent Scientist in CAE Key Project (*Internet of Things & Traffic Engineering*). Awarded by Chinese Academy of Engineering (CAE), 2011.
- 4) China Mao Yisheng Outstanding Research Award for Postgraduate in Engineering. Awarded by Chinese Technology & Development Council, 2007.
- 5) State Excellent Student Medal. Awarded by Department of Public Education of Hunan Province (State), China, 2008.
- 6) State Honors I Graduate Medal. Awarded by Department of Public Education of Hunan Province (State), China, 2008.
- 7) State Excellent Master Thesis Award. Thesis Title: *Strong Wind Speed Signal Modeling & Forecasting Optimization Algorithms for Qinghai-Tibet Railway Safety Protecting System*. Awarded by Academic Committee of Hunan Province (State), China, 2008.
- 8) Mittal Excellent Engineering Student Research Medal. Awarded by England Arcelor Mittal Steel Company, 2008.
- 9) University Excellent Postgraduate Award. Awarded by Central South University, 2006 and 2007.

## 8. Publications

***H-index Excluding Self-Citation 11 in Scopus***

**Google Scholar:** <https://scholar.google.de/citations?user=Rni6S94AAAAJ&hl=en>

**● Mobile Robotics:**

- (1) Liu, H.; Stoll, N.; Junginger, S.; Thurow, K.: Human-Mobile Robot Interaction in Laboratories Using Kinect Sensor and ELM based Face Feature Recognition. Proceedings, IEEE HSI-IEEE International Conference on Human System Interaction, Portsmouth (UK), 6-8, July, 2016, pp. 197-202. **(SCOPUS)**
- (2) Liu, H.; Stoll, N.; Junginger, S.; Thurow, K.: New Localization Strategy for Mobile Robot Transportation in Life Science Automation Using StarGazer Sensor, Time Series Modeling and Kalman Filter Processing. Proceedings, IEEE ROBIO-IEEE International Conference on Robotics and Biomimetics, Zhuhai (China), 6-9, December, 2015, pp. 164-168. **(SCOPUS)**
- (3) Liu, H.; Stoll, N.; Junginger, S.; Thurow, K.: Human Face Orientation Recognition for Mobile Robot Transportation in Laboratory Automation using Hybrid Edge Detection and LVQ Neural Networks. Proceedings, IEEE ROBIO-IEEE International Conference on Robotics and Biomimetics, Zhuhai (China), 6-9, December, 2015, pp. 2003-2007. **(SCOPUS)**
- (4) Liu H.; Stoll, N.; Junginger S.; Thurow, K.: A Fast Approach to Arm Blind Grasping and Placing for Mobile Robot Transportation in Laboratories. International Journal of Advanced Robotic System, 2014. DOI: 10.5772/58253. **(SCOPUS & SCI Thomson Reuters)**
- (5) Liu, H.; Stoll, N.; Junginger, S.; Thurow, K.: A New Approach to Battery Power Tracking and Predicting for Mobile Robot Transportation Using Wavelet Decomposition and ANFIS Networks. Proceedings, IEEE ROBIO-IEEE International Conference on Robotics and Biomimetics, Bali (Indonesia), 5-10, December, 2014, pp. 253-258. **(SCOPUS)**
- (6) Liu, H.; Stoll, N.; Junginger, S.; Thurow, K.: Mobile Robotic Transportation in Laboratory Automation: Multi-robot Control, Robot-Door Integration and Robot-Human Interaction. Proceedings, IEEE ROBIO-IEEE International Conference on Robotics and Biomimetics, Bali (Indonesia), 5-10, December, 2014, pp. 1033-1038. **(SCOPUS)**
- (7) Liu H.; Stoll, N.; Junginger S.; Thurow, K.: Mobile Robot for Life Science Automation. International Journal of Advanced Robotic System, 2013, 10(7): 1-14. DOI: 10.5772/56670. **(SCOPUS & SCI Thomson Reuters)**
- (8) Liu H.; Stoll, N.; Junginger S.; Thurow, K.: A Fast Method for Mobile Robot Transportation in Life Science Automation, IEEE I2MTC-International Instrumentation and Measurement Technology Conference, Minneapolis (USA), 6-9, May, 2013, pp. 238-242. **(SCOPUS)**
- (9) Liu H.; Stoll, N.; Junginger S.; Thurow, K.: An Application of Charging Management for Mobile Robot Transportation in Laboratory Environments, IEEE I2MTC-International Instrumentation and Measurement Technology Conference,

- Minneapolis (USA), 6-9, May, 2013, pp. 435-439. **(SCOPUS)**
- (10) Liu H.; Stoll, N.; Junginger S.; Thurow, K.: A New Method for Mobile Robot Arm Blind Grasping Using Ultrasonic Sensors and Artificial Neural Networks, Proceedings, IEEE ROBIO-IEEE International Conference on Robotics and Biomimetics, Shenzhen (China), 11-14, December, 2013, pp. 1360-1364. **(SCOPUS)**
- (11) Liu H.; Stoll, N.; Junginger S.; Thurow, K.: A Common Wireless Remote Control System for Mobile Robots in Laboratory, Proceedings, IEEE I2MTC-International Instrumentation and Measurement Technology Conference, Graz (Austria), 13-16, May, 2012, pp. 688-693. **(SCOPUS)**
- (12) Liu H.; Stoll, N.; Junginger S.; Thurow, K.: A Floyd-Dijkstra Hybrid Application for Mobile Robot Path Planning in Life Science Automation, Proceedings, IEEE CASE-8th IEEE International Conference on Automation Science and Engineering, Seoul (Korea), 20-24, August, 2012, pp. 275-280. **(SCOPUS)**
- (13) Liu H.; Stoll, N.; Junginger S.; Thurow, K.: A Floyd-Genetic Algorithm Based Path Planning System for Mobile Robots in Laboratory Automation, Proceedings, IEEE ROBIO-IEEE International Conference on Robotics and Biomimetics, Guangzhou (China), 11-14, December, 2012, pp. 1550-1555. **(SCOPUS)**
- (14) Ghandour M.; Liu, H.; Stoll, N.; Thurow, K.: Interactive Collision Avoidance System for Indoor Mobile Robots based on Human-Robot Interaction. Proceedings, IEEE HSI-IEEE International Conference on Human System Interaction, Portsmouth (UK), 6-8, July, 2016, pp. 209-215. **(SCOPUS)**
- (15) Ghandour, M.; Liu, H.; Stoll, N.; Thurow, K.: A Hybrid Collision Avoidance System for Indoor Mobile Robots based on Human-Robot Interaction. Proceedings, 17th International Conference on Mechatronics – Mechatronika 2016, Prague (Czech Republic), 7-9, December, 2016. **(Accepted, SCOPUS)**
- (16) Abdulla A. A. A.; Liu H.; Stoll, N.; Thurow, K.: A New Robust Method for Mobile Robot Multi-Floor Navigation in Distributed Life Science Laboratories. Journal of Control Science and Engineering, 2016, pp. 1-17. **(SCOPUS)**
- (17) Abdulla A. A. A.; Liu H.; Stoll, N.; Thurow, K.: An Automated Elevator Management and Multi-Floor Estimation for Indoor Mobile Robot Transportation Based on a Pressure Sensor. Proceedings, 17th International Conference on Mechatronics – Mechatronika 2016, Prague (Czech Republic), 7-9, December, 2016. **(Accepted, SCOPUS)**
- (18) Ali, M. M.; Liu, H.; Stoll, N.; Thurow, K.: Intelligent Arm Manipulation System in Life Science Labs Using H20 Mobile Robot and Kinect Sensor. Proceedings, IEEE International Conference on Intelligent Systems (IS'16), Sofia (Bulgaria), 04-06, September, 2016, pp. 382-387. **(SCOPUS)**

- (19) Ali, M. M.; Liu, H.; Stoll, N.; Thurow, K.: Multiple Lab Ware Manipulation in Life Science Laboratories using Mobile Robots. Proceedings, IEEE International Conference on Mechatronics (Mechatronika), Prague (Czech Republic), 07-09, December, 2016. **(Accepted, SCOPUS)**
- (20) Ali, M. M.; Liu, H.; Stoll, N.; Thurow, K.: An Identification and localization Approach of Different Labware for Mobile Robot Transportation in Life Science laboratories. Proceedings, IEEE International Symposium on Computational Intelligence and Informatics (CINTI), Budapest (Hungary), 17-19, November, 2016. **(Accepted, SCOPUS)**
- (21) Thurow, K.; Liu H.: Mobile robotics for life science laboratories. Mobile Robotics: Principles, Techniques and Applications, ISBN: 978-163482665-5; 978-163482641-9, Book Chapter, 2015. **(SCOPUS)**
- (22) Ali M. M.; Liu H.; Stoll, R.; Thurow, K.: Arm Grasping for Mobile Robot Transportation Using Kinect Sensor and Kinematic Analysis. IEEE I2MTC-International Instrumentation and Measurement Technology Conference, Italy (Pisa), 11-14, May, 2015, pp. 516-521. **(SCOPUS)**
- (23) Abdulla A. A. A.; Liu H.; Stoll, N.; Thurow, K.: Multi-floor Navigation Method for Mobile Robot Transportation Based on StarGazer Sensors in Life Science Automation. IEEE I2MTC-International Instrumentation and Measurement Technology Conference, Italy (Pisa), 11-14, May, 2015, pp. 428–433. **(SCOPUS)**
- (24) Ghandour M.; Liu H.; Stoll, N.; Thurow, K.: Improving the Navigation of Indoor Mobile Robots Using Kalman Filter. IEEE I2MTC-International Instrumentation and Measurement Technology Conference, Italy (Pisa), 11-14, May, 2015, pp. 1434-1439. **(SCOPUS)**
- (25) Abdulla A. A. A.; Liu H.; Stoll, N.; Thurow, K.: A Robust Method for Elevator Operation in Semi-outdoor Environment for Mobile Robot Transportation System in Life Science Laboratories. IEEE 20th International Conference on Intelligent Engineering Systems, Hungary (Budapest), June 30-July 2, 2016, pp. 45-50. **(SCOPUS)**
- (26) Vorberg E.; Fleischer H.; Junginger S.; Liu H.; Stoll, N.; Thurow, K.: A Highly Flexible, Automated System Providing Reliable Sample Preparation in Element- and Structure-Specific Measurements. Journal of Laboratory Automation, 2015, DOI: 10.1177/2211068215595946. **(SCOPUS & SCI Thomson Reuters)**

## ● Control Engineering & Energy System & Wind Engineering:

- (27) Liu H.; Tian H.Q.; Liang X.F.; Li Y.F.: Wind speed forecasting approach using secondary decomposition algorithm and Elman neural networks. Applied Energy, 2015, 157(11): 183-194. DOI: 10.1016/j.apenergy.2015.08.014. **(IF: 5.613, JCR-Q1 Journal, SCOPUS & SCI Thomson Reuters)**

- (28) Liu H.; Tian H.Q.; Li Y.F.: Comparison of new hybrid FEEMD-MLP, FEEMD-ANFIS, Wavelet Packet-MLP and Wavelet Packet-ANFIS for wind speed predictions. *Energy Conversion and Management*, 2015, 89: 1-11. DOI: 10.1016/j.enconman.2014.09.060. **(IF: 4.380, JCR-Q1 Journal, SCOPUS & SCI Thomson Reuters, Global ESI Top 0.1% Hot Paper)**
- (29) Liu H.; Tian H.Q.; Li Y.F.; Zhang L.: Comparison of four Adaboost algorithm based artificial neural networks in wind speed predictions. *Energy Conversion and Management*, 2015, 92: 67-81. DOI: 10.1016/j.enconman.2014.12.053. **(IF: 4.380, JCR-Q1 Journal, SCOPUS & SCI Thomson Reuters, Global ESI Top 1% Highly Cited Paper)**
- (30) Liu H.; Tian H.Q.; Li Y.F.: Four Wind Speed Forecasting Models Using Extreme Learning Machines and Signal Decomposing Algorithms. *Energy Conversion and Management*, 2015, 100: 16-22. DOI:10.1016/j.enconman.2015.04.057. **(IF: 4.380, JCR-Q1 Journal, SCOPUS & SCI Thomson Reuters)**
- (31) Liu H.; Tian H.Q.; Liang X.F.; Li Y.F.: New Wind Speed Forecasting Approaches Using Fast Ensemble Empirical Model Decomposition, Genetic Algorithm, Mind Evolutionary Algorithm and Artificial Neural Networks. *Renewable Energy*, 2015, 83: 1066-1075. DOI: 10.1016/j.renene.2015.06.004. **(IF: 3.476, JCR-Q1 Journal, SCOPUS & SCI Thomson Reuters, Global ESI Top 0.1% Hot Paper)**
- (32) Liu H.; Tian H.Q.; Li Y.F.: An EMD-Recursive ARIMA Method to Predict Wind Speed for Railway Strong Wind Warning System. *Journal of Wind Engineering & Industrial Aerodynamics*, 2015, 141(6): 27-38. DOI: 10.1016/j.jweia.2015.02.004. **(IF: 1.414, JCR-Q2 Journal, SCOPUS & SCI Thomson Reuters)**
- (33) Liu H.; Tian H.Q.; Liang X.F.; Li Y.F.: Short-term wind speed intelligent prediction algorithm along strong-wind railways based on empirical mode decomposition and adaptive neural fuzzy inference system. *Journal of Central South University of Technology (Science and Technology)*, 2015, 141(6): 27-38. **(SCOPUS)**
- (34) Liu H.; Tian H.Q.; Li Y.F.: Study on Performance Comparison of Wind Speed Hybrid High-precision One-step Predicting Models along Railways. *Journal of the China Railway Society*, 2015, 38(8): 41-49. **(SCOPUS)**
- (35) Liu H.; Tian H.Q.; Pan D.F.; Li Y.F.: Forecasting models for wind speed using wavelet, wavelet packet, time series and artificial neural networks. *Applied Energy*, 2013, 107(7): 191-208. DOI: 10.1016/j.apenergy.2013.02.002. **(IF: 5.613, JCR-Q1 Journal, SCOPUS & SCI Thomson Reuters, Global ESI Top 1% Highly Cited Paper)**
- (36) Liu H.; Tian H.Q.; Chen C.; Li Y.F.: An experimental investigation of two Wavelet-MLP hybrid frameworks for wind speed prediction using GA and PSO

- optimization. International Journal of Electrical Power and Energy Systems, 2013, 52(11): 161-173. DOI: 10.1016/j.ijepes.2013.03.034. **(IF: 3.432, JCR-Q1 Journal, SCOPUS & SCI Thomson Reuters)**
- (37) Liu H.; Tian H.Q.; Li Y.F.: Comparison of two new ARIMA-ANN and ARIMA-Kalman hybrid methods for wind speed prediction. Applied Energy, 2012, 98(10): 415-424. DOI: 10.1016/j.apenergy.2012.04.001. **(IF: 5.613, JCR-Q1 Journal, SCOPUS & SCI Thomson Reuters, *Global ESI Top 1% Highly Cited Paper*)**
- (38) Liu H.; Chen C.; Tian H.Q.; Li Y.F.: A hybrid model for wind speed prediction using empirical mode decomposition and artificial neural network. Renewable Energy, 2012, 48(12): 545-556. DOI: 10.1016/j.renene.2012.06.012. **(IF: 3.476, JCR-Q1 Journal, SCOPUS & SCI Thomson Reuters)**
- (39) Liu H.; Tian H.Q.; Chen C.; Li Y.F.: A hybrid statistical method to predict wind speed and wind power. Renewable Energy, 2010, 35(8): 1857-1861. DOI: 10.1016/j.renene.2009.12.011. **(IF: 3.476, JCR-Q1 Journal, SCOPUS & SCI Thomson Reuters)**
- (40) Liu H.; Tian H.Q.; Li Y.F.: Short-term forecasting optimization algorithms for wind speed along Qinghai-Tibet railway based on different intelligent modeling theories. Journal of Central South University of Technology (English Edition), 2009, 16(4): 690-696. DOI: 10.1007/s11771-009-0114-3. **(IF: 0.464, JCR-Q3 Journal, SCOPUS & SCI Thomson Reuters)**
- (41) Liu H.; Tian H.Q.; Li Y.F.: Short-term forecasting optimization algorithm for wind speed from wind farms based on wavelet analysis method and rolling time series method. Journal of Central South University of Technology (Science and Technology), 2010, 41(1): 370-375. **(SCOPUS)**
- (42) Liu H.; Tian H.Q.; Li Y.F.: Short-term forecasting optimization algorithm for unsteady wind speed signal based on wavelet analysis method and neural networks method. Journal of Central South University of Technology (Science and Technology), 2011, 42(9): 2704-2711. **(SCOPUS)**
- (43) Liu H.; Pan D.F.; Li Y.F.: Qinghai-Tibet Railway Gale Forecasting Optimization Model and Algorithm Based on Train Running Safety. Journal of Wuhan University of Technology (Traffic & Transportation Edition), 2008, 32(6): 986-989. **(SCOPUS)**
- (44) Pan D.F.; Liu H.; Li Y.F.: A Short-Term Forecast Method for Wind Speed along Golmud-Lhasa Section of Qinghai-Tibet Railway. China Railway Science, 2008, 29(5): 128-133. **(SCOPUS)**
- (45) Pan D.F.; Liu H.; Li Y.F.: Optimization Algorithm of Short-term Multi-step Wind Speed Forecast. Proceedings of the CSEE, 2008, 28(26): 87-91. **(SCOPUS)**

## 9. Authorized Patents

- ✧ **Liu H.**; Tian H.Q.; Pan D.F.; Xu P.; Gao G.J.; Li Y.F.; Wang Z.G.: Method for Intelligently Forecasting Wind Speed in Wind Power Station, PRC Invention Application Publication (Source: SIPO); Publication No. CN 102609766A published on 25-Jul-2012; Application No. CN 201210036118.0 filed on 17-Feb-2012. **(Authorized Data: 12-March-2014)**
- ✧ **Liu H.**; Tian H.Q.; Liang X.F.; Yao S.; Yang M.Z.; Lu Z.J.; Zhang L.: Intelligent Hybrid Predicting Method for Wind Speed of High-Speed Railway Line, PRC Invention Application Publication (Source: SIPO); Publication No. 102609788A published on 25-Jul-2012; Application No. CN 201210036109.1 filed on 17-Feb-2012. **(Authorized Data: 6-August-2014)**
- ✧ Tian H.Q.; Yang M.Z.; **Liu H.**; Yang Z.G.; Xu P.; Li Z.W.: Method for Measuring and Analyzing Noise in Train and System Thereof, PRC Invention Application Publication (Source: SIPO); Publication No. CN 101650221 published on 17-Feb-2010; Application No. CN 200910169986.4 filed on 14-Sep-2009. **(Authorized Data: 15-December-2010)**
- ✧ Tian H.Q.; Liang X.F.; Pan D.F.; Yang M.Z.; Gao G.J.; **Liu H.**: Method for Forecasting Wind Speed along Railway, PRC Invention Application Publication (Source: SIPO); Publication No. CN 101592673 published on 02-Dec-2009; Application No. CN 200910009302.4 filed on 18-Feb-2009. **(Authorized Data: 15-December-2010)**
- ✧ Tian H.Q.; Xu P.; Xiong X.H.; Lu Z.J.; Liu T.H.; **Liu H.**: Determining Method and Measuring System of Safety Retreat Distance of Side Personnel under Action of Train Wind, PRC Invention Application Publication (Source: SIPO); Publication No. CN 101650255 published on 17-Feb-2010; Application No. CN 200910169985.X filed on 14-Sep-2009. **(Authorized Data: 15-December-2010)**

Rostock, 10 November 2016

Hui Liu



## Theses

1. An intelligent framework is proposed for the mobile robotics in laboratory automation. The proposed framework focuses on the latest challenges of the mobile robotics in the laboratory environments, including the multi-floor mobile robot indoor navigation, the multi-floor robot path planning, the human feature based robot collision avoidance, the intelligent mobile robot power forecasting and the robot arm manipulation.
2. A new universal multi-floor robot indoor localization method is proposed. The localization method adopts the StarGazer sensors to measure the installed ceiling landmarks to complete the universal robot positioning maps. All the equipped landmarks have a unique ID so that the whole laboratory environment and the corresponding small-zones can be identified correctly.
3. The installed ceiling landmarks do not consume any electrical power and can be extended conveniently to match any sizes and indoor laboratory environments. They also can be extended to different types of indoor environments such as the internal elevators to provide the running mobile robots satisfactory indoor localization performance.
4. A new intelligent signal filtering method is presented to improve the robustness of the adopted StarGazer sensors for the mobile robots under the indoor ceiling interferences, based on combining the TSA (*Time Series Analysis*) theory and the KF (*Kalman Filter*) theory.
5. In the proposed intelligent robot indoor localization filtering framework, both of the one-step tracking and the two-step forecasting computation are executed. All the calculated results are used by the mobile robots to find the false measured robot indoor coordinates under the ceiling interferences.
6. The ARIMA model from the TSA theory is established to identify the changing laws of the robot indoor coordinates and the built ARIMA equations are utilized to select and optimize the initial parameters of the KF model for the real-time computation. The combined ARIMA-KF model not only solves the mobile robot indoor navigation under the ceiling interferences but also provides a new strategy to initialize the KF model based on the ARIMA model.

7. In the ARIMA modeling for the real robot indoor coordinates, the auto-correlation and partial-correlation functions are chosen to determine the model types & orders, and the Yule-Walker estimation algorithm is adopted to calculate the specific parameters of the recognized time series models. The reason to adopt this kind of time series modeling is to guarantee the real-time performance of the proposed ARIMA-KF method for the running mobile robots.
8. A new human face based HRI (*Human-Robot Interaction*) approach is put forward for the collision avoidance in laboratories. In the proposed approach, the face orientations and the face moving directions being measured by Microsoft Kinect Sensors are proposed to control the mobile robots when they run in the narrow corridors and special areas where the standard collision avoidance functions become unavailable.
9. In the human face HRI based collision avoidance, the status of the human eye blinking is defined as the starting trigger and the eyebrow-eye hybrid zones in the face images are selected as the impacting parameters to differentiate the human face orientations and rotations. To find the eyebrow-eye hybrid zones, the standard image edge detecting method is used.
10. A LVQ (*Learning Vector Quantization*) neural network is established in the face HRI to classify the human orientations and moving directions for the mobile robots. In the built LVQ neural network, three-layer network architecture is used. To investigate and find the best image edge detecting algorithm combining with the LVQ neural network, a performance comparison is provided including mainstream edge detecting algorithms (*i.e., Sobel algorithm, Prewitt algorithm, Roberts algorithm, Log algorithm, Zero-cross algorithm and Canny algorithm*). The experimental results show that the Prewitt algorithm has the best performance either in the successful rate or in the consuming time.
11. Besides the face based HRI, another new gesture based HRI strategy is also proposed for the laboratory indoor collision avoidance. In the presented strategy, the human body skeletons and the corresponding gestures are all measured by the robot installed Microsoft Kinect Sensors to control the coming mobile robots. The proposed gesture based HRI works together with the proposed face based HRI.

12. A SVM (*Support Vector Machine*) model is built in the gesture HRI to recognize the dynamic gesture based commands for the mobile robots. In the built LVQ model, three-layer network architecture is adopted. To find the best parameters for the built SVM model for the real-time and accurate computation, several experiments are provided. The experimental results show that the SVM model needs less than one second to obtain the recognizing successful rate of 99.78%.
13. A new intelligent strategy is proposed for the mobile robot power forecasting combining two popular signal decomposing algorithms (*i.e., the Wavelet Decomposition-WD and the Empirical Mode Decomposition-EMD*) and the ANFIS (*Adaptive Neuro Fuzzy Inference System*) neural networks. Based on the proposed strategy, the mobile robots can decide whether to accept a distributed transportation task by considering the forecasted on-board power status.
14. In the proposed intelligent robot power forecasting framework, two hybrid methods named as the WD-ANFIS method and the EMD-ANFIS method are generated. The experimental results show that both of the proposed WD-ANFIS method and the proposed EMD-ANFIS methods have satisfactory robot power forecasting performance. For instance, the MAPE errors of the WD-ANFIS model and the EMD-ANFIS model are 0.22% and 0.24%, respectively.
15. In the proposed hybrid WD-ANFIS and EMD-ANFIS methods, both of the WD algorithm and the EMD algorithm decompose the originally measured robot power data successfully. To explore the contributions caused by the WD/EMD decomposition in the hybrid structures, a comparison is carried out and the results indicate that the decomposing strategies promote the performance of the standard ANFIS network considerably. For example, the promoting percentages of the MAE, the MAPE and the RMSE of the ANFIS by the WD decomposition are 55.04%, 55.10% and 50.76%, respectively.
16. A new intelligent blind strategy is presented for the mobile robots to complete the grasping & placing manipulations. The originality is to obtain satisfactory manipulating but does not need any additional sensors such as the arm cameras and request additional complex computation.
17. In the proposed intelligent blind arm manipulator, the ultrasonic sensors, which are always originally equipped with mobile robots for the collision detection, are adopted to measure the real-time distances between the robots' bases and the front

workstations. A MLP (*Multiple Layer Perceptron*) neural network is established to find the nonlinear relationship between the ultrasonic distances and the robot arm joint controlling values.

18. To build the best MLP neural network for the robot arm controlling, a comparison is provided based on the most popular network training algorithms. The comparing results show that the BFGS algorithm fit the MLP based robot blind arm controller best. The BFGS trained MLP network has good performance in both of the mapping accuracy and the real-time computation. It gets a successful rate 99.62% only consuming 0.72s with a normal laptop.
19. A new vision strategy is proposed to promote the accuracy threshold of the blind strategy from 2 cm to 0.5 cm for some high-accuracy situations. In the developed vision arm manipulator, the arm kinematic models are solved and embedded. At the same time, to make the proposed arm manipulator recognize and compensate the potential errors, the multiple lab-ware identification functions are included.

## Abstract

In this habilitation thesis a new intelligent framework is presented for the unsolved challenges of mobile robotics in laboratory automation, which includes the multi-floor robot indoor localization and path planning, the human feature based robot collision avoidance, the intelligent mobile robot power forecasting and the fast robot arm manipulations. The original innovations of this thesis are given as follows:

- ✧ A new StarGazer sensor based multi-floor robot indoor navigation method is presented and the corresponding multi-floor sub-zone shortest path planning approach is proposed. In the establishing multi-floor map, the StarGazer sensors work as the HEX reader to measure the ceiling landmarks for the robot indoor positioning & localization. In the sub-zone shortest path planning process, the whole laboratory environment is divided into a number of impacting zones where the Floyd-Dijkstra/Floyd-Genetic hybrid algorithms are executed to find the shortest paths for the running mobile robots. Based on the shortest paths of the sub-zones, the whole multi-floor paths can be generated directly.
- ✧ A new intelligent signal filtering method is put forward for the running mobile robots to forecast their corresponding indoor coordinates and correct the wrong measuring coordinates to avoid the robot-missing problems under the indoor ceiling interferences. In the proposed intelligent filtering method, a new hybrid computational method named as the TSA-KF method is proposed combining the TSA (*Time Series Analysis*) and the KF (*Kalman Filter*). The experimental results show that the MAPE errors of the one-step tracking and the two-step forecasting by the proposed TSA-KF method is only 1.03% and 1.92%, respectively. The consuming times for these MAPE errors are only 0.36s and 0.38s, respectively.
- ✧ A new human feature (*i.e., face, gesture*) based mobile robot controlling strategy is proposed for the robot-human smart collision avoidance. In the proposed strategy, the human face orientations and gestures are used to realize the controlling of the robot-human collision avoidance, the blinking status of the eyes or the defined gesture behaviors from the closest person are selected as the avoiding trigger. The eyebrow-eye edge detecting matrixes are utilized to classify

the real-time human face orientations in the proposed face strategy, and at the same time the human body skeletons and gestures are used to recognize the gesture behavior based commands. Based on the proposed human feature based architecture, the mobile robots can complete the smart human feature guiding avoidance.

- ✧ A new intelligent face feature classification computational method is presented using the LVQ (*Learning Vector Quantization*) neural networks. In the new method, the eyebrow-eye matrixes are chosen as the inputting neurons and the face orientations are selected as the outputting neurons in the LVQ network. Based on the recognized face orientations, the human face controlling purposes can be measured correctly. To build the best LVQ neural network model, four mainstream edge detecting algorithms are included in the performance comparison. The results of the experiments indicate that the Prewitt algorithm has the best performance either in the successful rate 99% or in the consuming time 3.17s. Similarly, a new intelligent gesture feature classification computational method is also proposed based on the SVM (*Support Vector Machine*). The results of the SVM based gesture recognizing experiments show that the built SVM model only needs less than 1s to reach the successful rate of 99.78%.
- ✧ A new intelligent robot power forecasting method is proposed for the running mobile robots to decide whether they should accept or reject a distributed transportation task, by combining two popular non-stationary signal decomposing algorithms (*i.e.*, *Wavelet Decomposition-WD* and *Empirical Mode Decomposition-EMD*) and the ANFIS neural networks. The original robot power is decomposed by the WD decomposition and the EMD decomposition, respectively. The suitable ANFIS models are established in the decomposed sub-layer signals.
- ✧ In the proposed robot power forecasting architecture two hybrid models are brought forward, the hybrid WD-ANFIS and the hybrid EMD-ANFIS. The experimental results show that the proposed two hybrid models have satisfactory performances and the adoption of the WD and EMD decomposition promotes the capacity of the ANFIS neural network considerably. *For instance, the promoting percentages of the MAE, the MAPE and the RMSE of the ANFIS by the wavelet decomposition are 55.04%, 55.10% and 50.76%, respectively.*

- ✧ A new intelligent blind approach is presented for the arm manipulations for the mobile robots. The proposed approach adopts the ultrasonic sensors which are originally equipped for the robot collision avoidance to realize the blind arm grasping and placing but does not need additional cameras. To make the blind strategy flexible, the MLP neural network is established to build the dynamic relationships between the measured ultrasonic distances and the corresponding arm joints' controlling values. The results of the experiments indicate that the proposed MLP based arm blind measure is effective (*the successful rate 99.62% and the consuming time 0.72s*) for the arm manipulations. Additionally, a new vision strategy is proposed to promote the accuracy threshold of the blind strategy from 2 cm to 0.5 cm by combining the robotic arm kinematic models and the multiple lab-ware identification.

## Zusammenfassung

In dieser Habilitationsschrift wird ein neues intelligentes Framework für die bisher ungelösten Herausforderungen der Anwendung mobiler Robotik in der Laborautomation vorgestellt. Dies beinhaltet eine Multi-Floor Indoorlokalisation und -pfadplanung, die Kollisionsvermeidung mit integrierter Objekterkennung / Unterscheidung, eine intelligente Batterieladungsvorhersage mit Lademanagement sowie die schnelle rückgekoppelte Steuerung des Roboterarms für Manipulationen. Nachfolgend werden die wesentlichen Innovationen dieser Arbeit genannt:

- ✧ Es wird ein auf der StarGazer™ Technologie basierendes Multi-Floor Indoor Navigationsverfahren vorgestellt, wobei zusätzlich Methoden der optimierenden Findung von Fahrwegen präsentiert werden. In der erstellten Multi-Floor Navigationskarten – Umgebung werden die StarGazer™ Sensoren als Code-Leser und Lokalisatoren der an den Labordecken installierten kodierten Landmarken eingesetzt. Bei der Pfadplanung mit Wegstreckenoptimierung wird die Gesamtlaborumgebung in eine Anzahl von Aktionsbereichen unterteilt, für die mit Floyd-Dijkstra- sowie Floyd-Genetic Hybrid-Algorithmen die kürzesten Fahrwege für die mobilen Roboter in den Teilbereichen gefunden werden. Darauf basierend können die Gesamtnavigationspfade für die gesamte Laborumgebung direkt generiert werden.
- ✧ Es wird ein neues intelligentes Signalfilterungsverfahren in der mobilen Roboternavigation eingesetzt, mit dessen Hilfe die folgenden korrespondierenden Indoorkoordinaten vorhergesagt werden können. Dies kann auch zur Plausibilitätsprüfung und Korrektur von Fehlinterpretationen von Landmarkensignalen infolge ungünstiger Umgebungsbedingungen eingesetzt werden. Somit werden Probleme bei der Selbstlokalisierung der Roboter vermieden. In dem vorgestellten intelligenten Filterverfahren wird eine neue hybride rechnergestützte Methode namens TSA-KF (*Time Series Analysis und Kalman Filter*) eingesetzt, welche die Zeitreihenanalyse und die Kalman Filter Technologie kombiniert. Die Ergebnisse der Untersuchungen zeigen, dass die mittleren absoluten prozentualen Fehler (MAPE) der TSA-KF Methode nur 1,92% betragen. Der Zeitbedarf für die Anwendung dieser Technologien liegt im Einschrittracking bei nur 0.36s und bei der ZweiSchrittvorhersage bei nur 0,38s.



- ✧ Es wird eine auf menschlichen Merkmalen basierende (z.B. Gesichtserkennung, Gesten) Steuerungsstrategie für die intelligente smarte Kollisionsvermeidung vorgestellt. Bei diesem Verfahren wird die Blickrichtung sowie Bewegungsrichtung des menschlichen Gesichts für die Steuerung der Kollisionsvermeidung verwendet. Das Muster der Schließbewegung der Augenlider der am nächsten befindlichen Person oder bestimmte Gesten werden als Trigger für Mechanismen der Kollisionsvermeidung verwendet. Für die Echtzeiterkennung der Orientierung des Gesichts werden Matrices zur Detektion der Augenbrauen / Augen verwendet. Gleichzeitig werden Gesten mittels Skelett-Motion Tracking erkannt und in Kommandos übersetzt. Auf allen diesen Techniken basierend wurde die intelligente gestenunterstützte Kollisionsvermeidung etabliert.
- ✧ Es wird eine auf Gesichtsmerkmalen basierende Erkennungsmethode vorgestellt, welches neuronale Netze mit Lernender Vektorquantisierung (LVQ) verwendet. Hier werden die Augenbrauen / Augen-Matrices als Eingangsneuronen und die Gesichtsorientierungen als Ausgangsneuronen im LVQ Netzwerk gewählt. Basierend auf den erkannten Gesichtsorientierungen können die gestenbasierten Steuerungskommandos korrekt interpretiert werden. Um das beste LVQ neuronale Netzwerk zu finden, werden vier Standardkanten-erkennungsalgorithmen in die Performancebewertung eingeschlossen. Die Ergebnisse der Untersuchungen zeigen, dass der Prewitt Algorithmus die beste Performance sowohl in der Erfolgsrate (99%) als auch in der Rechenzeit (3,17s) hat. Ebenso wird eine intelligente auf Gestenmerkmalen basierende Methode vorgestellt, die auf SVM (Support Vector Machine) basiert. Die Ergebnisse der Untersuchungen der Gestenerkennung mit SVM zeigen, dass das generierte SVM Modell weniger als eine Sekunde für die Verarbeitung benötigt und mit einer Erfolgsrate von 99,78% arbeitet.
- ✧ Es wird eine neue intelligente Akkuladezustandsvorhersage vorgestellt, die auf mobilen Roboterplattformen eingesetzt werden kann. Hier wird auf Basis der Ladezustandsvorhersage entschieden, ob die Roboter Transportaufträge annehmen oder ablehnen. Dabei werden zwei populäre nichtstationäre Signaldekompositionsalgorithmen (z.B. *Wavelet Decomposition-WD* and *Empirical Mode Decomposition -EMD*) und ANFIS Neuronale Netze

angewendet. Der echte Akkuladezustand wird jeweils mit Wavelet Dekomposition und Empirical Mode Dekomposition zeitlich zerlegt. Die ANFIS Modelle werden in den zeitlich zerlegten Sub-Layer Signalen verwendet.

- ✧ Es werden in der vorgestellten Akkuladezustandsvorhersage-Architektur zwei hybride Modelle verwendet: Das WD-ANFIS Modell und das EMD ANFIS Modell. Die Messergebnisse zeigen, dass die Modelle eine herausragende Performance besitzen und dass die WD und EMD Dekomposition die Vorhersagequalität des ANFIS Neuronalen Netzwerks erheblich verbessern. *Zum Beispiel werden die Fehlerwerte bei der Kombination von WD und ANFIS um mehr als 50% verbessert verglichen mit der Verwendung von ANFIS allein.*
- ✧ Abschließend wird ein intelligenter Ansatz für die blinde Armmanipulation der mobilen Roboter präsentiert. Das Verfahren nutzt Ultraschallsensoren des Roboters, die originär zur Kollisionsvermeidung eingesetzt werden, für die Positionierung, benötigt aber keine Kameras zur Verfolgung von Armbewegungen. Für eine flexible Strategie wurde ein MLP Neuronales Netz implementiert, um dynamische Beziehungen zwischen den gemessenen Ultraschallabständen und den Steuerwerten der korrespondierenden Armgelenke der Roboter herzustellen. Die Ergebnisse der Evaluierung dieses Ansatzes zeigen, dass das MLP basierte Verfahren mit einer Erfolgsrate von 99,62% und einer Rechenzeit von 0,72 Sekunden wirkungsvoll für präzise Armbewegungen ist. Zusätzlich wird eine auf Bildverarbeitung basierende Strategie vorgestellt, welche die Positioniergenauigkeit von 2cm beim blinden Greifen auf 0,5cm verbessert. Dabei werden kinematische Modelle der Roboterarme, als auch die Erkennung der Labwarepositionen an Hand von individuellen Mustern angewendet.